HIGH-TECH METAL POTENTIAL OF SPHALERITE FROM EASTERN ALPINE LEAD-ZINC DEPOSITS AND DEVELOPMENT OF A MATRIX-MATCHED SPHALERITE (ZnS) CALIBRATION MATERIAL (MUL-ZnS-1) FOR CALIBRATION OF IN SITU TRACE ELEMENT MEASUREMENTS BY LASER ABLATION INDUCTIVELY COUPLED PLASMA MASS SPECTROMETRY (LA-ICP-MS)

PhD Thesis

Montanuniversitaet Leoben

Department of Applied Geosciences

Chair of Geology and Economic Geology

Peter Onuk MSc

Supervisor: Univ. Prof. Dr. mont. Frank Melcher

April 2018

Herewith I affirm in the lieu of oath that I prepared this PhD thesis myself, using exclusively the references, cited in this volume

Leoben April 2018

Acknowledgement

First of all, I would like to thank my supervisor Univ. Prof. Dr Frank Melcher (Chair of Geology and Economic Geology, Universitaet Leoben) for his help and support during my research and for constructive critic and discussion during the writing process! I also want to thank Prof. Dr. Frank Melcher for staying cool after the explosion of a muffle furnace and fire alarm induced during this thesis.

This PhD thesis was partly financed by the Federal Ministry of Education, Science and Research (Austria) within the project fund of the Geological Survey of Austria: Identifikation und Klassifizierung potentieller Hochtechnologie-Metall Ressourcen in ostalpinen Blei-Zinklagerstätten.

For the sample preparation (thick sections) I want to thank Gustav Hanke and Sabine Feuchter. Many thanks to Regina Mertz (University Mainz), Simon Goldmann and Eike Gäbler (BGR) for their support during the quantification of the matrix matched reference material.

Furthermore I want to thank Univ. Prof. Dr. Walter Prochaska, Univ. Prof. Gerd Rantitsch, Dr. Heinrich Mali, Dipl.Ing. Birgit Kain-Bückner for their constructive critic and discussion during the research and writing process.

Thank you to Brigitte Mang for her administrative support.

Abstract

The “Ad-Hoc working Group on defining critical raw materials” of the European Union (EU) has identified twenty commodities as being critical; some of them are used in high-technology products and green technologies (EU, 2014). Austria hosts numerous mineralizations with significant potential of the rare high-tech metals germanium, gallium, indium and cobalt, as indicated by chemical data of sulphide ore concentrates. In the beginning of the 1990s, the long-lasting experience of Austrian companies in base metal mining from domestic sources was terminated by the closure of the zinc-lead mine at Bleiberg-Kreuth. Zinc, copper, lead and silver were the major commodities mined in deposits within Austria.

Erich Schroll was the first to analyze trace metals in domestic ores (Schroll, 1954; Cerny & Schroll, 1995). Modern, systematic research using state-of-the-art analytical methods, however, is almost completely missing. First LA-ICP-MS data from sphalerite, which is a major host for some high-technology metals like Ga, Ge, In and Co are presented as part of a re-evaluation of three major types of base metal deposits in the Eastern Alps.

In situ measurements of trace elements in natural sphalerite samples using LA-ICP-MS are hampered by a lack of homogenous matrix-matched sulphide reference materials available for calibration. The preparation of the MUL-ZnS1 calibration material containing the trace elements V, Cr, Mn, Co, Ni, Cu, Ga, Ge, As, Se, Mo, Ag, Cd, In, Sn, Sb, Tl, and Pb besides Zn, Fe and S is reported. Commercially available ZnS, FeS, CdS products were used as the major components, whereas the trace elements were added by doping with single element ICP-MS standard solutions and natural mineral powders. The resulting powder mixture was pressed to pellets and sintered at 400 °C for 100 hours using argon as inert gas. To confirm the homogeneity of major and trace element distributions within the MUL-ZnS1 calibration material, measurements were performed using EPMA, solution ICP-MS, ICP-OES and LA-ICP-MS. The results show that MUL-ZnS-1 is an appropriate material for calibrating trace element determination in sphalerite using LA-ICP-MS.

Additional to the in-situ trace element analysis, sulfur isotope ($\delta^{34}S$) composition was measured the first time in-situ by using a triple quadrupole ICP-MS in this study using N_2O as reaction gas to reduce the O_2 and NO interferences on sulfur isotopes. Therefore two Matrix matched sulfur isotopic reference materials were developed. The MUL-ZnS-S1 ($\delta^{34}S$ = 19.7 ‰ (relative to VCDT) and MUL-ZnS-S2 ($\delta^{34}S$ = 1.2 ‰ (relative to VCDT) reduce the problem of isotope fractionation during the ablation due to the ZnS matrix for sphalerite.

The three investigated ore types are:

(1) Carbonate-hosted “Alpine-type“ or “Bleiberg-type“ deposits hosted by Triassic limestones and dolomites of the Drau Range and the Northern Calcareous Alps are characterized by low Fe, high Cd (~2000 µg/g), Ge (200-400 µg/g) and Tl concentrations (~100 µg/g) in sphalerite and by the absence of Co (max. 1 µg/g), Cu, Ni. The Lafatsch deposit hosted in the Northern Calcareous Alps is a special case within this Group, hosting high amounts of Ag, but lower amounts in Mn, Ge, As and Tl compared to the other deposits of this type.
(2) In the Austroalpine nappe system, SEDEX-type deposits are known from the Graz Paleozoic and the Gurktal nappe. The Pb-Zn-Ba ores located in the Graz Paleozoic (Styria) formed in the Lower Devonian in a euxinic basin structure associated with submarine alkaline volcanism (Weber 1990). In a sphalerite concentrate from the deposit Arzberg-

Haufenreith, 10 µg/g Ge, 11 µg/g Ga, 1800 µg/g Cd, 29 µg/g In, and 5 µg/g Tl have been reported (Cerny and Schroll, 1995). In-situ LA-ICP-MS measurements of sphalerite grains collected from five ancient mining sites and one exploration adit reveal a large variation of trace element concentrations with median values of 4.7 wt% Fe, 1832 µg/g Cd, 138 µg/g Co, 18 µg/g Ag, 9 µg/g Ga, 0.36 µg/g Ge, 1 µg/g In, 1 µg/g Sn and 5 µg/g Sb. Maximum values reach 220 µg/g for Ge, 399 µg/g for Ag and 83 µg/g for In.

SEDEX deposits hosted in Palaeozoic units outside the Graz Palaeozoic like Meiselding (Gurktal nappe), sphalerite carries up to 1900 µg/g In, 250 µg/g Ge, 65 µg/g Ga, 282 µg/g Co and 2.9 wt% Cd. In the Walchen deposit located in Koralm-Wölz nappe system is characterised by high In values (98 µg/g) but low values in Co (55 µg/g), Ga (1.53 µg/g) and Ge (0.07 µg/g). Sphalerite from the Leogang deposit hosted by upper Silurian-Middle Devonian dolomite (Südfazies-Dolomit) at the border to the Ordovician Wildschönau Schiefer of the Graywacke Zone showed the most elevated In concentrations (Md= 247 µg/g), the measured values for Ga (1.05 µg/g), Ge (0.11 µg/g) and Co (128 µg/g) are in the range of the other investigated SEDEX deposits.

(3) Vein deposits of different genesis and age are widespread in the Eastern Alps. Pb-Zn-mineralization at Vellach-Metnitz in the Gurktal Nappe (Carintia) unit shows vein-like NW-SE trending structures (WEBER, 1997). Metnitz, sphalerite carries up to 65 µg/g In, 924 µg/g Ge, 381µg/g Ga, 679 µg/g Co and 4380 µg/g Cd. High indium concentrations have been previously reported for the Zn-Cu-Pb veins of Koprein (Palaeozoic of the Karawanken Range). Our LA-ICP-MS analyses of sphalerite show between 10 and 35 µg/g In (maximum 276 µg/g), Ge up to 2.2 µg/g, Ga 0,8- 9,8 µg/g, Co 217- 1221 µg/g, Cd 1121-3560 µg/g, and Fe 2.8 – 6.5 wt%. The Achselalm-Flecktrogalm deposit hosted in the Habach Group only contains slightly elevated Ga concentration (26 µg/g), In (1.5 µg/g) and Co 59 (µg/g) are low compared to the other vein-type deposits, Ge is below detection limit.

The sulfur isotopic composition shows no correlation between the trace element content and the $\delta^{34}S$ values. This leads to the conclusion that the origin of the sulfur or the process of sulfate reduction has no influence on the trace element mass fraction or variability.

Deposits with economic potential for Ge are mainly hosted in the Drau Range where Radnig shows the highest Ge values and Bleiberg the lowest .These lower Ge contend in sphalerite from Bleiberg can be compensated by the large size of this deposit. Cerny and Schroll (1995) estimated the remaining tonnage with 2 million tons of ore result in in 496 tons Ge metal. In values were evaluated in Leogang, due to the lack of reliable reserve data, no economic potential can be calculated. Sphalerite from Koprein holds the highest Co content of the investigated deposits. However due to the remote location and probably small size of these deposit, an economic production is very unlikely. Deposits from the Graz Paleozoic, the Achselalm- Flecktrogalm, Lafatsch, deposits of the Brenner Mesozoic, Drassnitz and Metnitz can be excluded as potential targets.

Zusammenfassung

Die “Ad-Hoc working group on defining critical raw materials” der Europäischen Union (EU) identifizierte im Jahr 2014 zwanzig Rohstoffe als kritisch. Einige dieser Rohstoffe werden in der Hochtechnologie Produkten und in „grüner“ Technologie eingesetzt (EU, 2014). Österreich ist bekannt für eine Vielzahl an Erzvorkommen mit signifikanten Potential dieser Rohstoffe wie Germanium, Gallium, Indium und Kobalt, welche durch Analysen an Erzkonzentraten bestätigt wurde. Anfang 1990 wurde die jahrhundertelange Tradition des Buntmetallerzbergbaues mit der Schließung des Bergbaues Bleiberg-Kreuth durch die Bleiberger Bergwerksunion eingestellt, und der Abbau von Zink, Kupfer, Blei und Silber fand ein Ende.

Erich Schroll war der erste, der Spurenelementanalyse an heimischen Erzen durchführte (Schroll, 1954; Cerny & Schroll, 1995). Sphalerit ist eines der Minerale, welches eine Vielzahl dieser Elemente wie z.B. Ga, Ge, In und Co in das Kristallgitter einbaut. In dieser Studie wurde eine Re-Evaluierung der Spurenelementverteilung in Sphalerit an drei Buntmetall Erztypen in den Ostalpen vorgenommen.

Für die Spurenelementanalyse an Sphalerit mittels LA-ICP-MS stehen keine homogenen Referenzmaterialien zur Verfügung. Bei dem LA-ICP-MS Messverfahren treten eine Vielzahl von polyatomaren Interferenzen (z.B. ArS^+ an allen Ge^+ Isotopen), und Fraktionierungseffekte (z.B. Schwefel) durch die Ablation bzw. die Ionisierung im Plasma auf. Um diese Einflüsse zu minimieren bzw. unterdrücken war die Entwicklung eines Referenzmaterials notwendig, welches der Sphalerit Matrix entspricht und dessen Spurenelementkonzentrationen in einem Bereich liegen, welcher der natürlicher Zinkblende entspricht. Im ersten Teil wird die Entwicklung dieses Referenzmaterials (MUL-ZnS-1) beschrieben, welches die Elemente V, Cr, Mn, Co, Ni, Cu, Ga, Ge, As, Se, Mo, Ag, Cd, In, Sn, Sb, Tl und Pb neben Zn, Fe und S (als Matrix) beinhaltet. Bei der Herstellung wurden im Handel erwerbliche Produkte wie ZnS, FeS und CdS, natürlich vorkommende Minerale sowie Einzelelement ICP-MS Standardlösungen herangezogen. Die Mixtur wurde gemahlen, mit den Standardlösungen in gewünschter Konzentration versetzt, getrocknet und zu Pulverpresslingen gepresst. Diese Pulverpresslinge unterliefen einem Sinterprozess bei 400 °C für 100 Stunden unter Argonatmosphäre. Die Konzentration wurde mittels Lösungsanalytik (ICP-OES, ICP-MS und AAS) bestimmt. Die Homogenität wurde mittels EPMA und LA-ICP-MS bestätigt, welche das MUL-ZnS-1 zu einem geeignetem Referenzmaterial für Sphalerit ausweist.

Zusätzlich zur in-situ Spurenelementanalytik war die Entwicklung einer Messmethode zur Bestimmung der Schwefelisotopenzusammensetzung mittels LA-QQQ-ICP-MS notwendig. Diese Methode wurde im Rahmen dieser Studie erstmals mittels Lachgas als Reaktionsgas durchgeführt und beschrieben. Um adäquate Ergebnisse zu liefern war es ebenfalls notwendig geeignete Referenzmaterialien herzustellen. Die Herstellung dieser Materialien folgte im weitesten der Sintermethode nach Onuk et al. (2017).

Bei den drei untersuchten Vererzungstypen handelt es sich um:

(1) Karbonatgebundene „Alpine-Type“ oder „Typ Bleiberg“ Blei-Zinklagerstätten der triassischen Karbonate im Drauzug und den nördlichen Kalkalpen, welche sich durch niedrige Fe, hohe Cd (~2000 µg/g), Ge (200- 400 µg/g) und Tl Konzentrationen um die 100 µg/g im Sphalerit hervorheben. Weiters ist Sphalerit aus diesem Typ nahezu frei von Co, Cu und Ni. Das Vorkommen Lafatsch scheint eine Ausnahme zu sein, da dort im

Gegensatz zu Sphalerit aus dem Drauzug (nahezu Ag frei) erhöhte Ag Konzentrationen (Md= 43 µg/g), aber erniedrigte Mn, Ge, As und Tl Werte nachgewiesen wurden.

(2) In den Ostalpen sind SEDEX- Vorkommen im Grazer Paläozoikum (Steiermark) und in der Gurktaler Decke (Kärnten) und aus dem Koralm-Wölz Deckensystem bekannt, welche bereits im Mittalter auf Blei abgebaut wurden. Die Pb-Zn-Ba Vorkommen wurden im Unter Devon in euxinischen Becken gebildet, welche mit submarinen alkalischen Vulkanismus in Zusammenhang gebracht werden (Weber 1990). Frühere Analysen an Sphaleritkonzentraten von Cerny und Schroll (1995) ergaben Werte für Ge = 10 µg/g, Ga = 11 µg/g, Cd = 1800 µg/g, In 29 µg/g und Tl 5 µg/g. In-situ LA-ICP-MS Analysen an Sphalerit von 20 unterschiedlichen Lokalitäten zeigten eine große Variation innerhalb des Erzbezirkes, Lokalität bis hin zum Maßstab einer Probe. Medianwerte von 4.7 wt% Fe, 1832 µg/g Cd, 138 µg/g Co, 18 µg/g Ag, 9 µg/g Ga, 0.4 µg/g Ge, 1 µg/g In, und 5 µg/g Sb wurden errechnet. Im Vorkommen Haufenreith konnten maximal Gehalte für In von 82 µg/g, die höchsten Ag Werte in Sphalerit von Arzberg (3556 µg/g), das maximale Ge mit 209 µg/g in Guggenbach nachgewiesen werden.
Sphalerit aus dem SEDEX Vorkommen Meiselding in der Gurktaler Decke inkorporierte bis zu 1900 µg/g In, 250 µg/g Ge, 65 µg/g Ga, 282 µg/g Co und 2.9 wt% Cd. Das Vorkommen Walchen (Koralm-Wölz Deckensystem) ist gekennzeichnet durch hohe In (98 µg/g) aber geringe Co (55 µg/g), Ga (1.5 µg/g und Ge (0.1 µg/g) Gehalte. Eine Sonderstellung bei diesem Lagerstättentypus nimmt das Vorkommen Leogang (Salzburg), welches in Ober Silurischen bis Mittel Devonischen Dolomiten an der Grenze zu ordovizischem Wildschönau Schiefer der Grauwackenzone eingebettet ist. Hier wurden die höchsten In Werte gemessen, welche einen Median von 247 µg/g ergaben, wobei aber Ga (1 µg/g), Ge (0.1 µg/g) und Co (59 µg/g) im Durchschnitt der SEDEX Vorkommen liegen.

(3) Ganglagerstätten unterschiedlicher Genese und Alter sind ein weitverbreiteter Vererzungstyp der Ostalpen. Sphalerit aus der Pb-Zn Mineralisation Vellach-Metnitz in der Gurktaler Decke (Kärnten) weist maximal Konzentrationen an In 65 µg/g, Ge 924 µg/g, Ga 381 µg/g Co 679 µg/ und 4380 µg/g Cd auf. Hohe In Werte im Vorkommen Koprein (Paläozoikum der Karawanken) wurden bereits von Cerny (1982) postuliert, neue Analysen zeigen In Werte zwischen 10 und maximal 276 µg/g. Koprein zeichnet sich auch durch seine hohen Co Gehalte (217- 1221 µg/g) aus. Die Ganglagerstätte Achselalm-Flecktrogalm ist nur durch leicht erhöhte Ga (26 µg/g) gekennzeichnet.

Eine Korrelation zwischen der Schwefelisotopen Zusammensetzung und den Spurenelementgehalten der einzelnen Sphalerite konnte nicht gefunden werden. Dies lässt darauf schließen, dass die unterschiedlichen Prozesse der Sulfat Reduktion keinen Einfluss auf den Spurenelementgehalt haben und von der Herkunft der Fluide abhängen.

Das höchste wirtschaftliche Potential für Ge konnte aufgrund der Größe des Vorkommens in Bleiberg gefunden werden (laut Cerny und Schroll (1995) 2 Millionen Tonnen Erz), welches eine Ge Tonnage von etwa 496 t entspricht. Für In konnte Leogang als Explorationsziel ausgemacht werden, da aber für dieses Vorkommen keine verlässlichen Zahlen zu den Reserven existieren, kann keine Tonnage errechnet werden. Für Co könnte Koprein interessant sein, aber aus wirtschaftlicher Sicht durch seine Abgeschiedenheit und kleinen Größe eher ausgeschlossen werden. Die Vorkommen im Grazer Paläozoikum, Achselalm-Flecktrogalm, Lafatsch, Vorkommen im Brenner Mesozoikum, Drassnitz und Metnitz kommen aufgrund ihrer geringen Spurenelementgehalte für eine wirtschaftliche Nutzung nicht in Frage.

Part 1

Development of a matrix-matched sphalerite (ZnS) calibration material (MUL-ZnS-1) for calibration of in situ trace element measurements by laser ablation inductively coupled plasma mass spectrometry (LA-ICP-MS)

Peter Onuk (1), Frank Melcher (1), Regina Mertz-Kraus (2), Hans-Eike Gäbler (3), Simon Goldmann (3

(1) Department of Applied Geological Sciences and Geophysics, Chair of Geology and Economic Geology, Montanuniversität, A-8700 Leoben, Austria

(2) Institute for Geosciences, Johannes Gutenberg University, 55099 Mainz, Germany

(3) Federal Institute for Geosciences and Natural Resources (BGR), 30655 Hanover, Germany

Abstract

Sphalerite (ZnS) is an abundant ore mineral and an important carrier of elements such as Ge, Ga and In used in high technology applications. In situ measurements of trace elements in natural sphalerite samples using LA-ICP-MS are hampered by a lack of homogenous matrix-matched sulphide reference materials available for calibration. The preparation of the MUL-ZnS1 calibration material containing the trace elements V, Cr, Mn, Co, Ni, Cu, Ga, Ge, As, Se, Mo, Ag, Cd, In, Sn, Sb, Tl, and Pb besides Zn, Fe and S is reported. Commercially available ZnS, FeS, CdS products were used as the major components, whereas the trace elements were added by doping with single element ICP-MS standard solutions and natural mineral powders. The resulting powder mixture was pressed to pellets and sintered at 400 °C for 100 hours using argon as inert gas. To confirm the homogeneity of major and trace element distributions within the MUL-ZnS1 calibration material, measurements were performed using EPMA, solution ICP-MS, ICP-OES and LA-ICP-MS. The results show that MUL-ZnS-1 is an appropriate material for calibrating trace element determination in sphalerite using LA-ICP-MS.

Contents

List of Figures

List of Tables

1. Introduction

Sphalerite (ZnS) is an abundant ore mineral in base metal deposits (e.g. volcanogenic massive sulphides (VMS), sediment-hosted massive sulphides (SEDEX), carbonate-hosted Pb-Zn (e.g. Mississippi Valley-type, MVT), stratiform copper, vein type as well as skarn deposits). It is a major carrier of Ge and other critical high-technology elements such as Ga and In (Melcher and Buchholz, 2014). Considerable abundances of trace elements such as V, Cr, Mn, Ni, Cu, As, Se, Mo, Ag, Cd, Sb, Tl, Pb, and Hg have been reported in sphalerite (e.g. Fleischer 1955; Hall & Heyl 1968; Sangster & Liberty 1971, Hall & Czamanske 1972).

LA-ICP-MS has become a well-established in situ technique for sulphide mineral analysis, but the accuracy of the results may be limited with respect to sphalerite since suitable homogenous matrix-matched ZnS reference materials for calibration are not available. Several authors have previously discussed two main reasons why application of matrix-matched reference materials is crucial:

1) nonstoichiometric sampling and aerosol transport as well as matrix-dependent ablation behaviour (Longerich et al.1996 A, Günther et al.1999, Durrant 1999, Guillong and Günther 2002) and 2) difficulties quantification LA-ICP-MS measurements on sulphides due to the large number of polyatomic interferences (e.g. $^{38}Ar^{36}S$ on ^{74}Ge, $^{38}Ar^{33}S$ on ^{72}Ga, $^{50}Cr^{16}O$ on ^{66}Zn, $^{52}Cr^{16}O$ on ^{68}Zn, $^{95}Mo^{16}O^{+}$ on ^{111}Cd). Kuhn and Günther (2005) reported significant elemental fractionation for zinc during the ablation process. Therefore, well-characterized reference materials that match the sample matrix are essential. Reference materials such as the NIST SRM 61X glasses in combination with Fe used as the internal standard are less suitable (Danyushevsky et al. 2011). Natural sphalerite samples as reference materials would be the ideal case, but homogenous natural sphalerite with a wide range of trace elements is extremely rare (Cook et al. 2009, Cerny 1989). The only commercially available sulphide reference material is MASS-1 (Wilson et al. 2002), a synthetic pressed powder pellet distributed by the USGS. It is based on a $(Fe,Cu,Zn)_{1-x}S$ matrix. The major element composition of MASS-1 (S 27.6 %m/m, Cu 13.4 %m/m, Fe 15.6 %m/m and Zn 21.0 %m/m) is far from the chemical composition of sphalerite. Additionally fractionation effects have been observed during ablation due to melt formation, while sphalerite in contrast shows minor to no fractionation during ablation (Wohlgemuth-Ueberwasser and Jochum 2015).

The issues outlined above demonstrate the need for the development of a matrix-matched sphalerite calibration material. Various authors described different techniques to develop sulphide reference materials (e.g. Ballhaus & Silvester 2000). Wohlgemuth-Ueberwasser et al. (2007) synthesized pyrrhotite under high pressure and temperature. Danyushevsky et al. (2011) described the synthesis of a sulphide reference material fused to a lithium borate containing glass. The MASS-1 sulphide reference material developed by Wilson et al. (2002) is precipitated from a solution. Dewaele et al. (2007) used a modified welding technique after Ødegard (1999) to produce a matrix-matched pyrite reference material. None of these reference materials represent a true matrix match for sphalerite, nor are they characterised well enough for the large number of trace elements desired for comprehensive in situ analysis of sphalerite.

In nature, zinc sulphides occur as hexagonal α-ZnS wurtzite, cubic β-ZnS sphalerite, and trigonal γ-ZnS matraite (Deer et al. 2011). All ZnS polymorphs show different chemical and physical properties at different temperatures and pressures. Sphalerite and wurtzite are the most common ZnS

polymorphs. The inversion temperature from sphalerite to wurtzite occurs at 1020 °C (Scott and Barnes 1967). Pure ZnS transforms into ZnO_2 and SO_2 in the presence of O_2 at temperatures of about at 850 °C. It sublimes at 1185 °C (Scott and Barnes 1972) and melts congruently at 1830 °C and 3.7 bar (Fleet 2006). This physical behaviour and the low melting point of some spiked trace elements (e.g. Se, Pb, As, Hg) were regarded as challenging factors for the production of a ZnS matrix-matched calibration material in the past.

In this study, we describe the preparation procedure of a suitable ZnS calibration material (MUL-ZnS-1) using commercially available basic starting material, natural minerals and single element ICP-MS standard solutions. The sintering of the pressed powder pellet under argon atmosphere increases the stability and allows easy refurbishment of the calibration material MUL-ZnS-1; that is, a new flat surface can be obtained by grinding and polishing. Different analytical techniques were applied in this study for the quantification of element massfraction (ICP-MS, ICP-OES, EPMA, AAS) and the assessment of small-scale homogeneity (EMPA, LA-ICP-MS) of MUL-ZnS-1. MUL-ZnS-1 contains Zn, Fe and S as major elements and V, Cr, Mn, Co, Ni, Cu, Ga, Ge, As, Se, Mo, Ag, Cd, In, Sn, Sb, Tl and Pb as trace elements. All these elements are typically present in natural sphalerite at variable mass fraction.

Wohlgemuth-Ueberwasser et al. (2007) produced a sulphide calibration material by melting $(Fe,Ni,Cu)_{1-x}S$ doped with trace elements in a SiO_2– Pyrex glass pipe. The cooled melt was finely ground, enclosed in SiO_2- Pyrex glass and hot pressed using a piston cylinder. The method described by Wilson et al. (2002) - doping powdered material which was precipitated from solutions and pressed into pellets - was not applied because we aimed for a more robust reference material that could easily be polished to expose a fresh surface. The welding technique described by Dewaele et al. (2007) and Ødergard (1999) was not suitable either, because sphalerite sublimes at 1185 °C and the temperature during the welding process is higher (1400 °C; Scott and Barnes 1972, Dewaele et al 2007). Ballhaus & Silvester (2000) synthetized a Fe-S mixture in a piston cylinder using 950°C and a pressure of 1GPa over a period of 2 days. Even if the synthesis was successful, the approach has some drawbacks. Firstly, only a small amount of sample is treated yielding ~ 100 mg of final material; secondly, only tiny (100 µm) spheres were produced; and thirdly, the process is quite cost intensive with the respect to the material used. The method described by Danyushevsky et al. (2011) producing a lithium borate glass was not applied because the resulting material is not matrix-matched to natural sphalerite.

In the beginning, we followed the sample preparation procedure of Wohlgemuth-Ueberwasser et al. (2007). However, the result was not satisfying due to the high exothermic reaction of ZnS (ΔH_R = -206 kJ/mol), which induced an explosion in the muffle furnace. The effect of this reaction could be reduced by using small amounts of material (<5 g); however, this would also reduce the intended efficiency of the production process.

This study presents an alternative method to produce a ZnS calibration material, examines the obtained homogeneity of the product (MUL-ZnS-1) and presents analytical data obtained from different methods to characterise MUL-ZnS-1.

2. Experimental procedure

2.1. Preparation of MUL-ZnS-1

The starting materials for the (Zn,Fe)S matrix were 87 g of zinc sulphide (reagent grade ≥97.0 % nanocrystal powder Sigma Aldrich, with D_{50} <0.5 µm), 8.6 g of iron(II) sulphide (technical grade Alfa Aesar), 1.5 g of cadmium sulphide (reagent grade 98% Alfa Aesar) and 0.15 g of silver(I) selenide (Johnson Matthey Ltd). For addition of Pb and Sb, 1.3 g of natural galena and 1.4 g of natural stibnite were ground in a Retsch PM100® planetary ball mill to homogenize both components. From this mixture, 0.3 g was added to the starting material. The powder mixture was subsequently transferred into a PTFE beaker, and the trace elements V, Cr, Mn, Ni, Cu, Ga, Ge, As, Se, Mo, In, Tl, and Bi were added as single element ICP-MS standard solutions to reach the target concentrations given in Table 1.

Table 1: Expected trace element concentration in the final calibration material MUL-ZnS-1

Element	Concentration [µg/g^{-1}]
V, Mo, Ni, Tl, As	50
Cr	100
Co	300
Ge, In	500
Ga, Mn	600
Sn, Cu	1000

Althought natural sphalerite may contain notenotable amounts of Hg, this element was not added to the mixture because Hg has a boiling temperature of 356 °C and degases during the sintering process. The resulting mixture was dried for 20 h on a hot plate at a temperature of 120°C under constant stirring using an overhead stirring machine. Subsequently the material was ground again using the planetary ball mill. To prevent the material from sticking to the wall of the tungsten carbide (WC) grinding beaker, ultrapure water (ELGA >18.5 MΩ cm^{-1}) was added to the powder until a "motor oil" like slurry was obtained. Grinding was performed operated the planetary ball mill with ~ 1 kg of 1 mm WC milling balls (diameter 1mm) and about 100 g of the above mentioned slurry at 550 rpm for 20 minutes. The grain size distribution (Fig. 1) was determined using a Horiba laser scattering particle size distribution analyser (Partica LA-960®) at Retsch, Austria.

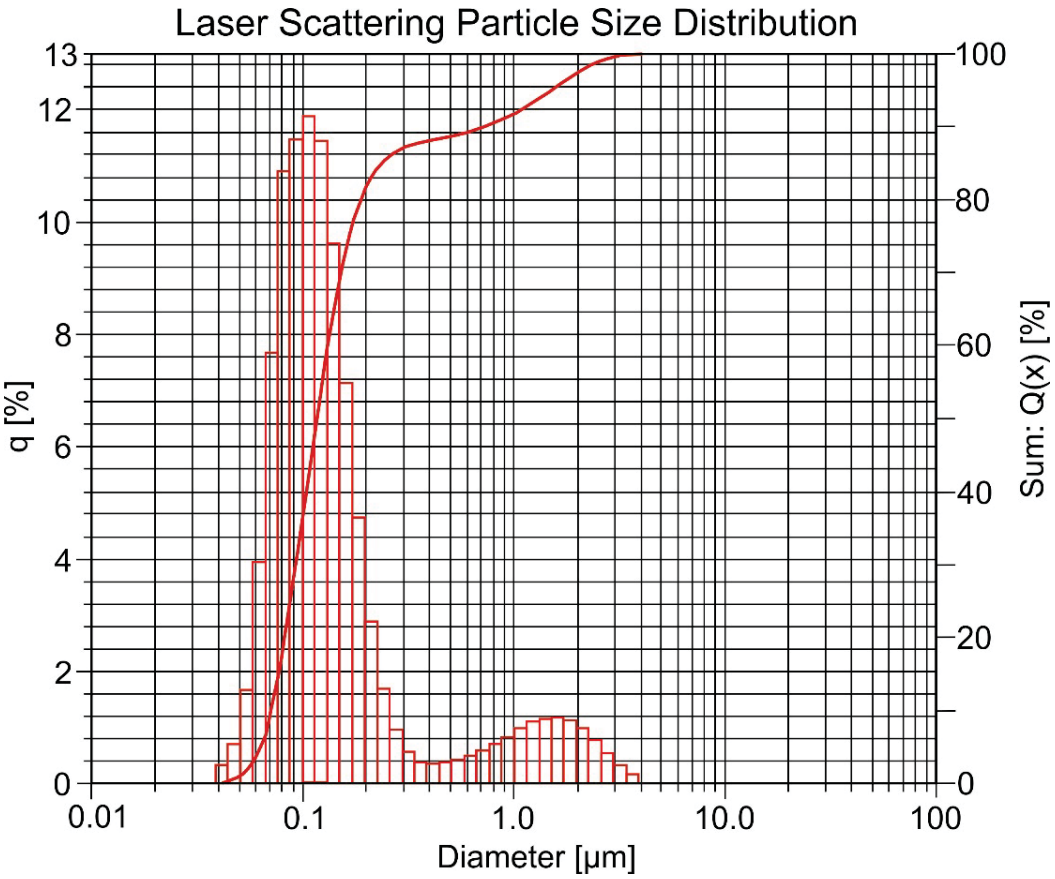

Fig. 1: Distribution of the single particle fraction q[%] of MUL-ZnS-1. Red sum curve demonstrates a D90 at 0.7 µm. The laser particle size distribution analysis shows two peaks: the peak at 0.1 µm represents the ZnS nanopowder, the peak at 1.5 µm represents FeS and the added natural minerals.

In order to prevent the suspension from agglomeration during drying, the material was freeze-dried with a Christ Alpha 2-4® at 0.22 mbar and a temperature of -85°C. The dry powder mixture was pressed into 32 mm pellets, each weighting 30 g, at a pressure of 0.17 x 10^6 kPa (10 tons) for 2 minutes. The three pressed pellets were bedded on refractory material in a self-made autoclave placed in a tube furnace (Fig. 2). Argon was used as inert gas to prevent the material from oxidizing.

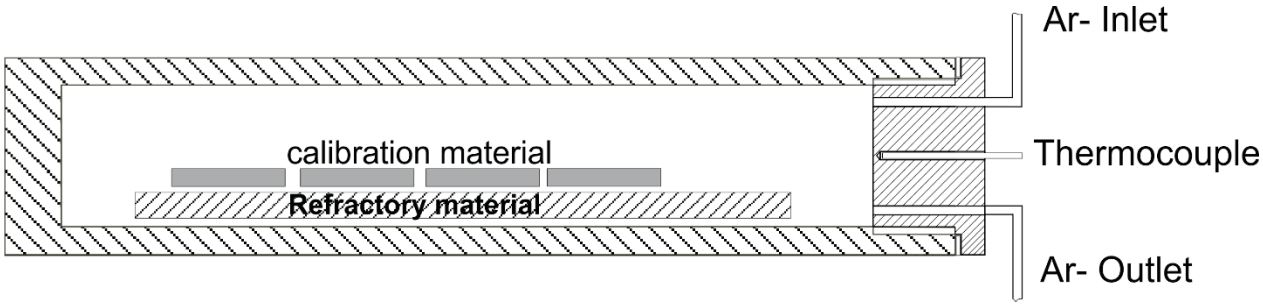

Fig. 2: Design drawing of the self-made stainless steel autoclave showing the sintering setup.

The samples were sintered at a temperature of 400°C ± 5°C over a period of 100 h. For temperature control, a Eurotherm 7100L® solid state single-phase contactor combined with an Eurotherm 3216® PID temperature control unit was used. The sintered pellets of MUL-ZnS-1 were cut into forty cubes with an edge length of 4 mm. Single pieces of the sliced material of MUL-ZnS-1 were mounted in epoxy resin resulting in round 1 inch sections for in situ analysis. The sections were polished with 3000 grit, 5000 grit and 12000 grit abrasive papers, successively.

2.2. Analytical methods

The mass fraction of MUL-ZnS-1 were determined by solution inductively coupled plasma-mass spectrometry (ICP-MS), atomic absorption spectrometry (AAS) and inductively coupled plasma-optical emission spectrometry (ICP-OES) after digestion. Two subsamples per sintered MUL-ZnS-1 pellet were digested using an high pressure asher (HPA-S, Anton Paar, Graz). For that purpose, 0.1 g of the fine ground sample was weighed in a 50 ml quartz vessel and 2 ml HCl (12 mol l^{-1}), 5 ml HNO_3 (14.5 mol l^{-1}) and 1 ml H_2O_2 (30 % m/m) were added. The HPA was set to run the digestion process at 250°C at a pressure of 100 bar in N_2 atmosphere over a period of 2 hours. After cooling the solution was diluted up to 50 ml with HNO_3 (0.1 mol l^{-1}). This solution was used for trace and main element determination by AAS, ICP-OES, and ICP-MS after dilution appropriate for each instrument.

Solution ICP-MS analyses were performed using an Agilent 8800® (QQQ)-ICP-MS at the Chair of Geology and Economic Geology, Montanuniversität, Leoben. The instrument was operated in no gas mode for some elements and for other elements to reduce isobaric interference in MS/MS mass shift mode (in reaction gas mode) using O_2 and NH_3 as reaction gases in brackets (Table 2). For external calibration of most trace elements, the Merck IV® multi-element ICP-MS standard solution, and for S, Zn and Sn single-element ICP-MS standard solutions were used in different concentrations. The instrument was tuned for low oxide formation rates (UO^+/U^+ <0.3 %) and to a minimum formation level of double charged ions (La^{2+}/La^+ < 0.9 %). AAS (Perkin Elmer 3030 flame AAS) at the Chair of Geology and Economic Geology, Montanuniversität, Leoben was used for the determination of Zn, Fe, Mn, and Cd mass fraction. ICP-OES (Perkin Elmer 8300 DV) at the Institute of Applied Geoscience, Graz University of Technology was applied to determine the mass fractions of S, Zn, Fe, Cd, Pb, Mn, Co, Cr, Ni, Cu, Ga, Ag, In, and Tl using the calibration standards Merck 21 and Fluka 3 for external calibration and NIST SRM 1640a and SW2 for quality control.

Table 2: Collision/reaction gases used for solution ICP-MS analysis on the Agilent 8800 ICP-MS

Collision/Reaction gas	no gas	O_2	10% NH_3 in He
Element	S, As, Se	V, Mn, Co, Ni, Cu, Ga, Ge, Mo, Ag, Cd, In, Sb, Sn, Tl, Pb, Bi	Fe, Zn, Cr

For small-scale in situ homogeneity tests within a polished section of MUL-ZnS-1, EPMA and LA-ICP-MS analyses were performed, as described below.

EPMA was carried out at the Federal Institute for Geosciences and Natural Resources, Hanover using a Cameca SX100 equipped with five wavelength-dispersive spectrometers. The acceleration voltage was set to 25 kV and the beam current to 150 nA for determination of the trace elements. The electron beam was defocused to a size of 10 µm. For each element the respective X-ray line, measuring time in seconds, spectrometer crystal, and reference material were as follows: MgKα, 100 s, TAP, metal; VKα, 660 s, LLIF, metal; CrKα, 480 s, LLIF, metal; MnKα, 60 s, LLIF, Mn-rich sphalerite; CoKα, 240 s, LLIF, metal; CuKα, 30 s, LLIF, metal; GaKα, 80 s, LLIF, synthetic gallium arsenide; GeKα, 120 s, LLIF, metal; AsLα, 600 s, TAP, synthetic gallium arsenide; SeLα, 200 s, TAP, metal; AgLα, 300 s, PET, metal; CdLβ, 30 s, LPET, metal; InLα, 60 s, LPET, metal; SnLα, 60 s, PET, metal; SbLα, 60 s, LPET, metal; BaLα, 240 s, PET, barite; PbMα, 300 s, PET, galena; BiMα, 900 s, LPET, metal. For determination of the major elements, the beam current was reduced to 20 nA and the respective X-ray line, measuring time in seconds, spectrometer crystal, and reference materials were as follows: SKα, 10 s, PET, Fe-rich sphalerite; FeKα, 10 s, LLIF, Fe-rich sphalerite; ZnKα, 10 s, LLIF, sphalerite.

line scan measurements over a length of 10 mm were performed on one slice of the sintered MUL-ZnS-1, using an ESI NWR213 laser ablation system (spot size 80 µm, fluence 2 J/cm^2, 10 Hz) coupled to an Agilent 8800 (QQQ)-ICP-MS in no-gas mode at the Chair of Geology and Economic Geology, Montanuniversität, Leoben. Additionally, spot measurements were performed by LA-ICP-MS on different polished pieces of MUL-ZnS-1 at three different laboratories: (1) three polished sections of MUL-ZnS-1 were analysed at the Montanuniversität Leoben, Chair of Geology and Economic Geology; (2) one polished section at the Federal Institute for Geosciences and Natural Resources in Hannover and (3) one polished section at the Johannes Gutenberg University Mainz, Institute for Geosciences. At each laboratory, three different spot sizes were applied (thirty spots of each spot size; see Table 3 for details of the key instrumental parameters): The following isotopes were monitored: ^{34}S, ^{66}Zn, ^{57}Fe, ^{111}Cd, ^{208}Pb, ^{51}V, ^{52}Cr, ^{55}Mn, ^{59}Co, ^{60}Ni, ^{63}Cu, ^{71}Ga, ^{74}Ge, ^{75}As, ^{82}Se, ^{95}Mo, ^{107}Ag, ^{115}In, ^{118}Sn, ^{121}Sb, ^{205}Tl, and ^{209}Bi.

The polymetallic sulphide pressed powder pellet MASS-1 from USGS and the glass NIST SRM 610 were used as calibration materials applying the preferred values reported in the GeoReM database (http://georem.mpch-mainz.gwdg.de/, Application Version 18) (Jochum et al., 2005, 2011).

Table 3: Instrumental parameters of the LA-ICP-MS measurements for the homogeneity test.

	Leoben	Mainz	Hanover
ICP-MS	Agilent 8800 (QQQ)-ICP-MS	Agilent 7500ce	Thermo Scientific Element XR, medium resolution mode
RF power	1280 W	1200 W	1200 W
Carrier gas flow rate (Ar)	0.85 l/min	0.85 l/min	1.1 l/min
Sampling depth	3.7 mm	6 mm	5.4 mm
Dwell time per mass	20 ms	10 ms	10 ms
Laser System	ESI NWR213 Nd:YAG laser	ESI NWR 193 ArF excimer	ESI NWR193 ArF excimer
Ablation cell	TwoVol[1] ablation cell	TwoVol[2] ablation cell	TwoVol[1] ablation cell
Wave length	213 nm	193 nm	193 nm
Pulse repetition rate	10 Hz	10 Hz	10 Hz
Fluence	2.2 J/cm^2	2.2 J/cm^2	3.2 J/cm^2
Spot size	30, 60, 90 µm	35, 50, 100 µm	35, 50, 100 µm

At Leoben, data reduction was performed using Iolite V3.2 software (Paton et al. 2011) and a Microsoft Excel® spreadsheet, subsequently. The element mass fractions of MUL-ZnS-1 were calculated and normalized to internal standardization using Zn, Fe and S as internal standard element for MASS-1, and Zn and Fe for Nist SRM 610.

At Hanover, a data-handling software tool written in Java processed the raw data (Gäbler et al., 2011). Quantitative analysis was obtained by normalization of the sum of all analysed metals to 67.1 % m/m.

At Mainz, data reduction was performed by calculating the blank-corrected count rates of the measured isotopes relative to the internal standard Zn (measured as ^{66}Zn) using an in-house Excel spreadsheet according to the calculations given in Jochum et al (2007).

To distinguish the ablation behaviour between MUL-ZnS-1 and natural sphalerite, laser ablation pits ablated using an ESI NWR 213 (Leoben) and an NWR193 ArF excimer (Mainz) laser system set to 2 J/cm^2 and a frequency of 10 Hz were investigated on MUL-ZnS-1 and natural sphalerite using an Alicona infinite focus microscope.

A Zeiss Gemini focused ion beam-scanning electron microscope (FIB-SEM) was used to observe the grain size distribution, porosity and sinter neck development of the sintered MUL-ZnS-1 (Fig. 3 and Fig. 4).

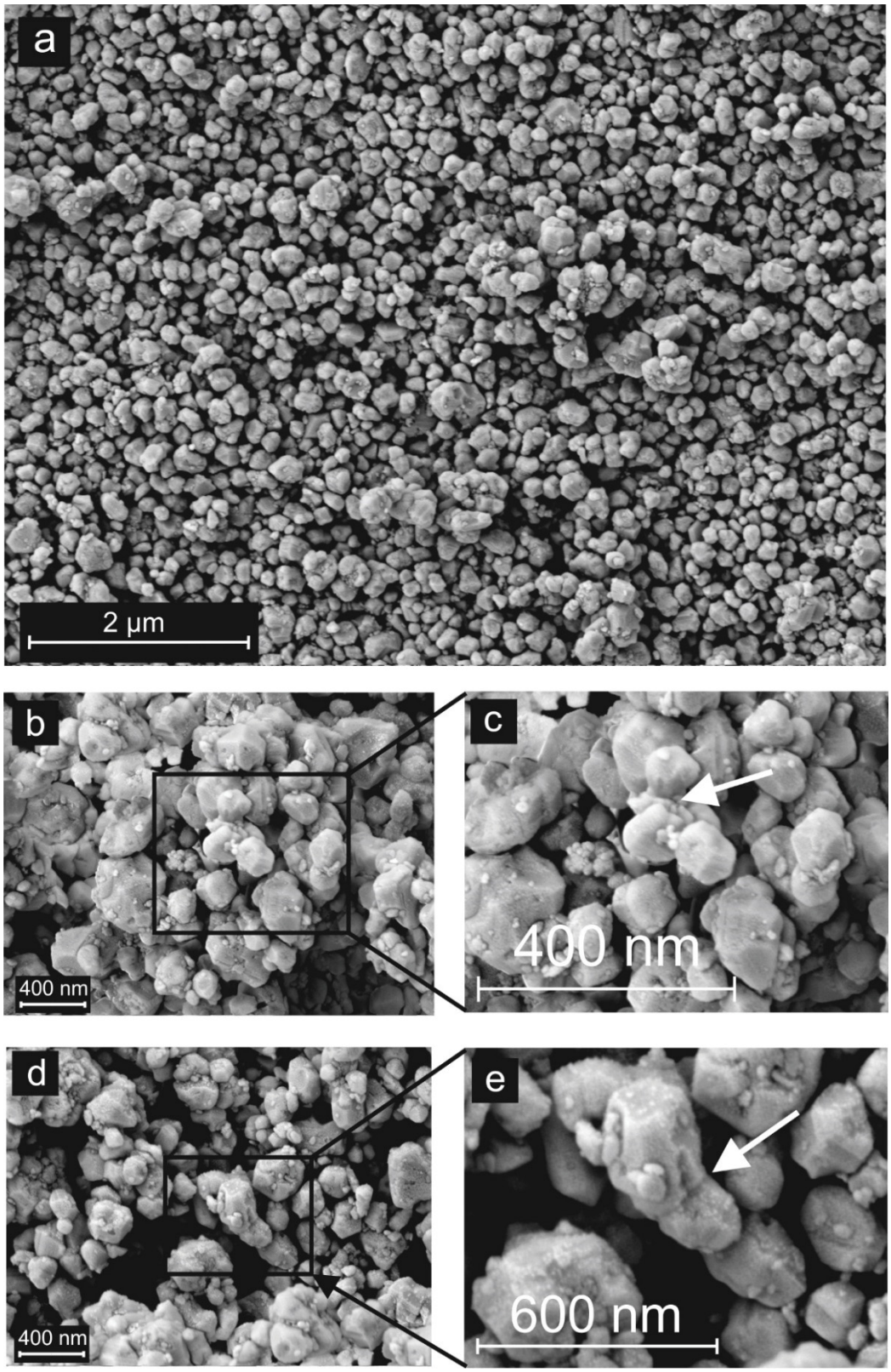

Fig. 3: Field emission scanning electron microscope images (Zeiss Gemini) of MUL-ZnS1 sintered at 400°C. (a) showing the homogenous grain size; (b, d) cluster of sintered material; (c, e) close-up of the insets of (c) and €. White arrows point to sinter necks.

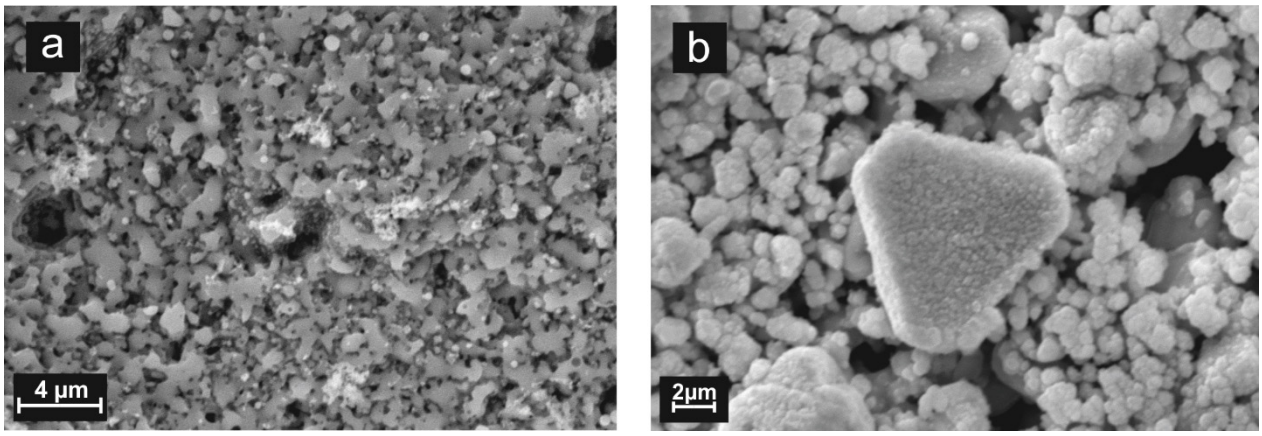

Fig. 4: Scanning electron microscope (Zeiss EVO MA 10) images of material sintered at 800°C. (a) improved sinter neck formation; (b) partial recrystallization of sphalerite.

3. Results and Discussion

3.1. Preparation of MUL-Zn-S1

Synthesis of a trace element reference material with a (Zn,Fe)S matrix for laser ablation ICP-MS analysis is possible if the material behavior of (Zn,Fe)S has to be considered thoroughly. To ensure homogeneity, small grain sizes and careful mechanical homogenization are essential (Fig 3a). Pressure higher than 10 tons (i.e., 0.17 x 10^6 kPa) during the production of the pellets leads to delamination. However, pressure less than 6 tons (i.e., 0.12 x 10^6 kPa) led to no or little mechanical robustness and a higher porosity. Sintering temperature had the greatest effect on the trace element content, due to degassing of the trace elements. The best balance between avoiding degassing and the formation of sinter necks for bonding was achieved at a sintering temperature of 400 °C (Fig. 3b-e). Higher temperature (> 450 °C) leads to better sinter neck formation but also to a higher degassing rate of the volatile elements and partial recrystallization of sphalerite (Fig. 4**Fehler! Verweisquelle konnte nicht gefunden werden.**). Low temperature (< 350 °C) results in insufficient sintering effects and thus in lower stability which would make it difficult to refurbish the material by, for example polishing.

3.2. Electron probe microanalysis

The sum of all element mass fractions analyzed by EPMA did not yield 100 %m/m. From fifty-three spot measurements, a quite constant mean for the sum of 81.6 %m/m was obtained (1σ= 0.2 %m/m). The constant deviation of the sum from 100 %m/m is attributed to the remaining porosity of the sintered material because a defined volume is stimulated by the electron beam instead of a defined sample mass. This porosity is visible from the SEM images (Fig. 3 and 4). As matrix-matched reference materials have been applied for the main elements Zn, Fe, and S, a matrix effect affecting the calibration for these elements can be ruled out. Porosity-corrected EPMA data have been calculated by dividing each element mass fraction by the sum of the mass fractions of all elements. Additional EPMA measurements were performed to quantify the O content of MUL-ZnS-1. The determined O mass fraction was between 4 and 6 %m/m. Stoichiometric calculations using these data (Table 4) indicate that the material is sphalerite since the ratio of S vs. Fe+Zn is approximately 1:1. Therefore, the presence of oxygen is not due to the formation of oxide or sulfate but probably

due to (1) the porosity of the material and (2) the presence of crystallisation water in the ZnS (because ZnS has been precipitated from a solution).

Table 4. EPMA measurements to quantify the O content of MUL-ZnS-1

at. % (normalized to 100 %)

S	Fe	Zn	O	Sum
41.35	4.33	37.84	16.48	100
41.13	4.34	38.01	16.53	100
41.27	4.22	38.43	16.08	100
41.13	4.34	38.01	16.53	100

3.3. Mass fractions and homogeneity test of MUL-ZnS-1

The mass fractions of the elements V, Cr, Mn, Ni, Cu, Ga, Ge, As, Se, Mo, Ag, Cd, In, Sb, Tl, Pb, Bi, Zn, Fe, and S obtained from six HPA digestions of MUL-ZnS-1 and analysed by ICP-MS, ICP-OES, EPMA and AAS are given in Table 5. The ICP-MS and ICP-OES results are given in Table 6.

*Table 5: ICP-MS, ICP-OES and AAS median values of six digestions and EPMA of the reference material MUL-ZnS-1. Elements marked with * in g/100g, other elements in µg/g (n.m. = not measured und bdl = below detection limit).*

Element	ICP-MS	RSD	ICP-OES	RSD	EPMA	RSD	AAS	RSD
S*	29.30	2.91 %	29.31	0.42 %	32.09	2 %	n.m.	
Zn*	58.24	2.49 %	58.85	0.27 %	59.12	2 %	58	7 %
Fe*	5.56	2.36 %	5.59	0.69 %	5.52	12 %	5.4	12 %
Cd*	1.16	1.79 %	1.11	3.88 %	1.56	4 %	1.14	8 %
Pb	1124	0.49 %	1173	3.21 %	1248	11 %	n.m.	
V	52	6.45 %	n.m.		bdl		n.m.	
Cr	124	2.75 %	130	7.56 %	106	17 %	n.m.	
Mn	616	3.25 %	604	1.32 %	623	11 %	660	10 %
Co	309	2.49 %	306	2.02 %	279	8 %	n.m.	
Ni	46	5.01 %	48	2.83 %	n.m.		n.m.	
Cu	925	2.58 %	1063	3.78 %	1036	7 %	n.m.	
Ga	599	2.33 %	603	1.51 %	339	16 %	n.m.	
Ge	505	6.43 %	n.m.		374	19 %	n.m.	
As	59	9.03 %	n.m.		bdl		n.m.	
Se	216	0.49 %	n.m.		295	10 %	n.m.	
Mo	59	8.93 %	n.m.		n.m.		n.m.	
Ag	610	3.18 %	603	1.58 %	764	6 %	620	8 %
In	531	2.71 %	498	1.76 %	583	11 %	n.m.	
Sn	1048	8.09 %	n.m.		1117	11 %	n.m.	
Sb	819	1.25 %	n.m.		952	13 %	n.m.	
Tl	11	51.26 %	10	48.07 %	n.m.		n.m.	

Table 6 shows the combined results of the ICP-MS and ICP-OES results.

Table 6: Calculated values for the reference material MUL-ZnS-1. Values are equally weighted means of the results from ICP-MS and ICP-OES data listed in Table 4. EPMA measurements to quantify the O content of MUL-ZnS-1

Element	g/100 g	± [g/100 g]
S	29.31	0.85
Zn	58.55	1.6
Fe	5.58	0.14
Cd	1.14	0.02

Element	µg/g	± [µg/g]
Pb	1149	5.7
V	52	3.1
Cr	127	3.8
Mn	610	42.7
Co	308	7.7
Ni	47	2
Cu	994	25.9
Ga	602	13.8
Ge	505	32.3
As	66	3.3
Se	200	2
Mo	60	5.4
Ag	607	18.2
In	515	13.9
Sn	1048	83.9
Sb	819	10.7
Tl	11	0.4

To confirm the large-scale homogeneity between the three sintered pellets of MUL-ZnS-1, the mass fractions of the different elements were plotted against the relative standard deviation (RSD) of the elements obtained from the 6 HPA digestions (Fig. 5). The results demonstrate that the homogeneity decreases with decreasing mass fractionation. With de exception of Mo (12.1 % RSD) and Tl (51.8 % RSD), the mass fractions of all elements had a RSD values of < 10 %.

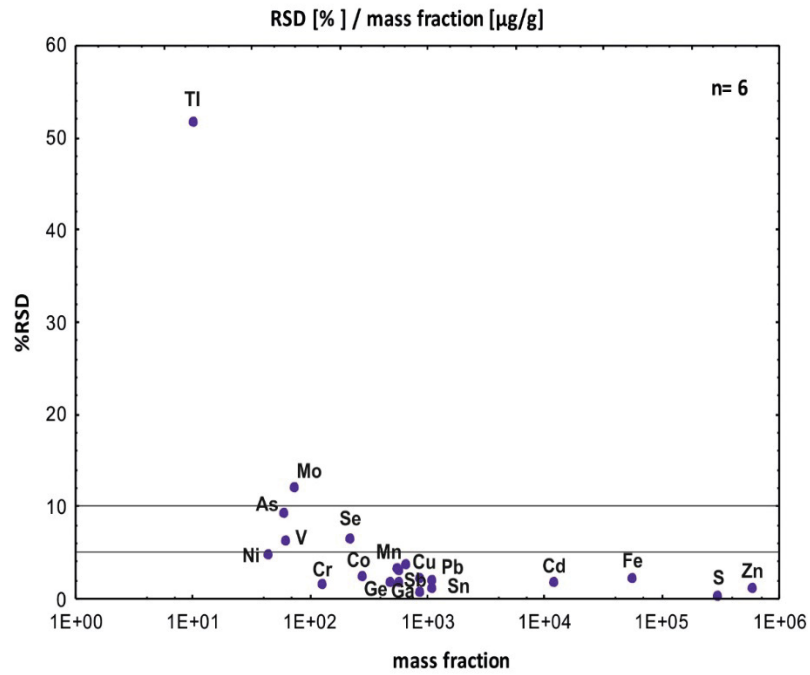

Fig. 5: Relative standard deviation in % RSD vs. mass fraction [µg/g-1] for different elements of six digestions from three different sintered pellets of MUL-ZnS-1 determined by solution ICP-MS

Fig. 6 shows a profile of a LA-ICP-MS line scan (intensity in counts per second vs. distance in millimeters) across a section of MUL-ZnS-1 demonstrating that the elements are quite homogeneously distributed across a sintered pellet. The variation, expressed as one standard deviation (1 RSD), is smaller than 10 % for most of the analytes.

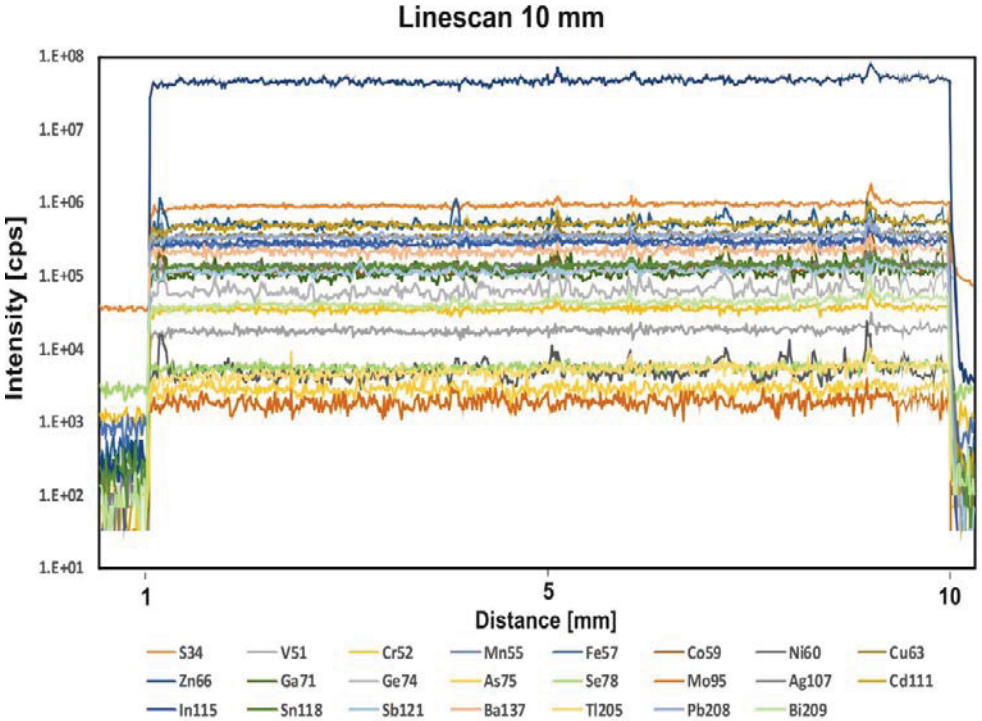

Fig. 6: Intensities of a 10 mm line scan across MUL-ZnS-1 using LA-ICP-MS at a spot size of 80 µm in diameter

This result is consistent with the homogeneity tests by LA-ICP-MS performed at different laboratories using five different section of MUL-ZnS-1 were ninety spots on the surface of each section were analysed (thirty spots 90/100 µm, thirty spots 60/65 µm and thirty spots 30/35 µm). However, mass fractions below 60 $\mu g/g^{-1}$ (V, Ni, As, Mo, Tl) show decreasing RSDs at increasing spot size due to better counting statistics (Fig. 7).

Homogeneity tests of MUL-ZnS-1 by EPMA using 53 single spots (10 µm in diameter) distributed randomly over the polished section result in RSDs of >10% for most elements. The higher variability of the determined mass fractions are probably due to the small analytical volume stimulated by EPMA and thus in inhomogeneity of the material at this scale.

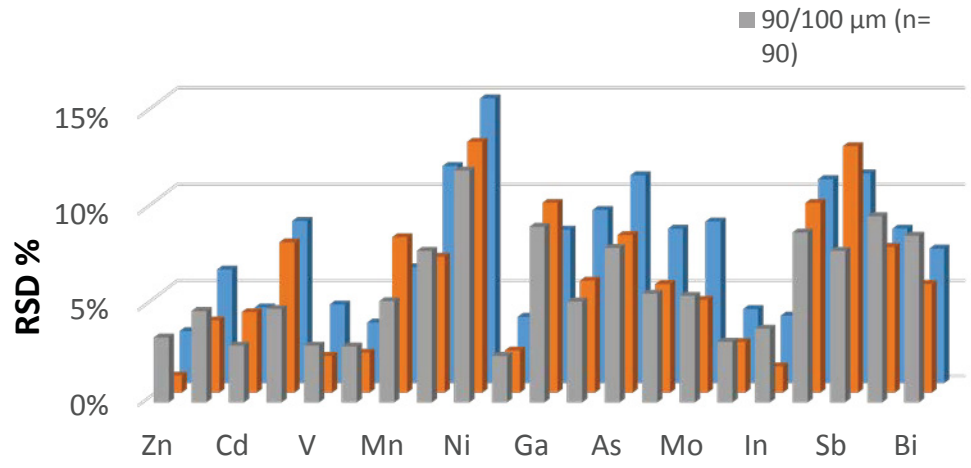

Fig. 7: Homogeneity of trace metals in MUL-ZnS-1 based on LA-ICP-MS analysis expressed as relative standard deviation (%RSD) at different spot sizes.

This is supported by the fact that the median element fractions obtained from all spots of the porosity corrected EPMA measurements are similar to the ICP-MS and ICP-OES obtained from the digestions (Table 5). Low totals of the measurements on MUL-ZnS-1 are due to the porosity of the material. Nevertheless, the data are consistently stoichiometric for sphalerite.

3.4. Ablation behavior of the calibration material

Typical laser ablation craters produced on MUL-ZnS-1 by 213 nm Nd:YAG and 193 nm ArF excimer laser systems are shown in Fig. 8. Both laser systems produce well-defined craters with sharp rims and constant depth at an energy density of about 2 J/cm^2. This low energy leads to appropriate signal intensities and a minimum deposition of ablated material at the crater rim. The base of the crater has no melt bonds (Fig. 8). Higher energies lead to larger coronas and more ejected material around the ablation pits. The ablation behavior of MUL-ZnS-1 is nearly the same as for natural sphalerite. Fig. 9 displays three profiles through ablation craters obtained by a laser beam diameter of 90 µm and a fluence of 2 J/cm^2 on MUL-ZnS-1 and a natural sphalerite.

3.5. SEM investigation

Scanning electron microscope investigations show that the formation of sintering necks is sufficient (Fig. 3). It gives MUL-ZnS-1 the mechanical stability to be refurbished, e.g. by polishing. The grain size distribution of MUL-ZnS-1 is homogeneous and no recrystallized minerals (e.g., sphalerite) were detected.

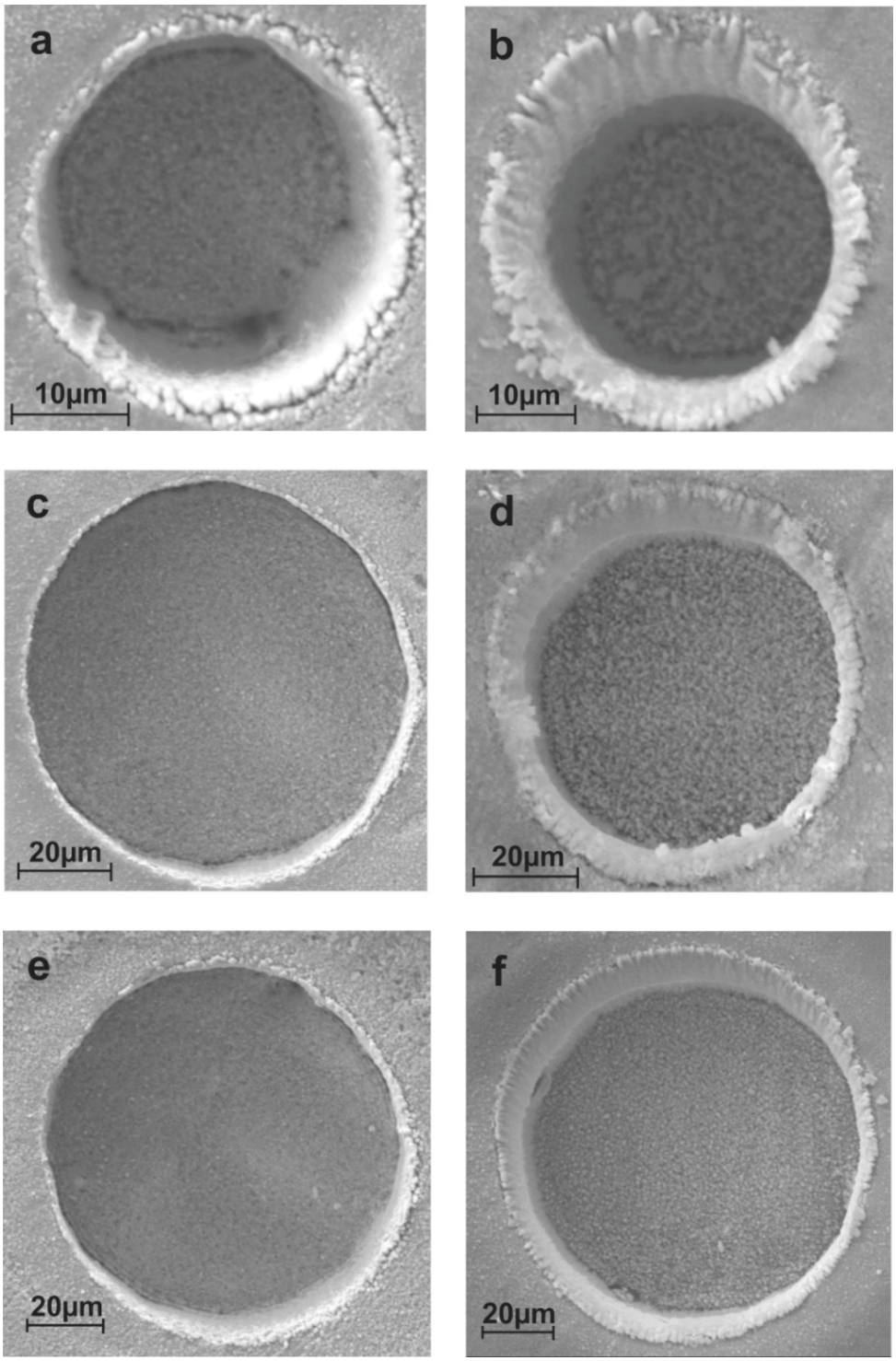

Fig. 8: Secondary electron images (Zeiss EVO MA 10) of laser ablation craters on MUL-ZnS-1 with different spot sizes using laser ablation systems at a pulse repetition rate of 10 Hz and a fluence of about 2 J/cm^2; left column ESI NWR 213 Nd:YAG, right column ESI NWR 193 ArF excimer, a, b: 30 µm, c,d: 60 µm and e,f: 90µm spot size.

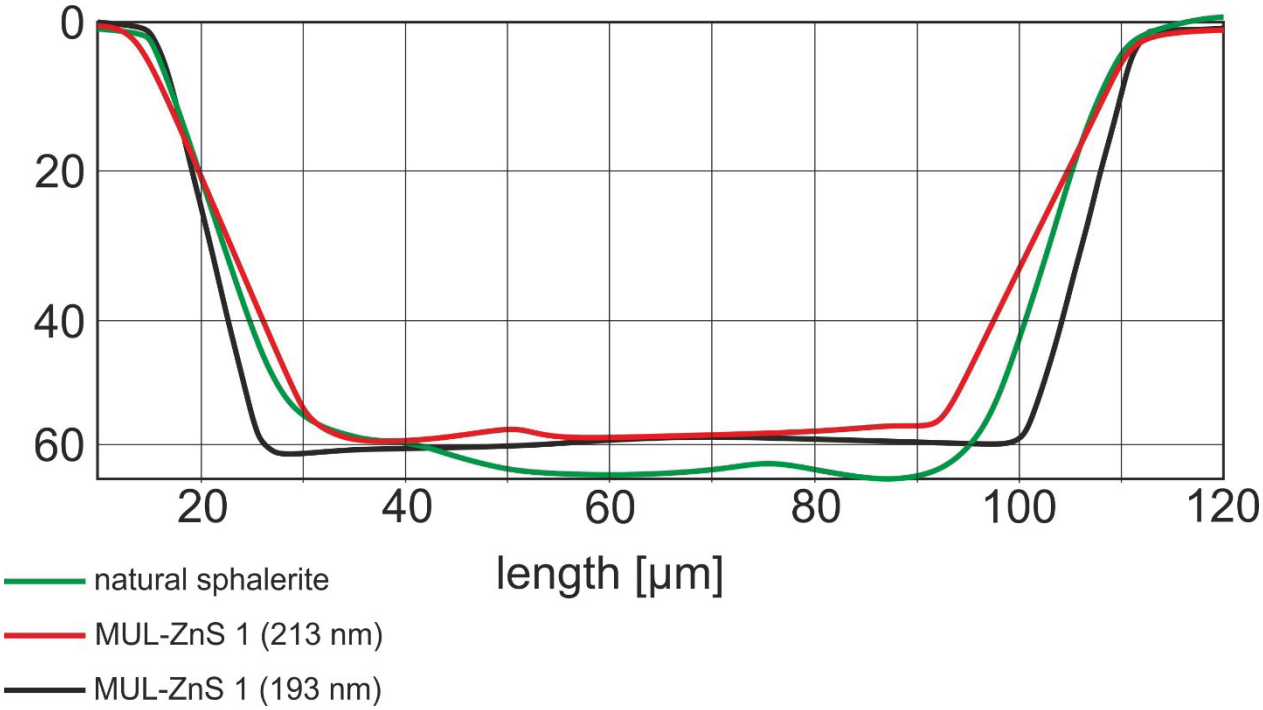

Fig. 9: Depth profiles of the laser ablation craters produced using a spot size of 90 µm; green profile: laser ablation crater in natural sphalerite using an ESI NWR 213, red profile: ESI NWR 213 in the new reference material MUL-ZnS-1, black profile: ESI NWR 193 in MUL-ZnS-1.

4. Conclusion

Synthesis of a trace element reference material with a (Zn,Fe)S matrix for laser ablation ICP-MS analysis is possible if the material behavior of (Zn,Fe)S is taken into account. The synthesized material MUL-ZnS-1 is homogenous within a single pellet and between different sintered pellets on a scale typically used for LA. MUL-ZnS-1 shows similar ablation behavior and element fractionation than natural sphalerite (Fig. 9). The trace element content and the matrix are adjusted to cover a wide range of natural sphalerite compositions. MUL-ZnS-1 is applicable as trace element reference material for matrix-matched calibration of LA-ICP-MS analyses for spot sizes larger than 30 µm. It is of no use for EPMA trace element analysis because the porosity of the sintered material leads to low totals of 81.6 %m/m due to reduced sample material present within the activated volume.

Acknowledgements

The authors are grateful to Christoph Walkner (General and Analytical Chemistry, Montanuniversität) for helping with the HPA digestion and solution ICP-MS measurements and Andreas Prethaler (General and Analytical Chemistry, Montanuniversität) for depth profile measurements of the ablation craters. Andre Balderman (Applied Mineralogy, TU Graz) is thanked for conducting the ICP-OES measurements and Corinna Grasser (Environmental and Energy Process Engineering, Montanuniversität) for freeze-drying the samples. Walter Prochaska for AAS measurements.

References

Ballhaus C. and Sylvester P. (2000)
Noble metal enrichment processes in the Merensky Reef, Bushveld Complex. **Journal of Petrology, 41,** 545-561.

Fleet M.E. (2006)
Phase equilibria at high temperatures. **In: Bowels J.F.W., Howie R.A., Vaughan D.J. and Zussman J. (2011) Rock-Forming Minerals Second Edition Vol. 5A. The Geological Society London,** 802-856.

Cook N.J., Ciobanu C.L., Pring A., Skinner W., Shimizu M., Danyushevsky L., Saini-Eidukat B. and Melcher F. (2009)
Trace and minor elements in sphalerite: A LA-ICPMS study. **Geochemica et Cosmochimica Acta, 73**, 4761-4791.

Cerny I. (1989)
Die karbonatgebundenen Blei-Zink-Lagerstätten des alpinen und außeralpinen Mesozoikums. Die Bedeutung ihrer Geologie, Stratigraphie und Faziesgebundenheit für Prospektion und Bewertung. **Archiv für Lagerstättenforschung Geologische Bundesanstalt, 11,** 5-125.

Danyushevsky L., Robinson P., Gilbert S., Norman M., Large R., McGoldrick P. and Shelley M. (2011)
Routine quantitative multi-element analysis of sulphide minerals by laser ablation ICP-MS: Standard development and consideration of matrix effects. **Geochemistry, 11**, 51-60.

Deer W.A., Howie R.A., Zussman J., Bowles J.F.W. and Vaughan D.J. (2011)
Rock-forming minerals. Volume 5A: Non-silicates, oxides, hydroxides and sulphides (2nd edition. Geological society of London, 932.

Dewaele S., Muchez P. and Hertogen J. (2007)
Production of a matrix-matched standard for quantitative analysis of iron sulphides by laser ablation inductively coupled plasma-mass spectrometry by welding: A pilot study. **Geologica Belgica, 10/1-2**, 109-199.

Durrant S.F. (1999)
Laser ablation inductively coupled plasma mass spectrometry: achievements, problems, prospects. **Journal of Analytical Atomic Spectrometry, 14**, 1385-1403.

Fleet M.E. (2006)
Phase Equilibria at High Temperatures. **Reviews in Mineralogy & Geochemistry, 61**, 365-419.

Fleischer M. (1955)
Minor elements in some sulphide minerals. **Economic Geology, Fiftieth Anniversary,** 970-1024.
Gäbler H.-E., Melcher F., Graupner T., Bahr A., Sitnikova M. A., Henjes-Kunst F., Oberthür T., Brätz H. and Gerdes A. (2011)
Speeding up the analytical workflow for coltan fingerprinting by an integrated mineral liberation analysis/LA-ICP-MS approach. **Geostandards and Geoanalytical Research, 35/4,** 431-448.

Guillong M. and Günther D. (2002)
Effect of particle size distribution on ICP-induced elemental fractionation in laser ablation-inductively coupled plasma-mass spectrometry. **Journal of Analytical Atomic Spectrometry, 17**, 831-837.

Günther D., Jackson S.E. and Longerich H.P. (1999)
Laser ablation and arc/spark solid sample introduction into inductively coupled plasma mass spectrometry. **Spectrochimica Acta, 54B**, 381-409.

Hall W. E. and Heyl A. V. (1968)
Contribution of minor elements in ore and host rock, Illinois, and Upper Mississippi Valley zinc rich district. **Economic Geology, 63**, 655-670.

Hall W.E. and Czamanske G. K. (1972)
Mineralogy and trace element content of the Wood River lead-silver deposits, Blain Country, Idaho. **Economic Geology, 67**, 350-361.

Jochum K.P., Nohl U., Herwig K., Lammel E., Stoll B. and Hofmann A.W., 2005.
GeoReM: a new geochemical database for reference materials and isotopic standards. Geostand. Geoanal. Res. 29, 87-133.

Jochum K.P., Stoll B., Herwig K. and Willbold M. 2007
Validation of LA-ICP-MS trace element analysis of geological glasses using a new solid-state 193nm Nd: YAG laser and matrix-matched calibration. J. Anal. At. Spectrom. 22, 112-121. doi: 10.1039/B609547J

Jochum K.P., Weis U., Stoll B., Kurmin D., Yang Q., Raczek I., Jacob D.E., Stracke A., Birbaum K., Frick D.A., Günther D. and Enzweiler J., 2011.
Determination of reference values for NIST SRM 610-617 glasses following ISO guidelines. Geostand. Geoanal. Res. 35, 397-429.

Kane J.S. (1998)
A history of the development and certification of NIST glass SRMs 610-617. **Geostandards Newsletter: The Journal of Geostandards and Geoanalysis, 22,** 7–13.

Kuhn H.R. and Günther D. (2003)
Elemental fractionation studies in laser ablation inductively coupled plasma mass spectrometry on laser induced brass aerosols**. Analytical Chemistry, 75**, 747-753.

Longerich H.P., Günther D. and Jackson S.E. (1996 A)
Elemental fractionation in laser ablation inductively coupled plasma mass spectrometry. **Fresenius Journal of Analytical Chemistry, 355**, 538-542.

Longerich H.P., Jackson S.E. and Günther D., (1996 B)
Laser ablation inductively coupled plasma mass spectrometric transient signal data acquisition and analyte concentration calculation. **Journal of Analytical Atomic Spectroscopy. 11,** 899–904.

Melcher F. and Buchholz P. (2014)
Germanium. **In: Critical Metals Handbook: Germanium,** ed. Gus Gunn, John Wiley & Sons, Ltd. 177-203.

Ødergard M. (1999)
Preparation of synthetic calibration materials for use in the microanalysis of oxide minerals by direct fusion in high- purity graphite electrodes: Preliminary results for quartz and rutile**. Geostandards Newsletter, 23**, 173-186.

Sangster D. F. and Liberty B. A. (1971)
Sphalerite Concretions from Bruce Peninsula, Southern Ontario, Canada. **Economic Geology, 66**, 1145-1152.

Paton C., Hellstrom J., Paul B., Woodhead J. and Herdt J. (2011)
IOLITE: Freeware for the visualisation and processing of mass spectrometric data. **Journal of Analytical Atomic Spectroscopy 12**, 2508-2518.

Scott S.D. and Barnes H.L. (1967)
Nonstochiometric phase changes in sphalerite and wurtzite. **In: Rock-Forming Minerals Second Edition Vol. 5A.** The Geological Society London, 802-856.

Scott S.D. and Barnes H.L. (1972)
Sphalerite-wurtzite equilibria and stoichiometry. **Geochemica et Cosmochimica Acta, 86**, 1275-1295.

Wohlgemuth-Ueberwasser C.C., Ballhaus C., Berndt J., née Paliulionyte V. S. and Meisel T. (2007)
Synthesis of PGE sulfide standards for laser ablation inductively coupled plasma mass spectrometry (LA-ICP-MS). **Contributions to Mineralogy and Petrology, 154**, 607-617.

Wilson S.A., Ridley W.I. and Koenig A.E. (2002)
Development of sulfide calibration standards for the laser ablation inductively-coupled plasma mass spectrometry technique. **Journal of Analytical and Atomic Spectrometry, 17**, 406-409.

Wohlgemut-Ueberwasser C.C. and Jochum K.P. (2015)
Capability of fs-LA-ICP-MS for sulfide analysis in comparison to ns-LA-ICP-MS: reduction of laser induced matrix effects? **Journal of Analytical and Atomic Spectrometry, 30**, 2469-2480.

Woodhead J., Hellstrom J., Hergt J., Greig A. and Maas R. (2007)
Isotopic and elemental imaging of geological materials by laser ablation Inductively Coupled Plasma mass spectrometry. **Journal of Geostandards and Geoanalytical Research, 31,** 331-343.

Part 2

HIGH-TECH METAL POTENTIAL OF SPHALERITE FROM EASTERN ALPINE LEAD-ZINC DEPOSITS

Peter Onuk

Abstract

The “Ad-Hoc working Group on defining critical raw materials” of the European Union (EU) has identified twenty seven commodities as being critical; some of them are used in high-technology products and green technologies (European Commission 2017). Austria hosts numerous mineralizations with significant potential of the rare high-tech metals germanium, gallium, indium and cobalt, as indicated by chemical data of sulfide ore concentrates. In the beginning of the 1990s, the long-lasting experience of Austrian companies in base metal mining from domestic sources was terminated by the closure of the zinc-lead mine at Bleiberg-Kreuth. Zinc, copper, lead and silver were the major commodities mined in deposits within Austria.

Erich Schroll was the first to analyze trace metals in domestic ores (SCHROLL, 1954; CERNY & SCHROLL, 1995). Modern, systematic research using state-of-the-art analytical methods, however, is almost completely missing. More than 5500 LA-ICP-MS data from sphalerite, which is a major host for some high-technology metals like Ga, Ge, In and Co are presented as part of a re-evaluation of three major types of base metal deposits in the Eastern Alps. Additional to in-situ trace element analysis, sulfur isotope ($\delta^{34}S$) composition was measured for the first time in-situ by using a triple quadrupole ICP-MS and N_2O as reaction gas to reduce the O_2 and NO interferences on sulfur isotopes.

Carbonate-hosted “Alpine-type“ or “Bleiberg-type“ deposits, hosted by Triassic limestones and dolomites of the Drau Range and the Northern Calcareous Alps, are characterized by low Fe, Cd (~2000 µg/g), Ge (200-400 µg/g) and Tl concentrations (~100 µg/g) in sphalerite and by the absence of Co (max. 1 µg/g), Cu, Ni. The Lafatsch deposit in the Northern Calcareous Alps is a special case within this group, hosting high amounts of Ag, but lower concentrations of Mn, Ge, As and Tl compared to other deposits of this type.

In the Austro Alpine nappe system, SEDEX-type deposits are known, among others, from the Graz Paleozoic and the Gurktal nappe. The Pb-Zn-Ba ores located in the Graz Paleozoic (Styria) formed in the Lower Devonian in an euxinic basin structure associated with submarine alkaline volcanism (Weber 1990). In a sphalerite concentrate from the deposit Arzberg-Haufenreith, 10 µg/g Ge, 11 µg/g Ga, 1800 µg/g Cd, 29 µg/g In, and 5 µg/g Tl have been reported (Cerny and Schroll, 1995). In-situ LA-ICP-MS measurements of sphalerite grains collected from five ancient mining sites and one exploration adit reveal a large variation of element concentrations with median values of 4.67 wt% Fe, 1832 µg/g Cd, 138 µg/g Co, 18 µg/g Ag, 9 µg/g Ga, 0.36 µg/g Ge, 1 µg/g In, 1 µg/g Sn and 5 µg/g Sb. Maximum values reach 220 µg/g for Ge, 399 µg/g for Ag and 83 µg/g for In.

In SEDEX deposits hosted in Paleozoic units outside the Graz Paleozoic, e.g. Meiselding (Gurktal nappe), sphalerite carries up to 1900 µg/g In, 250 µg/g Ge, 65 µg/g Ga, 282 µg/g Co and 2.9 wt% Cd. The Walchen deposit located in the Koralm-Wölz nappe system is characterized by high In values (98 µg/g) but low values in Co (55 µg/g), Ga (1.53 µg/g) and Ge (0.07 µg/g). Sphalerite from the Leogang deposit hosted by upper Silurian-Middle Devonian dolomite (Südfazies-Dolomit) at the border to the Ordovician Wildschönau Schiefer of the Greywacke Zone showed the most elevated In concentrations (Md= 247 µg/g); the measured values for Ga

(1.05 µg/g), Ge (0.11 µg/g) and Co (128 µg/g) are in the range of the other investigated SEDEX deposits.

Vein deposits of different genesis and age are widespread in the Eastern Alps. Pb-Zn-mineralization at Vellach-Metnitz in the Gurktal Nappe (Carinthia) unit shows vein-like NW-SE trending structures (WEBER, 1997). At Metnitz, sphalerite carries up to 65 µg/g In, 924 µg/g Ge, 381µg/g Ga, 679 µg/g Co and 4380 µg/g Cd. High indium concentrations have been previously reported for the Zn-Cu-Pb veins of Koprein (Paleozoic of the Karawanken Range). Our LA-ICP-MS analyses of sphalerite show between 10 and 35 µg/g In (maximum 276 µg/g), Ge up to 2.2 µg/g, Ga 0,8- 9,8 µg/g, Co 217- 1221 µg/g, Cd 1121- 3560 µg/g, and Fe 2.8 – 6.5 wt%. The Achselalm-Flecktrogalm deposit hosted in the Habach Group of the Subpenninic nappe system in the Tauern Window contains only slightly elevated Ga concentration (26 µg/g), whereas In (1.5 µg/g) and Co 59 (µg/g) are low compared to the other vein-type deposits, and Ge is below detection limit.

Deposits with economic potential for Ge are mainly hosted in the Drau Range where Radnig shows the highest Ge values and Bleiberg the lowest these lower Ge content in sphalerite from Bleiberg can be compensated by the large size of this deposit. Cerny and Schroll (1995) estimated the remaining tonnage with 2 million tons of ore result carrying 496 tons Ge metal. Indium values were evaluated in Leogang, due to the lack of reliable reserve data, no economic potential can be calculated. Sphalerite from Koprein holds the highest Co content of the investigated deposits. Deposits from the Graz Paleozoic, the Achselalm- Flecktrogalm, Lafatsch, deposits of the Brenner Mesozoic, Drassnitz and Metnitz can be excluded as potential targets of critical metals.

Content

List of Figures

List of Tables

1 Introduction

High-tech metals (HT) are elements that are extensively used in the electronics industry, in technologies such as green technologies and in communication technology. Some of these are critical metals because of the economic importance and the supply risk (e.g. REE from China, Co from the DR Congo), in many cases supply is largely prevented by the establishment of large mining and processing infrastructures, leading to monopolistic market structures. As it can be seen in Table 1 many of these metals show a high Substitutability index (above 0.5) and a low End of life recycling input rate, below 10 % (EU 2014). Nearly all of these metals are related to sulfide minerals (see Table 1) and are produced as by-product in copper, zinc and lead refineries (except Ga, where the main source is bauxite ore). In many cases those elements are not extracted due to the fact that no production infrastructure exists that is coupled to the metallurgical plant or it is not economical and these elements end up on the dumpsite.

Some of the HT metals show an increasing production rate of between 3 and 5 % per year. Pb-Zn deposits have a high rate of co-products like In, Ge, Ga and Co, which seldom form discrete minerals but are frequently substituted in the lattice of common base metal sulfides (BMS). They may be produced as sweeter during the hydro- or pyro-metallurgical refinery process of the primary metal (Fig. 1), but they are more often regarded as penalty elements (e.g. In). The worldwide demand for these elements is driving the research for controlling factors during mineral precipitation and understanding the geological setting where there HT-metals can be found in economical relevant concentrations.

Table 1: HT-metals and their most abundant ore minerals, substitutability index, end of life recycling, application and yearly production modified after EU (2014).

Metal	Ore minerals	Substitutability index	End of life recycling input rate	Application	Annual production (metal)
Co	Cobaltite, Carrollite…	0.71	16%	Batteries, super alloys, magnet alloys	100000 tons
Ga	Bauxite, Sphalerite	0.60	0%	Semiconductor, LED	200 tons
Ge	Sphalerite	0.86	0%	Semiconductor, fiber optics, solar cells	~80 tons
In	Sphalerite	0.82	0%	Semiconductor, LED, LCD display	650 tons

This work presents a mineralogical and geochemical study of sphalerite samples from the most important Eastern Alpine Pb-Zn deposits of different age and origin. It aims at a new insight into the HT-metal potential of Eastern Alpine Pb-Zn deposits. This also includes a $\delta^{34}S$ isotope study using LA-QQQ-ICP-MS, a novel technique developed during the thesis work.

Sphalerite (ZnS) is an abundant tetrahedral sulfide mineral in many BMS deposits. In numerous Pb-Zn deposits, sphalerite is the main carrier of Ga, Ge, and In. The geochemical features of sphalerite were first investigated by Oftedal (1941) who pointed out the link between trace element content and ore type. Bernstein (1985), (Möller, Dulski 1993, 1996) showed the temperature control on the substitution of Ge and Ga. The simple formula ZnS and Zn within its tetrahedral sites allow the incorporation of a broad range of trace elements by direct, e.g. $Cd^{2+} \leftrightarrow Zn^{2+}$,and coupled substitution, e.g. $[Cu^{+}In^{3+}] \leftrightarrow 2Zn^{2+}$ (Cook et al. 2009; Höll et al. 2007). Sphalerite incorporates also hazardous elements like Cd, Hg, Tl and As. Due to the broad range of substituted elements, the color spectrum of natural sphalerite ranges from white to dark black (Cook et al. 2009). Studies by Cook et al. (2009), Lockington et al. (2014) and others demonstrated that e.g. Fe, Mn, and Co are the coloring elements. LA-ICP-MS studies by Cook et al. (2009), Melcher et al. (2006), Lockington et al. (2014) demonstrated that low-temperature deposits like MVT deposits are characterized by high Ge and low Ga and In contents, whereas low Ge and high Ga and In contents can be expected in high-temperature mineralizations like SEDEX and VMS deposits. All these studies pointed out that low Ge concentrations can be an analytical issue by using LA-ICP-MS due to the isobaric interferences like $^{40}Ar^{34}S$ on ^{74}Ge (Belissont et al. 2014; Danyushevsky et al. 2011). This effect can be reduced by using matrix matched reference materials (Onuk et al. 2016).

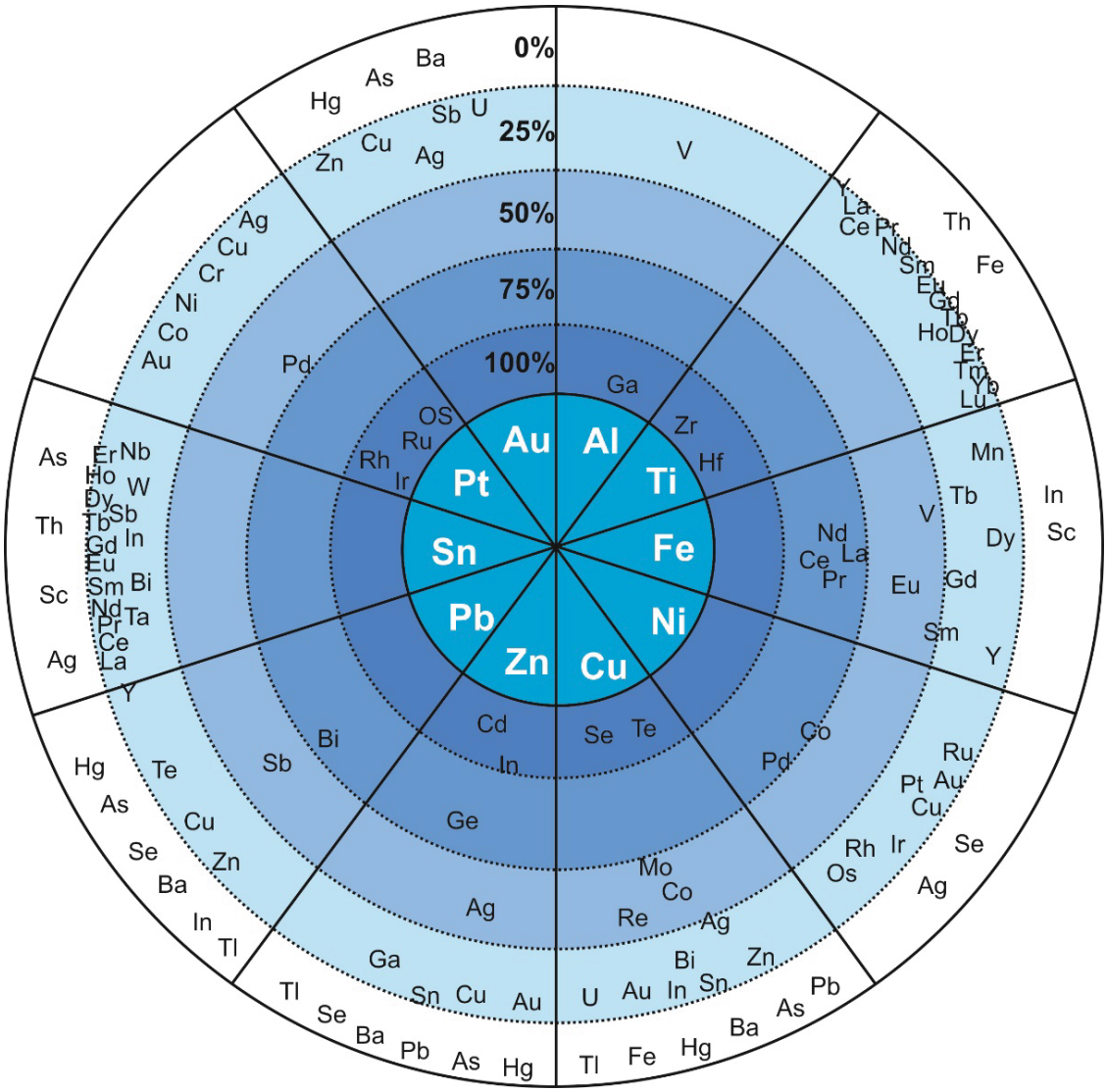

Fig. 1: The wheel of metal companionality modified after (Reuter, Verhoef 2004). The primary host metal are listed in the centre circle, the companion elements appear in the outer circles proportional to their primary production associated with the host metal.

Many authors investigated the trace element content of Eastern Alpine Pb-Zn deposits over the last decades (Cerny 1989c; Weber 1990; Cerny and Schroll 1995) on sphalerite concentrate samples, using methods like spark spectroscopy. These analyses gave an overview on the bulk trace element content and do not reflect the variability of these elements within a grain or even more within a mineralization. The Eastern Alpine Pb-Zn deposits show potential for some of the HT- metals due to different ore-forming processes: Co and Ga in Paleozoic SEDEX deposits, vein deposits show elevated concentrations of Co, Ga, and Sn. The Mesozoic carbonate-hosted, strata-bound Pb-Zn-deposits (Alpine type MVT deposit) of the Drau range and the Northern Calcareous Alps are characterized by significant enrichment in Ge, As, Tl and Cd, whereas sphalerite from the Northern Calcareous Alps is additionally enriched in Ag. The Austrian Mineral Resources Plan (Weber 2012) has identified areas in Austria that should be protected for future mining activities. The Geological Survey of Austria financed the project by funds from the Federal Ministry of Education, Science and Research (Austria): Identifikation und Klassifizierung potentieller Hochtechnologie-Metall Ressourcen in ostalpinen Blei-

Zinklagerstätten; The investigation of trace elements in some of these safeguarded deposits are part of this thesis.

1.1 Minor and trace element substitution in sphalerite

Metal speciation in aqueous solution and precipitation of minerals depend on parameters like temperature, pressure, salinity, pH, fO_2 and fS_2. All these parameters can be observed in sphalerite, one of the compositionally most inhomogeneous sulfide minerals. The variable chemistry of sphalerite can be observed as zoning and cation distribution as a product of different genetic conditions (Di Benedetto 2005). Sphalerite can host a wide range of ions by direct substitution (Fe^{2+}, Mn^{2+}, Cd^{2+}, Co^{2+}, Hg^{2+}) or by coupled substitution (Ge^{4+}, Ga^{3+}, In^{3+}, Cu^{+}, Ag^{+} and many more)(Di Benedetto 2005; Johan 1988).

Iron, Cd, and Mn show the highest element proportion next to Zn and S. Iron is present in almost every natural sphalerite in concentrations of a few 100 µg/g up to more than 15 wt.% (Lepetit et al. 2003). The Fe content of sphalerite has been used as a geological barometer for deciphering ore-forming conditions and determination of the metamorphic grade of ore deposits (Scott, Barnes 1971). Fe^{2+}, $Mn^{2+,}$ and Cd^{2+} can be incorporated in ZnS by isovalent substitution (Fe^{2+}, Mn^{2+}, Cd^{2+}) $\leftrightarrow$ Zn^{2+}; this can lead to zoned crystals that reflect the physio-chemical variation during crystal growth (Di Benedetto 2005). Different element proportions among crystallographic faces, e.g. if the crystal surface becomes enriched in Fe the Mn accumulates in the fluid next to the surface, this leads to an oversupply of Mn and the Mn starts to be chemisorbed. This competition between the ions leads to the formation of oscillatory zoning (Di Benedetto 2005; Belissont et al. 2016).

Manganese plays no role in sphalerite from an economic point of view; the concentrations range from a few µg/g to a few thousand µg/g. Manganese variation in sphalerite within one sample or mineralization is very common (Cerny 1989c). Investigations by Bernardini et al. (2004) and Di Benedetto (2005) show that the presence of Cd influences the Mn and Fe distribution in sphalerite due to competition on the mineral and fluid interface. Manganese is incorporated into sphalerite by simple direct substitution Zn^{2+} $\leftrightarrow$ Mn^{2+} (Di Benedetto 2005; Bernardini et al. 2004).

Sphalerite is the chief host of Cd. This element can perpetrate major environmental hazards on mine dumps and abandoned mine sites. Cadmium concentrations normally vary between 0.1-1 wt.% in sphalerite but can be significantly higher in some Mississippi Valley type deposits (Kelley et al. 2004; Cook et al. 2009; Schwartz 2000).

Germanium is an element of low crustal abundance of ~1.3 µg/g (Rudnick, Gao 2005). The stable oxidation states of Ge are Ge^{2+} (in aqueous solution) and Ge^{4+} in minerals. Due to isomorphous substitution of Ge^{4+} for Si^{4+}, Ge can be found in silicate minerals, especially in topaz and mica hosted by granitic pegmatites (Höll et al. 2007). In the same way Ge can be incorporated in sulfide minerals, particularly in sphalerite, up to a concentration of 3000 µg/g Ge (Bernstein 1985). Limited numbers of ore mineralizations host Ge-minerals like germanite [$Cu_{26}Ge_4Fe_4S_{32}$] (e.g. Tsumeb, Khusib Springs sulphide deposit, Namibia the Tres Marias, Mexico (Cook et al. 2015; Melcher et al. 2006)). Belissont et al. (2016) described the coupled

substitution $3Zn^{2+} \leftrightarrow Ge^{4+}$ + 2 monovalent cations as the main mechanism of Ge incorporation.

Gallium has a crustal abundance of ~16 µg/g (Rudnick, Gao 2005). There are only a few of Ga sulphides known, e.g. gallite [$CuGaS_2$] (Strunz et al. 1958). Most of them occur in the Tsumeb sulphide deposit (Namibia). The only oxidation state is Ga^{3+}. Ga behaves geochemically similar to Al. Sphalerite can host several hundred µg/g of Ga which is incorporated by coupled substitution like $3Zn^{2+} \leftrightarrow 2Cu^{+} + Ga^{3+}$ (Belissont et al. 2016).

Indium is a rare element with a crustal abundance of 52 ppb (Rudnick, Gao 2005). Only 12 indium mineral phases have been defined until now. Roquesite [$CuInS_2$] is the most important mineral (Schwarz-Schampera 2014). Indium is chalcophile. Sphalerite and chalcopyrite are the main sources of indium where it is incorporated as In^{3+} (Figueiredo et al. 2012). Indium is substituted within the sphalerite lattice via coupled substitution $2Zn^{2+} \leftrightarrow Cu^{+} + In^{3+}$ with a typical concentration of <1 µg/g up to several 1000 µg/g (Cook et al. 2011; Johan 1988). Natural sphalerite also shows sector zoning next to band zonation, with significantly increased Cu, In and decreased Fe values (Belissont et al. 2014).

Cobalt has a total crustal abundance of 26.5 µg/g (Rudnick, Gao 2005). Due to its chalcophile and siderophile properties, it is bound to Fe, Ni, S and Cu. It forms cobalt sulphides and arsenides like cobaltite (Co,Fe)AsS and carrollite ($CuCo_2S_4$) (Roberts, Gunn 2014). Cobalt can be substituted into the ZnS structure in a range of some µg/g to several 100 µg/g by direct substitution $Zn^{2+} \leftrightarrow Co^{2+}$ (Cook et al. 2012).

Copper as Cu^{+} is considered to be incorporated into the sphalerite lattice in a range between some µg/g up to several thousand µg/g by coupled substitution like $3Zn^{2+} \leftrightarrow 2Cu^{+} + Ga^{4+}$ (Johan 1988). No evidence for the presence of Cu^{2+} in sphalerite was found by Belissont et al. (2016). Copper can also be incorporated into sphalerite as blebs, dusty or worm-like chalcopyrite inclusions formed by diffusion-induced segregation (DIS) better known as so called copper disease (Bente, Doering 1993).

Sphalerite is the major host mineral for Tl; the concentrations range from a few µg/g to several hundred µg/g. Kelley et al. (2004) reported up to 355 µg/g from the Red Dog deposit. Xiong (2007) proposed the substitution of Tl in low-temperature environment (up to 150°C) in terms of $Tl^{+}_{0.5}As^{3+}_{0.5}S$ solid solution. As thallium exhibits a high potential for environmental hazards on dumpsites, refineries charge penalties for high thallium concentrates.

Several authors suggest that high Ag concentrations (up to 1720 µg/g) in sphalerite probably are the result of mineral inclusions of galena, fahlore and/ or chalcopyrite (Kelley et al. 2004). Cook et al. (2009) proposed that Ag concentrations up to ~100 µg/g (if they are homogenously distributed) can be incorporated into the sphalerite lattice by coupled substitution $3Zn^{2+} \leftrightarrow 2Ag^{+} + Sn^{4+}$.

Tin concentrations can be elevated in sphalerite; in samples where the tin concentration is higher than 100 µg/g discrete stannite minerals can be found as inclusions in sphalerite. Ono et al. (2004) found Sn contents up to 3.59 wt. % in the Suttu vein-type deposit. These investigations indicate a solid solution of Sn in sphalerite. Studies from George et al. (2016) show that elevated Sn concentrations are related to In enriched zones. Belissont et al. (2014)

also found a correlation between In and Sn and proposed two substitution mechanisms, i.e. $3Zn^{2+} \leftrightarrow In^{3+} + Sn^{2+} + (Cu,Ag)^{+}$ or $4Zn^{2+} \leftrightarrow In^{3+} + Sn^{4+} + (Cu,Ag)^{+} + \square$ (□ denotes a vacancy).

High levels of As (up to 1 wt. %) can be found in low-temperature environments. Clark (1970) proposed a solid solution of the form Zn(As, S) as a stable phase in the As-Zn-S system at low temperatures. The substitution is prevented by minor amounts of Fe. Xiong (2007) proposed the substitution of As in low-temperature environment (up 150°C) in terms of $Tl^{+}_{0.5}As^{3+}_{0.5}S$ solid solution. Similar to Tl, As contamination leads to penalties for high As concentrates.

There are only limited data available on how much Pb can be incorporated in the sphalerite lattice, but there is a strong correlation between Sb, Ag, As and Pb suggesting the probability of galena and fahlore inclusions in sphalerite (Kelley et al. 2004).

Sphalerite is the chief host for Hg in Pb-Zn deposits ranging from 0.04 to 5000 µg/g. Proterozoic exhalative deposits show the highest Hg content (Schwartz 1997). Grammatikopoulos et al. (2006) describe an almost perfect substitution between Hg and Zn ($Zn^{2+} \leftrightarrow Hg^{2+}$). Mercury degases during the roasting process leading to hazardous environmental contamination leading in concentrates charge penalties for high mercury concentrates (Grammatikopoulos et al. 2006).

2 Ore forming processes

2.1 Carbonate hosted Pb-Zn mineralization

Alpine Pb-Zn deposits are commonly epigenetic, stratabound, carbonate hosted ore bodies composed of sphalerite, galena, iron sulfides (pyrite, marcasite), carbonates, fluorite and barite. Organic material, such as hydrocarbon is common in some deposits and can be used to reconstruct the thermal history (Rantitsch 2001). The Triassic Alpine Type (APT) deposits of the Eastern Alps occur mainly in highly brecciated dolomite and limestone as open space fillings, breccias, and/or as replacement of the carbonate host rock as emplaced after lithification of the host rock. Host rocks formed along the passive continental margin of the Tethys; this stage was followed by the opening of the Meliata ocean, and the final subduction of this ocean during the Alpine orogeny (Schmidt et al. 1991). The ore fluids have low temperatures (80 °C to 150 °C). The sulfur isotope composition of APT is highly variable ranging from -31 up to -3 ‰ for sphalerite, -32 to – 4 ‰ galena and 8 to 16 ‰ for barite (Schroll, Rantitsch 2005), indicating bacteriogenetic (BSR) and thermal sulfate reduction (TSR) (Schroll 2008).

The salinity of fluid inclusions found in MVT deposits is typically between 10 and 30 wt.% NaCl equivalent; the similarity between these fluids and oil field brines led to the acceptance of a basin-generated origin of MVT fluids (Leach et al. 2010b). Fluid inclusion studies performed by (Leach et al. 2005) yielded formation temperatures from 80° up to 200 °C. Heat, metal and other solutes of the fluid are necessary during migration along aquifers. Chloride rich fluids are able to leach metals from the source rock during migration. Sulfur is derived from crustal sources, evaporates, sulfur bearing organic material or seawater, involving sulfate reduction. MVT deposits are characterized by $\delta^{34}S$ values that indicate a thermal sulfate reduction e.g. Pine Point (NW-Territory, Canada) shows $\delta^{34}S < 6$ ‰ (Schroll 2008).

The differences in the ore forming fluid temperatures, the fluid composition (APT are not related to oil field brines), the sulfur and lead (B-type) isotopic composition and trace element content provoked Schroll (1985) to introduce the term Austro Alpine Pb-Zn deposit (APT) to distinguish the carbonate hosted Triassic Pb-Zn deposits of the Eastern Alpine from Mississippi Valley Type deposits. Kucha et al. (2005, 2010) confirmed this model showing that framboidal pyrite and sphalerite originate from bacterial sulfate reduction to form microscale globular sphalerite.

2.2 SEDEX mineralizations

Sediment-hosted Pb-Zn deposits contain more than 50 % of the known Pb and Zn resources. Most of the known SEDEX deposits are of Lower to Middle Proterozoic (1.7 to 1.4 Ga) and Lower to Middle Paleozoic (500 to 320 Ma) age and form large ore bodies exceeding 20 to > 100 million tons (Robb 2011). They are typically formed within intracontinental euxinic rift basins and are hosted by a wide variety of siliciclastic and carbonate rocks and appear as stratiform, stratabound and discordant ores in the host rock. In some deposits, vein ores are important. Typical sulfide assemblage is galena, sphalerite, pyrite, pyrrhotite and minor chalcopyrite and as gangue mineral barite. Possible by-products are the high-tech metals Co, Ga, Ge, In and the toxic elements Cd, As, Se and minor Tl. Zinc concentrates from the largest known SEDEX deposit Red Dog (~100 million tons of ore grading 18 % Zn, 5 % Pb and 85 g/t Ag), Alaska, carry about 100 µg/g Ge which is extracted at the TECK zinc smelter in Trail, B.C. (Melcher and Buchholz 2014; Kelley et al. 2004). In the eastern Alps, SEDEX deposits are known from the Paleozoic of Graz (formed in the Lower Devonian) and the Gurktal nappe, both part of the Austro Alpine Paleozoic basement units (Fig. 3). The deposits of the "lead-zinc ore district Graz Paleozoic" within the Rannach and Hochlantsch facies and the Meiselding mineralization within the Gurktal nappe show low-grade metamorphic conditions (Weber 1990).

2.3 Volcanic-hosted massive sulfide deposits „VMS"

VMS-deposits are formed during episodes of extensional setting throughout the earth history, forming stratiform syngenetic sulfide and sulfate mineralization forming from hot (300– 400°C) metal-rich fluids, circulating in volcanically active submarine environments on and below the seafloor in association with mafic or bimodal mafic-felsic volcanic activity along oceanic spreading ridges or center (Robb 2011). Actuogeologic equivalents of these exhalative processes are the black and white smokers discovered in 1979 on the Eastern Pacific Rise where hot (up to 400°C), acidic, H_2S-rich Fe, Mn, Zn and Cu bearing hydrothermal fluid is released into cold sea water, forming chimneys on the sea floor (Pohl 2011). Usually these deposits are small containing 0.1-10 million tons ore grading <10% Cu + Pb + Zn. One of the largest occurrences, Kidd Creek (Ontario), reached a size of 100 million tons of ore. The ore includes critical metals like In, Ge, Co, Te and Bi typical by-products are Ag and Au. In the Eastern Alps numerous Cu and "Kies", (pyritic) ores are known within the Austro Alpine and Penninic units. Examples include the Subpenninic Habach Series, the Penninic Bündnerschiefer Formation, the Austro Alpine Ennstal quartz phyllite and the Greywacke Zone.

2.4 Vein-type deposits

Vein-type deposits in the Eastern Alps of variable age and origin that formed during Eoalpine and Paleogene orogenic events may be attributed to one of the before mentioned ore types by

remobilization of originally stratiform mineralization by later processes (Pohl and Belocky 1999). For example, the Gurktal nappe shows deformed and metamorphosed SEDEX Pb-Zn-ores in Meiselding and vein-type Pb-Zn ores at Metnitz (Weber et al. 1997). Processes like these may also account for some of the fahlore-dominated Cu – barite ores in Paleozoic carbonates, e.g. in the polymetallic Cu-Ni-Co-Hg ore district Leogang. Ores from vein-type deposits include the critical metals Co, Ga, Ge, In, Sb and sometimes Ni, Ag and Au.

3 Analytical Methods and Samples

3.1 Samples

The 288 samples were taken from 18 locations with the focus on central and eastern Austria, mainly Carinthia, Styria and Salzburg, with a few samples from Tyrol. Sample locations in Austria are displayed in the simplified geological map (Fig. 3). Additional ore samples from Italy (Raibl, Salafossa, Schneeberg) and Slovenia (Mezica) were analyzed for comparative reasons but not their geological settings described in this thesis in detail (Table 4). Zinc-Pb ores from the "Stubai-Ötztal complex (Tösens)" are currently evaluated separately in a parallel MRI project led by Dr. Thomas Angerer from the University of Innsbruck in cooperation with the Chair of Geology and Economic Geology, MU Leoben. GPS data of the sample locations can be found in the appendix.

The samples were collected with the focus on high sphalerite content and are therefore not representative for the bulk ores.

Due to the age of the host rock the samples were subdivided into two groups, a Mesozoic (Table 2) and a Paleozoic (

Table 3) group. The sampling campaign was structured in two phases: (1) sampling on site: underground mine, open pit, dump site and backfilling material. (2) Samples from collections (see Appendix) from Joanneum Graz, Montanuniversität Leoben MUL and Leopold Franzens Universität Innsbruck.

Table 2: Number of samples and analyses of Mesozoic rock hosted mineralizations.

Location	No. of samples	spot analyses trace elements	spot analyses $\delta^{34}S$ analyses
Jauken	6	93	22
Radnig	19	318	10
Bleiberg-Kreuth	38	797	166
Fladung	21	282	67
Lafatsch	26	439	80
Total	118	2111	345

Table 3: Number of samples and analyses of Paleozoic rock hosted mineralizations

Location	No. of samples	spot analyses trace elements	spot analyses $\delta^{34}S$ analyses
Guggenbach	15	364	44
Arzberg	11	181	21

Rabenstein	9	190	29
Elisabeth adit	8	150	29
Friedrich adit	6	110	9
Silberberg	3	54	0
Haufenreith	6	80	20
Meiselding	19	302	76
Walchen	10	109	25
Leogang/Schwarzleo	5	78	10
Koprein	21	399	87
Metnitz	14	364	30
Achselalm/Flecktrogalm	43	812	28
Total	170	3130	408

Table 4: Overview on numbers of additional locations and analyses that

Location	No. of samples	spot analyses trace elements
Brenntal (Mühlbachtal)	1	12
Drassnitz	5	104
Mezica (Slovenia)	2	47
Raibl (Italy)	8	234
Salafossa (Italy)	1	20
Schneeberg (Italy)	4	70
Seibach-Griesbach	3	59

Samples from Pirkach and Oberzeiring (collection MUL and Johanneum Research) were screened but not further taken into account due to the lack of sphalerite.

3.2 Sample preparation

For petrographic, Scanning Electron Microscopy (SEM) and Laser Ablation Inductively Coupled Plasma Mass Spectrometry (LA-ICP-MS) investigations 350 polished thick sections (size = 46 x 27 mm) of ores of different deposits were prepared using samples from historic collections and self-picked samples. However, it is not possible to see the differences in trace element contents in reflected light and by scanning electron microscopy. The samples were first

analyzed using LA-ICP-MS to identify the samples with elevated amounts of high-tech elements. Afterwards, these samples were investigated petrographically by optical microscopy. SEM analyses were used to identify minerals and mineral inclusions that were not identified by reflected light microscopy.

3.3 SEM investigations

Major-element composition of sphalerite was determined by SEM using the Zeiss EVO MA 10 coupled to a Bruker Quantax 40 mm^2 energy dispersive detector installed at the Chair of Geology and Economic Geology, Montanuniversität Leoben (Austria). This technique allows a non-destructive analysis of minerals and the identification of mineral inclusions down to the lower micrometer scale. The best results were achieved using an acceleration voltage of 20 kV and a beam current of 60 mA.

3.4 Major and Trace element analysis

3.4.1 LA-ICP-MS Analysis

Major and trace element contents of sphalerite were mainly determined by using LA-ICP-MS with a New Wave Research (NWR 213) Nd:YAG 213 nm Nano second laser ablation system updated with a TV2 ablation cell, coupled to an Agilent 8800 triple quadrupole ICP-MS (QQQ-ICP-MS) installed at the Chair of Analytical Chemistry, Montanuniversität Leoben (Austria). For quantification of the element content the matrix matched sintered powder pressed pellet MUL-ZnS 1 reference material (Onuk et al. 2016) and for quality control, the USGS powder pressed polysulfide reference material MASS-1 (Wilson et al. 2002) was used. Sphalerite shows stoichiometric sulfur composition, therefore sulfur was used as internal standard. The LA-QQQ-ICP-MS was optimized to maximum sensitivity on mid-mass isotopes. Production of molecular oxide species to reach $^{232}Th^{16}O/^{232}Th$ and doubly charged species measured on $^{140}Ce^{++}/^{140}Ce^{+}$ was maintained to a level below 0.3% using the NIST standard reference material NIST 612 as reference material. Laser ablation was performed in pure helium atmosphere (750 ml/min), the laser beam size was 80 µm with a repetition rate of 10 Hz and a laser energy density (fluency) of 2 J/cm^2. The aerosol-He mixture from the ablation cell was gas diluted with 0.9 l/min Ar within a glass bulb signal smoothing device (Günther, Heinrich 1999). Each analysis was performed in a time-resolved mode, which includes sequential peak hopping throughout the mass spectrum using dwell times per isotope depending on the mass fraction between 10 and 50 msec. The analysis time for each sample was 120 seconds, 30 seconds for measuring the background (and Laser warm-up with closed aperture), 60 seconds analysis with laser on and 30 seconds wash out time. The following isotopes were monitored: ^{33}S, ^{34}S, ^{51}V, ^{52}Cr, ^{55}Mn, ^{56}Fe, ^{57}Fe, ^{59}Co, ^{60}Ni, ^{63}Cu, ^{66}Zn, ^{71}Ga, ^{74}Ge, ^{75}As, ^{82}Se, ^{95}Mo, ^{107}Ag, ^{111}Cd, ^{115}In, ^{118}Sn, ^{121}Sb, ^{205}Tl, ^{208}Pb and ^{209}Bi. Data reduction was carried out using the Iolite V3.1 software (Paton et al. 2011).

3.5 Sulfur isotope analysis on Sphalerite

Sulfur isotope ($\delta^{34}S$) ratios on sphalerite were determined by LA-ICP-MS with a New Wave Research (NWR 213) Nd:YAG 213 nm Nano second laser ablation system coupled to an Agilent 8800 QQQ-ICP-MS installed at the Chair of Analytical Chemistry, Montanuniversität Leoben (Austria). For quantification of the element content the matrix matched sintered powder pressed pellet MUL-ZnS-S1 and MUL-ZnS-S2 reference materials were used (Onuk et al. 2017a). The LA-QQQ-ICP-MS was optimized to maximum sensitivity on mid-mass isotopes. The

sulfur isotope ratios ($\delta^{34}S$) of the sulfides were measured in situ using the method of Onuk et al. (2017). The natural variation of the $\delta^{34}S$ ratio varies between -30‰ and +30‰ or even greater (Ohmoto 1972). This large variation implies that a precision of 1‰ is sufficient for many geological investigations. To reduce the polyatomic interferences e.g. $^{16}O_2^+$, $^{14}N^{18}O^+ \rightarrow {}^{32}S$, $^{16}O^{18}O^+$, $^{17}O_2^+ \rightarrow {}^{34}S$, N_2O was injected into the collision/reaction cell (Fig. 2) to a level that the gas blank was at a minimum (Onuk et al. 2017b). Laser ablation was performed in pure helium atmosphere (800 ml/min), the laser beam size was 80 µm with a repetition rate of 10 Hz and a laser energy density (fluency) of 2 J/cm^2. The aerosol-He mixture from the ablation cell was gas diluted with 0.95 l/min Ar within a glass bulb signal smoothing device (Günther, Heinrich 1999). Each analysis was performed in time-resolved mode that includes sequential peak hopping throughout the mass spectrum using dwell times per isotope depending on the mass fraction between 10 msec. The analysis time for each sample was 210 seconds, 30 seconds for measuring the background (and laser warm-up with closed aperture) 60 seconds analysis with laser on and 120 seconds wash out time. The $\delta^{34}S$ ratio was referred to the Vienna-Canyon Diablo Troilite (VCDT) defined by the assignment of $\delta^{34}S$ of -0.30‰ to the IAEA S-1 reference material (Krouse, Coplen 1997) using the expression:

$$\delta^{34} = \left(\frac{\frac{^{34}S_{sample}}{^{32}S_{sample}}}{\frac{^{34}S_{standard\ V\text{-}CDT}}{^{32}S_{standard\ V\text{-}CDT}}} - 1 \right) * 1000$$

The data reduction was performed using an Excel® spread sheet (Onuk et al. 2017a).

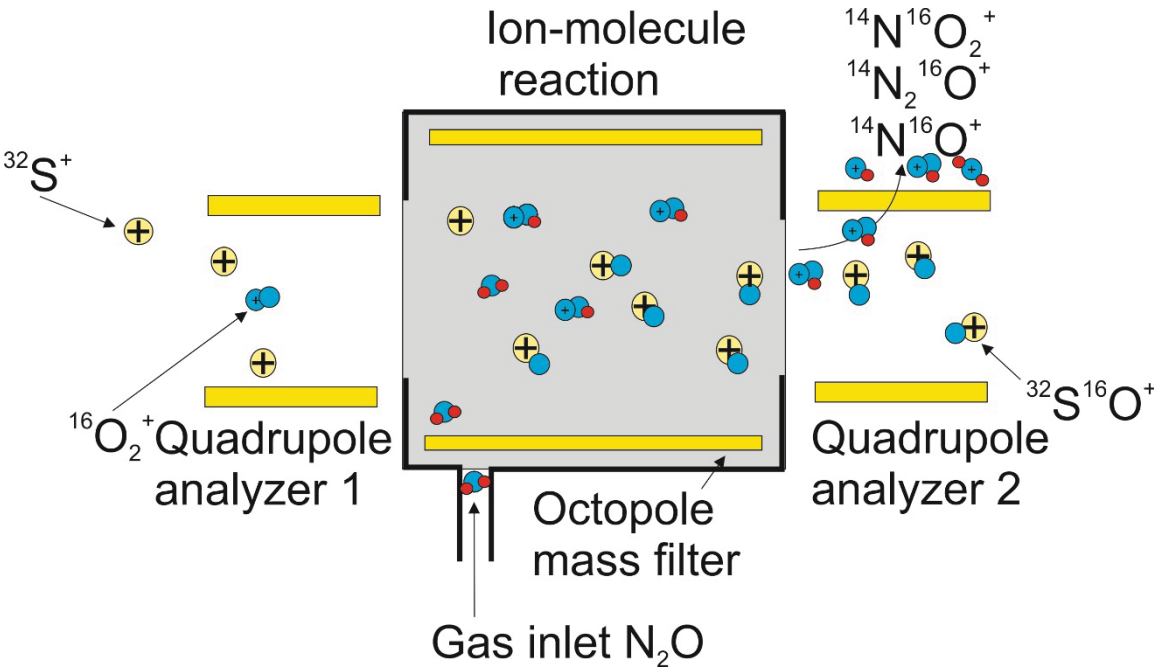

Fig. 2: Simplified sketch of the collision-reaction cell and the ion-molecule reaction of N_2O as reaction gas in the case of ^{32}S.

4 Geological Settings

The Eastern Alps are separated geographically from the Western Alps by avirtual line from the Rhine valley along the Splügenpass to the Lake Como. They are divided into four major tectonic units: Molasse Basin, Helvetic, Penninic and Austro Alpine nappe system. The Periadriatic lineament (Fig. 1) separates the South Alpine from the Austro Alpine unit.

The Austro Alpine nappe stack hosts numerous sedimentary exhalative deposits (SEDEX) within the Paleozoic of Graz (Fig. 3: GP), Gurktal Nappes (Fig. 3: Mei), Noric Nappe and other units.

Large volcanic massive sulfide deposits (VMS) are not known in the Eastern Alps, but there are numerous base metal sulfide deposits (BMS) in the Penninic unit and Austro Alpine nappe systems, for example, the Cu deposit Walchen located in the Ennstal Quartzphyllite (Fig. 3: Wa). The Pb-Zn deposit of Koprein, hosted in Paleozoic volcanic rocks of the Karawanken range (Fig. 3: Kop) shows vein-like appearance but is in context of this type of ore.

Vein type deposits are widespread in the Eastern Alps and were mined since medieval times for numerous metals like Au and Cu. Samples from this type were collected from the Achselalm/ Flecktrogalm deposit located in the Penninic Habachserie (Fig. 3: AA) and Metnitz from the Gurktal nappe system (Fig. 3: Met) and Drassnitz (Fig. 3: Dr).

Triassic carbonate-hosted Pb-Zn deposits of the Austro Alpine nappe system are present in the Drau Range (Fig. 3: BB, Ra, Ja, Fl), Lechtal and Inntal nappes of the NCA (Fig. 3: LaT). These deposits are assigned to the `Alpine or Bleiberg type` deposits. Bleiberg has been mined over the last 700 years until 1993. In this world class deposit, more than 3 million tons of Pb-Zn ore with a Zn/Pb ratio of 5-6 was produced (Cerny, Schroll 1995).

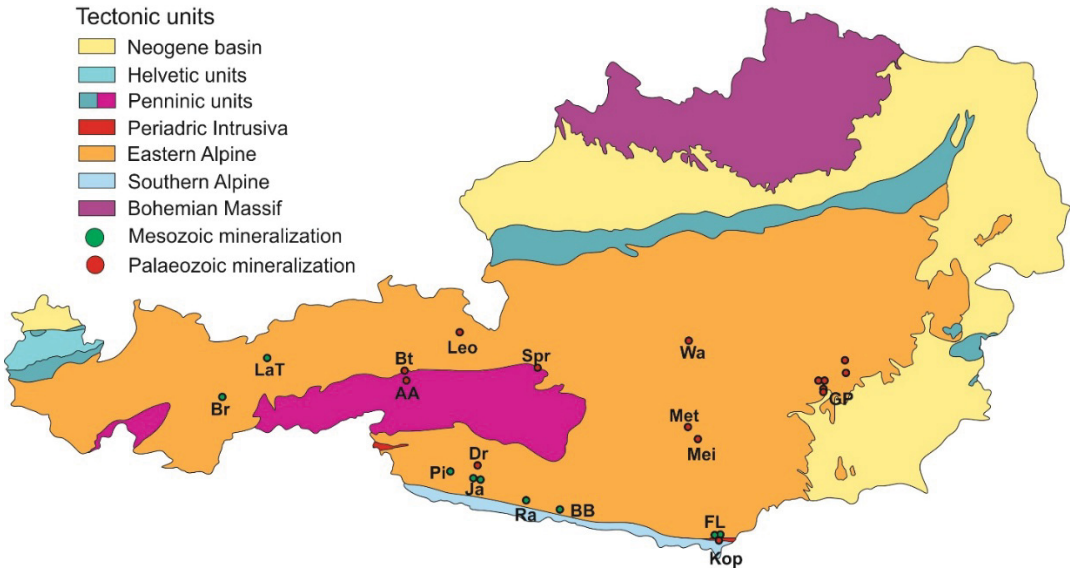

Fig. 3: Simplified geological sketch map of the Eastern Alps modified after Egger et al. (1999): red dots indicate Paleozoic deposits or deposits hosted in Paleozoic units, green dots indicate

Mesozoic deposits. AA, Achselalm; BB, Bleiberg-Kreuth; Fl, Fladung-Hochobir; GP, Graz Paleozoic; Ja, Jauken; KOP, Koprein; LaT, Lafatsch; Leo, Leogang; Mei, Meiselding; Met, Metnitz; Ra, Radnig; Wa, Walchen. Br, Brenner Mesozoic; Spr, Sprinzgasse; Pi, Pirkach; Dr, Drassnitz; Bt, Brenntal.

4.1.1 Mesozoic carbonate-hosted Pb-Zn mineralizations

The genesis of Mesozoic carbonate-hosted Pb-Zn mineralizations has been debated by generations of geologists. The focus of their work was mostly devoted to the Pb-Zn-deposit Bleiberg-Kreuth.

The Northern Calcareous Alps (NCA) and the Drau Range (DR) host more than 200 Pb-Zn-deposits. Cerny (1989b) identified mineralizations in three stratigraphic units (Fig. 4).

Alpine Muschelkalk Formation (Anisian)

Wetterstein Formation (Ladininan- Carnian)

Raibler Schichten (Carnian)

The sediment stratigraphy (upper Permian-upper Jurassic) of a passive continental margin can be seen in Fig. 4. Mesozoic carbonate hosted Pb-Zn deposits were deposited in the same environment. The Drau Range was paleogeographically the western most part of the Calcareous Alps that was transported before deposition of the Gosau Group in the Upper Cretaceous by a strike slip fold to its current position (Brandner, Sperling 1995). The Pb-Zn deposits from the NCA show differences to the deposits of the DR: NCA does not show mineralization in the Raibl strata. The second big difference is that galena and sphalerite from NCA deposits host Ag up to 250 µg/g, whereas these minerals are nearly Ag free in the DR (Schroll 2006).

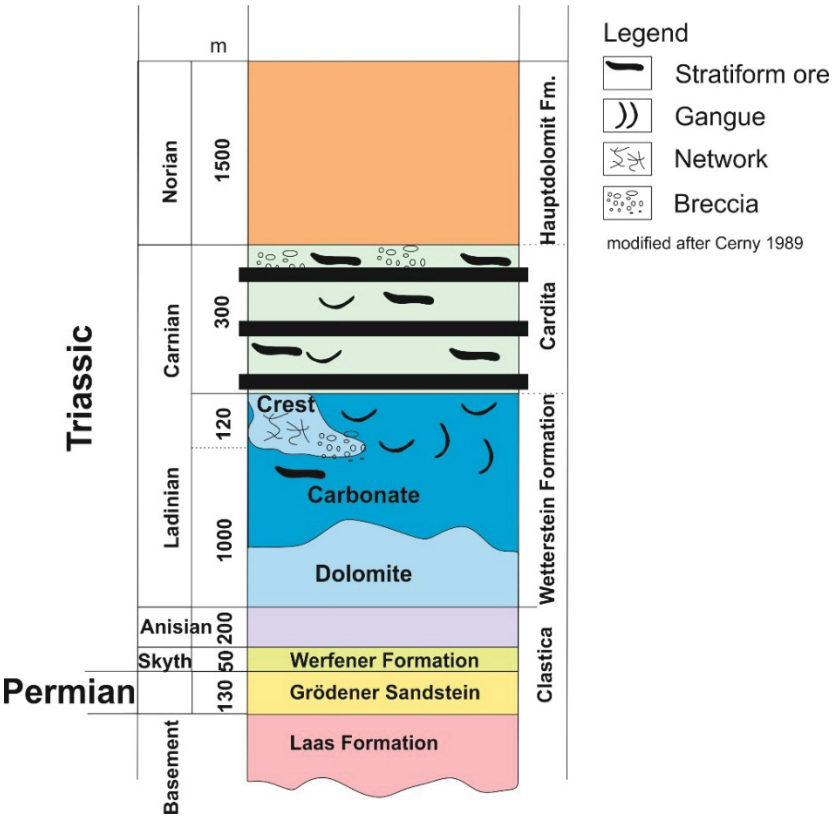

Fig. 4: Stratigraphy of Austro-Alpine Mesozoic carbonate-hosted Pb-Zn deposit.

4.1.1.1 Mesozoic Pb-Zn deposits of the Drau Range

The Mesozoic carbonates of the Drau Range host numerous Pb-Zn-deposits. The largest of them, Bleiberg-Kreuth, has been mined since the last 700 years producing approximately 3.5 x 10^6t of metals from ores hosted by Ladinian to Carnian carbonate rocks (Schroll 2006). The origin of the deposit was described by Cerny (1989a); Schroll, Rantitsch (2005) and Schroll (2008) as an Alpine Type deposit. Further investigations of Kucha et al. (2005) and Kucha et al. (2010) show that the evolution of these Pb-Zn ores is in context with microbial activity of sulfate-reducing bacteria. The stratigraphy is comprised of Scythian red beds (Alpine Bundsandstein), Anisian shallow water carbonates, Ladinian to Carnian lagoonal carbonates and the reef facies of the Wetterstein Formation, carbonate and clastic Carnian Raibl Group with the Cardita shales and the lagoonal dolomites of the Hauptdolomit Formation (Schroll, Rantitsch 2005; Cerny 1989a). In the western part of the Drau Range Jurassic hemi pelagic to Cretaceous flysch sediments were deposited in an oblique slip zone (Schmidt et al. 1991). This sedimentary pile reflects an unstable shelf at a passive continental margin of the Tethys, followed by the opening of the Meliata Ocean, and the final subduction of this ocean during the Alpine orogeny (Schroll 2008. Rantitsch 2001) calculated the thermal evolution and showed that the temperature during the Mesozoic to Cenozoic burial reached up to 130°C. Cerny (1989b) described that the ore bodies of the Drau Range are exposed along the axis Mezica via Bleiberg to Salafossa (both South alpine) in the west. Henjes-Kunst (2014) investigated sphalerite from different ore horizons from the Bleiberg deposit resulting in Rb/Sr ages for the Crest horizon 204±3.2 Ma and the Revier Erlach 195±2.6 Ma. Due to the high uncertainty, it was not possible for her to give an accurate age for the 1st Raibl horizon.

The Jauken deposit (Fig. 5) in the summit area of the Jauken ridge occurs as stratabound stratiform layers and veins along tectonic structures at the top of the Wetterstein Formation (Cerny, Schroll 1995).

The Pb-Zn mineralization Radnig (Fig. 5) 4 km north of Hermagor occurs as two stratabound stratiform concordant layers at the top of the Wetterstein Formation (Cerny, Schroll 1995).

The Bleiberg-Kreuth deposit shows three different geometries, stratabound mineralizations with primary ore textures, vein- fault (breccia) shaped and large scale stock like ore bodies (Cerny, Schroll 1995).

Fladung (Fig. 5) located at the Eisenkappler Hüttenstrasse (Hochobir)occurs as layered ZnS-PbS rhythmite with colloidal ore textures at the top of the Wetterstein Formation (Cerny, Schroll 1995).

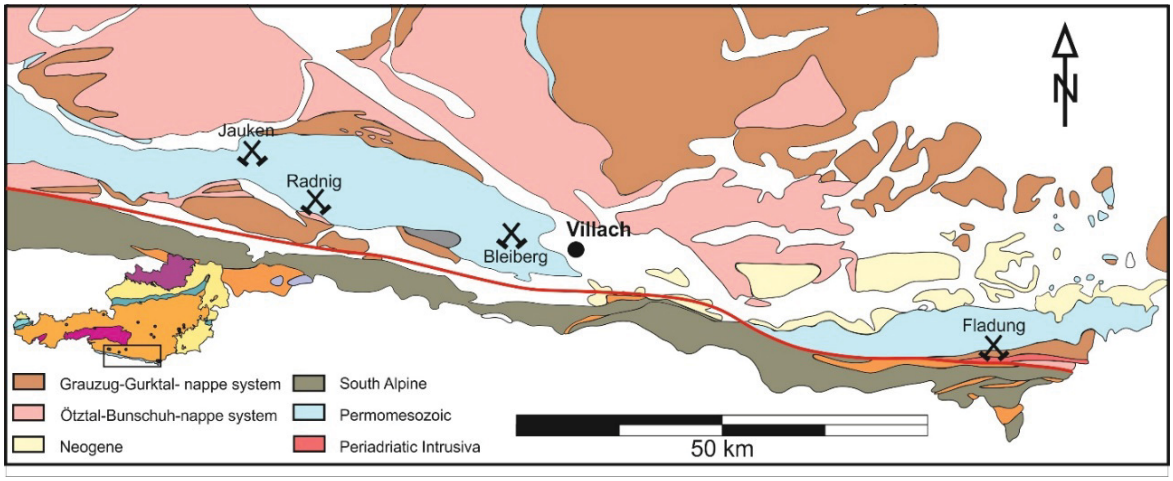

Fig. 5: Simplified geological sketch of a part of the Drau Range (modified after GBA: IRIS Online 2017). Crossed hammer symbols mark the Mesozoic deposits Jauken, Radnig, Bleiberg and Fladung. PAL (Peri-Adriatic-Lineament).

The reported values from Cerny and Schroll (1995) for Mesozoic carbonate hosted Pb-Zn deposits of the Drau Range are listed in Table 5

Table 5: Reported data of Cerny and Schroll (1995) from Pb-Zn deposits of the Drau Range

Deposit	Ge	Ga	Cd	Tl
Jauken	1500	36	1318	70
Radnig	320	345	1634	8
Bleiberg	173	16.5	1745	74
Fladung/Hochobir	900	66	3828	190

4.1.1.2 Mesozoic Pb-Zn deposits of the Northern Calcareous Alps

In the Northern Calcareous Alps (NCA) there are Pb-Zn deposits in Permomesozoic units north of the Inn valley and west of Kufstein (Cerny 1989a). Pb-Zn- deposits occur in the Inntal Nappe

at the top of the Wetterstein Formation and in the dolomitic part of the Alpine Muschelkalk (Anisian and Carnian age) as stratiform to podiform ore bodies with a thickness between 3 to 5 m. The Raibl group is not mineralized (Cerny, Schroll 1995; Weber, Cerny 1997). Weber and Cerny (1997) describe that galena and sphalerite are Ag bearing in contrast to the Drau Range (Ga ~ 200 µg/g and Sph ~270 µg/g).

Anisian mineralizations: The Heiterwand deposit located in the Inntal nappe, on the northern edge of the NCA located in the Anisian Wetterstein Formation is characterized by a complex ore paragenesis bearing next to sphalerite and galena also fahlore, enargite, luzonite and many more (Weber, Cerny 1997). The Tegestal mineralization located in the Lechtal nappe is restricted to the Anisian Alpine Muschelkalk and was sporadically mined for galena, galmei and Ag from the 15th century and closed 1929 (Cerny 1989b).

The biggest deposit in the Northern Calcareous Alps, Lafatsch-Vomperloch (~ 600 000 t of ore) was mined for Pb and Ag. The mineralization within a W-E oriented syncline is characterized by Wetterstein limestone, Raibl strata and Hauptdolomit and shows similarities to the Bleiberg Sonderfacies (Weber, Cerny 1997). The country rock has Carnian age, mineralization is strictly related to the uppermost 240 m of the Wetterstein limestone forming cloud- and nest-shaped ore bodies, that were sheared and folded during alpine orogenesis (Schulz 1981). The paragenesis is dominated by galena, sphalerite, marcasite, calcite and fluorite. Small mines operated since medieval time up to 1963 leading to around 150 small adit (Schulz 1981).

The Pb-Zn-deposits from the NCA show paragenetic and geochemical differences to the Pb-Zn deposits of the Drau Range (DR). In contrast to those of the DR, sphalerite and galena of the NCA show higher Ag and Cu concentrations. In the NCA deposits fahlore is associated with the Pb-Zn ore, fluorite is the main additional mineral and barite is missing (Cerny 1989b).

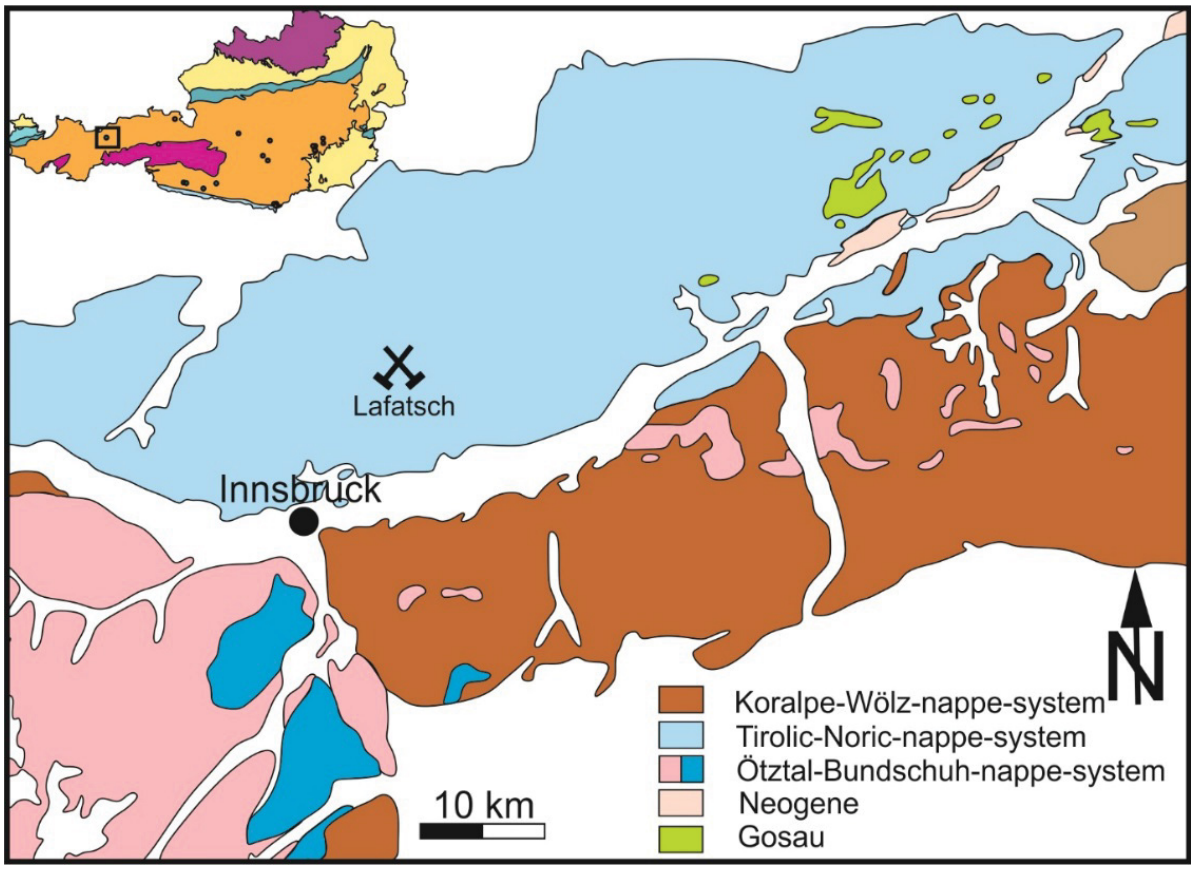

Fig. 6: Simplified geological sketch of a part of the Eastern Alpine Permomesozoic (modified after GBA: IRIS Online 2017). Crossed hammer symbol marks the Lafatsch deposit.

Cerny and Schroll (1995) reported values for Ge 150 µg/g, Ga 15 µg/g, Cd 2300 µg/g, Tl 45 µg/g and Ag 120 µg/g.

4.1.2 Paleozoic of Graz

The Graz Paleozoic Nappe Complex (GPNC) is part of the Upper Austro Alpine Nappe Complex. The ca. 30 x 50 km-sized nappe complex (see Fig. 7) consists of low- to very low-grade (greenschist facies) carbonates, schist's and metavolcanics of Paleozoic age (Gasser et al. 2010). The GPNC is in tectonic contact with the structurally deeper Koralm Crystalline Complex in the southwest, the Gleinalm Crystalline Complex to the north-west, the Anger Crystalline Complex in the northeast and the Radegund Crystalline Complex to the south-east. In the south, Neogene sediments overlie the GPNC (Piller et al. 2004). The GPNC is covered by the Cretaceous Gosau basin in the west.

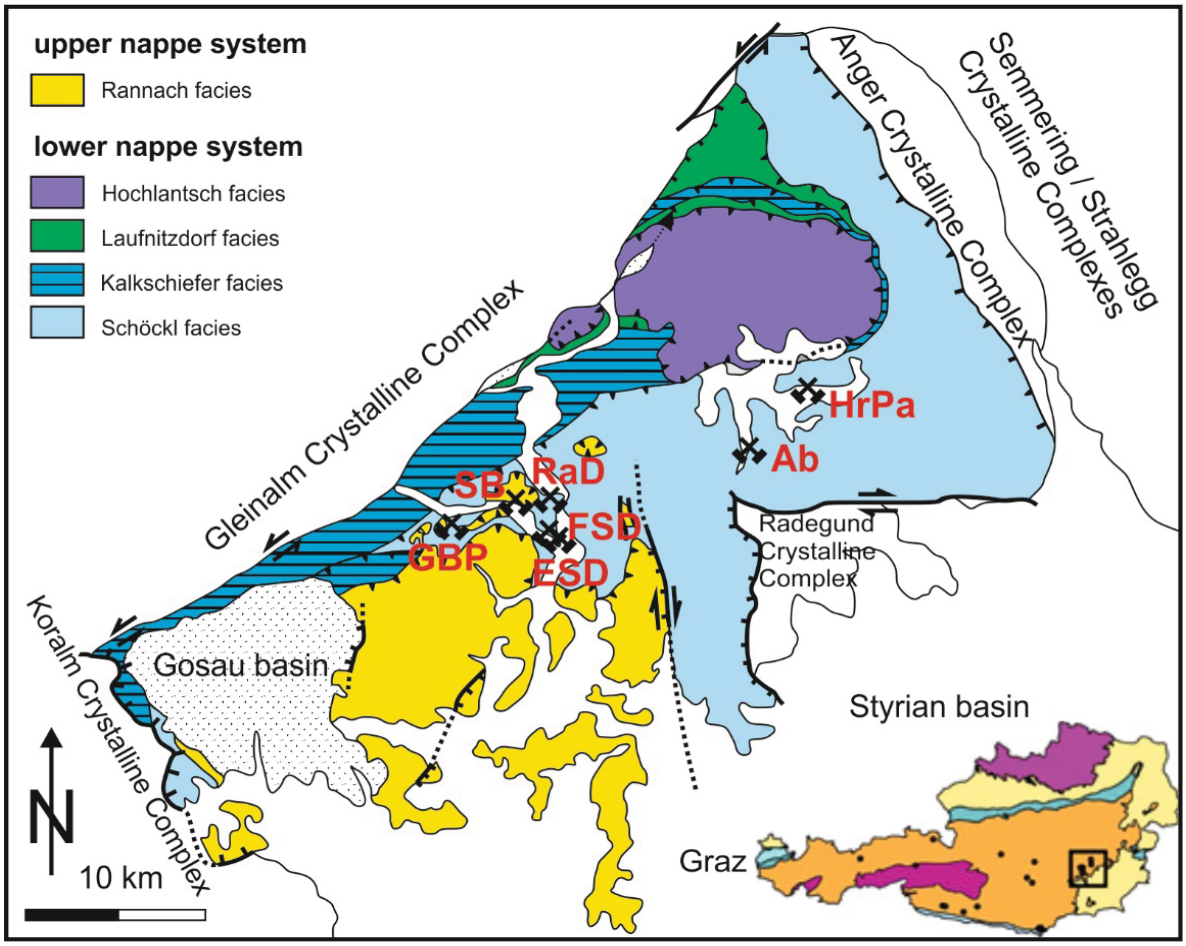

Fig. 7: Geological sketch map of the Graz Paleozoic modified after Gasser et al. (2010), crossed hammer indicates sample collection site. SB, Silberberg; GBP, Guggenbach-Poyd; ESD, Elisabeth-Adit; FSD, Friedrich Adit; RaD, Rabenstein-Deutschfeistritz, Ab, Arzberg; HrPa, Haufenreith-Passail.

The GPNC is subdivided into two nappe groups. The upper nappe system is represented by the Rannach nappe, the lower nappe system (from bottom to top) is composed of the Schöckl nappe, Kalkschiefer nappe, Laufnitzdorf nappe and the Hochlantsch nappe (Gasser et al. 2010).

The Pb-Zn-barite mineralizations of the GPNC are related to Silurian to early Devonian continental rifting and submarine exhalative volcanism in euxinic basins (Leach et al. 2010a). Weber (1990) confirmed that the Pb-Zn-barite deposits of the GPNC are SEDEX-type mineralizations, which formed in the lower Devonian and are exclusively hosted by the Schönberg formation (lower nappe system). The ore bodies are parallel to the layer of the

former basins, and are strictly stratiform and facies-bound (Weber 1990). The ore paragenesis mainly consists of galena, sphalerite and barite, pyrite and chalcopyrite are minor components. As Ag bearing accessorial minerals freibergite, pyrargyrite, polybasite and Ag-Au-Hg alloy was described by (Feichter, Mogessie 2003).

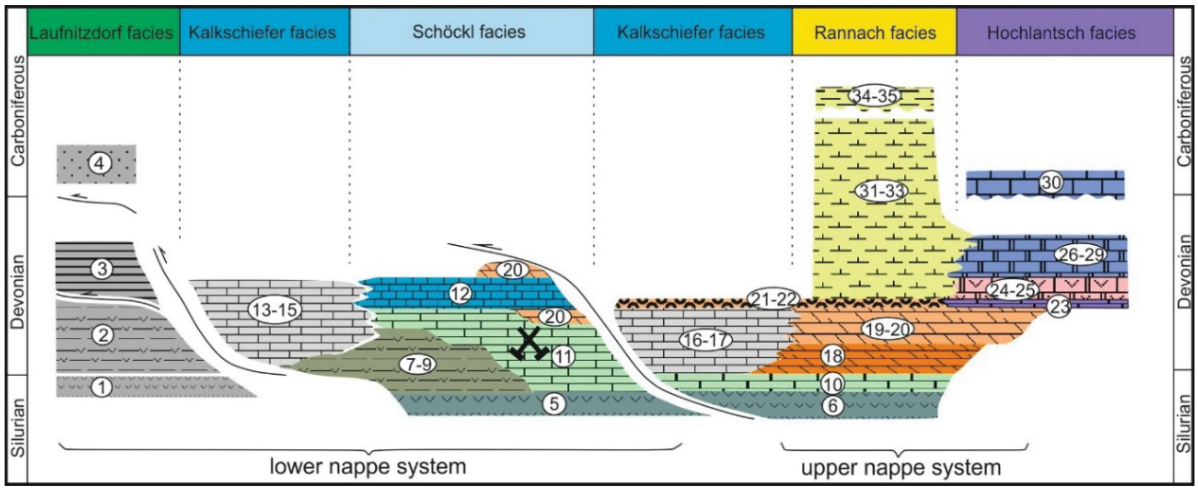

Fig. 8: Stratigraphy of the Graz Paleozoic modified after Gasser et al. (2010). Formation numbers: 1 Hackensteiner Fm, 2 St. Jakob Fm, 3 Harrberger Fm, 4 Dornerkogel Fm, 5 Taschen Fm, 6 Kehr Fm, 7 Semriach Phyllite Fm, 8 Heilbrunn Phyllite Fm, 9 Hirschkogel Phyllite Fm, 10 Kötschberg Fm, 11 Schönberg Fm, 12 Schöckl Fm, 13 Kogler Fm, 14 Hochschlag Fm, 15 Hubenhalt Fm, 16 Bameder Fm, 17 Heigger Fm, 18 Parmasegg Fm, 19 Flösserkogel Fm, 20 Raasberg Fm, 21 Plabutsch Fm, 22 Draxler Fm, 23 Osser Fm, 24 Tyrnaueralm Fm, 25 Rotmüller Fm, 26 Zachenspitz Fm, 27 Hochlantsch Fm, 28 Schweinegg Fm, 29 Fahrneck Fm, 30 Bärenschütz Fm, 31 Kollerkogel Fm, 32 Steinberg Fm, 33 Sanzenkogel Fm, 34 Höchkogel Fm, 35 Hahngraben Fm. Crossed Hammer indicates mineralized formation.

Median values of data from Cerny and Schroll (1995) give for Ge 10 µg/g, Ga 20 µg/g, In 15 µg/g, Ag 26 µg/g, Co 105 µg/g and Tl 5µg/g.

4.1.3 Pb-Zn mineralizations hosted in the Drauzug-Gurktal nappe system

The Drauzug-Gurktal nappe system (DGN) is a key structure of the Austro Alpine units east and south of the Tauern window (Neubauer 1987). The footwall rocks of the DGN are part of the Upper Austro Alpine basement nappes. The Variscan metamorphic basement was overprinted during Eoalpine greenschist to amphibolite facies metamorphism (Neubauer 1987). The DGN is subdivided into two units (Schmid et al. 2004):

1. Murau Nappe: The Murau Nappe consists mostly of Ordovician to Silurian phyllites, greenschist and Devonian carbonates (Neubauer 1987).
2. Stolzalpe Nappe: The Stolzalpe Nappe contains Upper Ordovician to Lower Carboniferous slightly metamorphosed rocks (Variscian and Alpine metamorphism), which are covered by Upper Carboniferous to Permian sediments (Neubauer 1987).

The Pb-Zn deposit of Meiselding (Fig. 9) is hosted by phyllites of the Murrau Nappe and forms stock- to mushroom shaped mineralizations (Cerny, Schroll 1995). It was mined underground for Pb, Zn, and Ag. The paragenesis is dominated by galena, sphalerite, pyrrhotite, pyrite and chalcopyrite.

The Metnitz mineralization (Fig. 9) was described by Cerny and Schroll (1995) as three parallel veins with a thickness of 0.4– 4 m at the contact between marble and graphite schist. The mineralization was mined for Pb and Zn in an open pit and underground along a NW-SE striking and SW dipping fault.

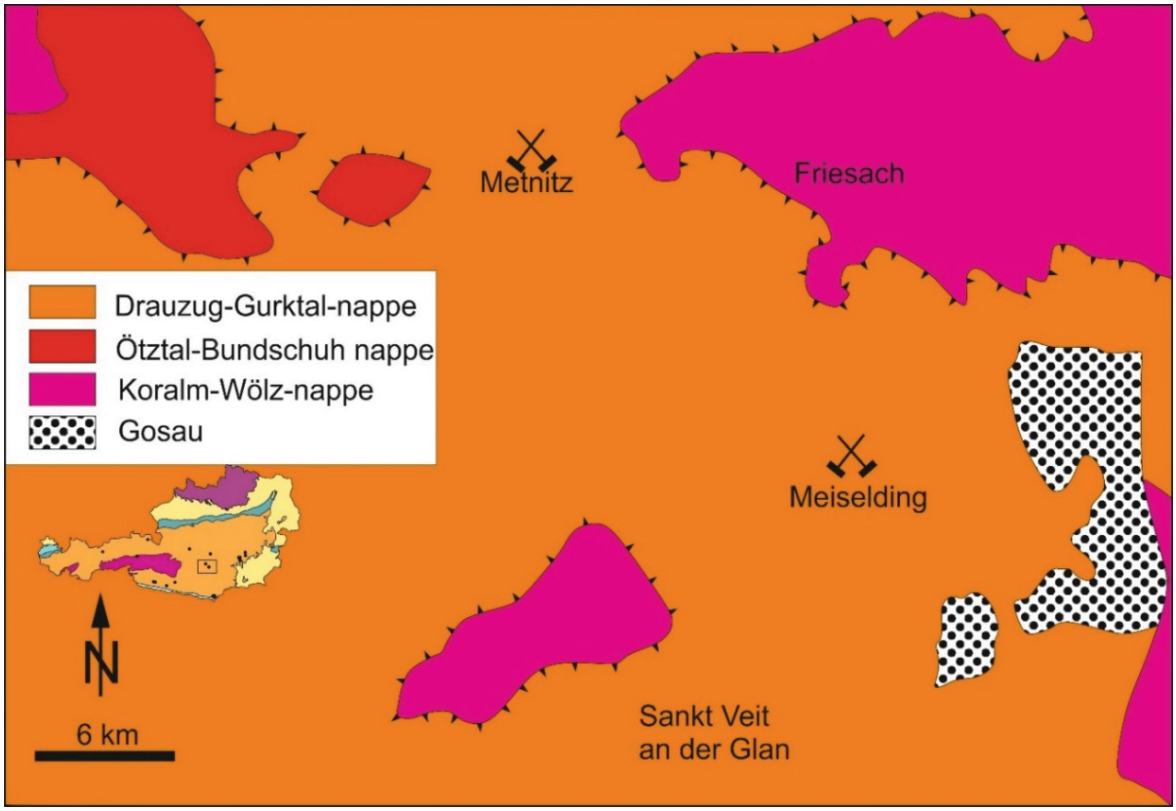

Fig. 9: Simplified geological sketch of a part of the Paleozoic Drauzug-Gurktal nappe system next to the city of Sankt Veit an der Glan (modified after GBA: IRIS Online 2017). Crossed hammer symbols mark the Meiselding and Metnitz deposits.

For Metnitz values are reported for Ge 370 µg/g, Ga 200 µg/g, In 9 µg/g, Co 470 µg/g, Ag 66 µg/g and Cd 216 µg/g (Cerny, Schroll 1995), no reliable data exist for Meiselding.

4.1.4 Pb-Zn mineralizations hosted in the Habach Group

The Habach Group is part of the Obere Schieferhülle that together with the Untere Schieferhülle overlies the Zentralgneis core of the Tauern Window (Fig. 10). The vein-type Pb-Zn-fluorite mineralization Achselalm Flecktrogalm is hosted by the Venediger nappe system, a folded stack of nappes deformed to a duplex structure (Kozlik 2015). The Venediger nappe system shows tectonic boundaries to the Glockner- and Modereck nappe systems. The Subpenninic units were derived from the distal European continental margin or an island arc (Eichhorn et al. 2001) which was covered by post-Variscian sequences of the "Untere Schieferhülle", (Schmid et al. 2004). The metabasites of the Venediger nappe system host numerous mineralizations, e.g. the economic scheelite mineralization at Felbertal. Kreis and Unger (1971) describe the Achselalm and Flecktrogalm deposit as hydrothermal stratiform Pb-Zn-fluorite deposit of unknown age, which was sporadically mined from medieval times up to 1946 (Feitzinger et al. 1998). The NE-SW striking mineralization shows a thickness of maximum 3 m, and is intercalated parallel to Habach phyllite and amphibolite. The deposit is divided into two separate tunnels divided at the surface by an avalanche corridor. The ore paragenesis consists of galena, yellow to dark brown sphalerite, fluorite calcite and quartz as gangue minerals.

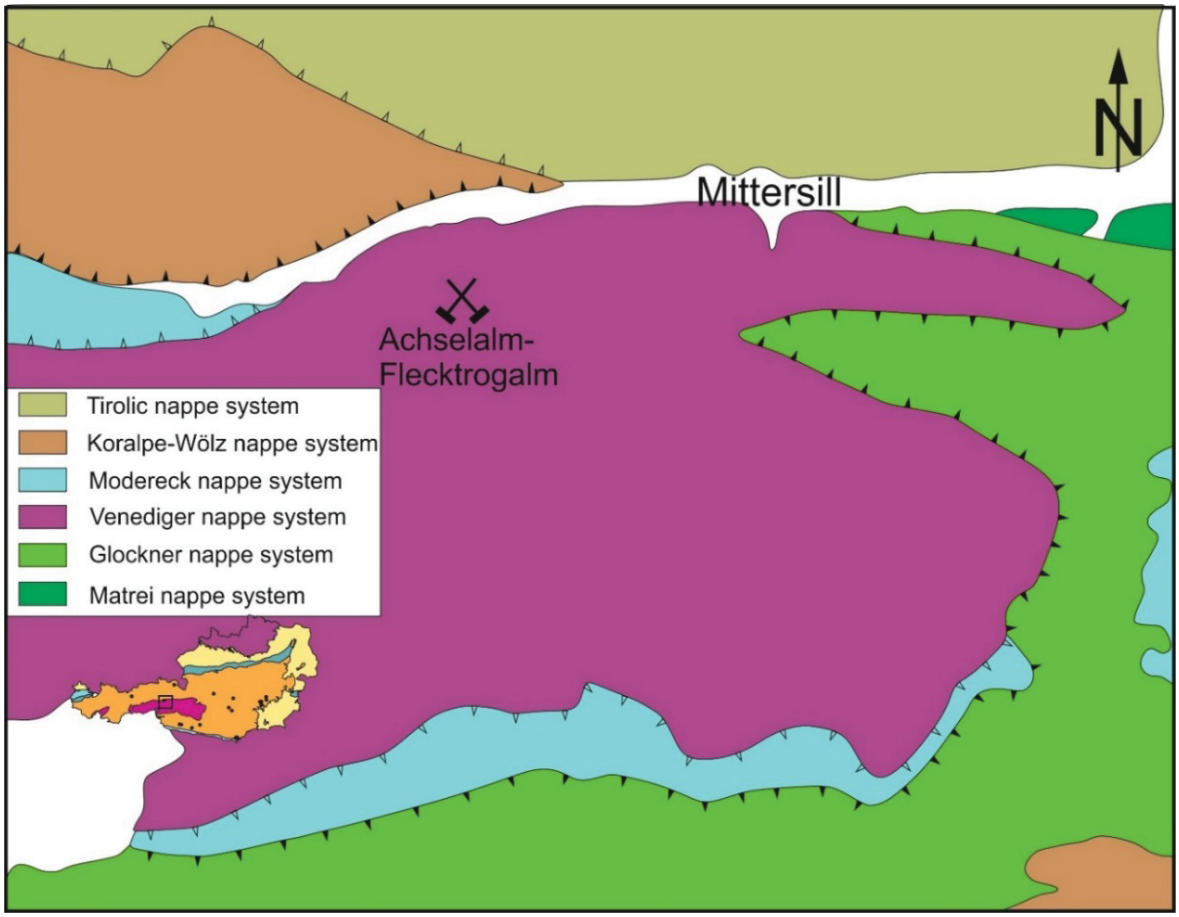

Fig. 10: Simplified geological sketch of a part of the Subpenninic Habach group next to the city of Mittersill (modified after GBA: IRIS Online 2017). Crossed hammer symbol marks the Achselalm Flecktrogalm deposit.

No reliable trace element data exist for the Achselalm/Flecktrogalm.

4.1.5 BMS mineralization Walchen

The stratiform BMS mineralization Walchen is located in Ennstal phyllites, a part of the Koralm-Wölz nappe system (Keil, Neubauer 2011). Schlüter et al. (1984) classify the Walchen mineralization as an intracontinental stratiform sedimentary submarine exhalative volcanic deposit related to a Paleozoic rift system leading into a small basin with oceanic crust similar to the recent Red See. The ore horizons lie concordant in the Ennstal phyllites above of the paragneisses of the Koralpe-Wölz nappe (Fig. 11) (Unger 1969). It consists of five 1-2m thick layers of massive to disseminated pyrite-pyrrhotite-chalcopyrite and sphalerite ore occurring within phyllite (Fig. 11).

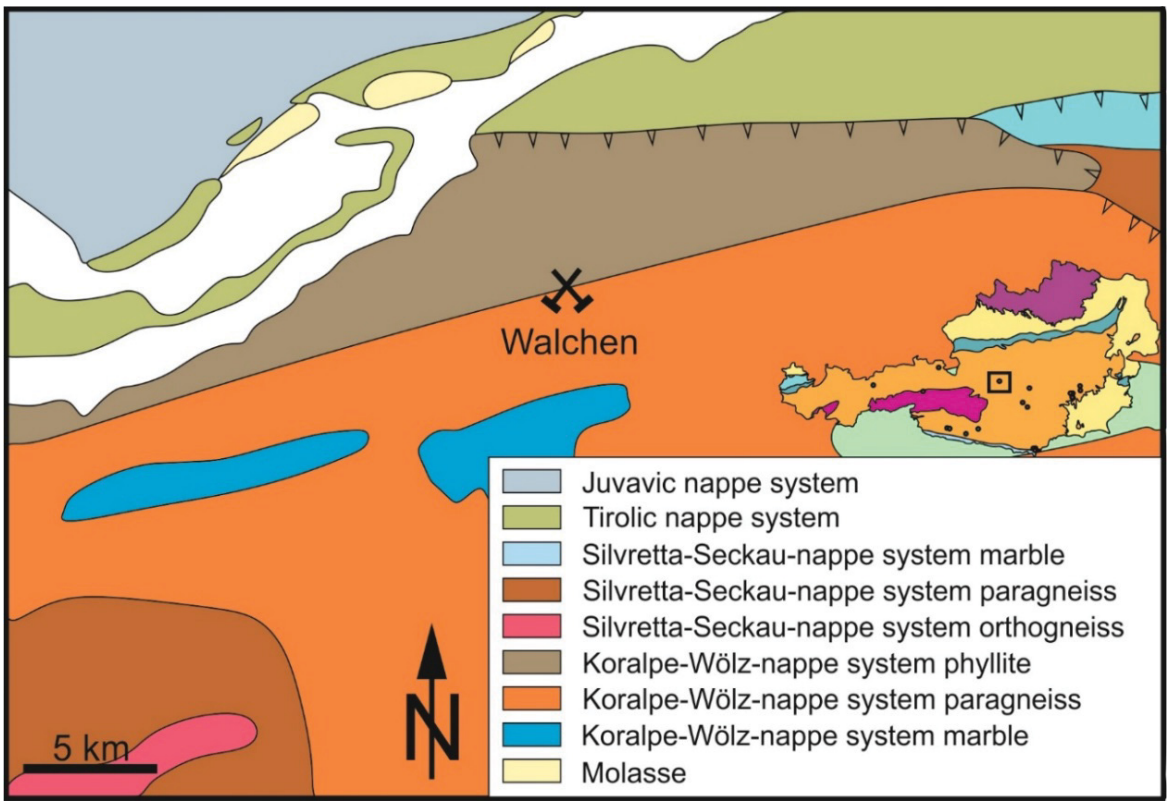

Fig. 11: Simplified geological sketch of a part of the Koralpe-Wölz- nappe system (modified after GBA: IRIS Online 2017). Crossed hammer symbol marks the Walchen deposit.

4.1.6 The Cu-Ni-Co mineralization Leogang-Schwarzleo

The Cu-Ni-Co mineralization Leogang-Schwarzleo was sporadically mined from 15th to the 19th century (Mostler 1967). It is hosted by upper Silurian-Middle Devonian dolomite (Südfazies-Dolomit) at the border to the Ordovician Wildschönau Schiefer of the Graywacke Zone with enrichment near the major Leogang thrust fault (Haditsch, Mostler 1970; Paar, Chen 1986) (Fig. 12). Paar and Chen (1986) identified in the dolomite matrix two ore types: type 1 is Cu-Fe-Ni (Co)-(Pb)-Sb dominated with the sulfide/ sulfosalt paragenesis bornite, chalcopyrite, tetraedrite and pyrite (high temperature mineralization), type 2 is Pb-Au-Cu-Hg dominated (low temperature mineralization) with the paragenesis bornite, pyrite, chalcopyrite and balkanite. The Ge sulfide renierite has been described by Paar and Chen (1986); Cerny and Schroll (1995) reported high Ge (700 µg/g) values in fahlore from the Leogang-Nöckelberg unit.

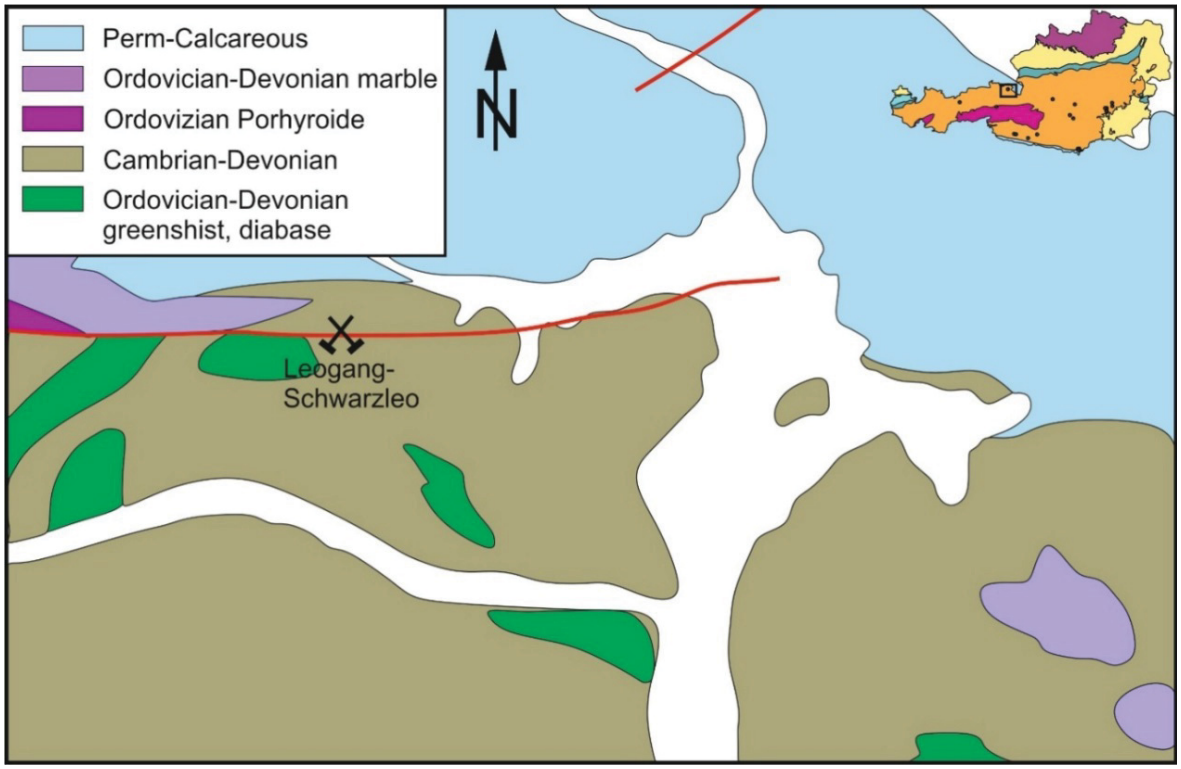

Fig. 12: Simplified geological sketch of a part of the Greywacke zone next to the village of Leogang (modified after GBA: IRIS Online 2017). Crossed hammer symbol marks the Leogang-Schwarzleo deposit.

4.1.7 Koprein

The mineralization of Koprein is located in the Leppen Valley, east to Eisenkappel (Fig. 13)in the Eisenkappel diabase formed at lower Visean time as a result of Variscian active plate margin a collisional regime following the extensional tectonic at the border between Devonian and lower carboniferous time (Schönlaub, Histon 1999). The mineralization is intercalated in south dipping greenschist and diabase (Cerny et al. 1982). The mineralization occurs as three veins of unknown age, hosted by greenschist. Cerny et al. (1982) found two short (30 m) tunnels in a distance of 10 m and described the thickness of the veins as 1.5 to 3 m. Hand specimen collected at the dumpsite carry galena and sphalerite rich brecciated ore in a white calcite and quartz matrix.

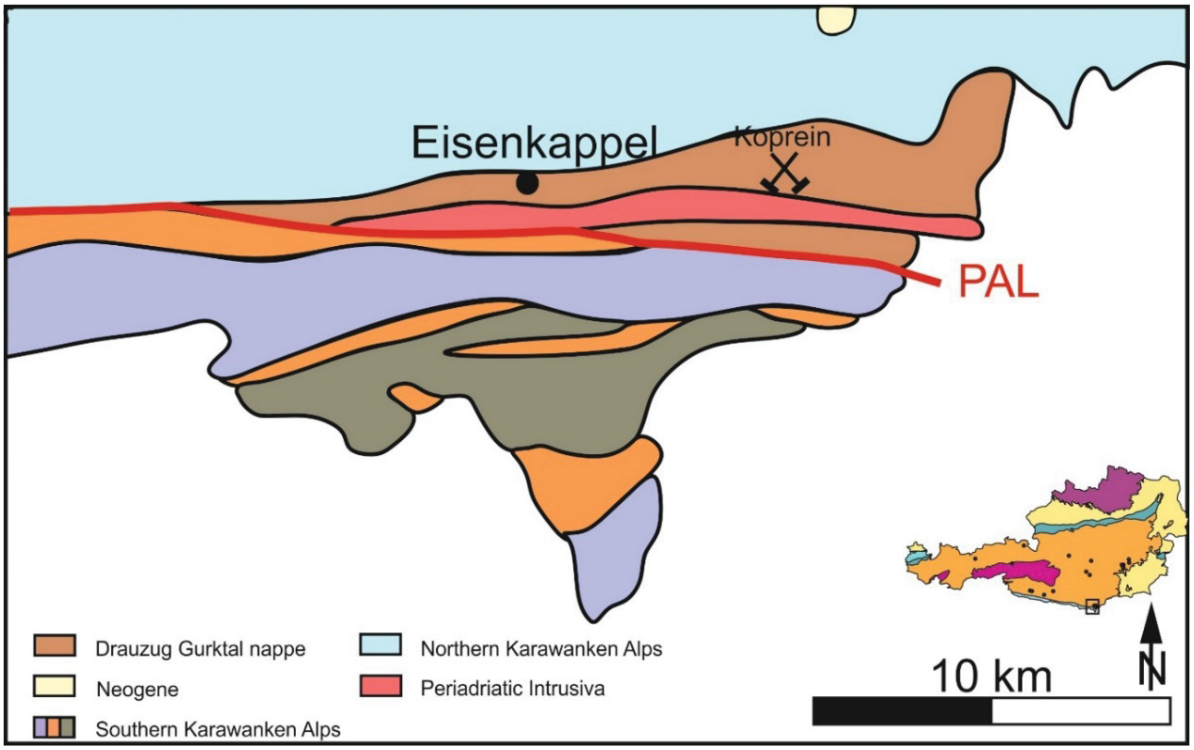

Fig. 13: Simplified geological sketch of the Southern Karawanken Alps (modified after GBA: IRIS Online 2017). Crossed hammer symbol marks the Koprein deposit.

4.1.8 Additional Samples

Brenntal/Mühlbach (Salzburg)

The vein-type deposit Brenntal/Mühlbach (IRIS No. 1749) is located in the south of the Salzach valley at the border between the `Schieferhülle`of the Tauernwindow (Subpeninnic) and the Quartzphyllite zone (Lower Austroalpine). The country rock consists of Proterozoic to Palaeozoic volcanosedimentary rocks of the Habach formation (Feitzinger et al. 1998). On pyrite-rich sample collected on the old dumps and donated by H. Grill, 12 analyses were performed.

Sprinzgasse (Salzburg)

The stratiform Pb-Zn mineralization Sprinzgasse (IRIS No. 2629) is hosted by graphitic quartzite and black schist of the Venediger Nappe system of the Subpenninic unit (Murtörlserie, Upper Carboniferous). The three analysed samples carry: chalcopyrite, pyrite, galena, sphalerite and gold are derived from the W. Paar collection (MUL). On these samples 60 in-situ analyses were performed.

Seibach-Griesbach

The stratiform and strata-bound Seibach Griesbach Fe-Pb-Zn-(Mo) mineralization is hosted by the dark Anisian ´Basisdolomit` of the Brenner Mesozoic overlying the Oetztal-Stubai crystalline complex, as part of the Upper Austroalpine unit (Melcher and Krois 1992). Three samples composed of pyrite, galena and sphalerite (54 in-situ analyses) from the F. Melcher (MUL) collection were analysed (Melcher and Krois, 1992). Sulphur isotope values of ore samples range from -20 to -34.6 ‰ (Melcher, Schroll E., unpublished data in Weber, Cerny 1997). The ores have low trace element concentrations, but carry elevated Mo (up to 50 ppm) as molybdenite flakes in pyrite. Oxidised goethite-rich ores have up to 800 ppm Mo.

Drassnitz (Carinthia)

The Ag bearing vein-type base metal deposit of Drassnitz is located in the Early Paleozoic “Altkristallin” of the Austroalpine Kreuzeck Massif. The mineralization occurs as bundles of quartz veins in altered phyllites (Feitzinger et al. 1995). Feitzinger gave a K/Ar age for this pyrite rich, pyrrhotite chalcopyrite sphalerite and galena bearing mineralization of 30-40 million years. The investigated samples were collected by F. Melcher at a surface outcrop close to Hubertushaus. 20 analyses were made on 1 samples.

Mezica (Slovenia)

The Mezica deposit is hosted in the upper 600m of the Ladinian to early Carnian Wetterstein formation of the Northern Karawanken Mountains that are part of the Austroalpine Drau Range. The mineralization is hosted in the carbonates as stratabound, brecciated and vein like ore bodies (Cerny 1989). The two analysed samples (47 analyses) were taken from BGR collection.

Raibl (Italy)

The Pb-Zn province Raibl is located south of the city Tarvisio. The orebody is hosted by the `Ugovizza Breccia` which is part of the Anisian limestone of the South Alpine unit (Cerny 1989).

The Carnian Raibl formation consists in the area of the orebody of the upper and lower `Dolomita Metallifera (Cerny 1989b). Eight samples (224 analyses) were taken from the MUL and BGR collections. An exact allocation of the samples was not possible.

Salafossa (Italy)

The carbonate hosted Pb-Zn mineralisation of Salafossa is mainly restricted to the South Alpine `Cassian Dolomite` (Ladinian, Carnian), The stock-like orebody had been mined from 1957 until it was depleted in 1986 yielding 10 million tons of ore (Cerny 1989). 20 analyses were performed on one sample of the BGR collection.

Schneeberg (Italy)

The stratiform sediment hosted Pb-Zn deposit Schneeberg is hosted by muscovite-rich and/or albite bearing micaschists, paragneises and graphite-schists of the polymetamorphic Oetztal-Stubai Complex in the northern Part oft South Tyrol (Holzman and Tropper 2013). 70 analyses were performed on 4 samples provided by F. Melcher, MUL.

5 Results

5.1 Petrography and sample description of Mesozoic carbonate-hosted Pb/Zn mineralizations

5.1.1 Jauken

The collected samples from the Jauken waste dump can be divided in two groups by the crystal size of the carbonate matrix, fine-crystalline (Fig. 14b) and coarse-crystalline calcite (Fig. 14a) (up to 2 mm). The grain size of the matrix is also reflected in the crystal size of the sphalerite. Sphalerite surrounded by fine-grained calcite shows smaller groups than the sphalerite in coarse-grained matrix. Coarse-grained sphalerite shows rims of fine-grained sphalerite (Fig. 14d). Some samples show nests of idiomorphic to hypidiomorphic sphalerite (Fig. 14c). The samples are poor in galena and the sphalerite is free of other sulfide mineral inclusions but shows many dark mono-phase gas and two-phase liquid-rich inclusions.

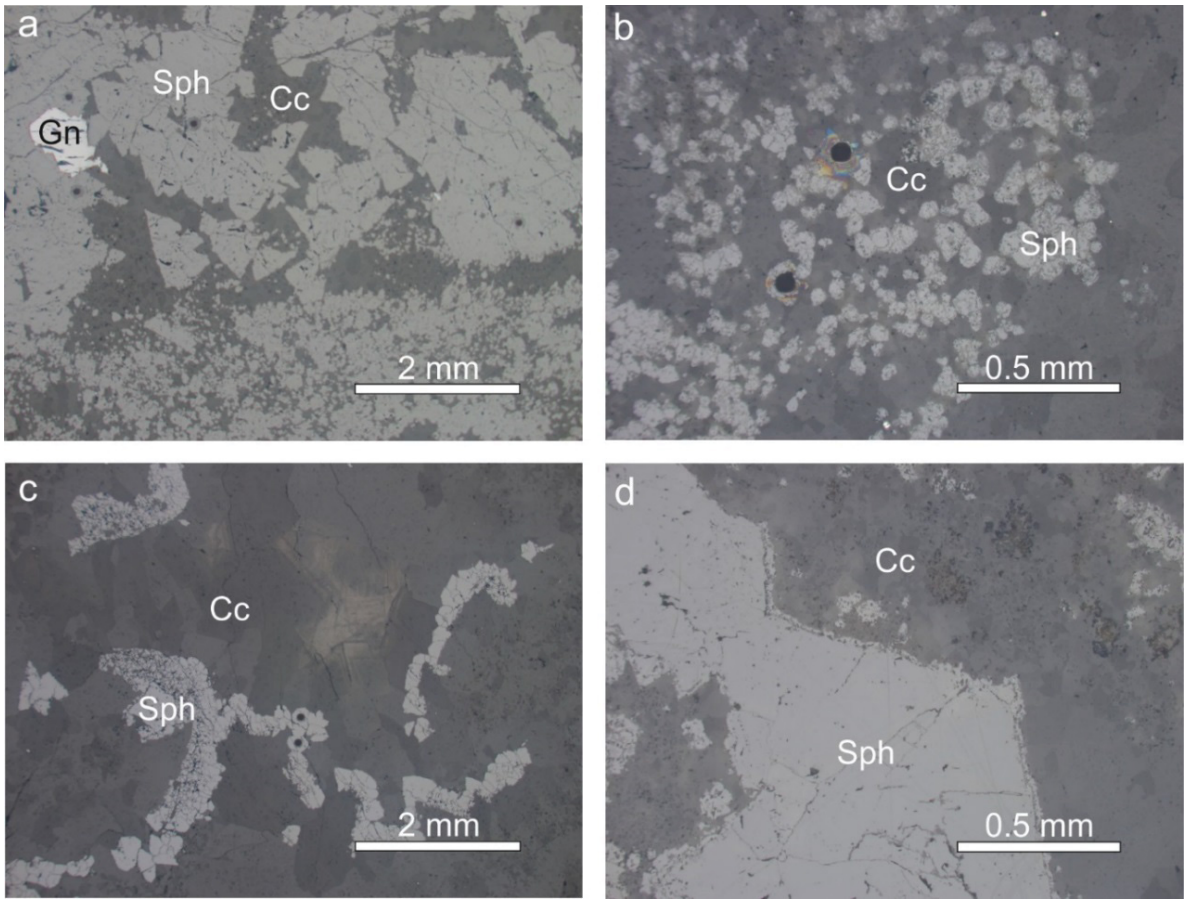

Fig. 14: Reflected light microscope images from the Jauken dumpsite a: coarse and fine-grained sphalerite surrounded by coarse and fine-grained calcite (JS 1). b: fine-grained colloform sphalerite (JS 5). c: cords of sphalerite in calcite matrix (JS 8). d: large sphalerite crystals surrounded by a fine-grained sphalerite rim (JS 10).

5.1.2 Radnig

The investigated samples collected from the tailings of the Kaiser Leopold adit shows two different ore types:

1. Rhythmic layers (zebra ore) of calcite, barite, and yellow, inclusion-free hypidiomorphic sphalerite (Fig. 15a).

2. Brecciated ore consisting of calcite, barite, fluorite, sphalerite and galena (Fig. 15b).

The sphalerite occurs in two color varieties, yellow and brown. The yellow sphalerite is linked to large calcite crystals, the brown sphalerite to small (sugar like) calcite.

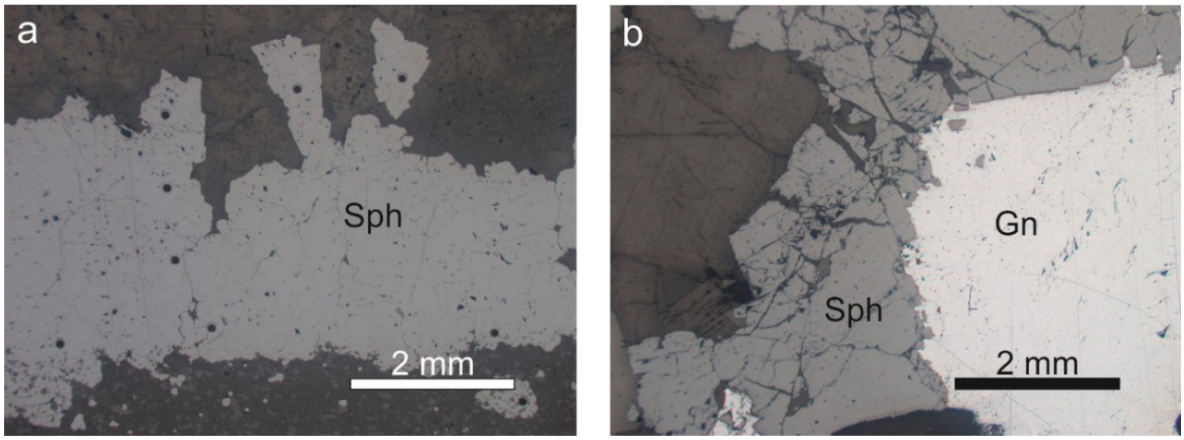

Fig. 15: Reflected light microscope images from the Radnig dumpsite a: layer of hypidiomorphic sphalerite in calcite matrix (Ra 5). b: brecciated sphalerite intergrown with galena (Ra 16).

5.1.3 Bleiberg-Kreuth

The investigated samples show two different types of sphalerite, colloform sphalerite (Fig. 16a) and sphalerite– galena breccia with carbonate matrix (Fig. 16b). The ore consists mainly of carbonate matrix, sphalerite, galena, pyrite and marcasite. Sphalerite crystals are often tectonically stressed and show cracks that are filled with carbonate. The color of the colloform sphalerite ranges from creamy white to middle brown. The sphalerite crystals of the brighter zones are larger (up to 1.5 mm) and the darker zones show small sphalerite crystals (up to 20µm) and pyrite/ marcasite contamination (Fig. 17a). The bright colloform sphalerite species is nearly free of inclusions, whereas the darker one shows pyrite, marcasite and galena inclusions.

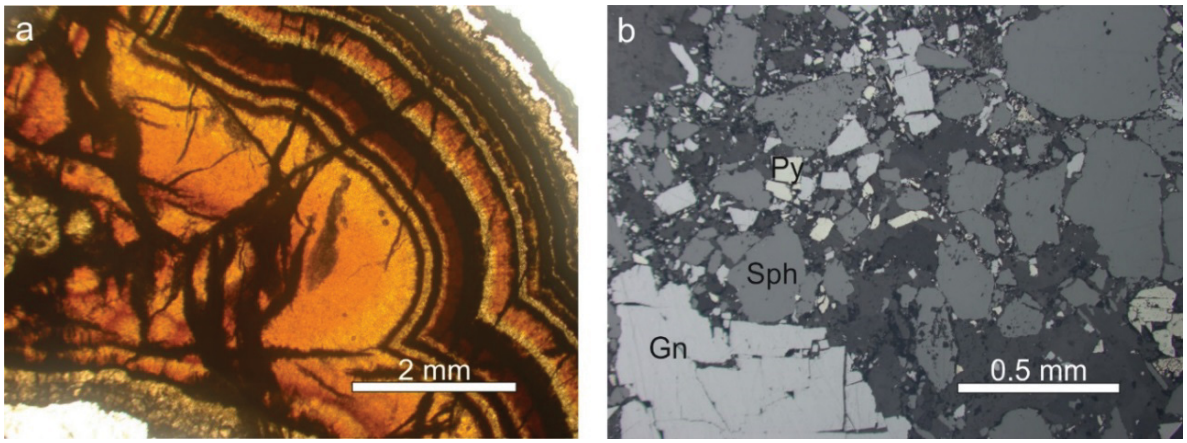

Fig. 16: a: transmitted light microscope images of colloform sphalerite (BB 10), b: reflected light microscopy image of sphalerite, pyrite and galena breccia in carbonate matrix (BB 11).

Pyrite occurs as rims in and around the colloform sphalerite and galena (Fig. 17a), and as idiomorphic small (up to 20µm) discrete minerals in the carbonate matrix (Fig. 17b).

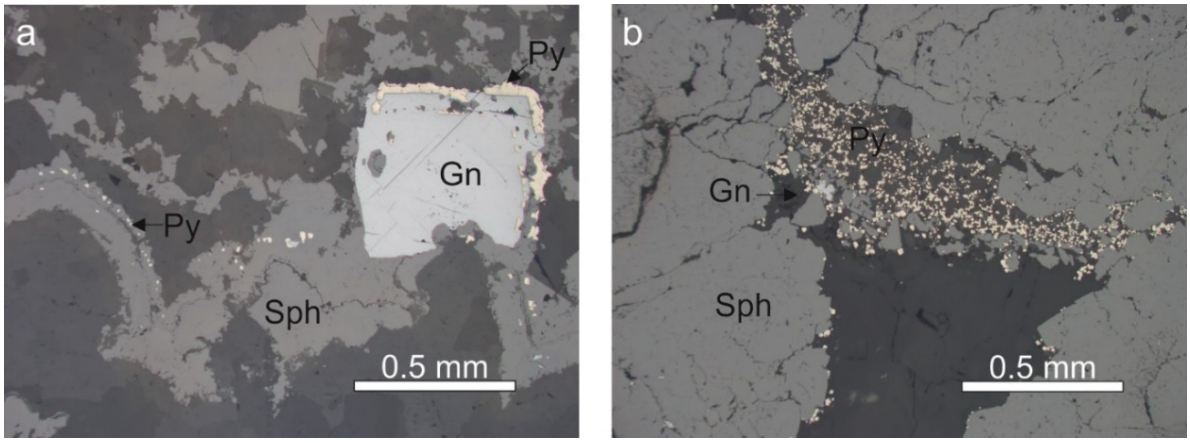

Fig. 17: Reflected microscope images of a: colloform sphalerite and idiomorphic galena with pyrite rim (BB-K 6), b: idiomorphic pyrite hosted in carbonate vein (BB-K 3).

Galena can be found as idiomorphic to xenomorphic crystals in colloform sphalerite (Fig. 17a), as breccia next to sphalerite in calcite matrix (Fig. 16b) and as skeleton crystal (Fig. 18b).

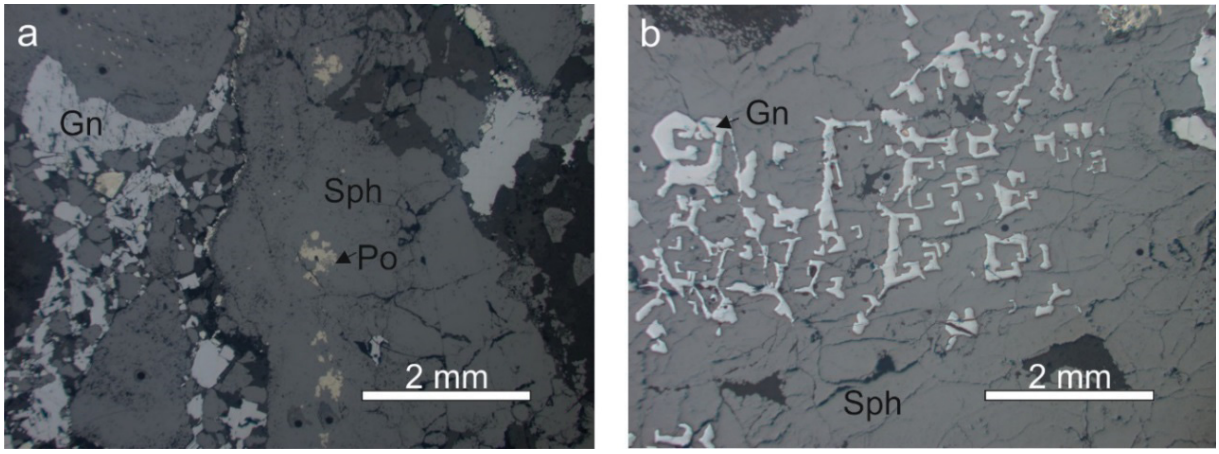

Fig. 18: a: idiomorphic to xenomorphic galena crystals (BB 11-4). b: galena skeleton crystals in sphalerite (BB 12)

5.1.4 Fladung (Hochobir)

Samples collected from the dumpsite of Fladung show three different types of sphalerite:

1. large and small idiomorphic sphalerite (Fig. 18a, c).

2. massive bands of brecciated brown sphalerite with galena inclusions (Fig. 18b).

3. colloform sphalerite, ranging from creamy white over bright brown to dark brown color, showing pyrite inclusions at the border to the carbonate (Fig. 18d).

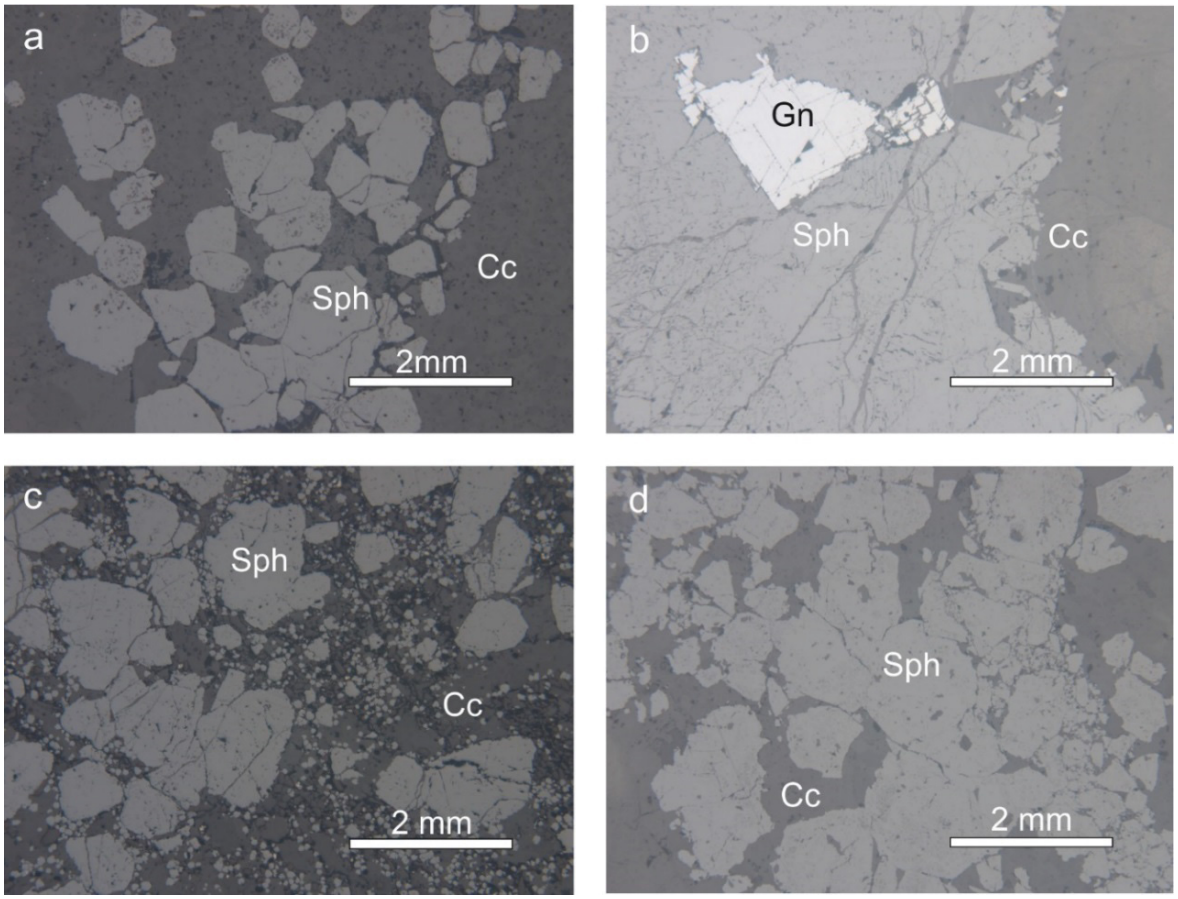

Fig. 19: Reflected light microscope images of ores from the Fladung dumpsite a: idiomorphic sphalerite crystals in calcite matrix (Fl 5). b: massive brecciated sphalerite band with galena (Fl 22). c: two generations of large hypidiomorphic sphalerite and fine crystalline sphalerite (Fl 7). d: large colloform sphalerite crystals (Fl 22).

5.1.5 Lafatsch

The Lafatsch samples mostly from the Stefanie adit (complete list see appendix) provided by the Leopold Franzens University of Innsbruck (Austria; Oskar Schulz collection) shows three different sphalerite varieties:

1. Massive colloform inclusion-free sphalerite that is brecciated perpendicular to the surface between calcite and sphalerite; the cracks are filled with calcite (Fig. 20a).

2. Colloform sphalerite showing a rhythmic layering of large (yellow) and small (brownish) sphalerite grains. Size and color of the sphalerite is related to the size of calcite (Fig. 20b).

3. Strongly brecciated sphalerite with galena as seam between sphalerite and calcite.

Some samples show framboidal pyrite as void filling (Fig. 20d).

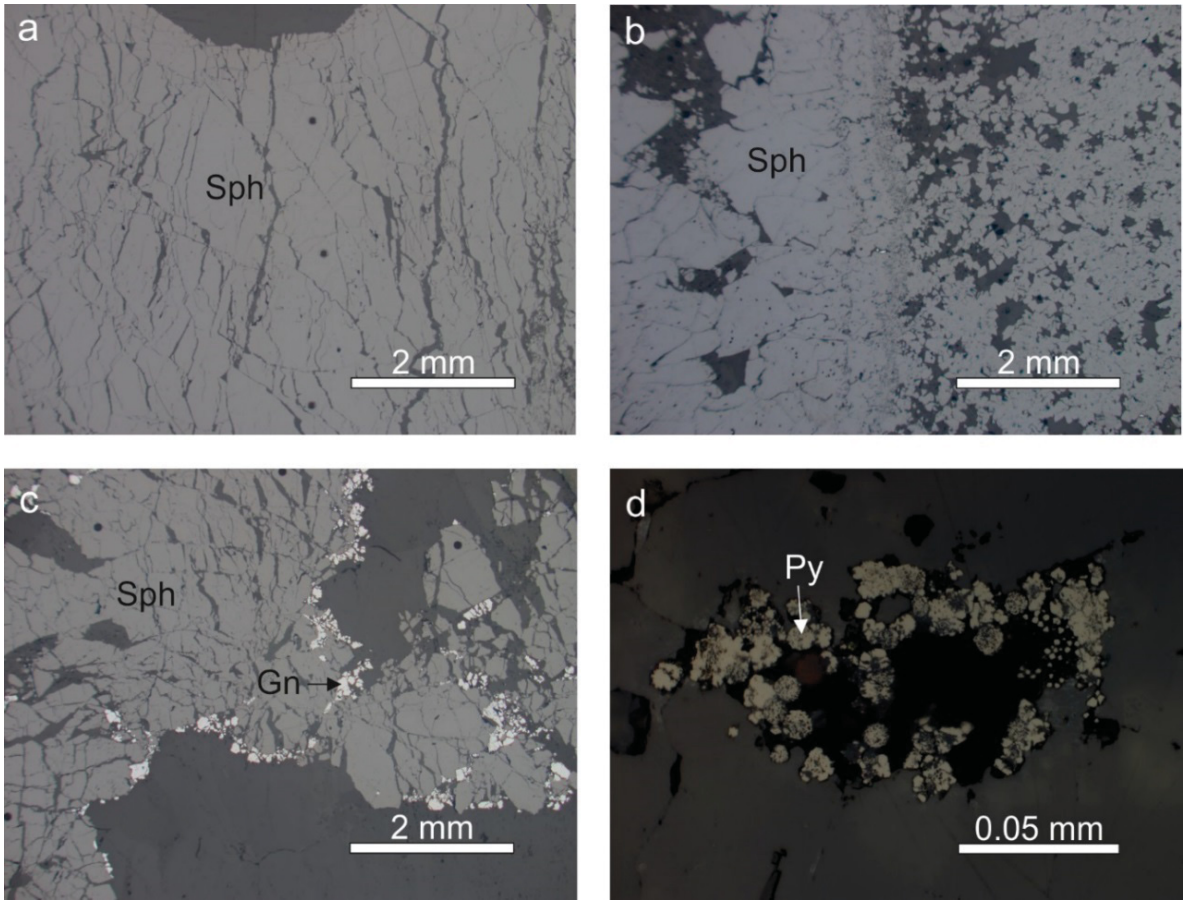

Fig. 20: Reflected light microscope images from Lafatsch. a: brecciated colloform sphalerite (LaT 1). b: transition between large colloform sphalerite and fine crystalline sphalerite (LaT 21). c: brecciated sphalerite with galena seam (LaT 3). d: nest of framboidal pyrite in calcite matrix (LaT 13).

5.2 Petrography and sample description of Paleozoic Pb/Zn mineralizations

5.2.1 Guggenbach

The carbonate bearing phyllite from Guggenbach, collected at the dumpsite near the Poyd farm is pyrite dominated; sphalerite, galena and pyrrhotite are minor minerals. Pyrite appears, as idiomorphic crystal close to the border of sphalerite (Fig. 21a), as idiomorphic to hypidiomorphic minerals in the host rock (Fig. 21d) and as inclusion in sphalerite (Fig. 21a). Sphalerite forms layers (Fig. 21a), diffusely distributed and as vein filling (Fig. 21b). Galena can be found as discrete crystals, as inclusion in sphalerite and as vein filling (Fig. 21b, c). Pyrrhotite occurs as discrete mineral in the host rock and as inclusion in sphalerite (Fig. 21a).

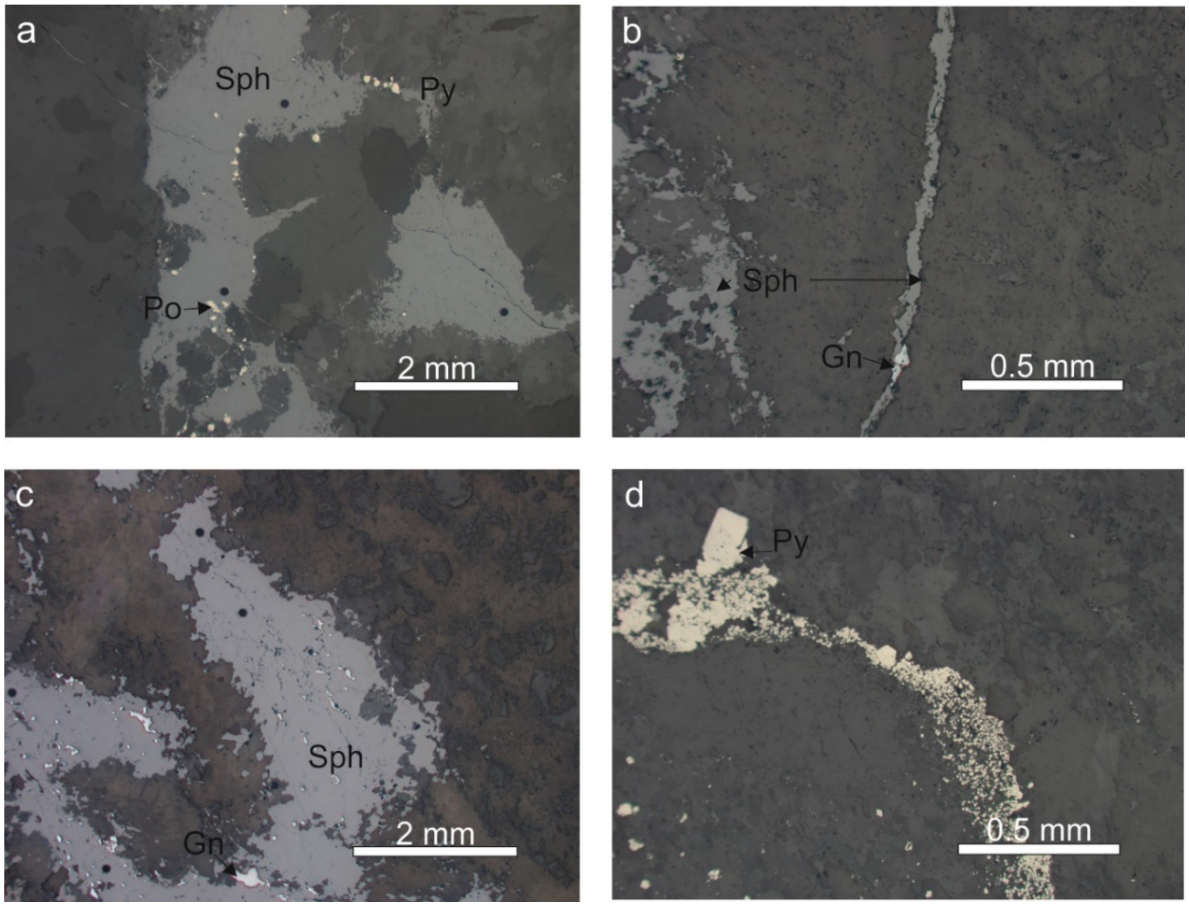

Fig. 21: Reflected light microscope images from the Guggenbach adit. a: large (up to 5 mm) xenomorphic sphalerite crystals with pyrite seam and pyrrhotite inclusions (GB 1). b: xenomorphic sphalerite grains (left) and vein filling of sphalerite and galena (GB 1). c: sphalerite with galena inclusions (GB-P 1). d: idiomorphic pyrite (GB-P1).

5.2.2 Arzberg

The samples from the Raab adit (chlorite schist and black schist) show folded massive sphalerite layers (Fig. 22a) and individual sphalerite crystals (Fig. 22c) concordant to the schistosity. Sphalerite is associated with galena, pyrrhotite and pyrite (Fig. 22b). Pyrrhotite occurs as idiomorphic to hypidiomorphic minerals next to and within sphalerite (Fig. 22b). Pyrite can be found as idiomorphic to hypidiomorphic mineral and as vein filling (Fig. 22d)

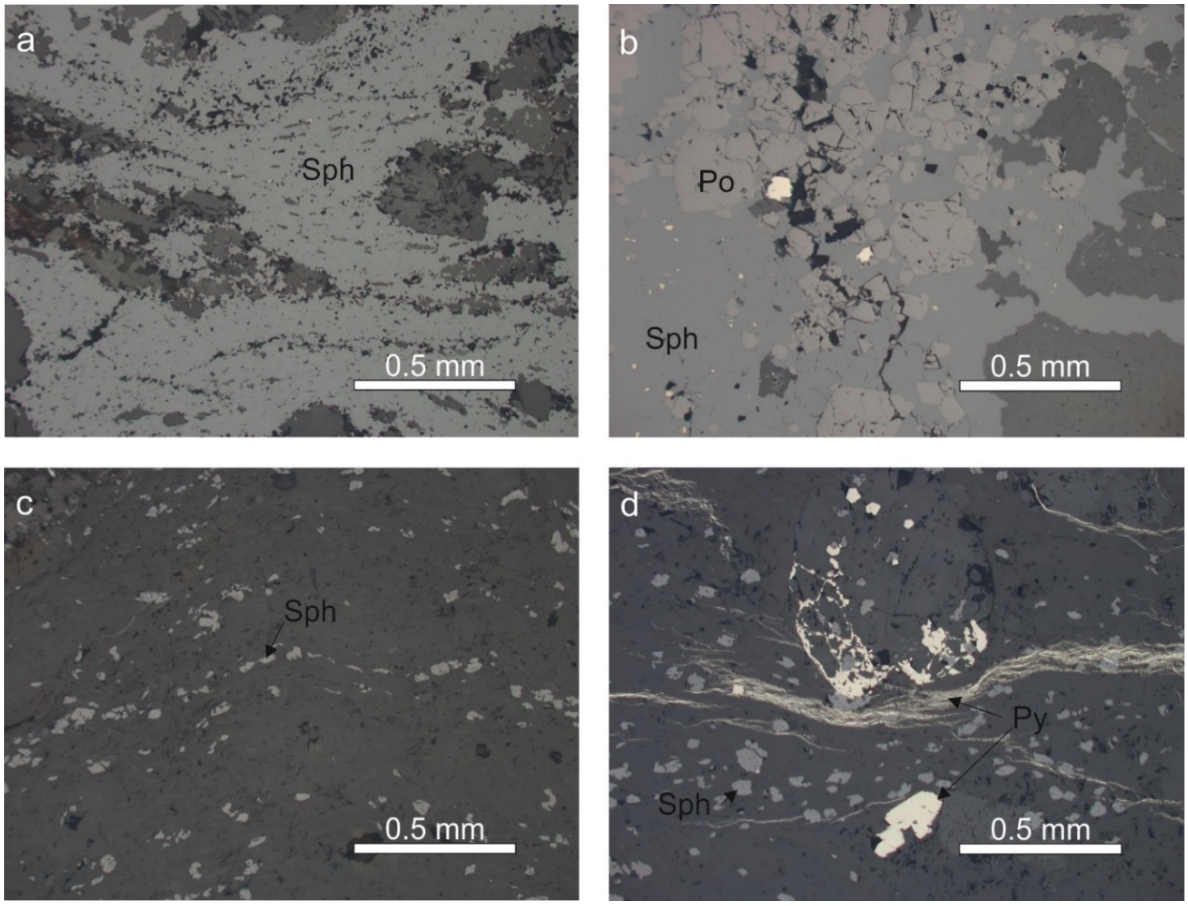

Fig. 22: Reflected light microscope images from the Arzberg adit. a: massive sphalerite layers concordant to the schistosity with small pyrrhotite inclusions (AB 1-1). b: massive sphalerite with idiomorphic to hypidiomorphic pyrrhotite and pyrite grains (AB 3-19). c: small (0.05 to 0.1 mm) idiomorphic to hypidiomorphic sphalerite grains concordant to the schistosity (AB 1-1). d: idiomorphic to xenomorphic pyrite as discrete minerals and as network like vein filling (AB 6).

5.2.3 Rabenstein

Ore samples collected at the dumpsite of Rabenstein show carbonate and barite bearing phyllite as host rock, carrying hypidiomorphic to xenomorphic crystals associated with galena and pyrite. Sphalerite occurs in massive folded layers and as single minerals (Fig. 23a, d). Galena can be found as gap filling (Fig. 23b) and as inclusion in sphalerite (Fig. 23c). Pyrite exists as discrete mineral in the host rock (Fig. 23a), as inclusion in sphalerite (Fig. 23c) and as seam at the border between sphalerite and the host rock (Fig. 23d).

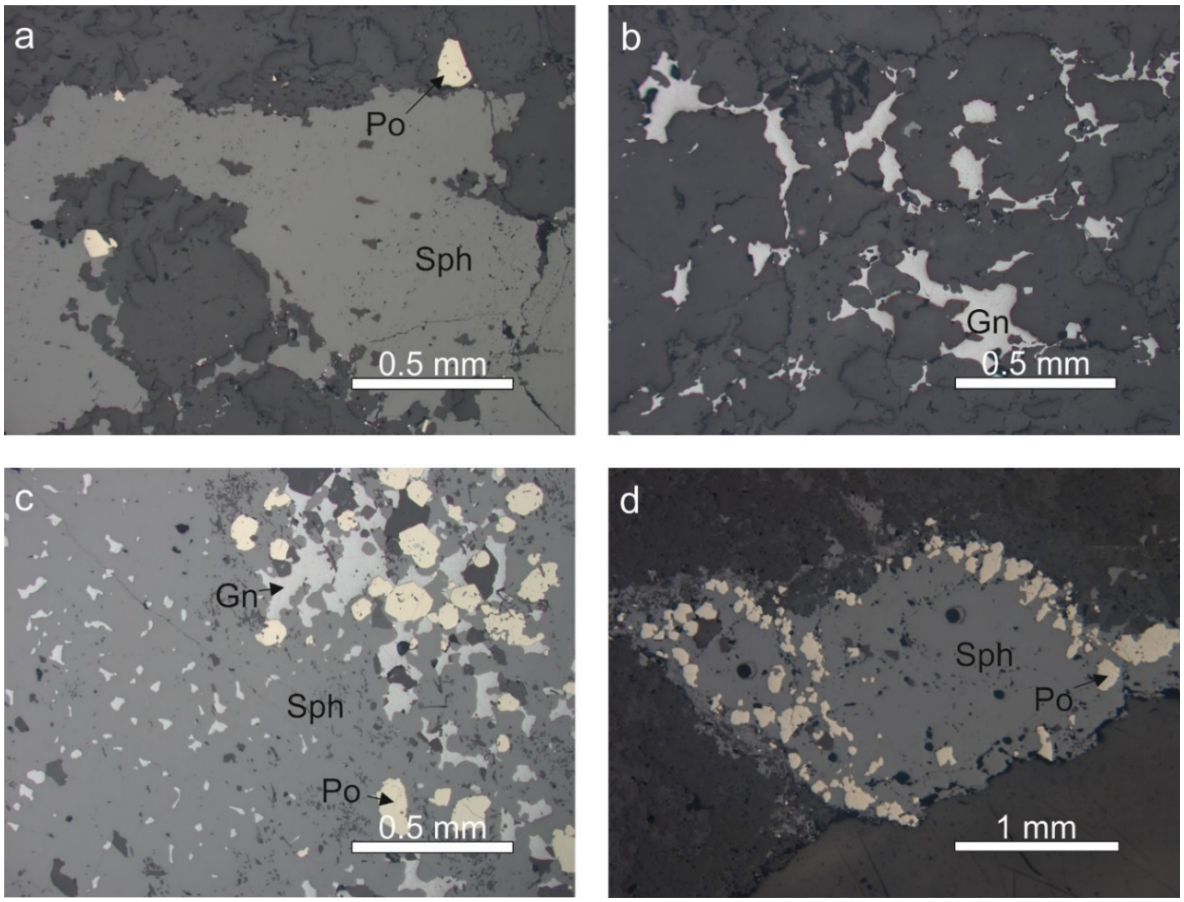

Fig. 23: Reflected light microscope images from the Rabenstein adit. a: massive sphalerite hosted in shale, pyrite occurs as idio.- hypidiomorphic minerals in the host rock and as inclusions in sphalerite (RaD 1). b: Galena as filling between quartz and carbonate (RaD 1). c: massive sphalerite with galena and pyrite inclusions (RaD 7). C: Sphalerite grains with pyrite seam (RaD 8).

5.2.4 Elisabeth Adit

Sphalerite hosted in carbonate bearing phyllite as hypidiomorphic crystals associated with galena, pyrite, pyrrhotite and marcasite gives evidence of at least four mineralization events. Sphalerite occurs as concordant mineralization and as mineralization around carbonate and quartz (Fig. 24a, b). Galena exists mostly as gap filling between calcite or vein filling and as inclusions in sphalerite (Fig. 24d). Pyrrhotite crystals can only be found as inclusions in sphalerite, whereas pyrite is present as idiomorphic crystals in the host rock and as inclusions in sphalerite (Fig. 24c, d). The host rock mainly consists of idiomorphic to hypidiomorphic carbonate and quartz. Mica appears as layered aggregations and in the interstices between quartz and carbonate. The layered mica aggregates show a high amount of Ti-oxides (Fig. 24a). According to the mineral assemblage and textural occurrence, three different mineralization events can be identified.

1. Massive sphalerite concordant to the schistosity, showing galena inclusions, sphalerite surrounding quartz and carbonate crystals with no galena or pyrrhotite inclusions.
2. Small to medium sized hypidiomorphic sphalerite, with galena and pyrrhotite inclusions.
3. Fine-grained network-like galena inclusions replace the carbonate.

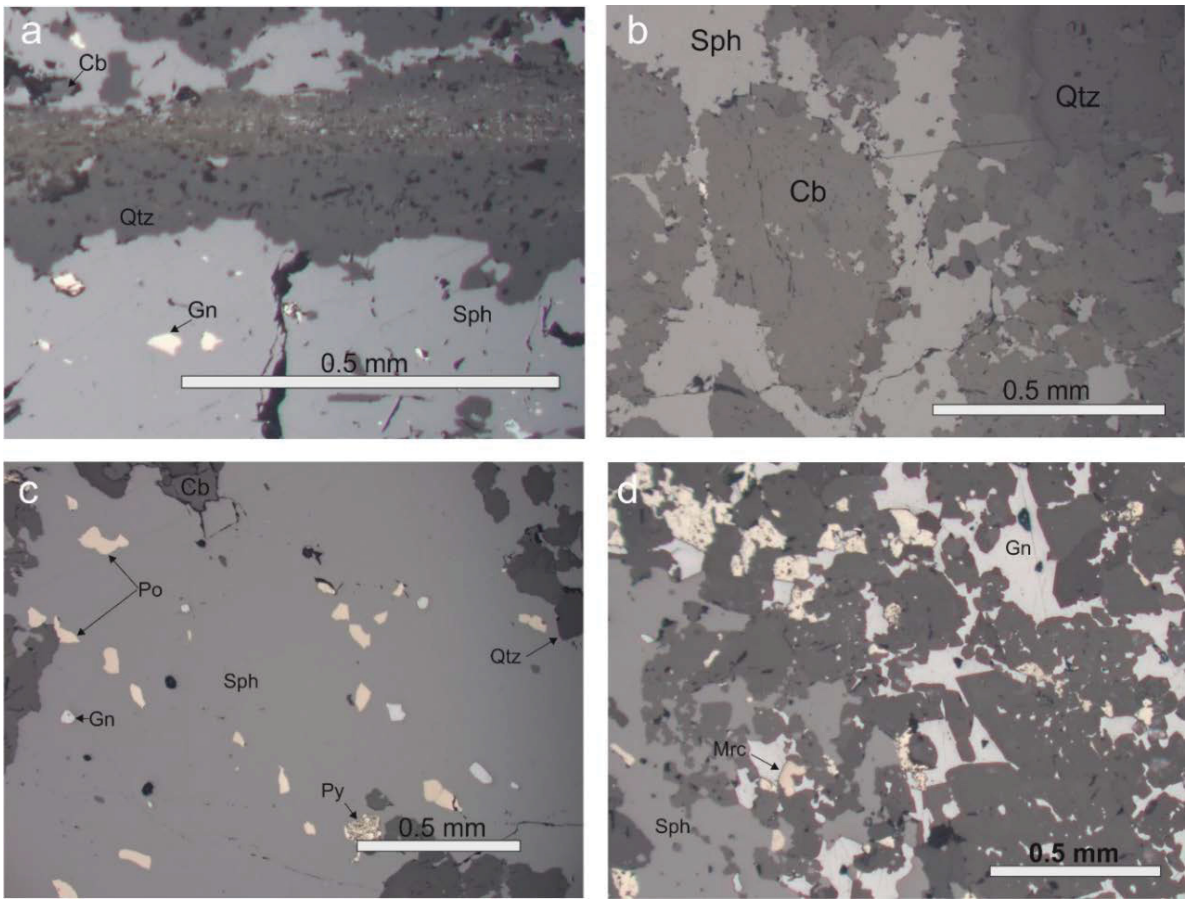

Fig. 24: Reflected light microscope images from the Elisabeth adit. a: concordant ZnS mineralization (ESD 6), b: ZnS mineralization surrounding carbonate minerals (ESD 3), c: Sphalerite crystal with galena, pyrrhotite and pyrite (ESD 1), d: galena as gap filling, pyrrhotite and pyrite (ESD 1).

5.2.6 Friedrich Adit

Hypidiomorphic sphalerite is hosted by carbonate bearing phyllite and is associated with galena, pyrite and pyrrhotite. Galena exists mostly as layer and as inclusions in sphalerite (Fig. 25a). Sphalerite exists as layers parallel to the schistosity (Fig. 25a), as large (up to 1.5 cm) undeformed minerals and as breccia (Fig. 25b,c). Pyrite and pyrrhotite can be found as inclusions in sphalerite and as idiomorphic to hypidiomorphic crystals in the host (Fig. 25d). The host rock mainly consists of idiomorphic to hypidiomorphic carbonate and quartz. Mica appears as layered aggregates and in the pendentive between quartz and carbonate.

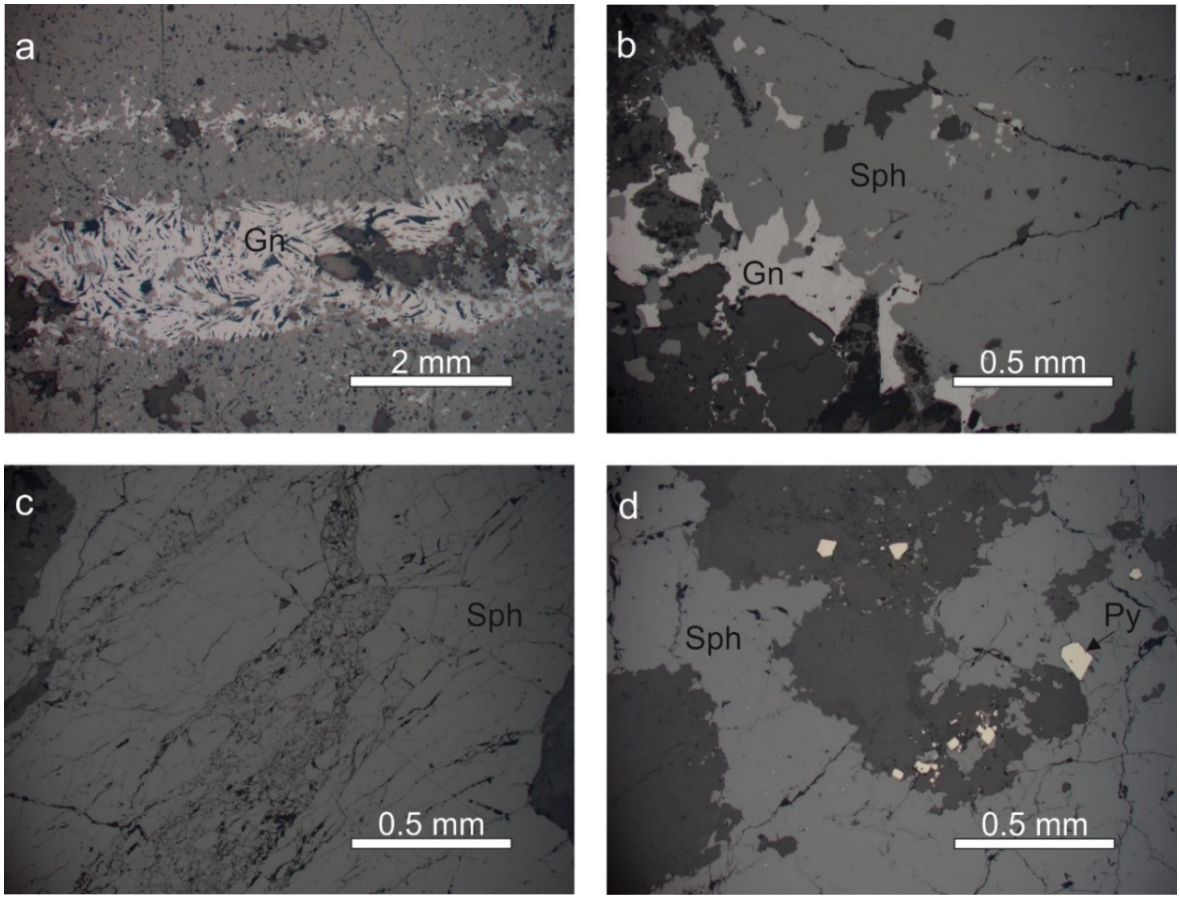

Fig. 25: Reflected light microscope images from the Friedrich adit. a: Galena as layers parallel to the schistosity (FSD 2). b: massive sphalerite with galena as inclusions and as discrete minerals at the border to the host rock (FSD 1). c: massive tectonically brecciated sphalerite (FSD 5). d: pyrite as discrete idiomorphic minerals hosted in gangue and as inclusion in sphalerite (FSD 6).

5.2.7 Silberberg

The barite bearing black shale collected in the Silberberg adit shows a rhythmic layering of sulfide minerals and the host rock. The sulfide paragenesis comprises sphalerite, galena and pyrite. Chalcopyrite exists as copper disease in sphalerite (Fig. 26c, d). Sphalerite can be found next to galena as massive layers and as distinct xenomorphic crystals (Fig. 26a). Pyrite occurs as idiomorphic to hypidiomorphic mineral next to sphalerite.

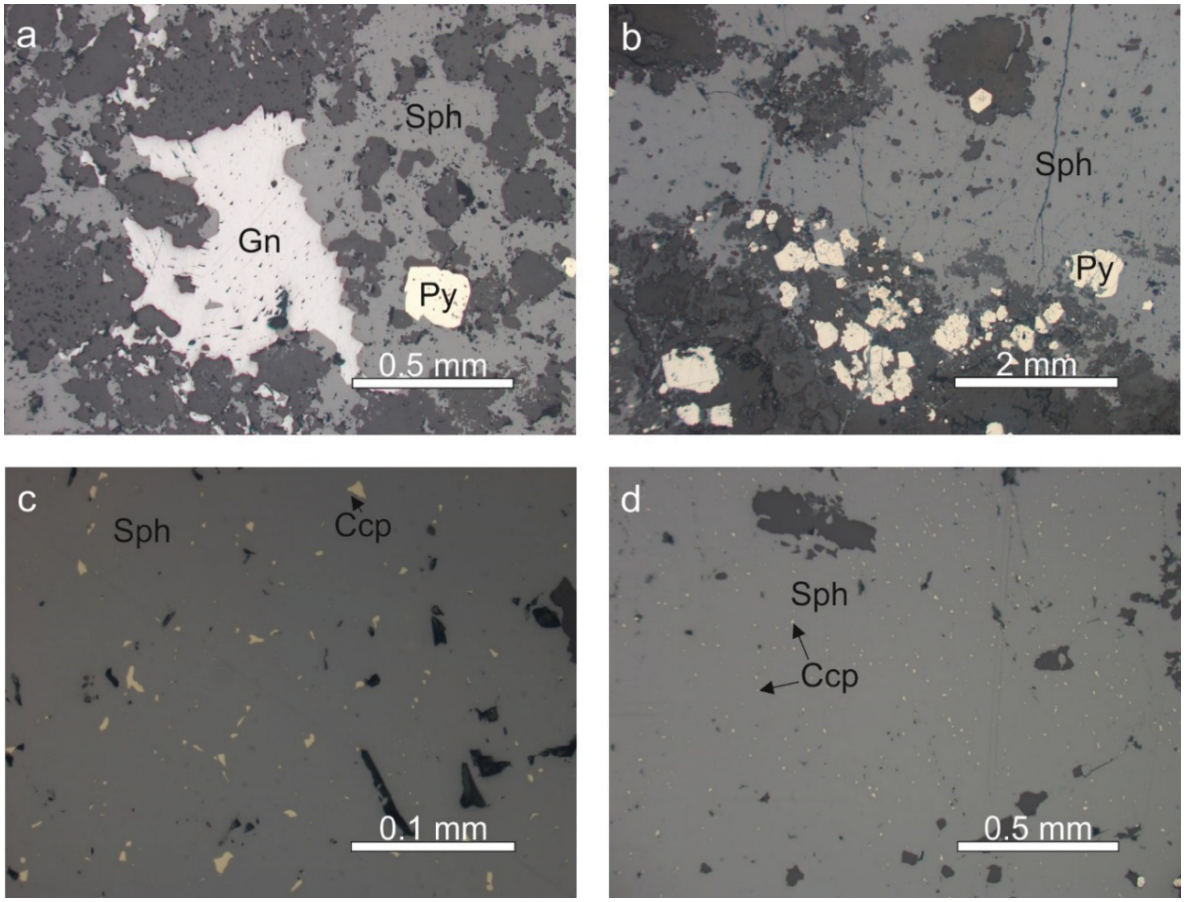

Fig. 26: Reflected light microscope images from the Silberberg adit. a: carbonate surrounded by inclusion free sphalerite, galena and an idiomorphic pyrite crystals (SB-600). b: massive sphalerite with hypidiomorphic pyrite (SB- EG). c: massive sphalerite with sporadic distributed chalcopyrite inclusions (SB EG). d: massive sphalerite with trail like copper-diseases (SB-EG).

5.2.8 Haufenreith

Sphalerite from Haufenreith occurs as folded massive layers parallel to the schistosity (Fig. 27a) and as distinct minerals in carbonate bearing phyllite (Fig. 27b). The layered sphalerite shows galena inclusions. Sphalerite is manly surrounded by altered pyrrhotite that shows birds eye structures (Fig. 27b). Most of the pyrites show cracks whereas the other sulfide minerals next to them are not tectonically affected (Fig. 27b).

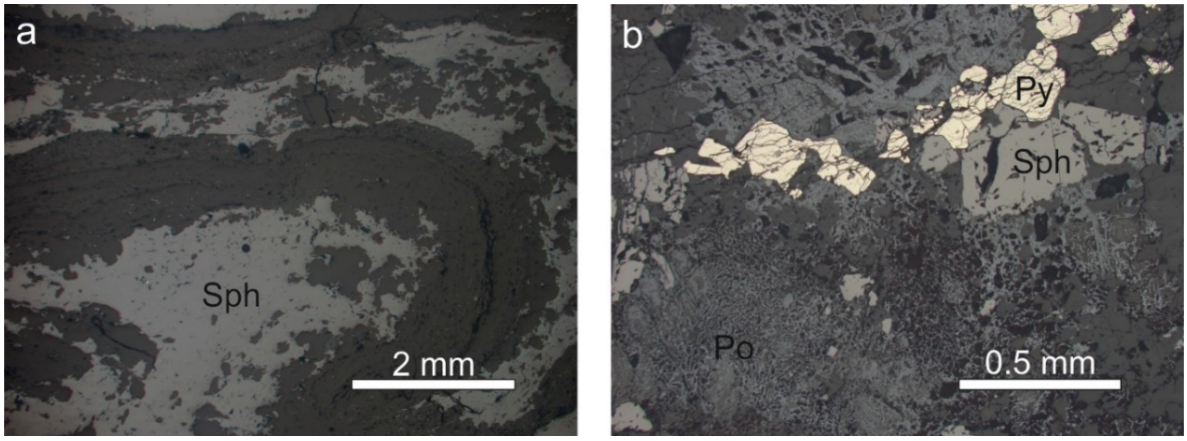

Fig. 27: Reflected light microscope images from Haufenreith. a: folded sphalerite bands (HrPa 1-2). b: altered pyrrhotite showing birds eye structure with sphalerite and pyrite (HrPa 1-2).

5.2.9 Meiselding

The ore bearing mica-schist of Meiselding, collected in the underground mine at the first and second level and from backfilling material consists of sphalerite, galena, pyrrhotite, pyrite and chalcopyrite. At least two generations of sulfide minerals can be observed in the specimen. The primary ore deposition is characterized by sulfide minerals that are parallel to the schistosity that is folded in some samples (Fig. 28a, b). Undeformed sulfide minerals mark the remobilization. Especially sphalerite can be assigned to both events (Fig. 28c, d). The primary sphalerite shows no inclusions of other sulfide minerals, conversely the secondary sphalerite shows inclusions of chalcopyrite, pyrrhotite and galena. Chalcopyrite is usually associated with sphalerite as flame like exolusions or as hypidiomorphic to xenomorphic inclusion (Fig. 28c). Galena was found as inclusions in sphalerite (Fig. 28d), and in the host rock. Pyrrhotite can be found in two shapes, as inclusion in sphalerite and as altered discrete mineral in the host rock. Pyrite exists only as vein filling.

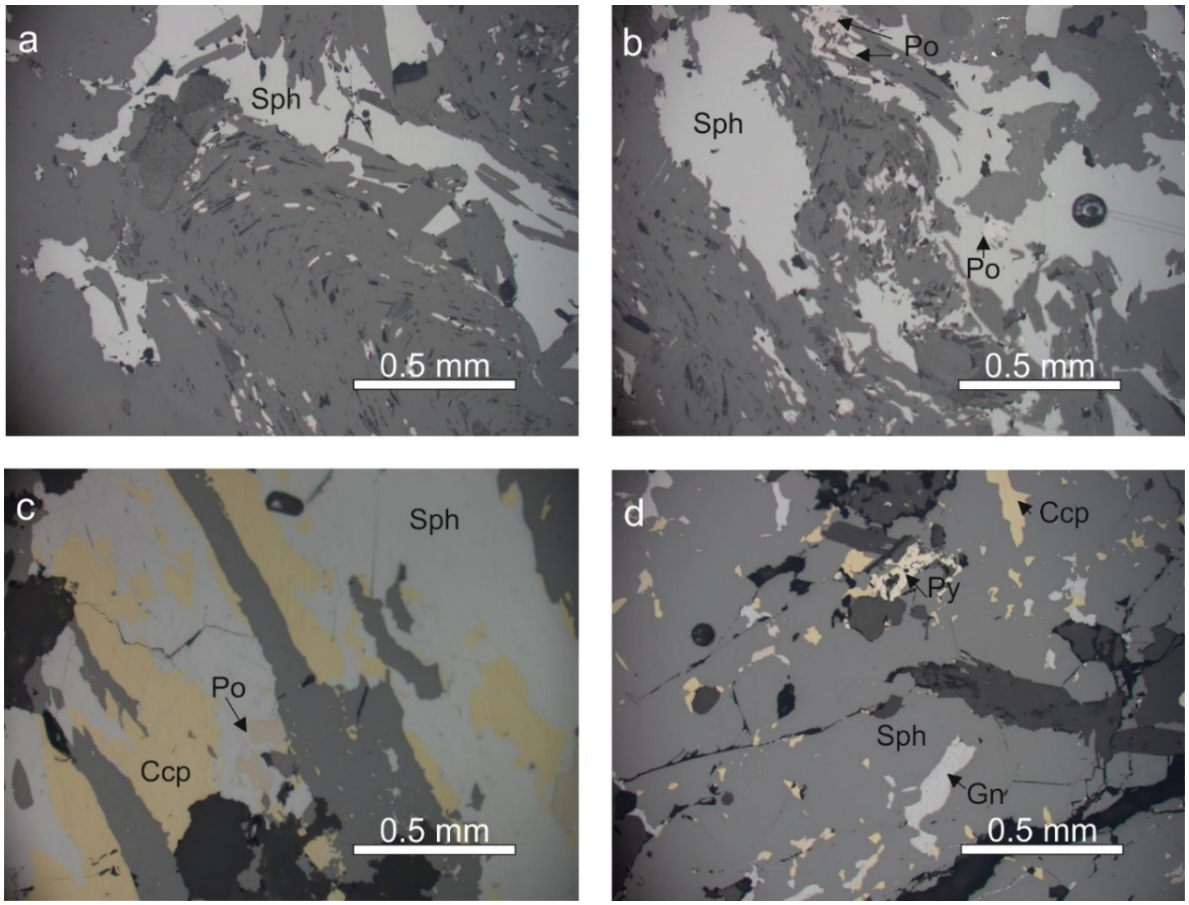

Fig. 28: Reflected light microscope images from the Meiselding adit. a: sphalerite concordant to the schistosity and large inclusion free hypidiomorphic sphalerite minerals (MEI 1). b: large and small sphalerite crystals partly concordant to the schistosity and as large crystals that are not affected by the schistosity of the host rock with pyrrhotite (MEI 1). c: flame like chalcopyrite inclusions in sphalerite, xenomorphic pyrrhotite at the border between galena and sphalerite (MEI 8). d: massive sphalerite with galena, pyrite and chalcopyrite inclusions (MEI 6).

5.2.10 Walchen

The samples collected at the dumpsite and in the Thaddäus adit are composed mostly of pyrrhotite, chalcopyrite, pyrite and minor sphalerite and galena. The ore is hosted by sericitic and quartzitic phyllites. Sulfide minerals are arranged parallel to the schistosity. The pyrrhotite is strongly altered and shows birds eye structures (Fig. 29a). Chalcopyrite exists as discrete hypidiomorphic to xenomorphic crystals, as inclusion in sphalerite and as vein filling (Fig. 29b, c, d). Sphalerite is mostly embedded in pyrrhotite but also in the phyllite and is associated with galena and chalcopyrite. Next to the copper disease, sphalerite also contains stannite needles.

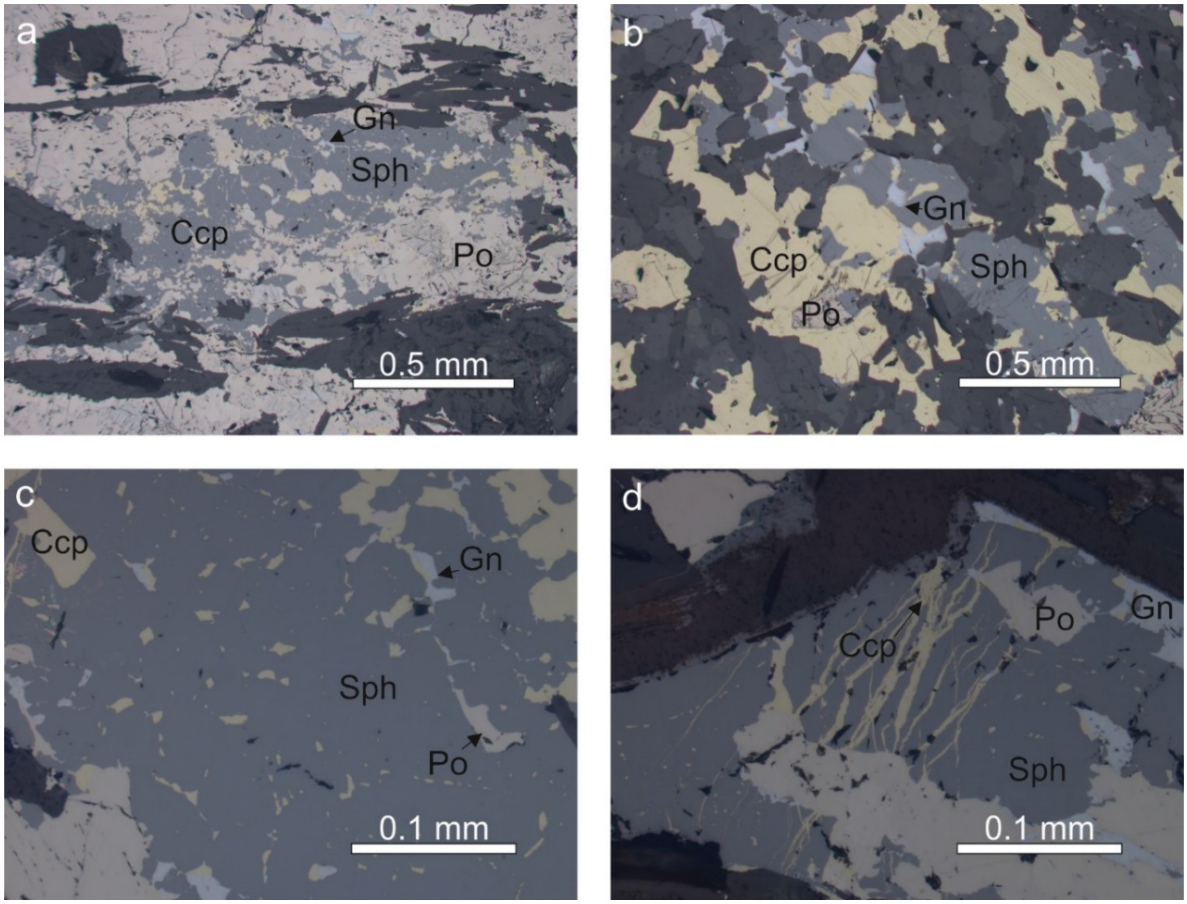

Fig. 29: Reflected light microscope images from the Walchen adit. a: pyrrhotite with galena chalcopyrite and sphalerite inclusions (Wa 6). b: typical sulfide mineral assemblage, hypidiomorphic to xenomorphic chalcopyrite, sphalerite, pyrrhotite and galena (Wa 2). c: sphalerite with pyrrhotite, galena and chalcopyrite inclusions (Wa 4). d: chalcopyrite as network like vein filling and as copper disease in sphalerite (Wa 4).

5.2.11 Leogang / Schwarzleo

The dolomitic samples taken from the Neuschurf adit and the Christoph adit are pyrrhotite dominated, sphalerite and galena are minor minerals (Fig. 30a, b). The altered pyrrhotite shows birds eye structures (Fig. 30c). Sphalerite shows hypidiomorphic to xenomorphic appearance and has galena und chalcopyrite inclusions (Fig. 30d).

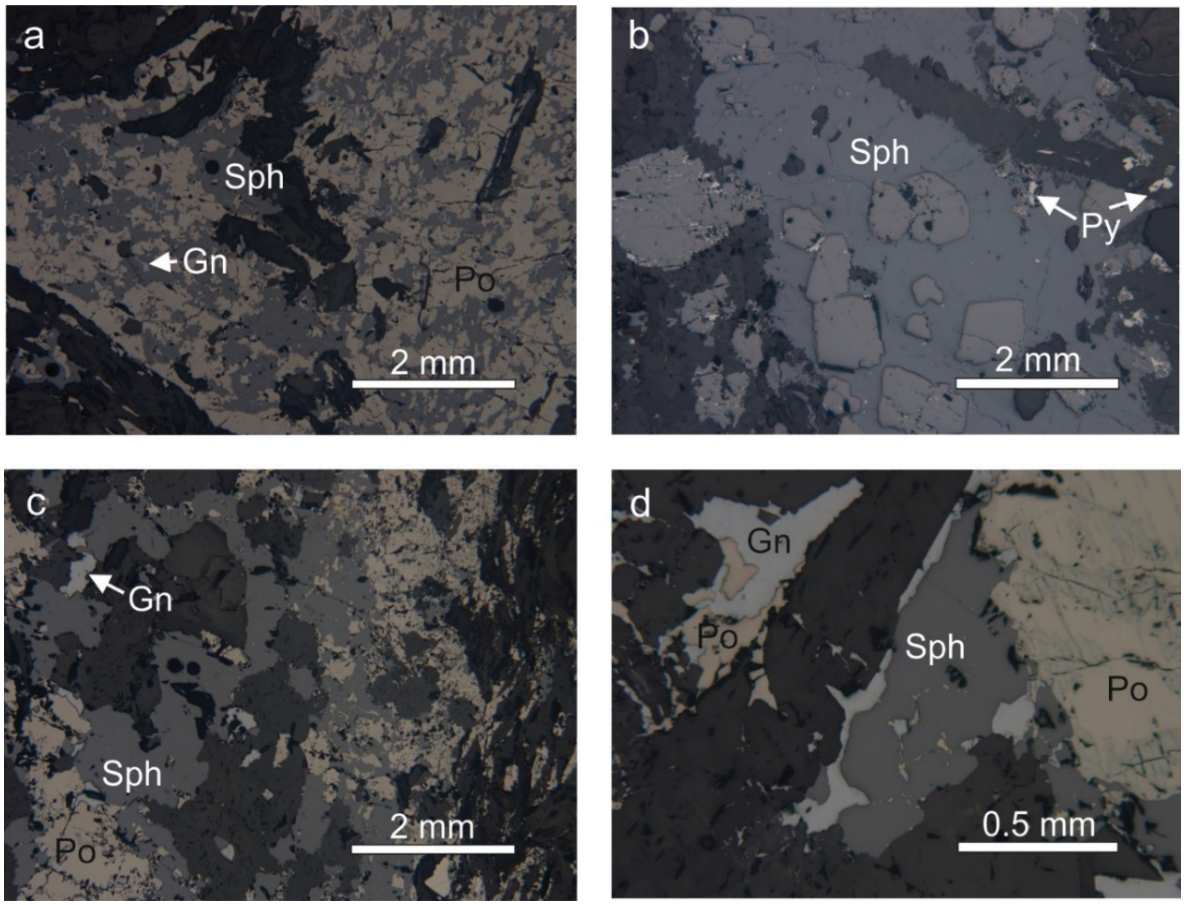

Fig. 30: Reflected light microscope images from the Leogang Neuschurf adit a: massive pyrrhotite with sphalerite and galena (Lg 16). b: massive sphalerite with hypidiomorphic pyrite inclusions (Lg 17). c: typical mineral assemblage consisting of pyrrhotite, sphalerite and galena (Lg 17). d: sphalerite associated with galena, pyrite and pyrrhotite (Lg 21).

5.3 Petrography and sample description of vein type Pb/Zn mineralizations hosted in Paleozoic units

5.3.1 Koprein

The sulfides occur in up to 20 cm wide veins hosted by greenschist. The gangue is tectonically deformed and consists mainly of quartz, carbonate and fine sericite. The dominant sulfides are sphalerite and galena (Fig. 31a), subordinate chalcopyrite, occurring as discrete minerals and as copper disease in sphalerite (Fig. 31b, c, d). Pyrite is rare and can be found as discrete mineral in the quartz/carbonate matrix. Sphalerite reaches a size up to 1 cm and form massive layers with a width up to 5 cm and fine minerals at the border between the massive sphalerite and the gangue minerals. Galena occurs as discrete minerals with a size up to 1 cm and as vein filling in the sphalerite (Fig. 31a). The copper disease shows two variations, parallel trails and irregular droplets (Fig. 31c).

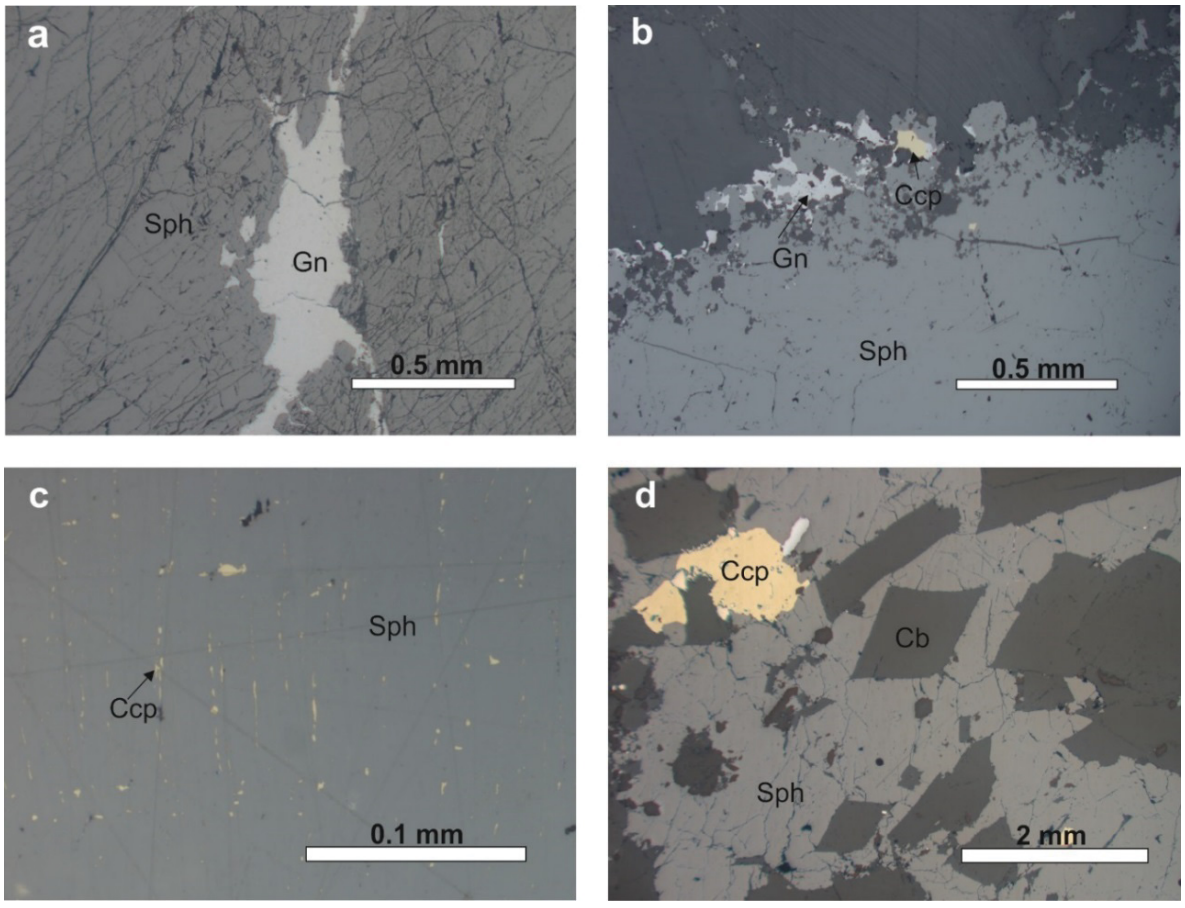

Fig. 31: Reflected light microscope images from Koprein tailing samples. a: sphalerite breccia with galena as crack filling (KOP 1-2). b: massive sphalerite with galena and chalcopyrite at the border to the carbonate (KOP 3). c: trail like copper disease in sphalerite (KOP 2). d: sphalerite surrounding idiomorphic carbonate minerals with chalcopyrite and galena (KOP 16).

5.3.2 Metnitz

The carbonate bearing phyllite samples from the open pit and underground mine Metnitz show the sulfide minerals sphalerite, galena and pyrite. Sphalerite can be found in veins as massive ore with a size of up to 5 mm and as breccia (Fig. 32a, b). Galena occurs as discrete mineral intergrown with sphalerite and as vein filling in sphalerite (Fig. 32a, b). Pyrite shows three varieties, discrete minerals (Fig. 32d), fillings between brecciated sphalerite (Fig. 32c) and seams around sphalerite (Fig. 32d).

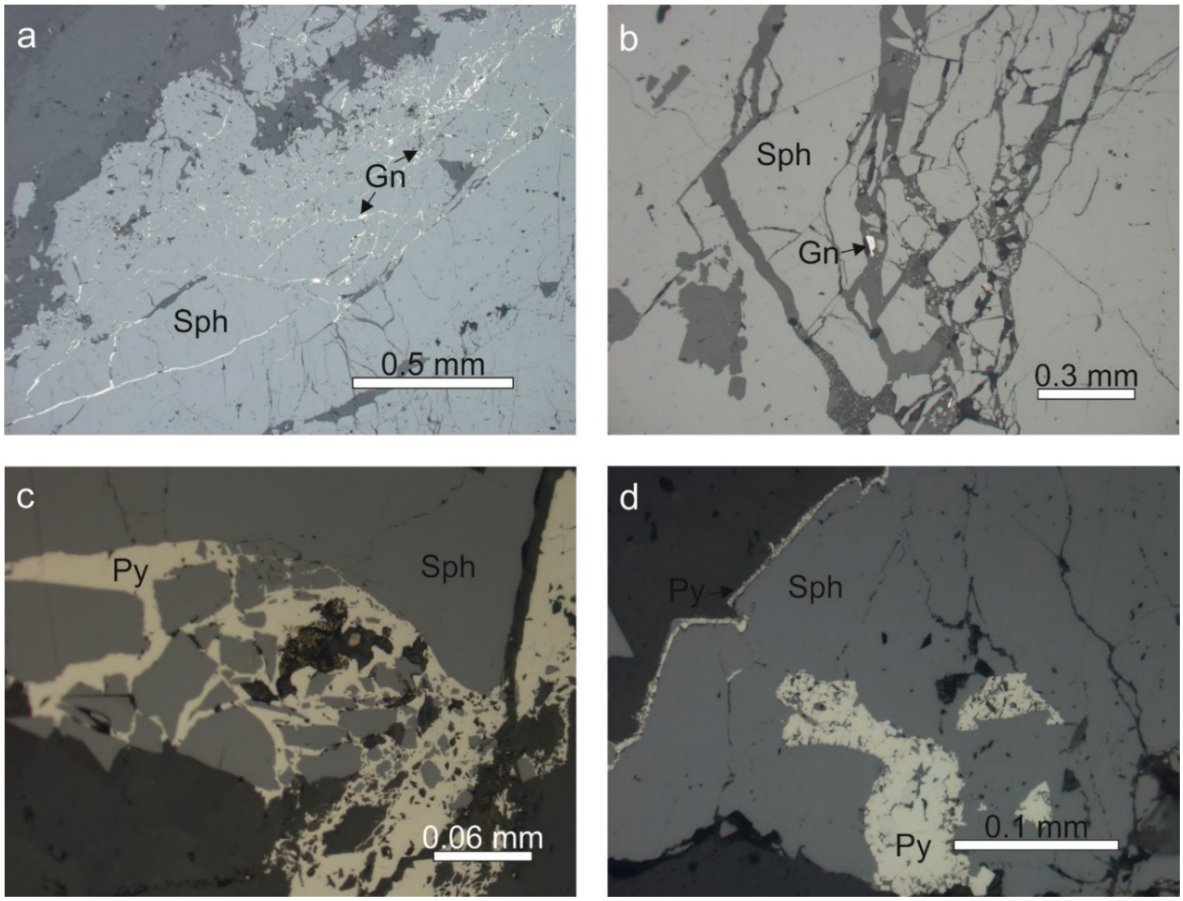

Fig. 32: Reflected light microscope images of Metnitz dump samples. a: tectonically stressed massive sphalerite with galena as vein filling (MET 7). b: sphalerite breccia with galena (MET 2). c: sphalerite breccia surrounded by chalcopyrite (MET 2). d: sphalerite with as pyrite seam and inclusion combined with marcasite (MET 7).

5.3.3 Achselalm/Flecktrogalm

The sphalerite of the Achselalm/Flecktrogalm adit occurs either disseminated in amphibolite associated with no other sulfide minerals (Fig. 33a) and more common in a sugar grain like fluorite – calcite vein together with galena (Fig. 33b). The sphalerite from the veins shows tiny (< 10 µm) galena inclusions. The color of the sphalerite ranges from creamy white to dark yellow.

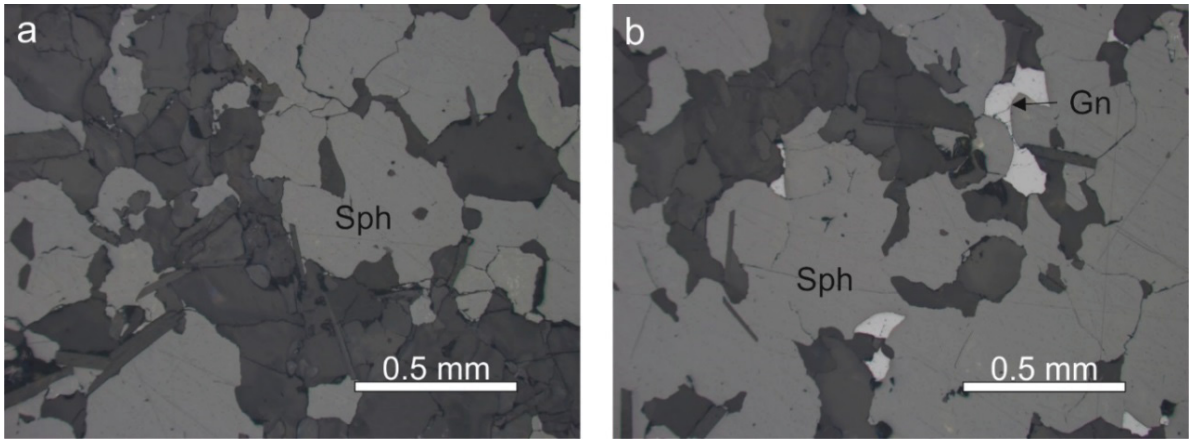

Fig. 33: Reflected light microscope images from the Achselalm / Flecktrogalm adit. a: hypidiomorphic to xenomorphic sphalerite in calcite, quartz and mica matrix (FT 2). b: sphalerite intergrown with galena (FT 2).

5.4 Sphalerite chemistry

5.4.1 Probability plots

The probability plots of the different deposits indicate single in-situ trace element values of the entire samples. All values are expressed in µg/g. Fig. 34 illustrates how lognormally distributed (Fig. 34A) and normally distributed data (Fig. 34B) look like in a histogram. Fig. 34C and D visualize the data in a logarithmic probability plot and Fig. 34E and F show the data in a linear probability plot. The differences between lognormally and normally distributed data can be seen best in Fig. 34E where the log normally distributed data follow a flexural line, whereas normally distributed data follow a nearly straight line (Fig. 34F). Normally distributed data in the probability plot look nearly similar; to visualize the differences blue lines were integrated in Fig. 34D and F. The curve in this case shows a concave shape below the blue line in the probability plot with logarithmic scale (Fig. 34D), whereas in the plot using a linear scale the data follow the blue line (Fig. 34F).

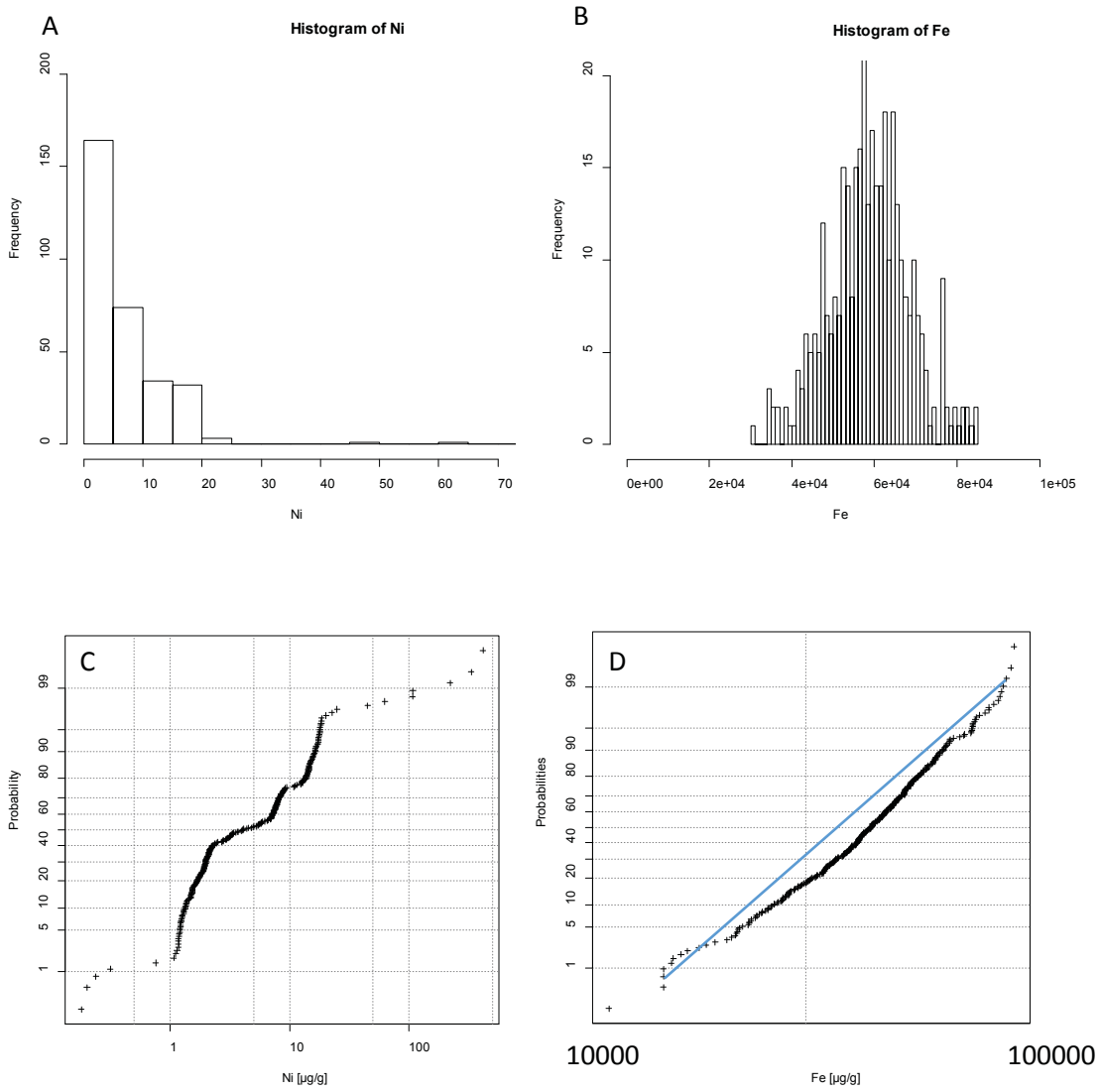

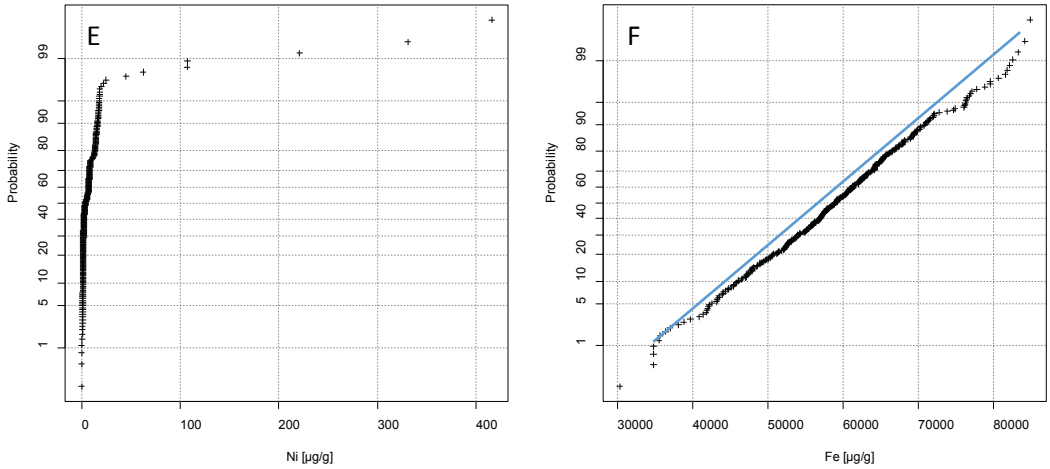

Fig. 34: Difference between lognormally (A) and normally (B) distributed data in the histogram plot (A,B), logarithmic probability plot (C,D) and linear probability plot (E,F).

5.5 Trace element chemistry

Main and trace element composition of sphalerite from the different Pb-Zn deposits was mainly obtained by LA-ICP-MS analysis. On each sample ~ 20 spot analyses were performed. The tables below show the median values of each location. The median values of each sample were taken and a median value for each location was calculated. Table 6 shows median values of all trace elements from Cook et al. 2009. In the following, the trace element data were normalized to this ´Cook trace element median` (CTEM). The median values of the different locations was normalized to the CTEM and plotted as spider plot.

Table 6: median values of all trace elements from Cook et al. 2009 (CTEM).

Mn	Fe	Co	Ni	Cu	Ga	Ge	As
2152	16959	26	0.85	443	4.585	1.19	14.95
Se	Ag	Cd	In	Sn	Sb	Tl	Pb
7.9	7.3	4968	16.8	1.425	1.23	0.14	13.95

5.5.1 Sphalerite chemistry of Mesozoic carbonate-hosted Pb/Zn mineralizations

Table 7 summarizes the median trace element data of 5 different locations (Jauken, Radnig, Bleiberg, Fladung and Lafatsch) including median values of 118 samples with 2111 in-situ trace element measurements.

Table 7: Trace element median values [µg/g] of all carbonate hosted Mesozoic Pb-Zn deposits (5)

Cr	Mn	Fe	Co	Cu	Ga	Ge	As
0.59	16.9	2590	0.07	92	1.9	325	74
Se	Ag	Cd	In	Sn	Sb	Tl	Pb
11.34	0.47	1911	0.02	0.06	0.52	16.4	330

Sphalerite from Mesozoic Pb-Zn deposits are compromised to the CTEM enriched in the elements Ge, As, Se, Tl, Pb and depleted in Mn, Fe, Co, Ni, Cu, Ga, Ag, Cd, In, Sn and Sb (see Fig. 35).

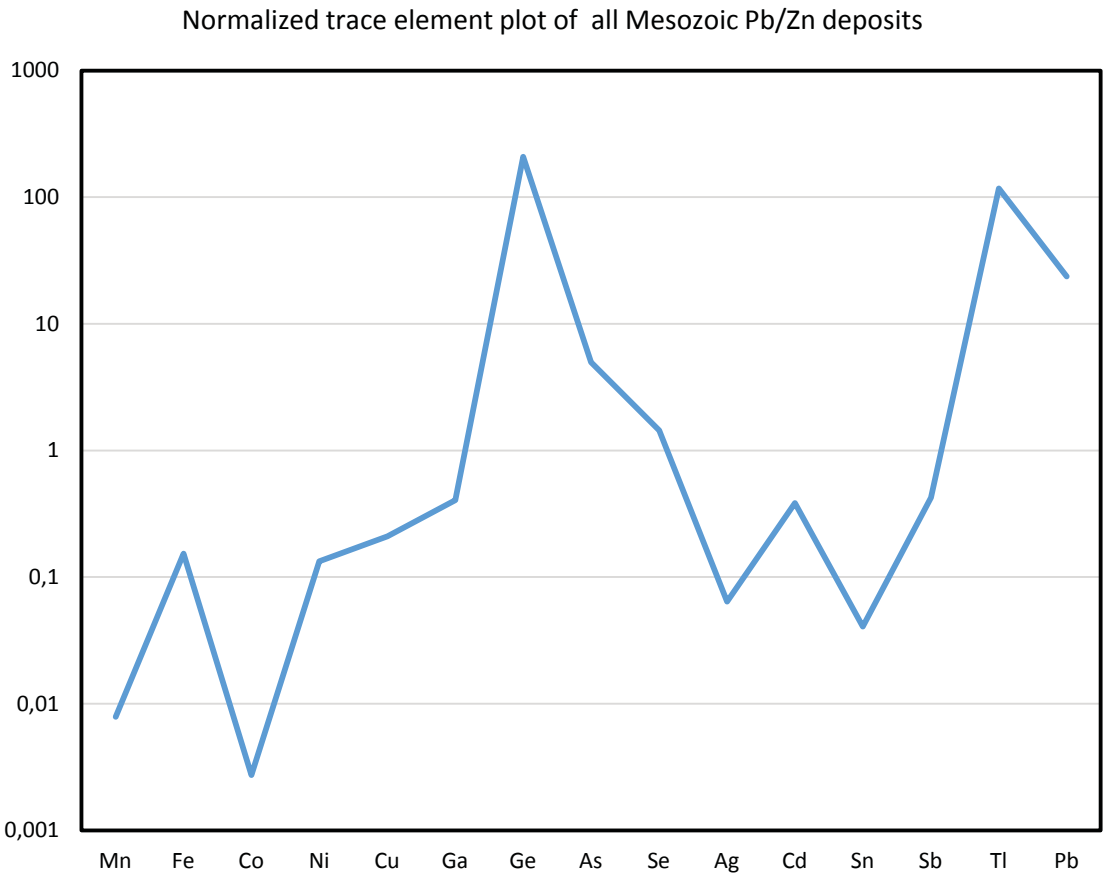

Fig. 35: Normalized trace element data from all Mesozoic Pb/Zn deposits normalized to the CTEM of table 4.

5.5.1.1 *Jauken*

Table 8 summarizes the chemical composition determined by LA-ICP-MS (6 samples, 93 spot analyses) for the major, minor and trace elements in sphalerite from the Jauken deposit.

Table 8: Statistics summarizing trace element data from 93 LA-ICP-MS measurements on sphalerite from the Jauken Pb/Zn deposit (values reported in µg/g).

	^{55}Mn	^{57}Fe	^{63}Cu	^{71}Ga	^{74}Ge	^{75}As	^{107}Ag	^{111}Cd	^{205}Tl	^{208}Pb
D90	68	9360	579	4.2	1253	106	0.7	2351	73	818
D75	51	5880	568	2.8	556	65	0.5	1496	45.3	467
Median	39.3	4508	554	1.6	389	37.8	0.3	1249	23.1	245
D25	29	3351	49.1	0.6	229	22.7	0.3	929	14	158
D10	19.4	2586	39.8	0.1	193	13.4	0.2	682	8.1	97
Min	11.3	1954	37.7	bdl	41.4	5.7	0.2	287	2.7	71
Max	142	34930	605	11.6	2411	234	3	3340	137	4390

Compared to the CTEM, the samples from Jauken are enriched in Cu, Ge, As, Se, Tl and Pb and depleted in Fe, Ga, Ag and Cd. Compared to the median of all Mesozoic deposits, sphalerite from Jauken is enriched in Mn (100%), Fe (74%), Cu (600%) and Ge (20%) . the other elements are nearly in the same range (Fig. 36).

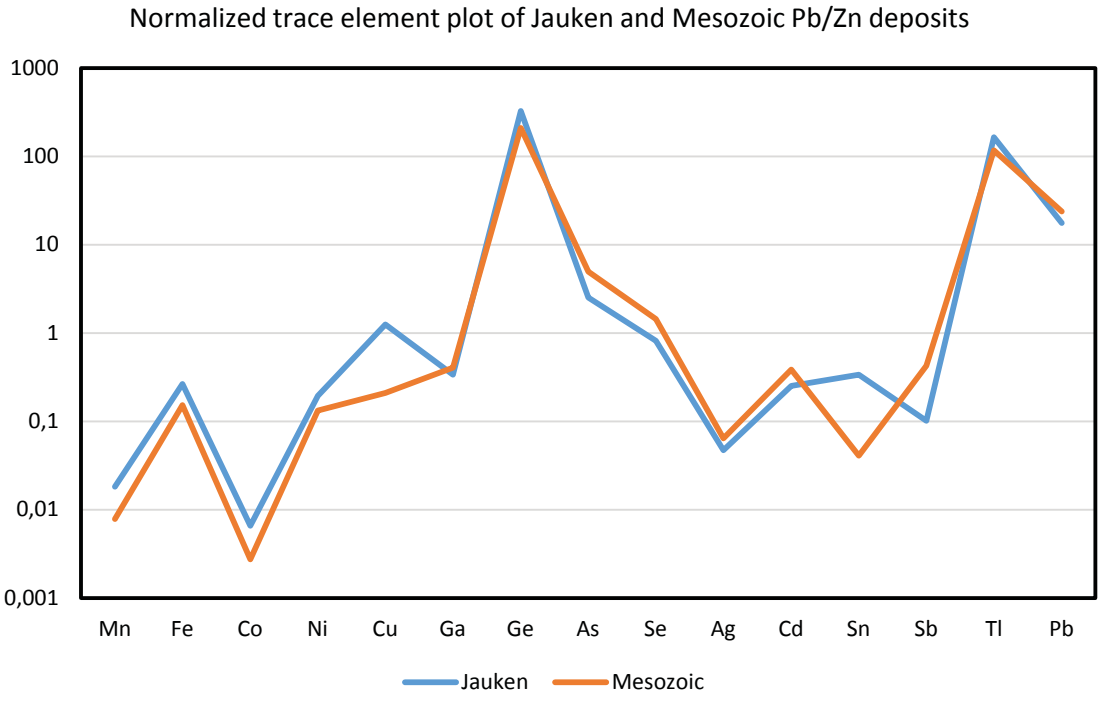

Fig. 36: Trace element plot from the Jauken Pb/Zn deposit and all Mesozoic Pb/Zn deposits normalized to the CTEM.

The probability plots in Fig. 37 show the large variation of the important trace elements Fe, Cd, Mn, Ge, As and Tl in samples from the Jauken Pb/Zn deposit. The elements Mn, Cd, and Tl (Fig. 37B, C, F) are linear normally distributed, Fe and As (Fig. 37A, E) are lognormally distributed and Ge (Fig. 37D) shows two linear distributed populations. The elevated Ge concentrations in Fig. 37D (blue ellipse) show a direct correlation with Tl. This sporadically occurrence in different samples cannot be correlated with microscopic observations.

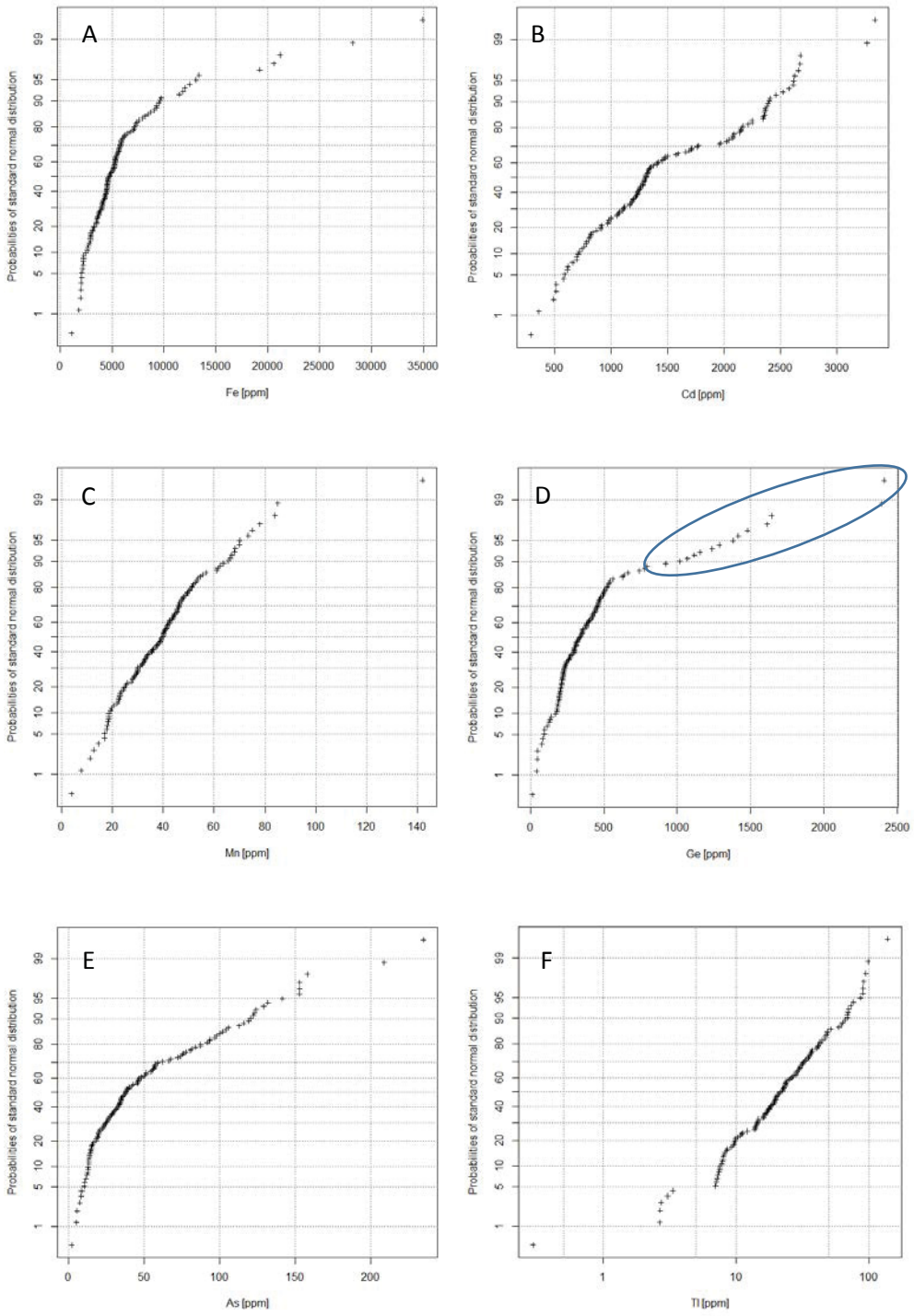

Fig. 37: Probability plots for the elements: A: Fe, B: Cd, C: Mn, D: Ge, E: As, F: Tl.

The $\delta^{34}S$ isotopic pattern measured on sphalerite (26 spot analyses) from the Jauken Pb/Zn deposit shows a unimodal distribution, ranging between +1 and +6 ‰ with a maximum at 3 ‰ (Fig. 38). compared to the other investigated deposits of the Drau Range the Jauken deposit shows the heaviest $\delta^{34}S$ values.

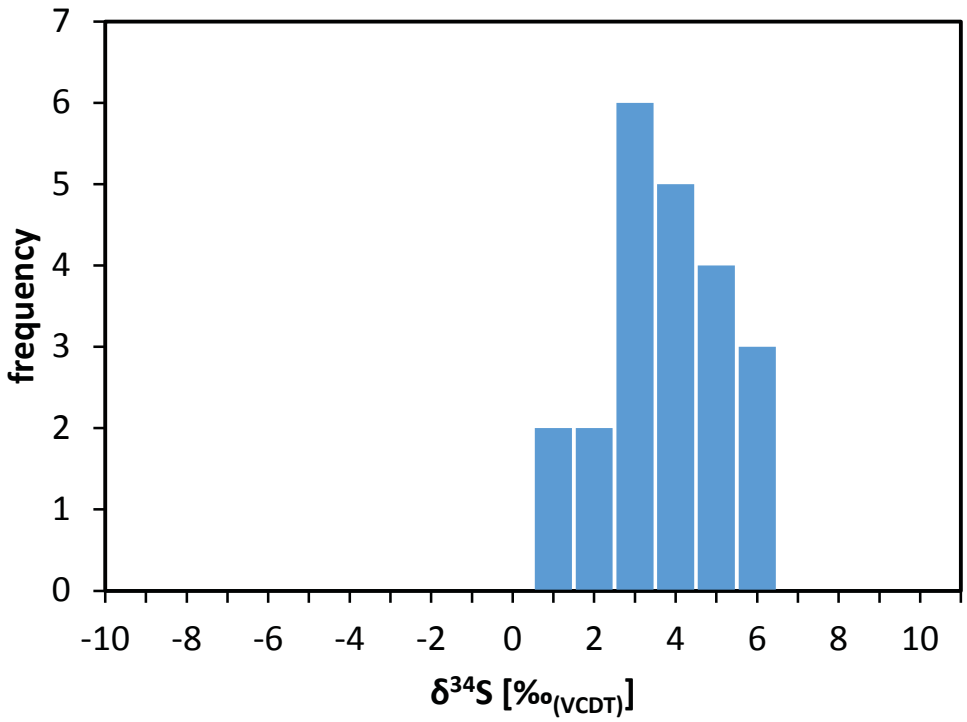

Fig. 38: Sulfur isotopic pattern of sphalerite from the Jauken Pb/Zn deposit.

5.5.1.2 Radnig

Table 9 summarizes the mineralogical composition determined by LA-ICP-MS (19 samples, 318 spot analyses) for the major, minor and trace elements in sphalerite from Radnig.

Table 9: Statistics of trace element contents from 318 LA-ICP-MS measurements on sphalerite from the Radnig Pb/Zn deposit (values reported in µg/g).

	^{55}Mn	^{57}Fe	^{63}Cu	^{71}Ga	^{74}Ge	^{75}As	^{82}Se	^{107}Ag	^{111}Cd	^{205}Tl	^{208}Pb
D90	55	13407	869	11	672	174	11.8	2.3	2171	51	647
D75	34.6	7573	50	5	522	129	10.9	0.7	1794	38.1	435
Median	24.3	4229	40.6	1.9	325	56	9.1	0.4	1383	16.4	243
D25	7.4	1277	1.4	0.8	121	6.1	5.6	0.3	954	2.5	56
D10	1.1	432	bdl	0.4	8.1	0.6	4.5	0.3	691	0.2	19
Min	bdl	146	bdl	bdl	bdl	bdl	2.7	0.2	403	bdl	0.4
Max	422	96800	8500	100	1318	266	72	107	3590	98	2992

Compared to the CTEM, the samples from Radnig are enriched in Ge, As, Se, Cd, Tl and Pb and depleted in Mn, Fe, Cu, Ga and Ag. Compared to the median of all Mesozoic deposits, sphalerite from Radnig is enriched in Mn, Fe, Ge and depleted in As, Se, Cd and Pb (Fig. 39).

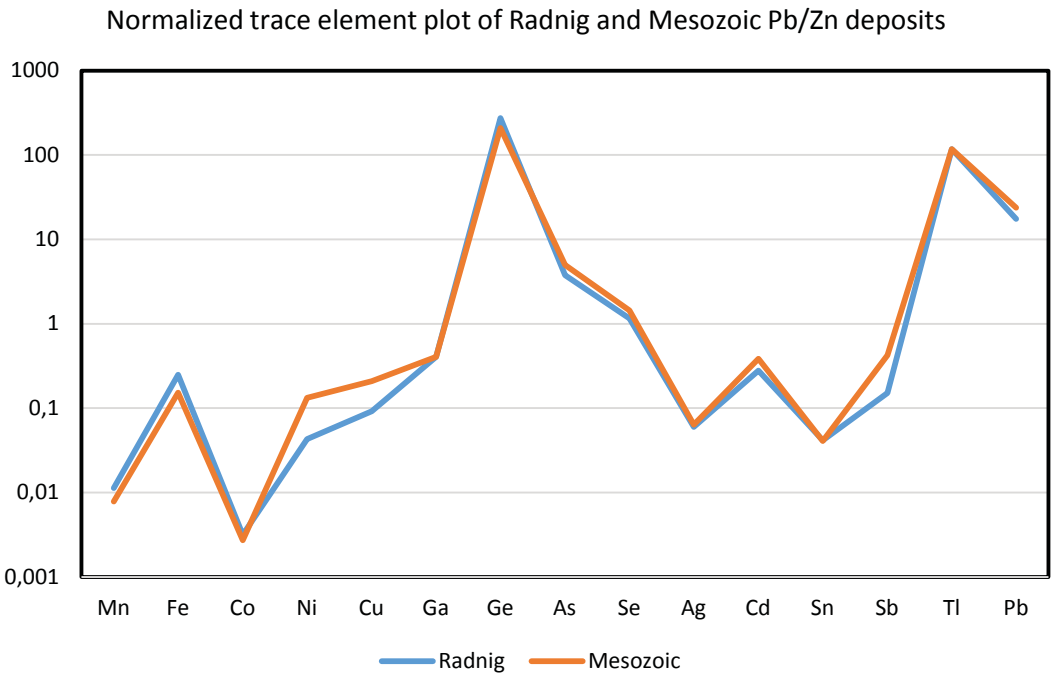

Fig. 39: Trace element plot from the Radnig Pb/Zn deposit and all Mesozoic Pb/Zn deposits normalized to the CTEM.

The probability plots in Fig. 40 show the variation of the important trace elements Fe, Cd, Mn, Cu, Ga, Ge, As and Tl in the samples of the Radnig Pb/Zn deposit. The Cu and Ge values in Fig. 40D, F, represent sphalerite from sample Ra6 with no visible copper disease. The element Fe, Mn, Cu, Ge, As and Tl show more than one sphalerite population (Fig. 40A, C, D, E, G, H). Cadmium is normally distributed, whereas Ga is lognormally distributed (Fig. 40B, F).

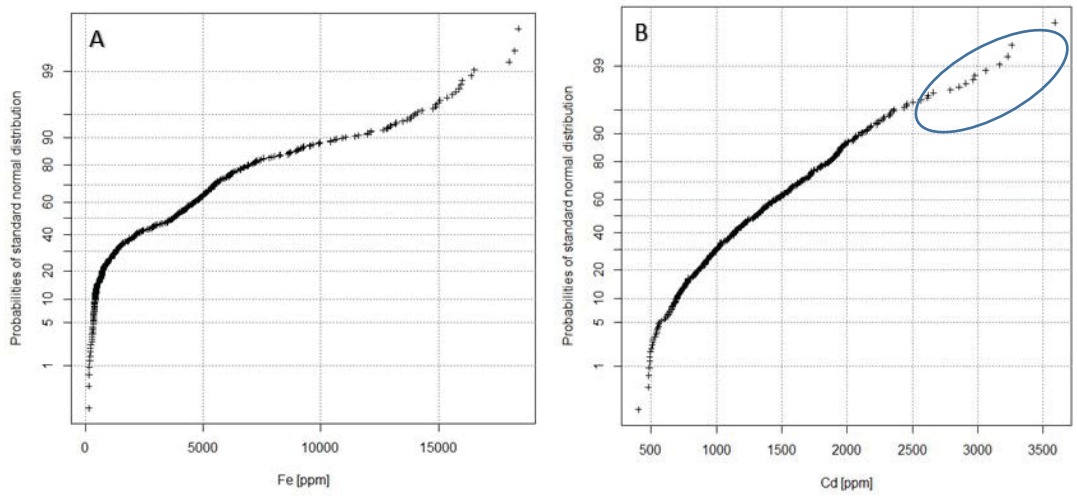

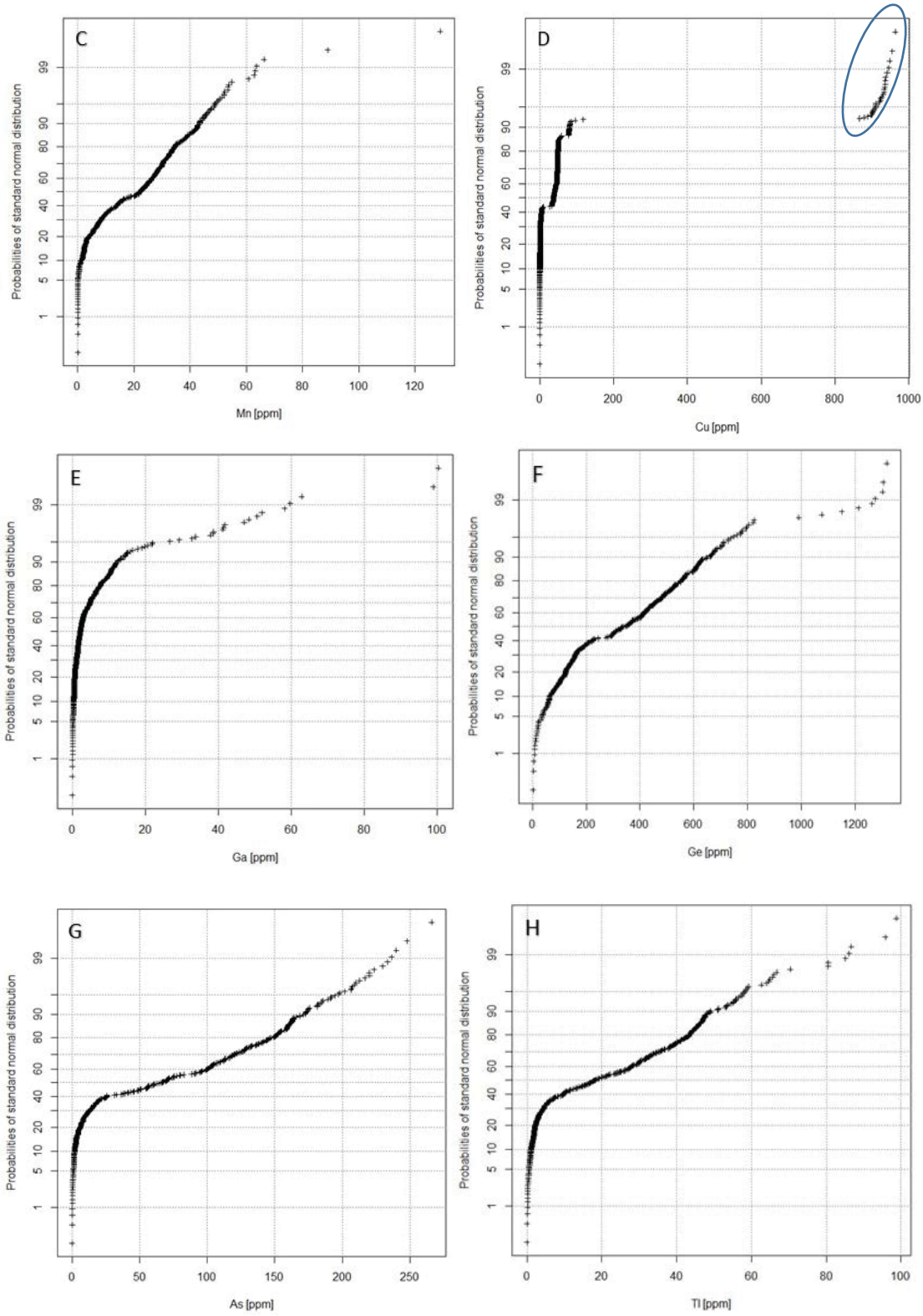

Fig. 40: Probability plots for the elements: A: Fe, B: Cd, C: Mn, D: Cu, E: Ga, F: Ge, G: As, H: Tl.

The $\delta^{34}S$ isotopic pattern of sphalerite (n= 38) from the Radnig deposit (Fig. 41) shows a unimodal distribution with a $\delta^{34}S$ maximum between -21 and -22 ‰; the values range from -16 to -28 ‰.

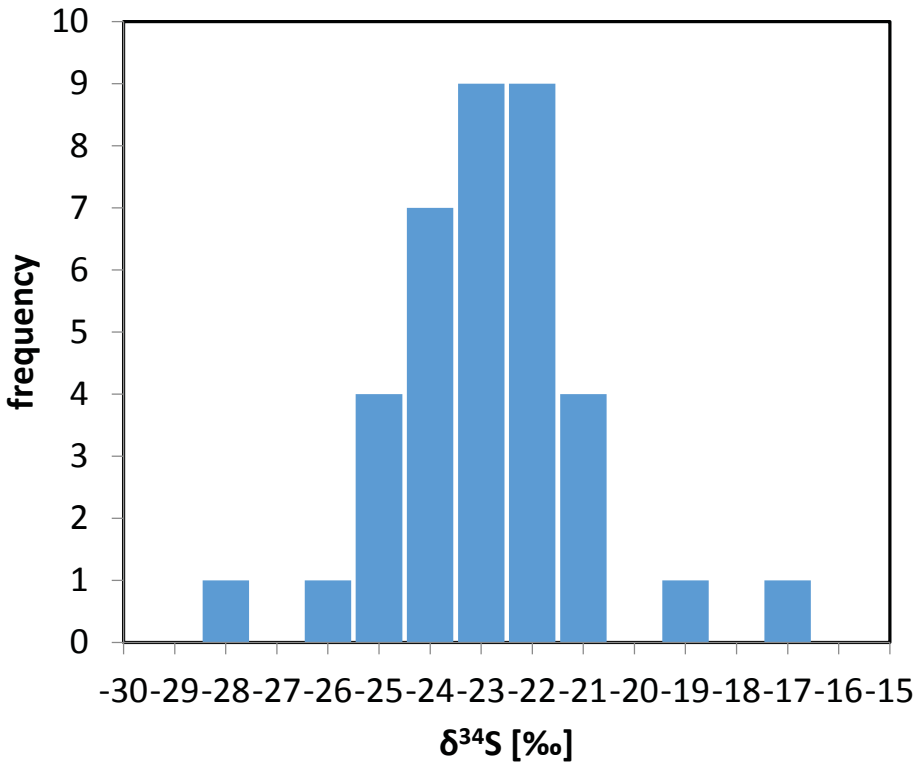

Fig. 41: $\delta^{34}S$ pattern from sphalerite of the Radnig ore deposit.

5.5.1.3 *Bleiberg*

Table 10 summarizes the chemical composition of sphalerite determined by LA-ICP-MS (38 samples, 795 spot analyses) for the major, minor and trace elements in sphalerite from Bleiberg. These data represent different ore types (Cardita ore, Wetterstein limestone ore).

Table 10: Statistics summarizing table of trace element contents from 795 LA-ICP-MS measurements on sphalerite hosted in the Bleiberg Pb/Zn deposit (values reported in µg/g).

	^{55}Mn	^{57}Fe	^{63}Cu	^{71}Ga	^{74}Ge	^{75}As	^{82}Se	^{107}Ag
D90	61	18912	83	8	1161	2073	13.3	14.8
D75	33.1	8415	60	3.2	526	824	12.4	3
Median	15.6	2590	51	1	248	234	11.2	0.7
D25	7.3	564	18.9	0.2	107	45.1	8.8	0.3
D10	2.3	267	0.5	bdl	34	12.7	5.1	0.3
Min	bdl	13.5	bdl	bdl	1.6	0.3	bdl	0.1
Max	242	55860	395	160	3703	10480	16.2	234

Compared to the CTEM, samples from the Cardita ore are enriched in Ge, As, Se, Tl and Pb and depleted in Mn, Fe, Co, Cu, Ga, Ag, Cd and Sb. Compared to the median of all Mesozoic deposits, sphalerite from Cardita ore is enriched in Mn, Fe, Co, Ge, Ag, As, Tl and Pb, depleted in Cu, Ga, Cd and Sb (Fig. 42: orange line).

Compared to the CTEM The samples from the Wetterstein limestone ore are enriched in Ge, As, Se, Tl and Pb and depleted in Mn, Fe, Co, Cu, Ga, Ag, Cd, Sn and Sb. Compared to the median of all Mesozoic deposits, sphalerite from Wetterstein limestone ore is enriched in As, Ag, Tl, Pb and depleted in Mn, Fe, Cu, Cd, and Ga (Fig. 42 blue line).

Compared to the Cardita ore, the Wetterstein ore shows only higher values in Ga. The other trace elements values are in the same range like them of the Cardita ore (Fig. 42).

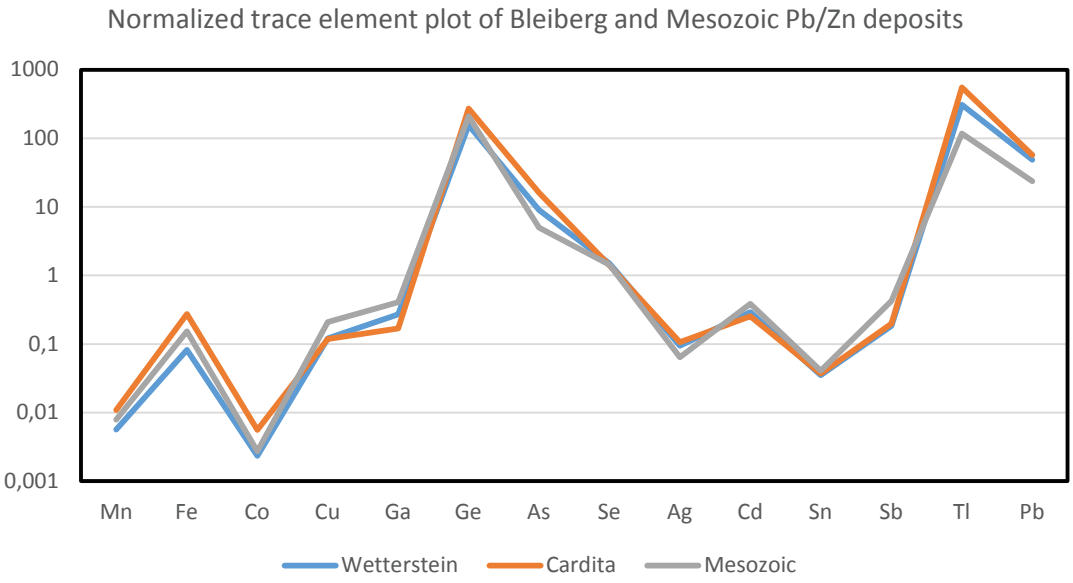

Fig. 42: Trace element plot of different Bleiberg ore types (blue: Wetterstein ore; orange: Cardita ore) and all Mesozoic Pb/Zn deposits (grey line) normalized to the CTEM.

The probability plots in Fig. 43 show the variations of the important trace elements Fe, Cd, Mn, Cu, Ga, Ge, As and Tl within the samples of the Bleiberg Pb/Zn deposit. The huge variation is a result of different ore types within the Pb/Zn deposit. The elements Fe, Cd, Mn, Ga, Ge and Tl are logarithmic normally distributed and show no evidence of more than one population (Fig. 43).

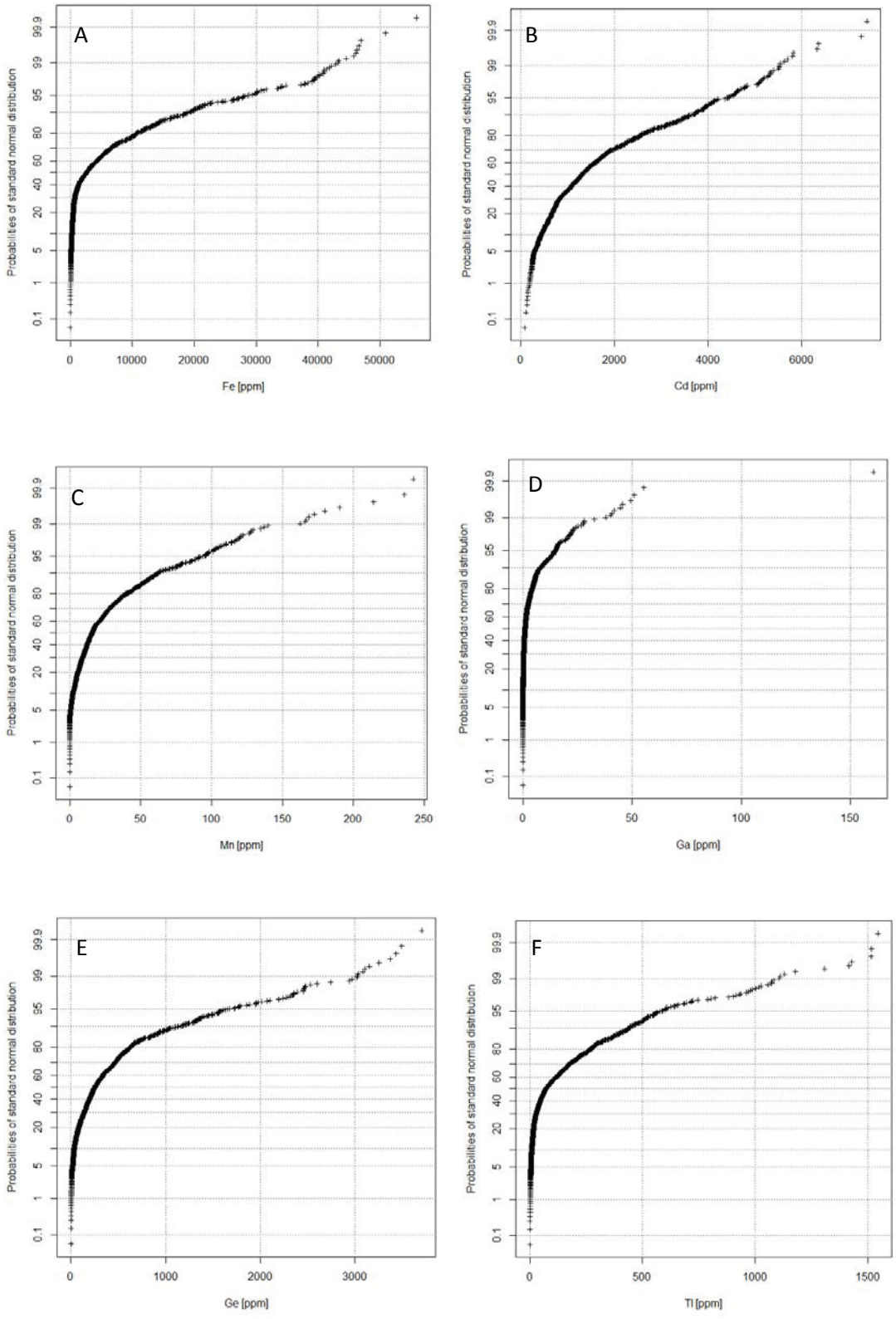

Fig. 43: Probability plots for the elements: A: Fe, B: Cd, C: Mn, D: Ga, E: Ge and F: Tl.

In situ $\delta^{34}S$- isotope ratios performed on 17 samples including 166 point analyses (Fig. 44) show a bimodal distribution with maxima at -27 ‰ and -10 ‰ relative to Vienna-Canyon Diablo Troilite (VCDT).

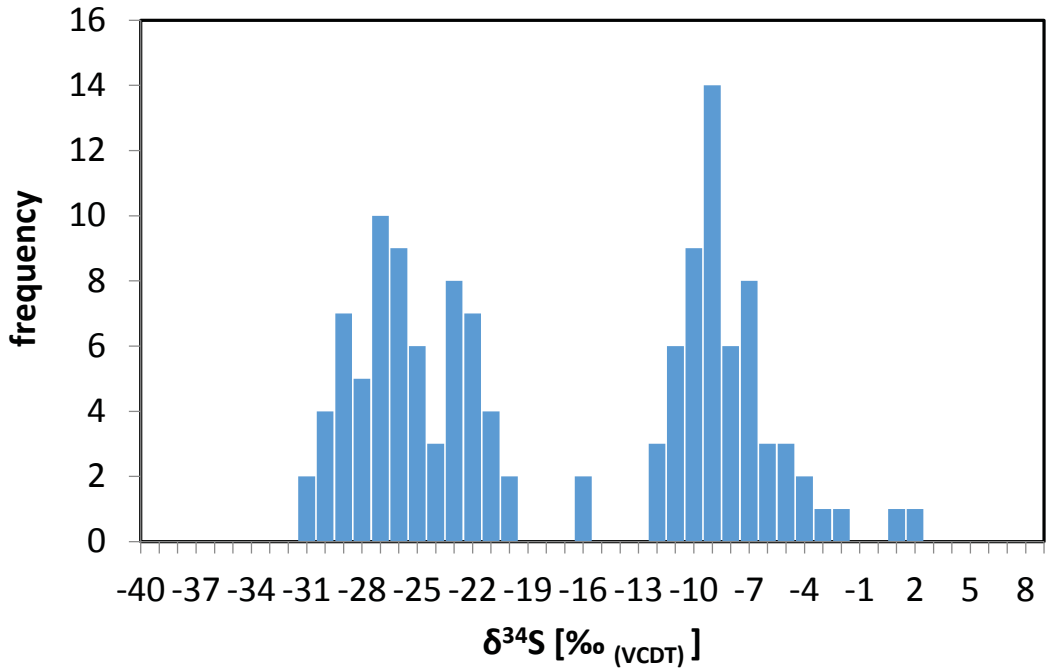

Fig. 44: Sulfur Isotope ratio histogram of all Bleiberg measurements (n= 166).

The $\delta^{34}S$ isotope pattern of sphalerite (n= 26) from the Cardita ore (Fig. 45) shows a bimodal distribution with a maximum at -30 ‰, the second maximum is at 8 ‰. Heavier values between -16 and -7 ‰ are rarer.

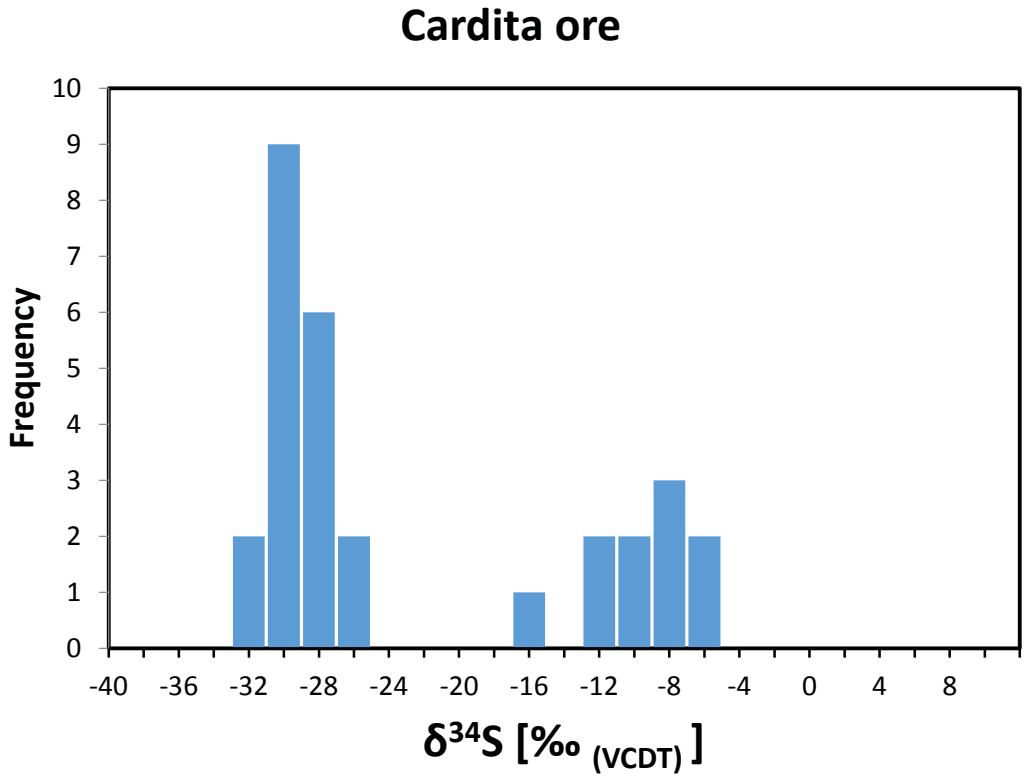

Fig. 45: In situ $\delta^{34}S$ values of the Cardita ore (n= 26).

The sulfur isotope analyses (n= 89) performed from the Wetterstein limestone ore type (Fig. 46) show a bimodal distribution, the first maximum at ~-26 ‰ represents the BSR and the second maximum at -8 ‰ indicates the TSR influence.

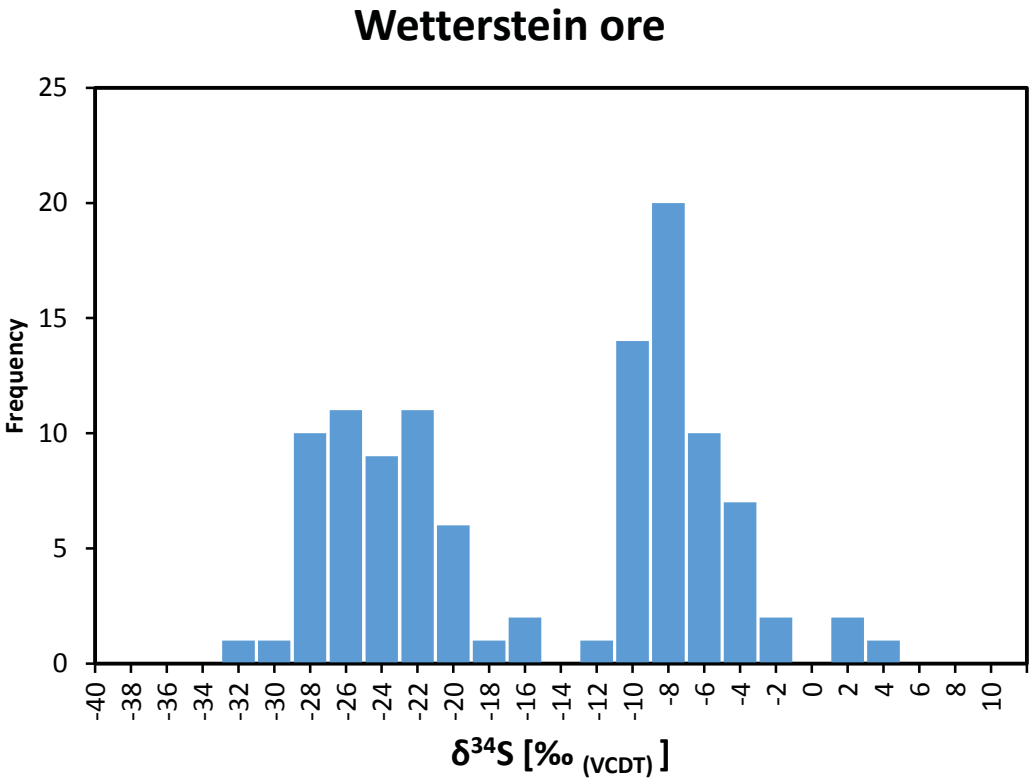

Fig. 46: Sulfur Isotopic composition of the Wetterstein limestone ore type.

5.5.1.4 Fladung

Table 11 summarizes the mineralogical composition determined by LA-ICP-MS (21 samples, 282 spot analyses) for the major, minor and trace elements in sphalerite from Fladung. Noticeable in this deposit are the high Ge values (Md= 845 µg/g), represents the highest median value of all investigated Pb-Zn deposits.

Table 11: Statistics summarizing trace element contents from 282 LA-ICP-MS measurements on sphalerite hosted in the Fladung Pb/Zn deposit (values reported in µg/g).

	^{55}Mn	^{57}Fe	^{63}Cu	^{71}Ga	^{74}Ge	^{75}As	^{82}Se	^{107}Ag	^{111}Cd	^{205}Tl	^{208}Pb
D90	28.7	11285	931	69	1537	567	13.5	3.7	9618	281	907
D75	20.4	8318	158	27.8	1127	445	12.3	1.6	7323	218	770
Median	16.9	5196	92	10.3	845	310	11.3	0.5	5515	137	593
D25	12.7	864	63	3.1	356	86	9.3	0.4	4099	25.4	396
D10	5.8	156	45.1	1	16.7	19.6	8.9	0.3	3205	2.5	148
Min	0.5	13.8	36.3	0.1	0.6	1.2	8.1	0.2	1851	0.1	20.5
Max	165	18720	2192	433	3080	1000	15	40.4	20740	408	1320

Compared to the CTEM, the samples from the Fladung Pb/Zn deposit are enriched in Ge, As, Se, Cd, Tl and Pb and depleted in Mn, Fe, Cu, Ga, and Ag. Compared to the median of all Mesozoic deposits, sphalerite from Fladung is enriched in Fe, Ga, Ge, As, Cd, Tl, Pb (Fig. 47).

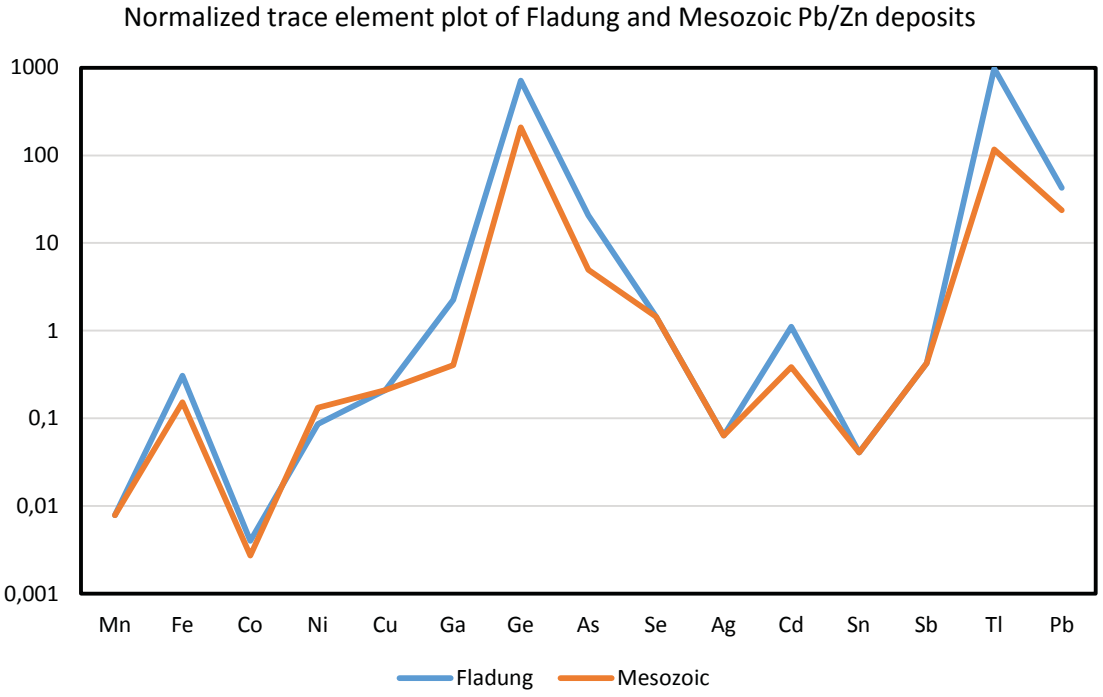

Fig. 47: Trace element plot from Fladung and all Mesozoic Pb/Zn deposits normalized to the CTEM.

The probability plots in Fig. 48 show the variation of the important trace elements Fe, Cd, Mn, Cu, Ga, Ge, As and Tl within the samples from the Fladung Pb/Zn deposit. The elements Cd and Ga (Fig. 48B, D) show logarithmic normally distribution, the elements Fe, Mn, Ge, As, Tl and Cu (Fig. 48: A, C, E, F, G, H) indicate at least two sphalerite populations. The elevated concentrations in Ge (Fig. 48: D, E, H) marked with a blue ellipse show a direct correlation to each other. These outlier concern to different samples and cannot be identified by reflected light microscopy due to different appearance

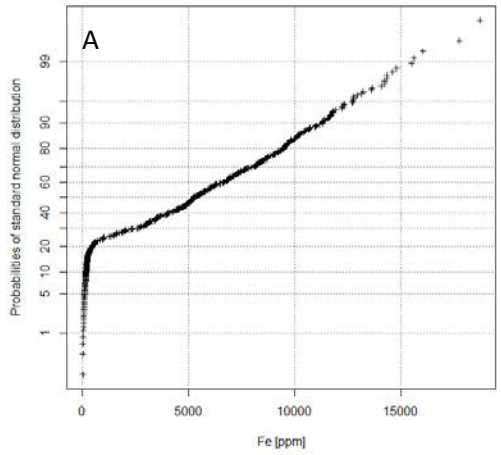
A
Probabilities of standard normal distribution
1
5
10
20
40
60
80
90
99
0
5000
10000
15000
Fe [ppm]

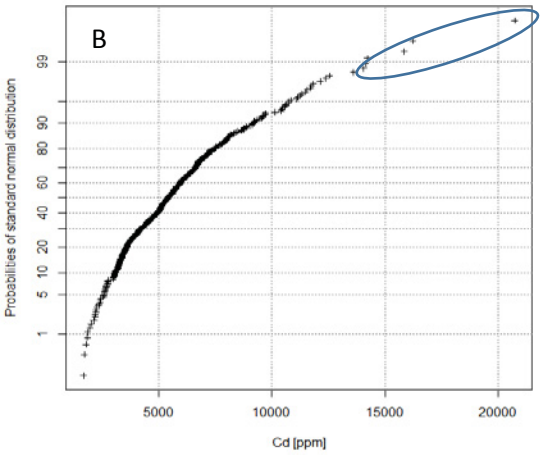
B
Probabilities of standard normal distribution
1
5
10
20
40
60
80
90
99
5000
10000
15000
20000
Cd [ppm]

.

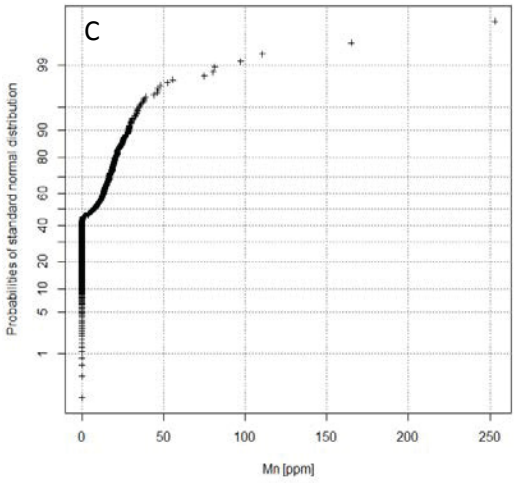
C
Probabilities of standard normal distribution
1
5
10
20
40
60
80
90
99
0
50
100
150
200
250
Mn [ppm]

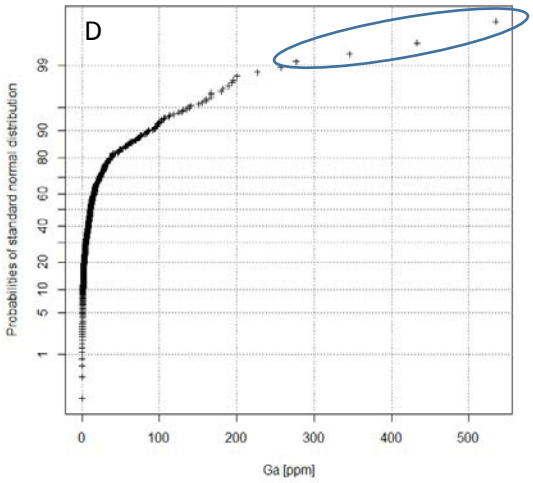
D
Probabilities of standard normal distribution
1
5
10
20
40
60
80
90
99
0
100
200
300
400
500
Ga [ppm]

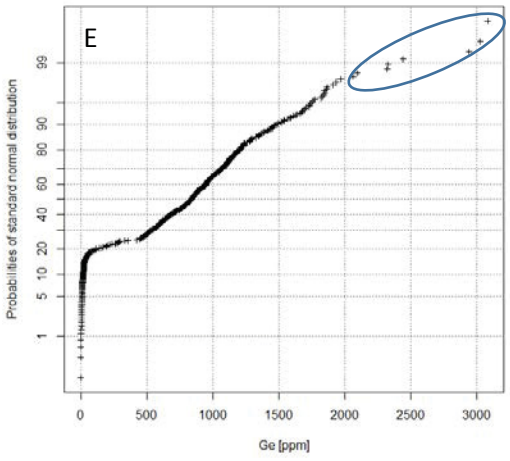
E
Probabilities of standard normal distribution
1
5
10
20
40
60
80
90
99
0
500
1000
1500
2000
2500
3000
Ge [ppm]

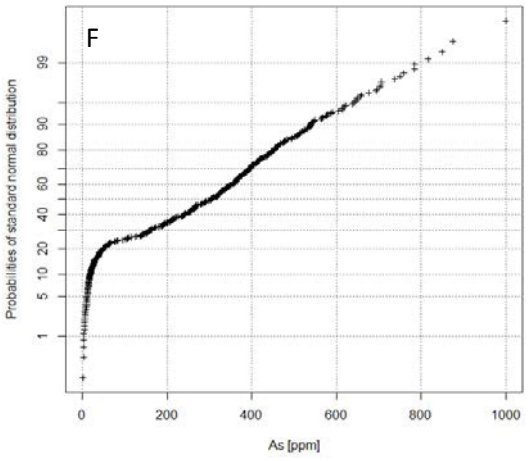
F
Probabilities of standard normal distribution
1
5
10
20
40
60
80
90
99
0
200
400
600
800
1000
As [ppm]

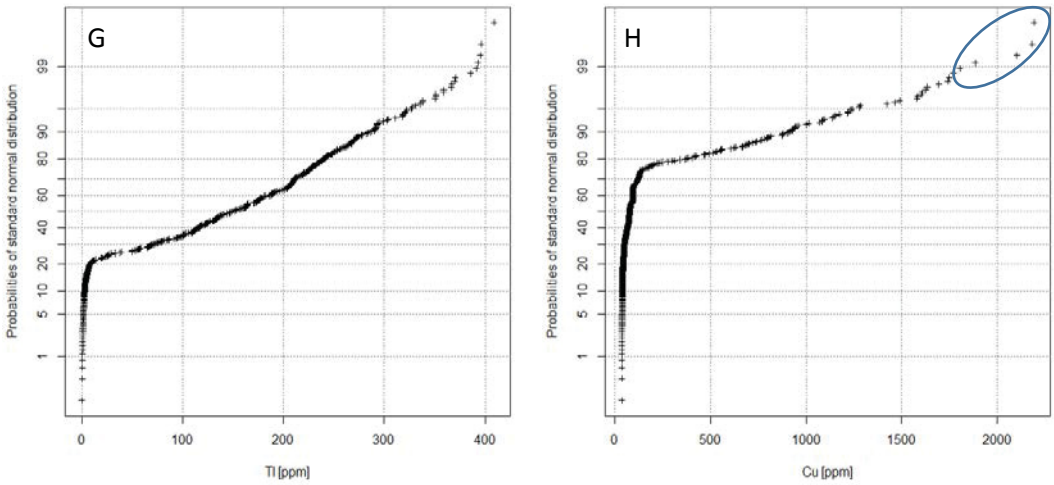

Fig. 48: Probability plots for the elements: A: Fe, B: Cd, C: Mn, D: Ga, E: Ge, F: As, G: Tl and H: Cu

Sphalerite from the Fladung Pb/Zn deposit shows a bimodal sulfur isotopic composition (

Fig. 49) with a first maximum at -22 ‰ and a second maximum at -17 ‰. The sulfur isotope composition ranges from -27 to -10 ‰ (n= 67).

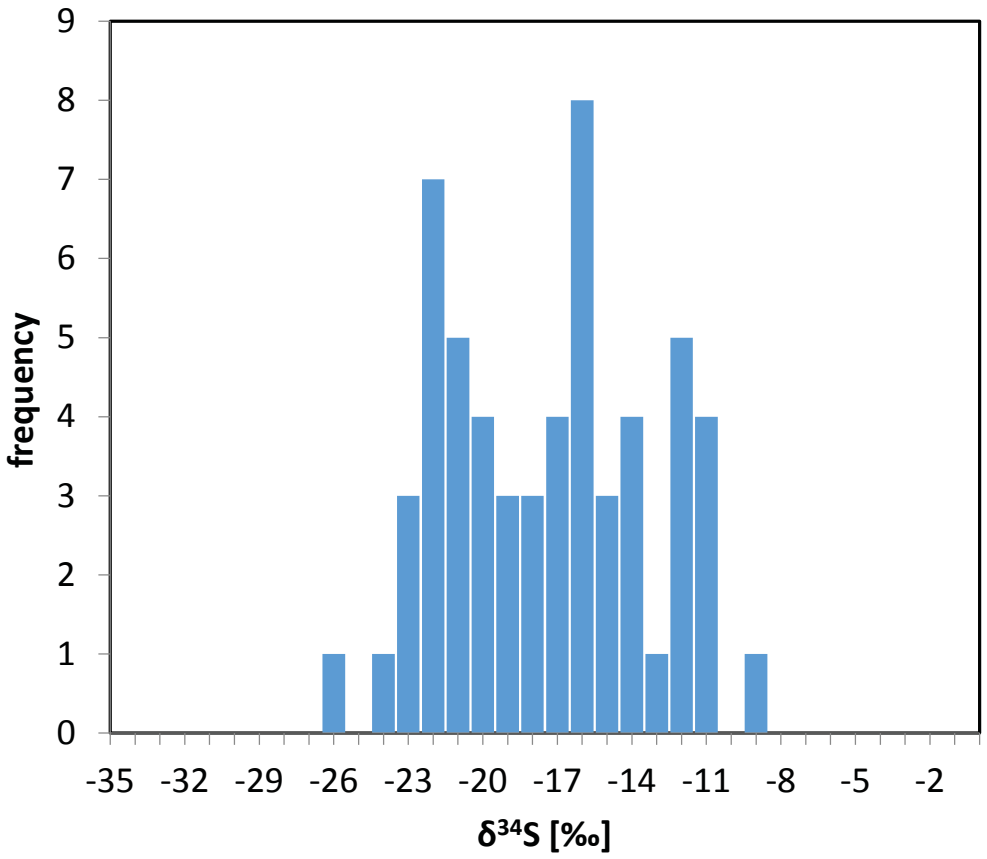

Fig. 49: $\delta^{34}S$ isotopic pattern, measured on sphalerite from the Fladung Pb/Zn deposit (n= 67).

5.5.1.5 *Lafatsch*

Table 12 summarizes the major, minor and trace element composition of sphalerite from Lafatsch determined by LA-ICP-MS (26 samples, 439 spot analyses). The Lafatsch deposit is characterized by the highest Ag and the lowest Mn and Fe values of all investigated carbonate hosted Pb-Zn deposits.

Table 12: Statistics summarizing trace element contents from 439 LA-ICP-MS measurements on sphalerite hosted in the Lafatsch Pb/Zn deposit (values reported in µg/g).

	55Mn	57Fe	63Cu	71Ga	74Ge	75As	82Se	107Ag	111Cd	205Tl	208Pb
D90	5	1513	1038	16.7	100	2912	12.4	247	5062	291	5506
D75	2.2	961	701	5.2	71	938	11.6	106	3443	86	1199
Median	0.9	520	132	1.2	41.7	273	10.7	43.4	1911	15.6	330
D25	0.2	192	68	0.3	25.3	74	7	17.6	1093	2.6	95
D10	bdl	95	62	0.1	11.7	27.2	4.2	7.7	495	0.7	32.7
Min	bdl	24.7	50	bdl	0.3	2.2	bdl	0.5	133	0.1	1
Max	26.5	7510	2400	89	226	20390	30.7	1351	9430	1387	22140

Compared to the CTEM the samples from the Lafatsch Pb/Zn deposit are enriched in Cu, Ge, As, Ag, Tl and Pb and depleted in Mn, Fe and Ga (Fig. 50). Compared to the median of all Mesozoic deposits, sphalerite from Lafatsch is enriched in Fe, Cu, Ga, As, Ag and depleted in Mn, Ge, Se, Tl and Pb. Lafatsch shows the highest Ag and the lowest Ge, Mn, As and Tl values of all measured Mesozoic Carbonate hosted Pb-Zn deposits.

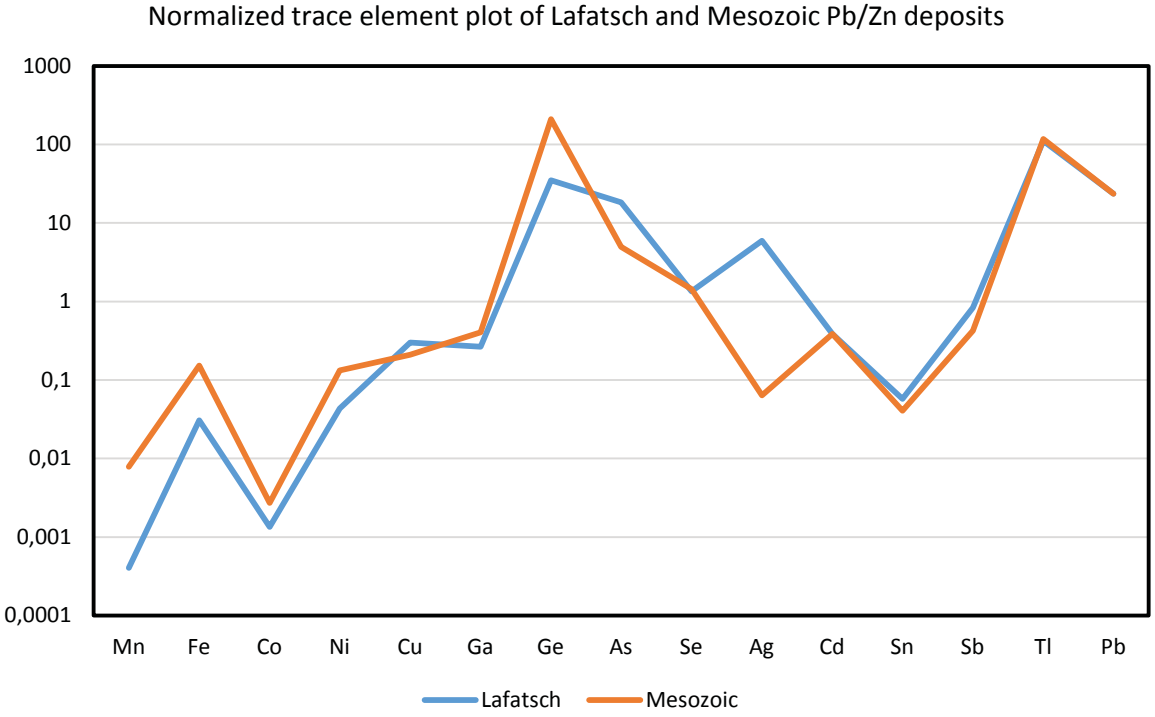

Fig. 50: Spider diagram of the Lafatsch Pb/Zn deposit and all Mesozoic Pb/Zn deposits normalized to the CTEM.

The probability plots in Fig. 51 show the variation of the important trace elements Fe, Cd, Mn, Cu, Ga, Ge, As and Tl within the samples of the Lafatsch Pb/Zn deposit. All the elements except

Cu, how a log- normally distribution (Fig. 51). The outlier of the elements Cd, Ga, Ge, and Cu, marked with blue ellipse in Fig. 51 do not correlate with other elements in the Lafatsch data set.

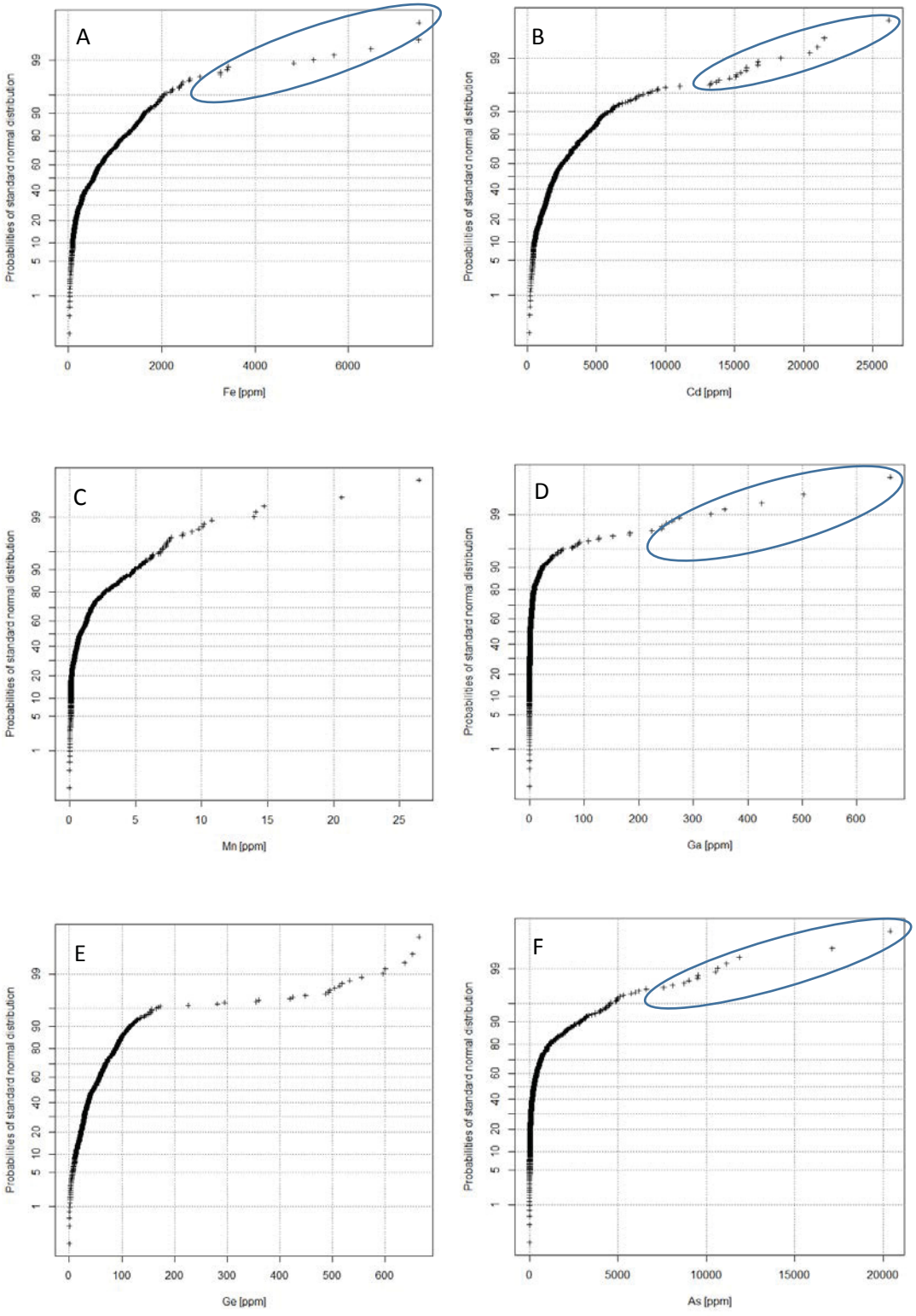

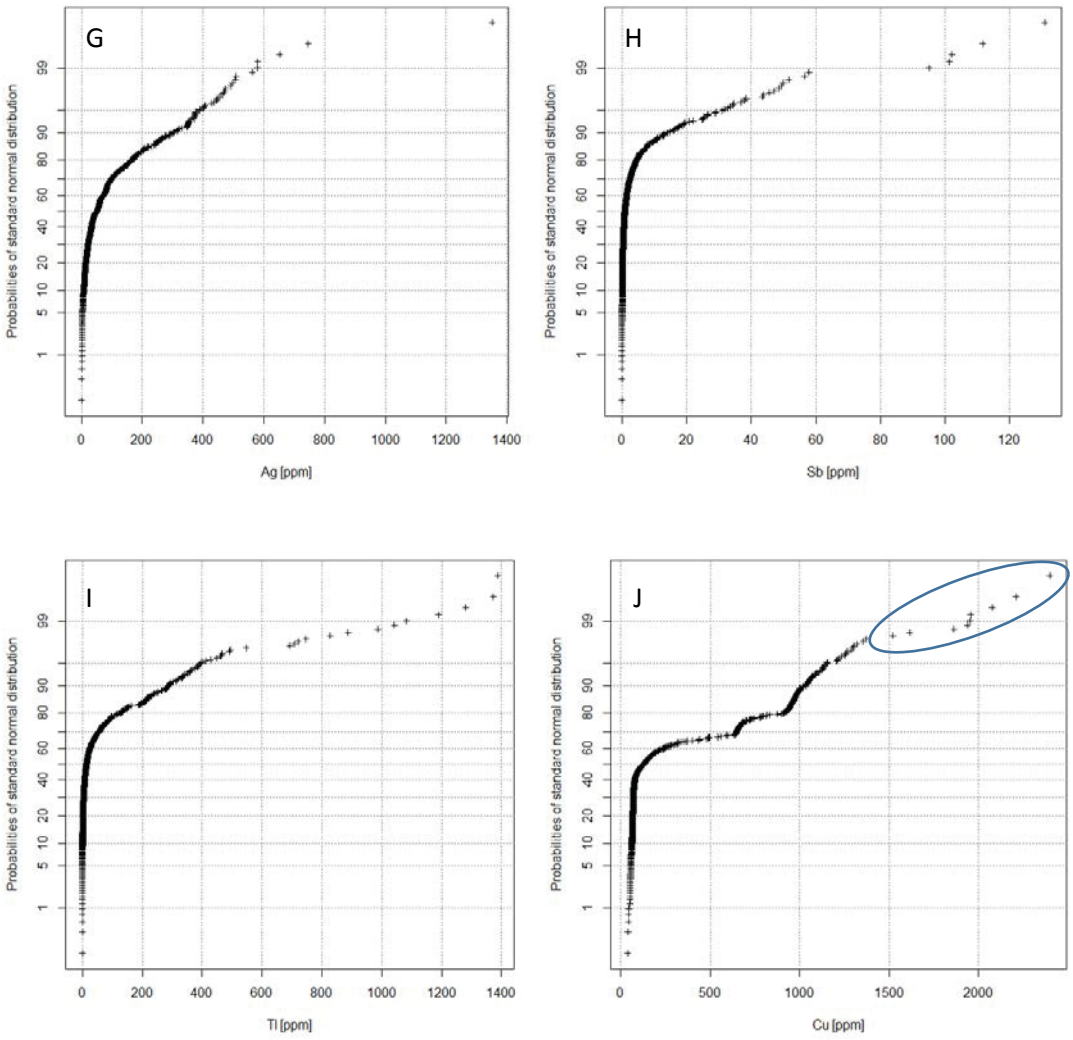

Fig. 51: Probability plots for the elements: A: Fe, B: Cd, C: Mn, D: Ga, E: Ge, F: As, G: Ag, H: Sb, I: Tl and J: Cu

In-situ sulfur isotope measurements (n= 80) of sphalerite from the Lafatsch Pb/Zn deposit shows a wide range (-35 to -10 ‰) with a maximum at -21 ‰ (Fig. 52). These values are comparable with data from the literature (Schulz 1981).

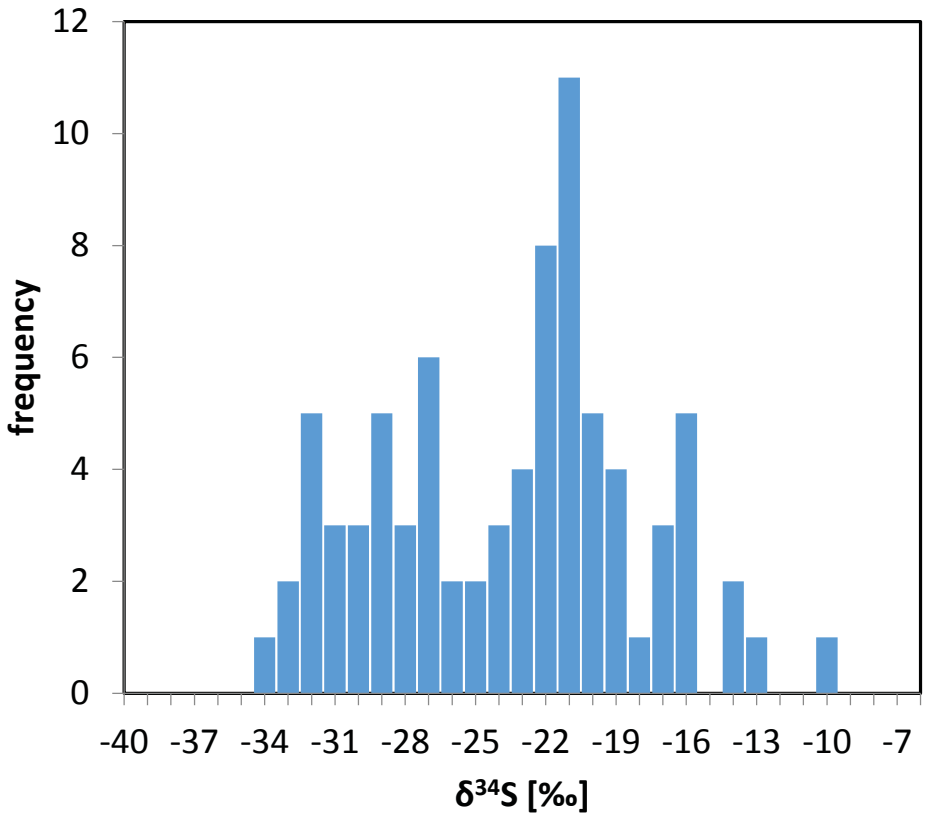

Fig. 52: Sulfur isotopic pattern of Sphalerite from Lafatsch Pb/Zn deposit.

5.5.2 Sphalerite chemistry of Paleozoic Pb/Zn mineralizations

Sphalerite from ten Paleozoic Pb-Zn deposits (Guggenbach, Arzberg, Rabenstein, Elisabeth adit, Friedrich adit, Silberberg, Haufenreith, Meiselding, Walchen, Leogang/Schwarzleo) are compared to the CTEM enriched in the elements Fe, Co, Cu, Ag, In, Sb and depleted in Mn, Ni, Ga, Cd, Sn and Pb (see Fig. 53). The plot in Fig. 53 visualizes the enormous variability of the dataset; some elements have a variation of 4 orders of magnitude. In this graph, 1436 in-situ measurements are plotted representing 10 deposits hosted in Paleozoic units.

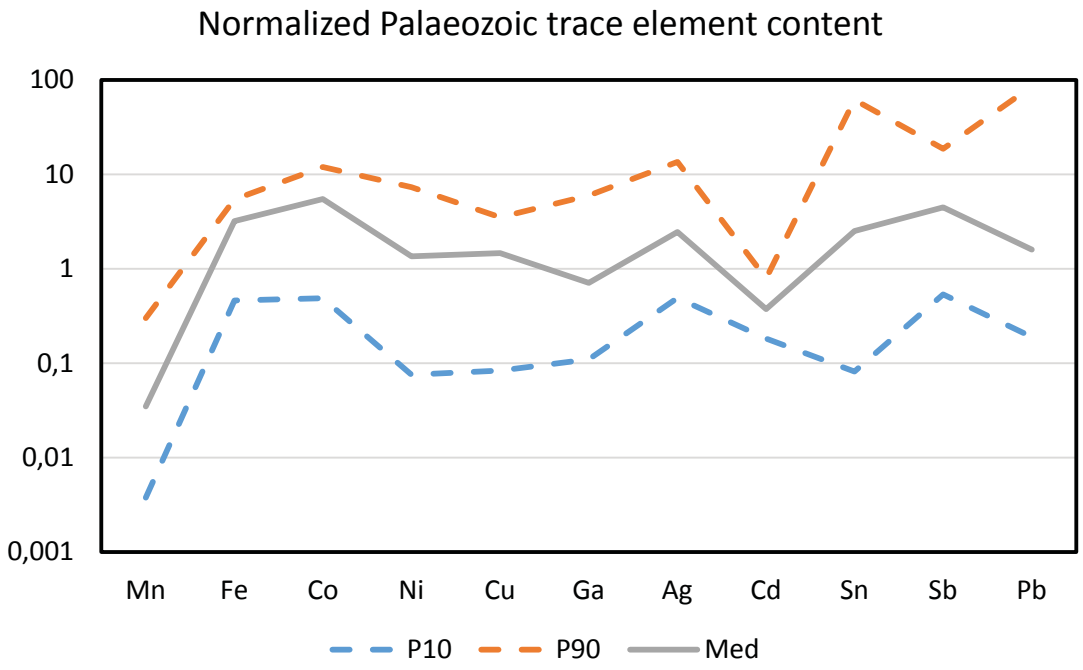

Fig. 53: Median, P10 and P90 values normalized trace element data from all ten Paleozoic Pb/Zn deposits (92 sample median values including 1618 analyses) normalized to the CTEM.

Table 13 shows calculated median values of ten Paleozoic Pb-Zn deposits (median values of 92 samples (10 locations) representing 1618 in situ trace elements measurements. These are used in the following as a ´Paleozoic trace element median`.

Table 13: Trace element median [µg/g] of all measured Paleozoic Pb-Zn deposits (10)

Cr	Mn	Fe	Co	Ni	Cu	Ga	Ge	As
0.45	88	49800	91	0.35	891	3.86	0.1	0.24

Se	Mo	Ag	Cd	In	Sn	Sb	Tl	Pb
6.5	0	18.5	1563	12.5	0.77	3.9	0.013	16.8

5.5.3 Graz Paleozoic

Sample median values from the deposits Guggenbach, Arzberg, Rabenstein, Elisabeth adit, Friedrich adit, Silberberg, Haufenreith were normalized to the CTEM plotted against the Paleozoic median. Compared to the Paleozoic median, median values of the Graz Paleozoic show enrichment in the elements Cr, Co, Ni, Ag, Sb, Pb and depleted in Mn, Fe, Se, Cd, In, Sn and Tl (Fig. 54).

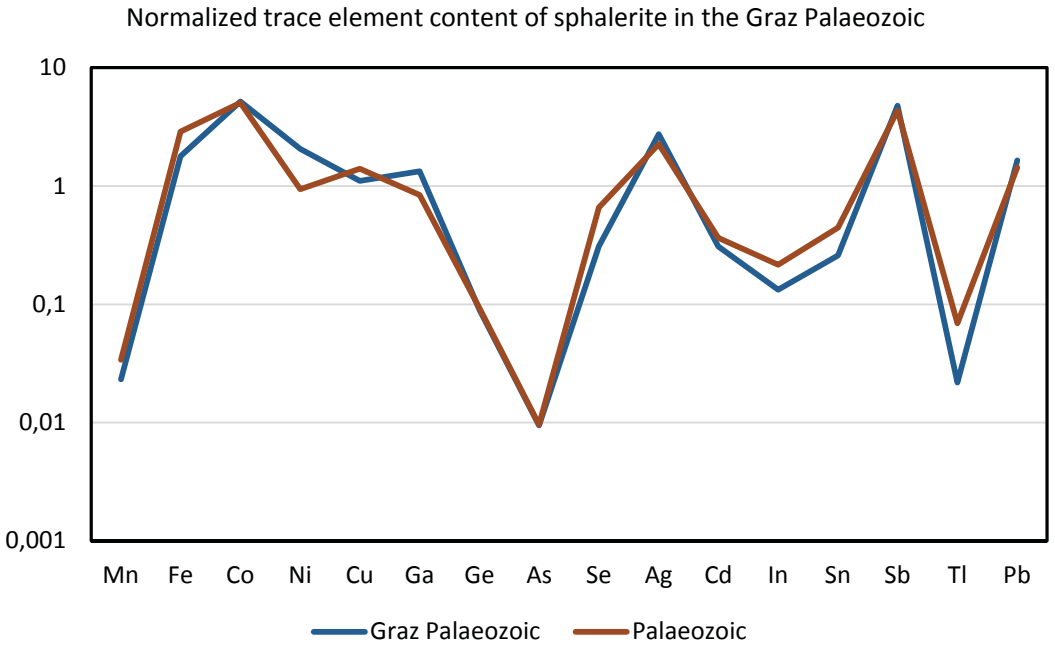

Fig. 54: Spider plot of the median from Graz Paleozoic Pb/Zn deposits and all measured Paleozoic deposits normalized to the CTEM.

The plot of all sulfur isotopic measurements (6 deposits, 152 spot analyses) performed on sphalerite shows a bimodal distribution with maxima at +1 and +7 ‰. The isotopic composition ranges from -3 to +13 ‰ (Fig. 55).

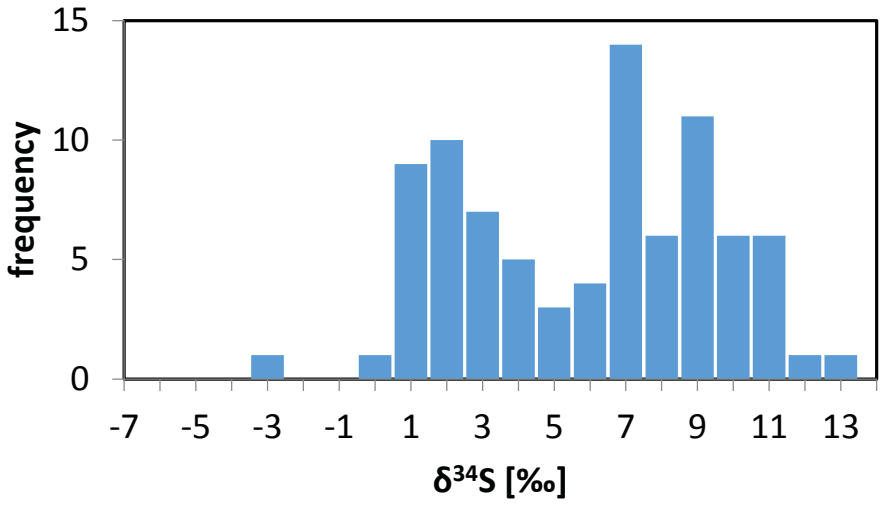

Fig. 55: Summarizing plot of all $\delta^{34}S$ measurements performed on sphalerite from the Graz Paleozoic Pb/Zn deposits.

5.5.3.1 Guggenbach

Table 14 summarizes the mineralogical composition determined by LA-ICP-MS (15 samples, 364 spot analyses) for the major, minor and trace elements in sphalerite from the Guggenbach deposit. The maximum value of Ge (209 µg/g) seems to be an outlier; the high Ge value does not correlate with other elements of this analysis.

Table 14: Statistics summarizing trace element contents from 364 LA-ICP-MS measurements on sphalerite hosted by the Guggenbach Pb/Zn deposit (values reported in µg/g).

	^{55}Mn	^{56}Fe	^{59}Co	^{63}Cu	^{71}Ga	^{74}Ge	^{107}Ag	^{111}Cd	^{115}In	^{118}Sn	^{121}Sb	^{208}Pb
D90	136	57940	179	1162	44.8	2.6	42.3	2028	4.3	1.9	15.1	241
D75	104	54800	156	1005	20.8	0.2	30.4	1558	3	1.4	8.7	59
Median	74	49800	134	918	7.4	0.1	18.5	1132	0.2	0.9	4.3	23
D25	64	44143	102	602	2.8	bdl	9.8	981	0.1	0.6	1.6	8.9
D10	55	29611	56	514	1.6	bdl	4.1	841	0.1	0.5	0.4	4.3
Min	16.6	13690	1.2	367	0.4	bdl	0.9	765	bdl	bdl	bdl	0.2
Max	2750	114000	289	10700	212	209	197	8200	83	47.8	119	18100

Most trace elements of the samples from the Guggenbach Pb/Zn deposit follow the trend of the Paleozoic and the Graz Paleozoic median. Compared to the CTEM, Cr, Fe, Co, Ni, Cu, Ag, Sn, Sb are enriched and Ga, Ge, In, Sb, Tl and Pb are depleted. Compared to the median of all Paleozoic deposits, sphalerite from Guggenbach is enriched in Cr, Co, Ni, Cu, As, Ag, Sn, Sb and depleted in Mn, As, Se, Cd, In and Tl (Fig. 56).

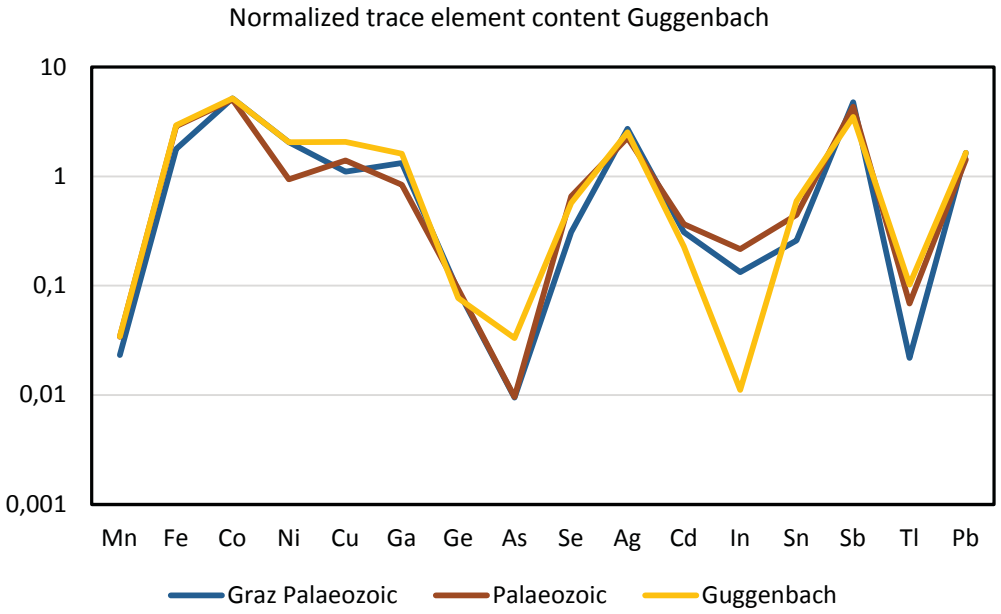

Fig. 56: Spider plot of the median from Guggenbach Pb/Zn deposits and all measured Paleozoic and Graz Paleozoic Pb/Zn deposits normalized to the CTEM.

The elements Fe, Co, Cu, Ge, As and In indicate at least three sphalerite populations (Fig. 57A, D, E, G, H and I). The probability plots of the elements Ni, Ga, Ag and Sb give evidence for a lognormally distribution of these elements (Fig. 57E, F, J and K). The sample GB-P4 shows

compared to the rest of the samples elevated values in Ga, In and Ag (Fig. 57 blue ellipse). This sample is also enriched in Mn, Cd and Sb, which can indicate a sulfosalt component.

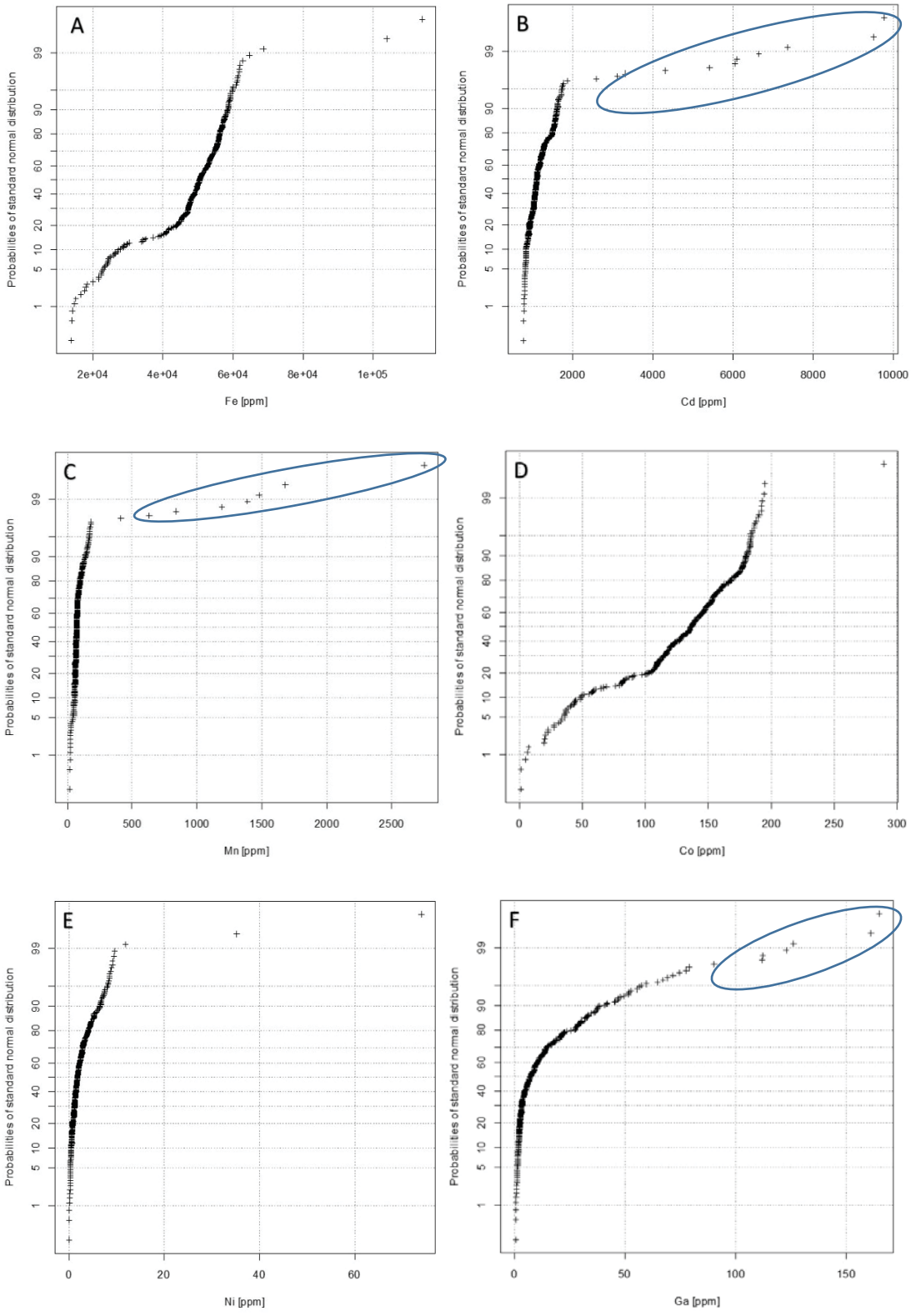

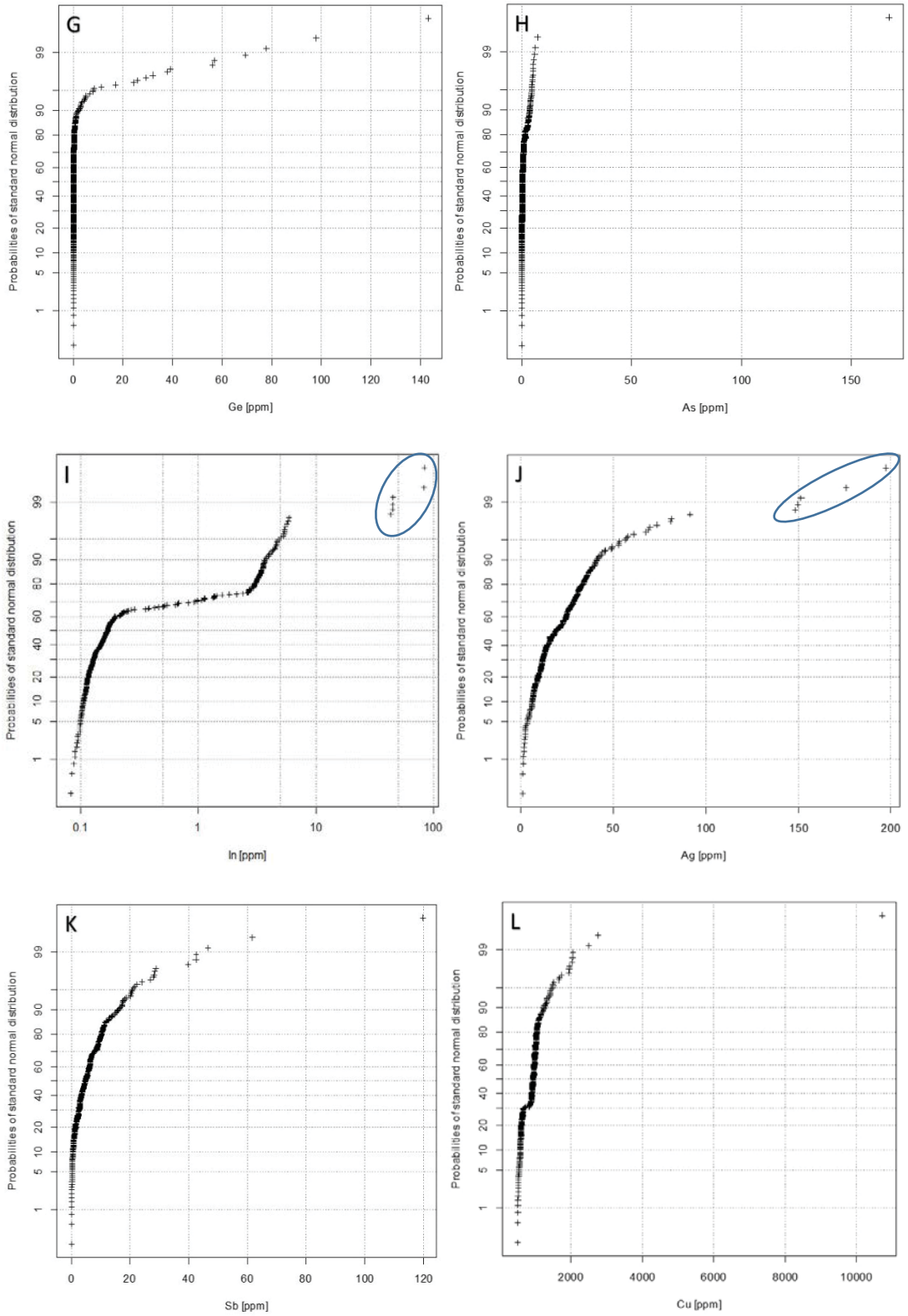

Fig. 57: Probability plots for the elements: A: Fe, B: Cd, C: Mn, D: Co, E: Ni, F: Ga, G: Ge, H: As, I: In, J: Ag, K: Sb and L: Cu

The Guggenbach Pb/Zn deposit shows a bimodal distribution in the sulfur isotopic composition (n= 44) ranging from -3 to +13 ‰ with two maxima, the first maximum at +2 ‰ representing the primary sphalerite, the second maximum at +7 ‰ might represent remobilized sphalerite (verbal confirmation of Weber L.) (Fig. 58).

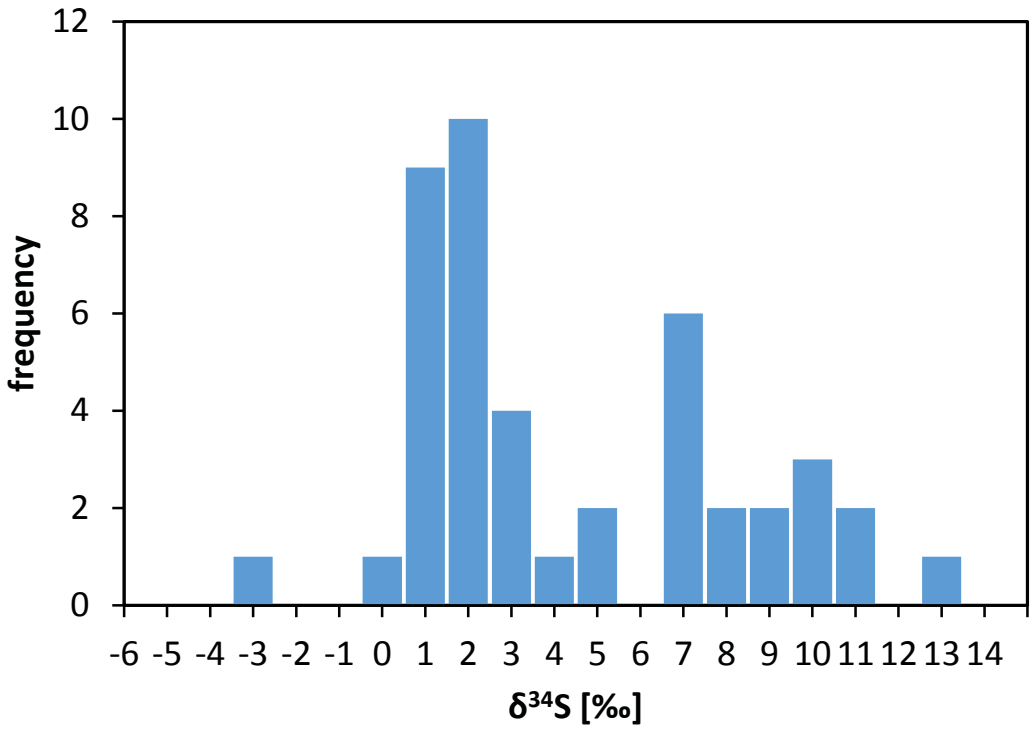

Fig. 58: Sulfur isotopic composition measured on sphalerite from the Guggenbach Pb/Zn deposit.

5.5.3.2 Arzberg

Table 15 displays the chemical composition of sphalerite from the Arzberg deposit determined by LA-ICP-MS (11 samples, 181 spot analyses) for the major, minor and trace elements.

Table 15: Statistics summarizing trace element contents from 181 LA-ICP-MS measurements on sphalerite hosted in the Arzberg Pb/Zn deposit (values reported in µg/g).

	^{55}Mn	^{56}Fe	^{59}Co	^{63}Cu	^{71}Ga	^{74}Ge	^{107}Ag	^{111}Cd	^{115}In	^{118}Sn	^{121}Sb	^{208}Pb
Q90	269	63300	351	2762	20.9	0.3	357	2001	10.3	1.2	29.9	1170
Q75	144	19100	233	1741	11	0.2	179	1851	8.4	0.7	13.9	330
Median	103	14020	27	936	2.1	0.1	78	1292	4	0.4	5.9	69
Q25	35.5	10490	11.3	125	0.6	bdl	11	975	2.6	0.2	2.4	15
Q10	23.2	6810	4	45	0.3	bdl	0.7	877	2	0.1	0.6	5.5
Min	6.6	2780	0.6	14.9	0.1	bdl	0.1	819	1	bdl	bdl	0.2
Max	3590	75500	387	5240	143	20	3556	2417	24.1	2.9	1953	41000

The sphalerite samples from the Arzberg Pb/Zn deposit follow the trend of the Paleozoic and the Graz Paleozoic median, but are enriched in Ag and Pb, due to inclusions of Ag bearing Galena and sulfosalt inclusions in sphalerite. Compared to the CTEM Cr, Mn, Cu, Se, Ag, In, Sb Tl, Pb are enriched and Fe, Co, Ni, Ga, Cd and Sn are depleted. In comparison to the median of all Paleozoic deposits, sphalerite from Arzberg is enriched in V, Cr, Ge, As, Se, Ag, Tl, Pb and depleted in Mn, Fe, Co, Ni, Ga and Cd (Fig. 59).

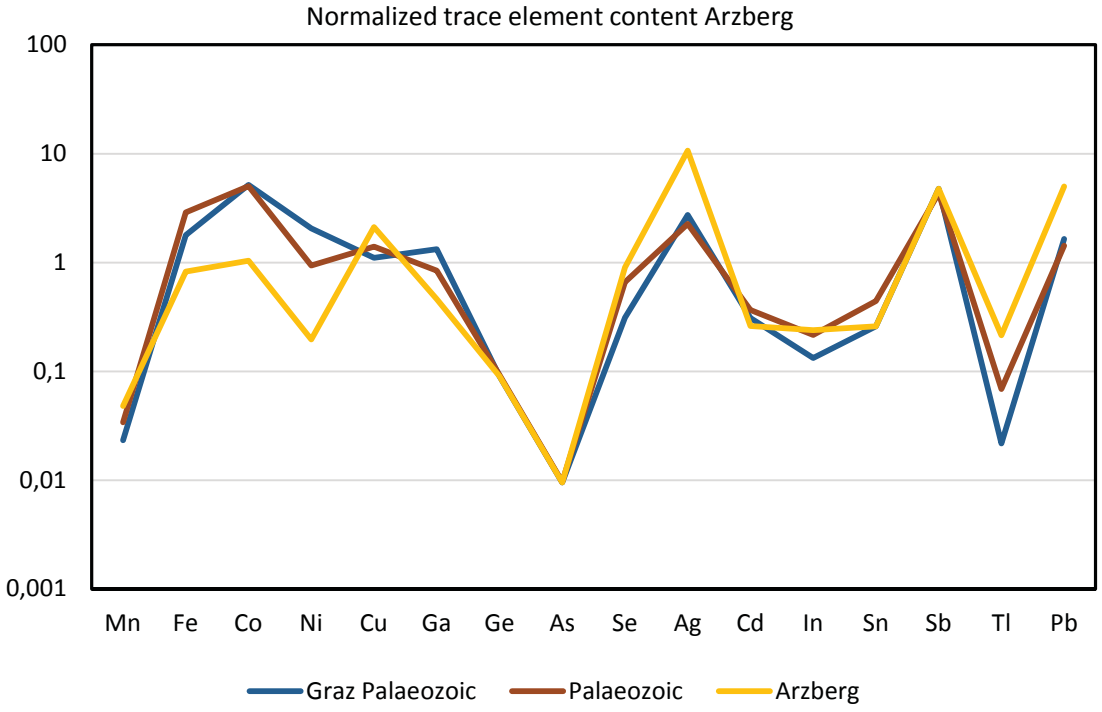

Fig. 59: Spider plot of the median from Arzberg Pb/Zn deposits and all measured Paleozoic and Graz Paleozoic Pb/Zn deposits normalized to the CTEM.

The probability plots in Fig. 60 indicates at least two sphalerite generations (Fe, Co poor and Fe, Co rich). The measured elements show no linear or lognormally distribution (Fig. 60). The elevated Ag, Cd and In concentrations plotted Fig. 60B, H and J give evidence for sulfosalt micro inclusions in sphalerite.

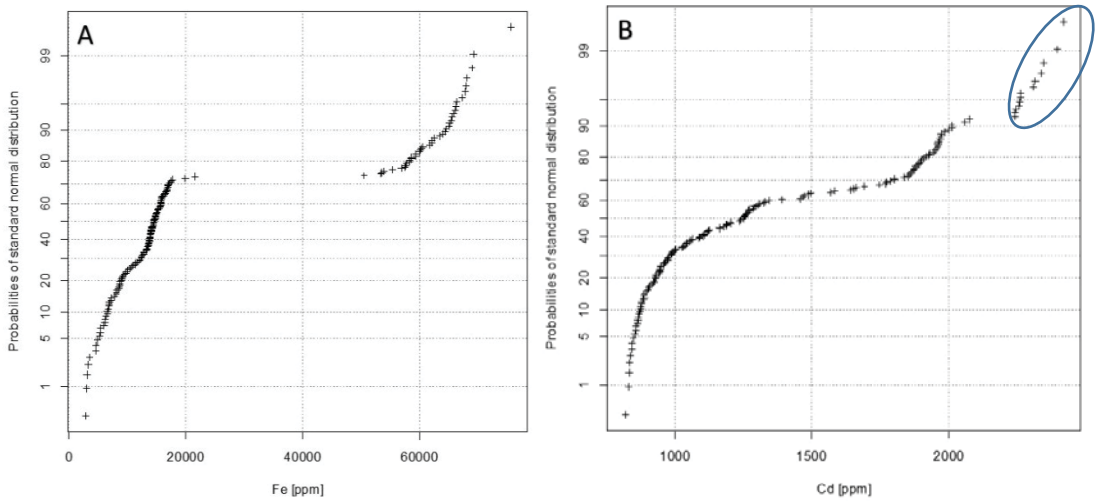

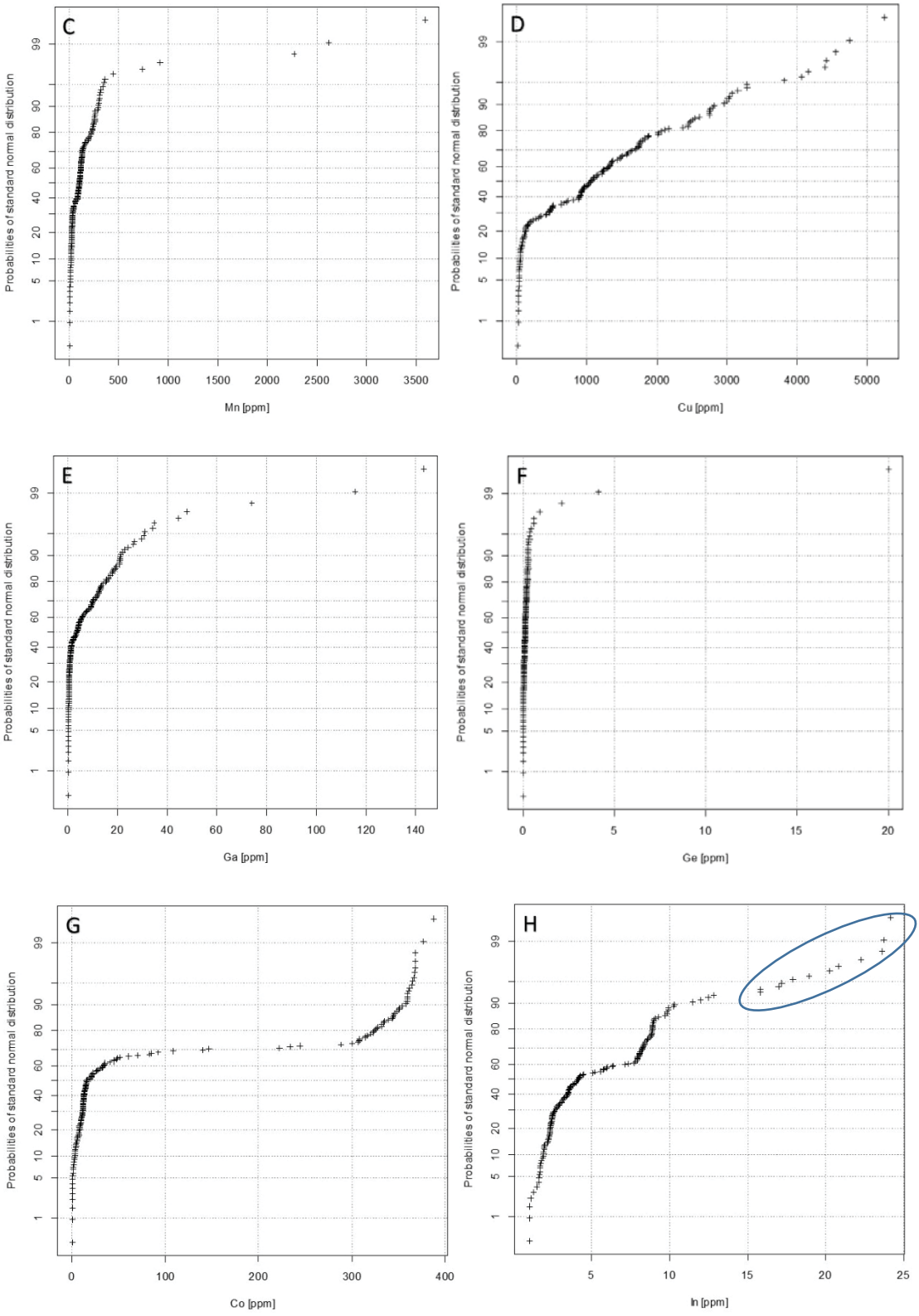
C
Probabilities of standard normal distribution
Mn [ppm]
D
Cu [ppm]
E
Ga [ppm]
F
Ge [ppm]
G
Co [ppm]
H
In [ppm]

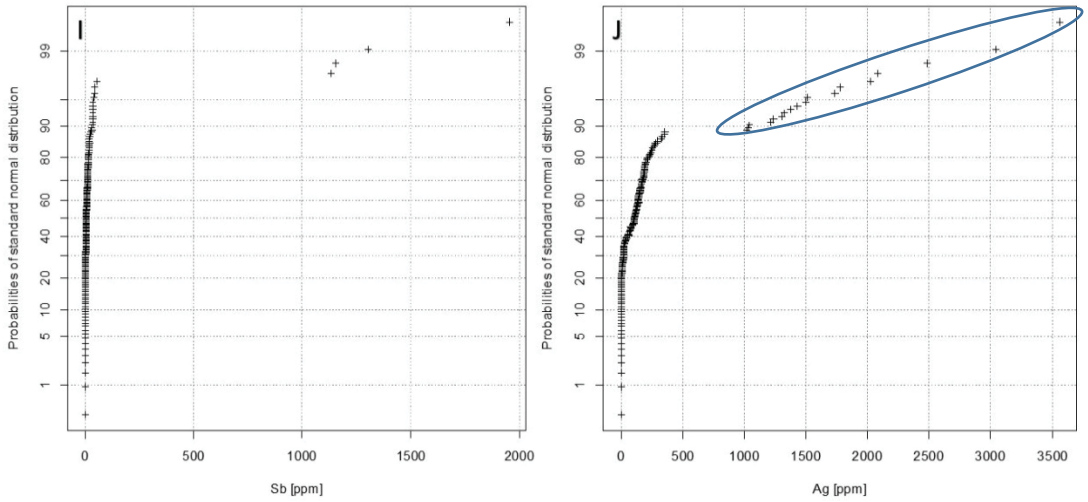

Fig. 60: Probability plots for the elements: A: Fe, B: Cd, C: Mn, D: Cu, E: Ga, F: Ge, G: Co, H: In, I: Sb and J: Ag

Sphalerite from the Arzberg Pb/Zn deposit shows a unimodal distribution in sulfur isotopic composition (n= 21) ranging from +2 to +11 ‰ (Fig. 61).

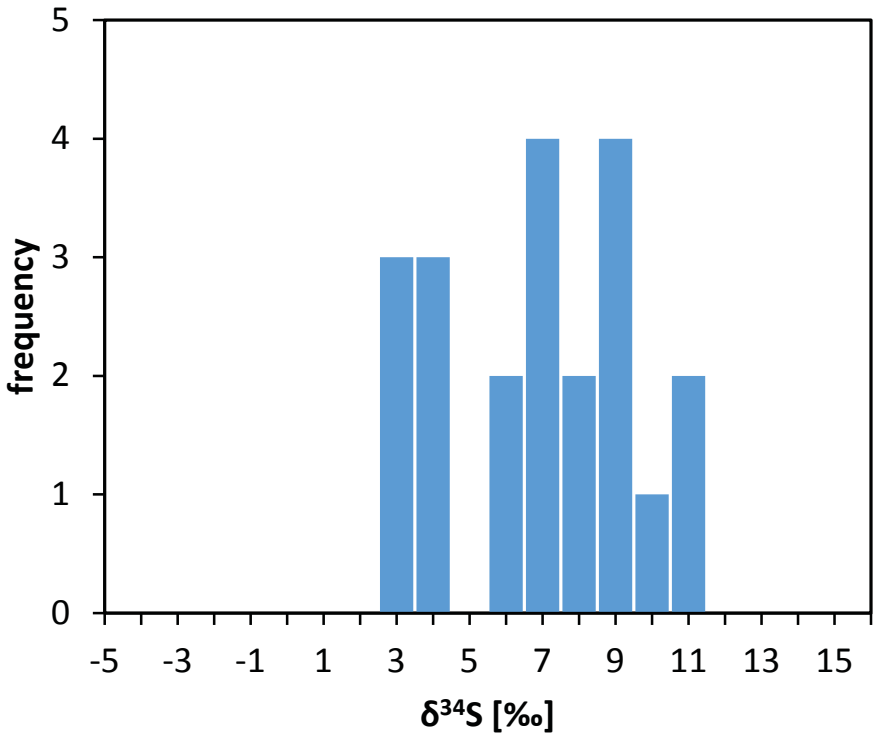

Fig. 61: $\delta^{34}S$ isotopic composition measured on sphalerite from the Arzberg Pb/Zn deposit.

5.5.3.3 *Rabenstein*

Table 16 displays the chemical composition of sphalerite from the Rabenstein deposit dumpsite determined by LA-ICP-MS (9 samples, 190 spot analyses) for the major, minor and trace elements.

Table 16: Statistics summarizing table of trace element contents from 190 LA-ICP-MS measurements on sphalerite hosted by the Rabenstein Pb/Zn deposit (values reported in µg/g).

	^{55}Mn	^{56}Fe	^{59}Co	^{63}Cu	^{71}Ga	^{74}Ge	^{107}Ag	^{111}Cd	^{115}In	^{118}Sn	^{121}Sb	^{208}Pb
D90	32.1	19656	169	1225	15.1	0.3	57	2117	15.6	1	25.1	531
D75	20.3	13010	44.7	1011	10.4	0.1	38.8	1801	8	0.7	13.3	38.7
Median	7	6300	28.3	940	5.6	0.1	20.2	1534	1	0.6	6.7	15.2
D25	4.9	4290	9.2	885	2.1	bdl	11.3	1209	0.4	0.4	3.4	7.2
D10	3.3	2001	2.5	574	0.7	bdl	7.3	769	0.2	0.3	1	3.3
Min	1.7	878	0.4	284	0.5	bdl	1.1	655	0.1	bdl	bdl	0.4
Max	630	34900	274	4170	21.8	5.3	399	2608	29.7	7	151	37000

Compared to the CTEM samples from Rabenstein Pb/Zn deposit are enriched in Cr, Ni, Cu, Ag, Sb and depleted in Mn, Fe, Co, Ga, Ge, As, Cd, In, Tl and Pb. In contrast to the median of all Paleozoic deposits, sphalerite from Rabenstein is enriched in Cr, Ni, Cu, As and depleted in Mn, Fe, Co, Ni, Ge and In (Fig. 62).

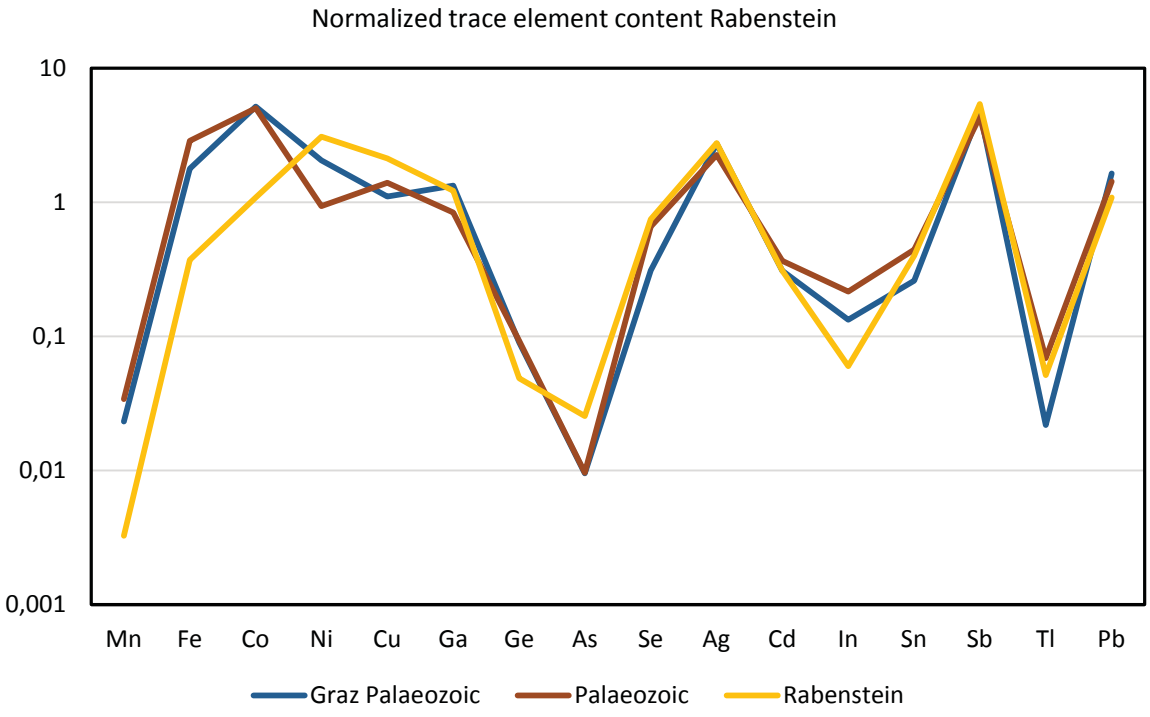

Fig. 62: Spider plot of the median from Rabenstein Pb/Zn deposits and all measured Paleozoic and Graz Paleozoic Pb/Zn deposits normalized to the CTEM.

The probability plots in Fig. 63 gives evidence for three sphalerite populations, none of the elements of interest is linear or lognormally distributed. The high Co values (up to 274µg/g) show a positive correlation with Fe (Fig. 63C).

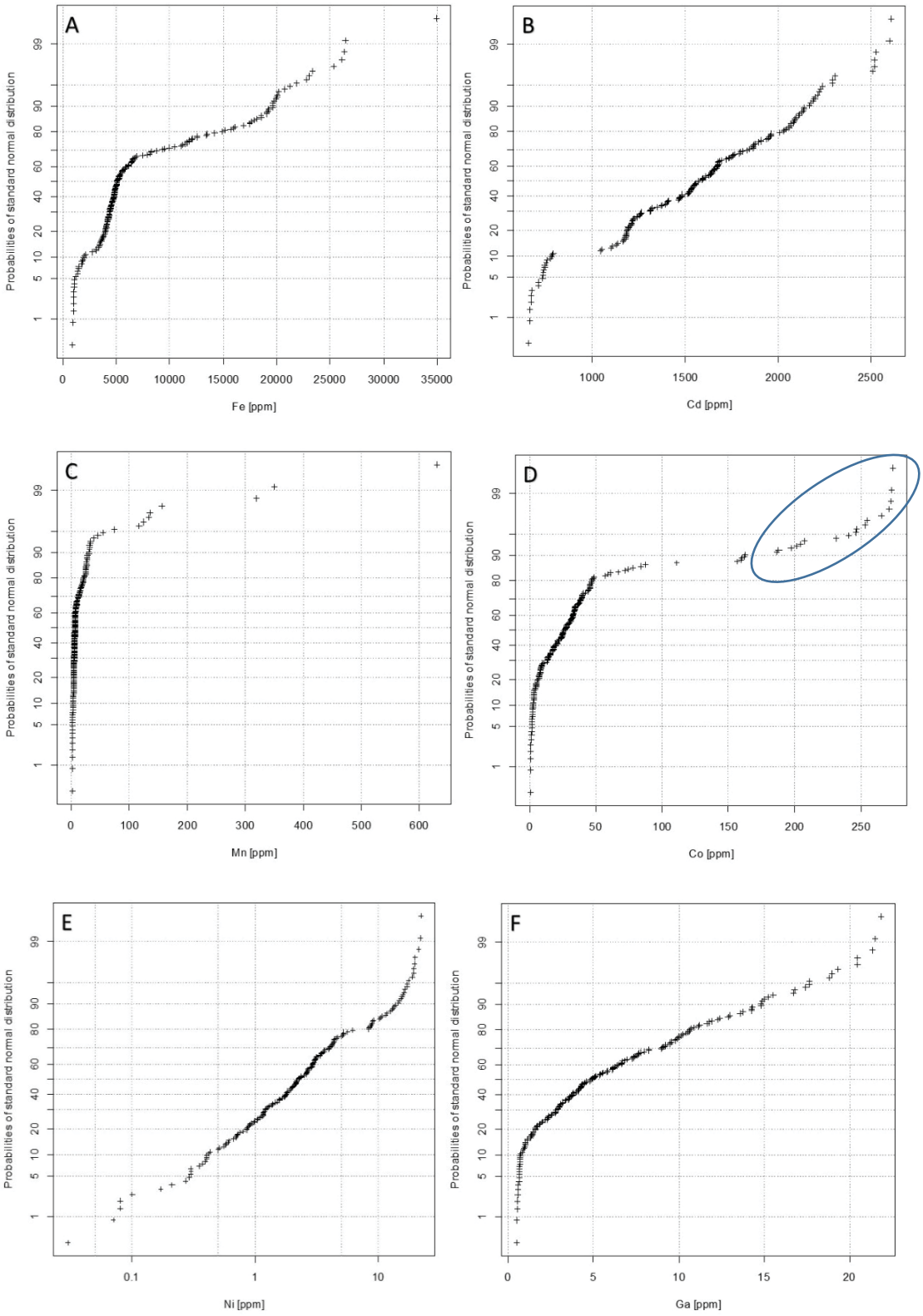
A
Probabilities of standard normal distribution
1 5 10 20 40 60 80 90 99
0 5000 10000 15000 20000 25000 30000 35000
Fe [ppm]
B
Probabilities of standard normal distribution
1 5 10 20 40 60 80 90 99
1000 1500 2000 2500
Cd [ppm]
C
Probabilities of standard normal distribution
1 5 10 20 40 60 80 90 99
0 100 200 300 400 500 600
Mn [ppm]
D
Probabilities of standard normal distribution
1 5 10 20 40 60 80 90 99
0 50 100 150 200 250
Co [ppm]
E
Probabilities of standard normal distribution
1 5 10 20 40 60 80 90 99
0.1 1 10
Ni [ppm]
F
Probabilities of standard normal distribution
1 5 10 20 40 60 80 90 99
0 5 10 15 20
Ga [ppm]

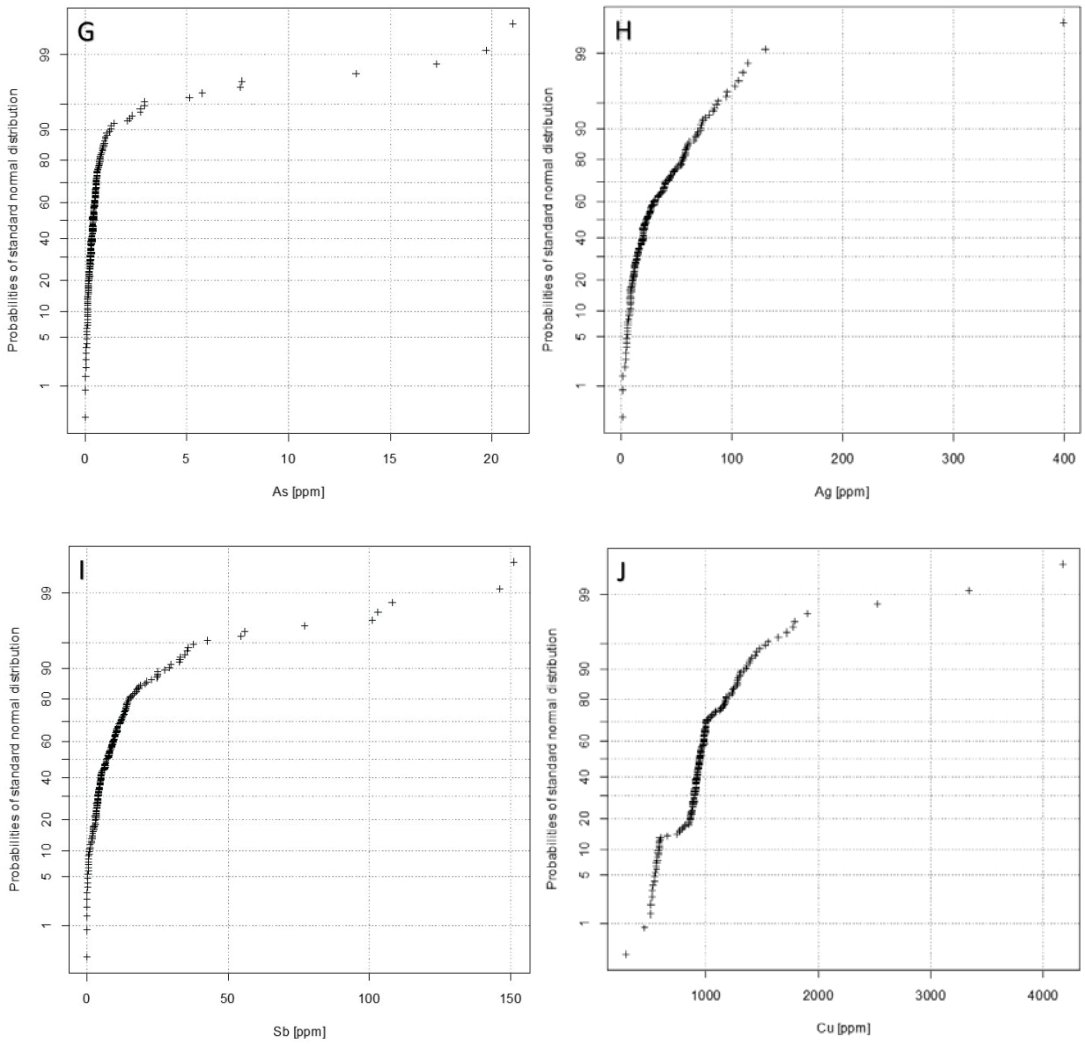

Fig. 63: Probability plots for the elements: A: Fe, B: Cd, C: Mn, D: Co, E: Ni, F: Ga, G: As, H: Ag, I: Sb and J: Cu

Sphalerite (n= 29) from Rabenstein deposit shows a sulfur isotopic composition that varies between +3 and +13 ‰, with a maximum at +11 ‰ (Fig. 64).

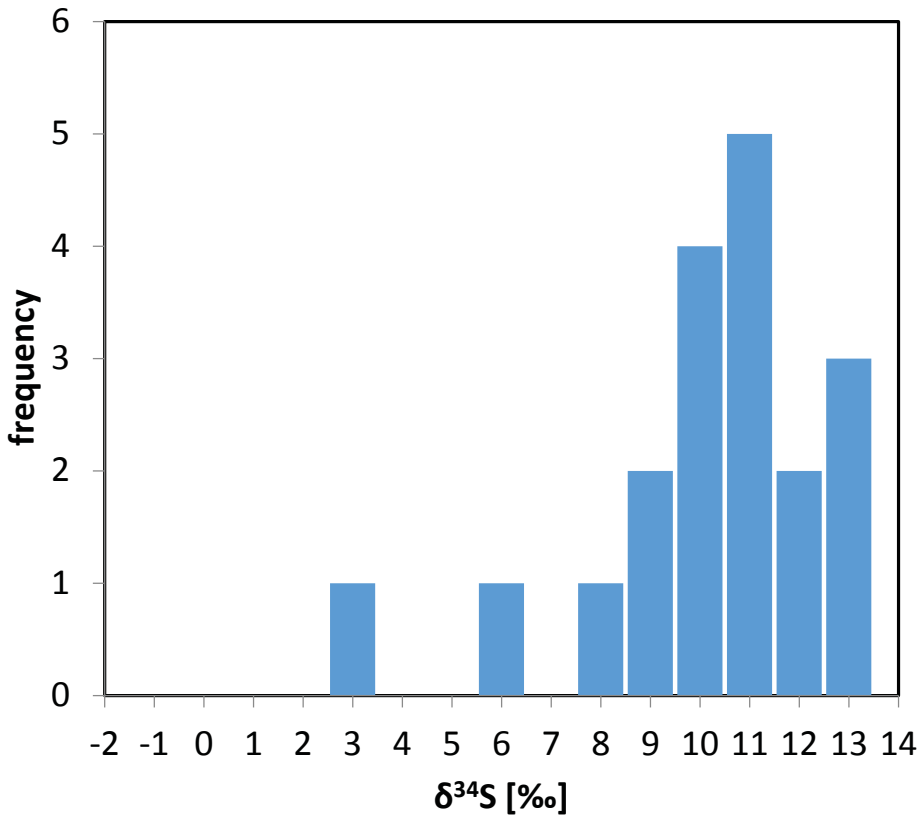

Fig. 64: $\delta^{34}S$ pattern measured on sphalerite from the Rabenstein mineralization.

5.5.3.4 Elisabeth adit

Table 17 displays the chemical composition of sphalerite from the Elisabeth adit, determined by LA-ICP-MS (8 samples, 150 spot analyses) for the major, minor and trace elements.

Table 17: Statistics summarizing table of trace element contents from 190 LA-ICP-MS measurements on sphalerite hosted in the Elisabeth adit (values reported in µg/g).

	^{55}Mn	^{56}Fe	^{59}Co	^{63}Cu	^{71}Ga	^{74}Ge	^{107}Ag	^{111}Cd	^{115}In	^{118}Sn	^{121}Sb	^{208}Pb
D90	133	65300	186	109	43.1	1.5	36.9	2829	0.5	0.4	17.6	686
D75	72	62175	177	63	22.8	0.4	24.4	2330	0.3	0.1	12.9	60
Median	55	57750	167	35.2	10.3	0.2	14.4	2168	0.2	bdl	7.8	26.4
D25	44.3	53450	147	24.8	4	0.1	9.6	2024	0	bdl	4.2	14.9
D10	35.7	40117	74	17.6	1.1	0	6.2	1910	0	bdl	2.1	7.5
Min	21.8	18920	55	11.2	0.5	0	2.3	1785	0	bdl	0.2	2.1
Max	2180	73200	213	701	188	21.3	99	3180	0.9	21.2	57	5100

In contrast to the CTEM, Elisabeth adit samples show enrichment in Fe, Co, Ag and are depleted in Cr, Mn, Cu, Ge, As, Se, Cd, In, Sn, Sb and Tl. In comparison to the median of all Paleozoic deposits, sphalerite from Elisabeth adit is enriched in Co, Ga, Ge and depleted in Cr, Ni, Cu, As, Ag, Sn, Tl and Pb (Fig. 65).

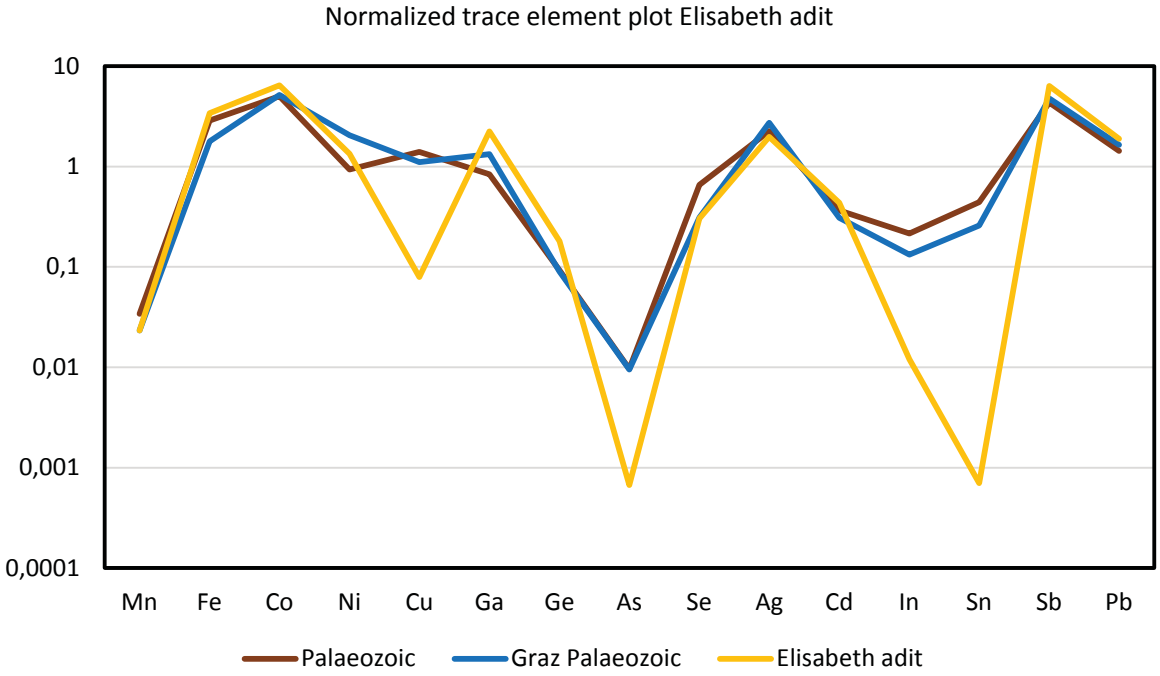

Fig. 65: Spider plot of the median from Elisabeth adit and all measured Paleozoic and Graz Paleozoic Pb/Zn deposits normalized to the CTEM.

Iron, Cd and Co in the probability plots in Fig. 66 indicates two sphalerite populations. The elements Mn, Ga, Ag, Sb and Cu (Fig. 66C, E, F, G, H) show a lognormally distribution.

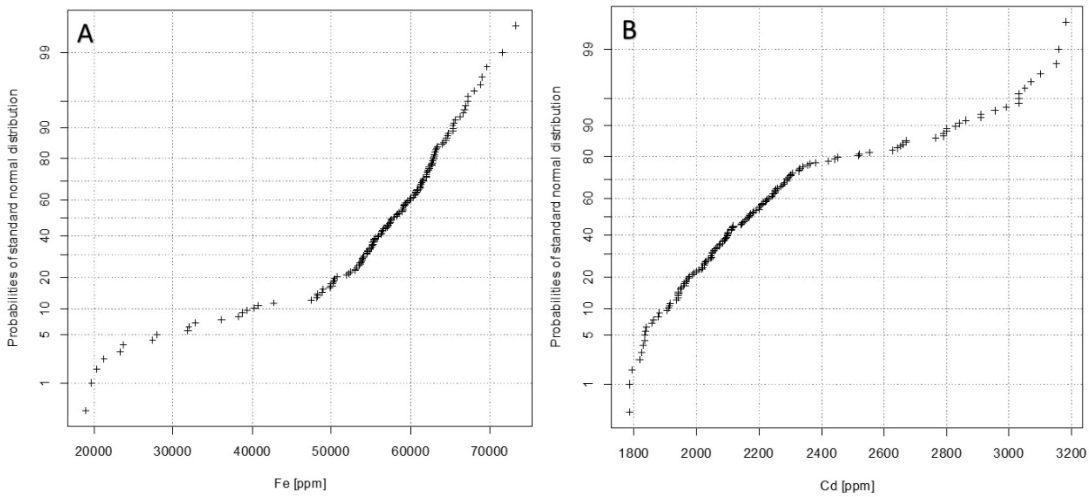

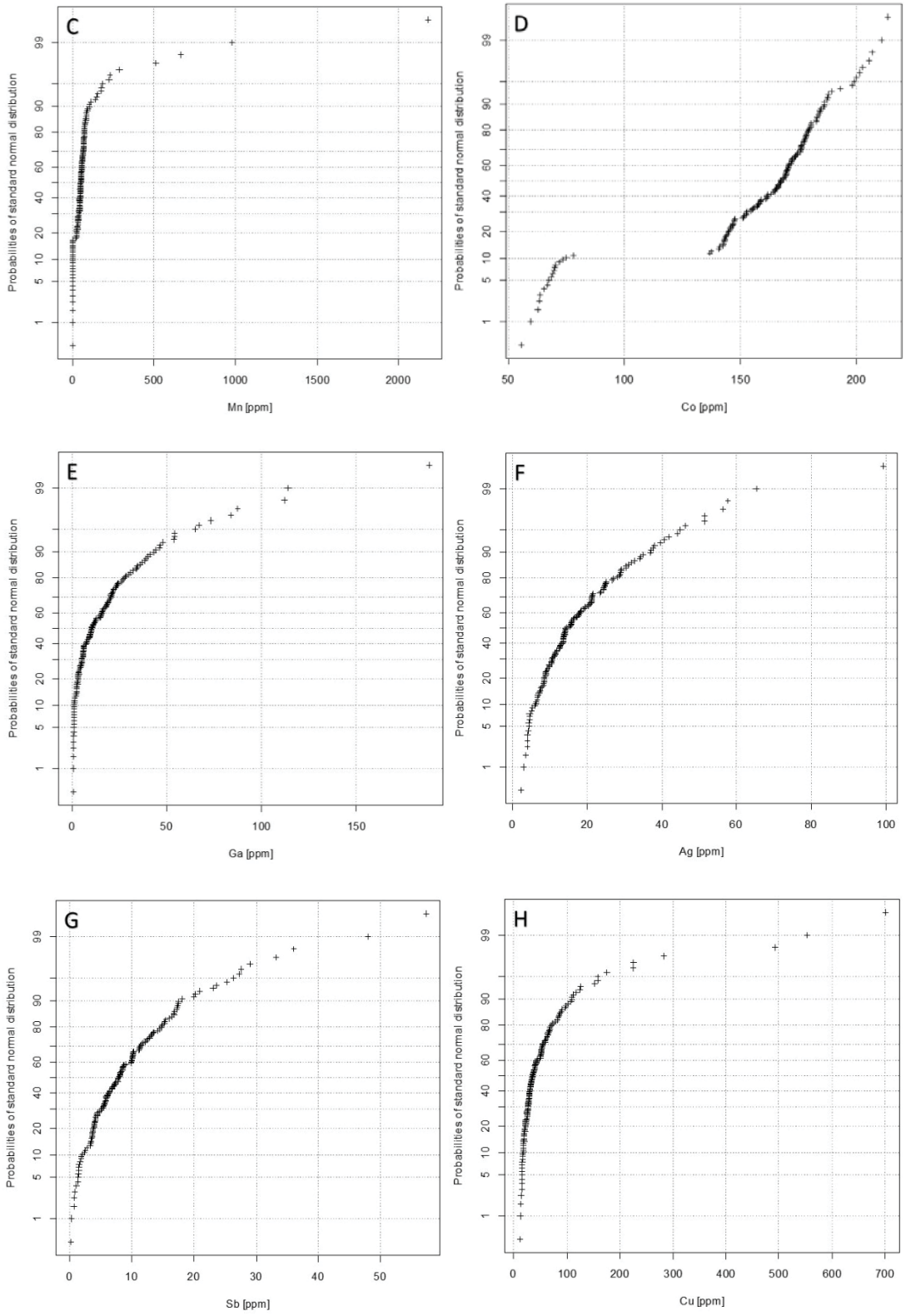

Fig. 66: Probability plots for the elements: A: Fe, B: Cd, C: Mn, D: Co, E: Ga, F: Ag, G: Sb, H: Cu.

Sphalerite samples (n= 29) from the Elisabeth adit show a variation in the $\delta^{34}S$ composition ranging from +6 to +12 ‰, with a maximum at +9 ‰ (Fig. 67).

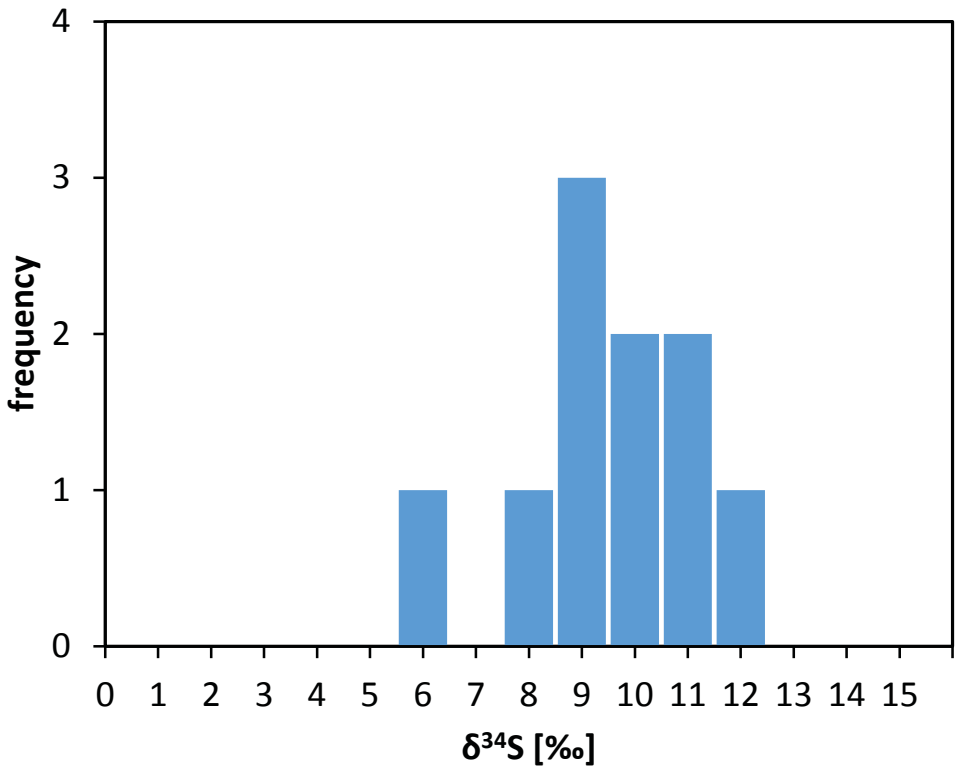

Fig. 67: Sulfur isotopic composition of sphalerite from the Elisabeth adit.

5.5.3.5 *Friedrich adit*

Table 18 displays the chemical composition of sphalerite from the Friedrich adit, determined by LA-ICP-MS (6 samples, 110 spot analyses) for the major, minor and trace elements.

Table 18: Statistics summarizing table of trace element contents from 110 LA-ICP-MS measurements on sphalerite derived from in the Friedrich adit (values reported in µg/g).

	^{55}Mn	^{56}Fe	^{59}Co	^{63}Cu	^{71}Ga	^{74}Ge	^{107}Ag	^{111}Cd	^{115}In	^{118}Sn	^{121}Sb	^{208}Pb
D90	84	59600	407	356	65	1.5	58	3242	31.8	1	16.8	290
D75	68	56650	338	158	33.7	0.4	40.2	3047	6.5	0.4	11.1	43.8
Median	48.5	48000	279	62	19.9	0.1	24.5	2673	2.2	bdl	7.6	22.9
D25	40.7	41650	162	32.5	9.4	bdl	14.5	2511	0.3	bdl	5.3	14.2
D10	33.9	37244	98	23.2	3.6	bdl	10.7	2391	0.1	bdl	2.5	10.3
Min	25	27700	33.5	5.8	1.3	bdl	2.6	2170	bdl	bdl	bdl	0.6
Max	282	62800	495	4500	111	72	183	3570	56	4.8	98	5330

In contrast to the CTEM Friedrich adit samples show enrichment in Fe, Co, Ni, Ga, Ag, Cd, In, Sb and are depleted in Cr, Mn, Cu, Ge, As, Se, In, Sn and Tl. In comparison to the median of all Paleozoic deposits, sphalerite from Friedrich adit is enriched in Fe, Co, Ni, Ga, Ag, Cd, Sb, Tl and depleted in Cr, Cu, Se and Sn (Fig. 68).

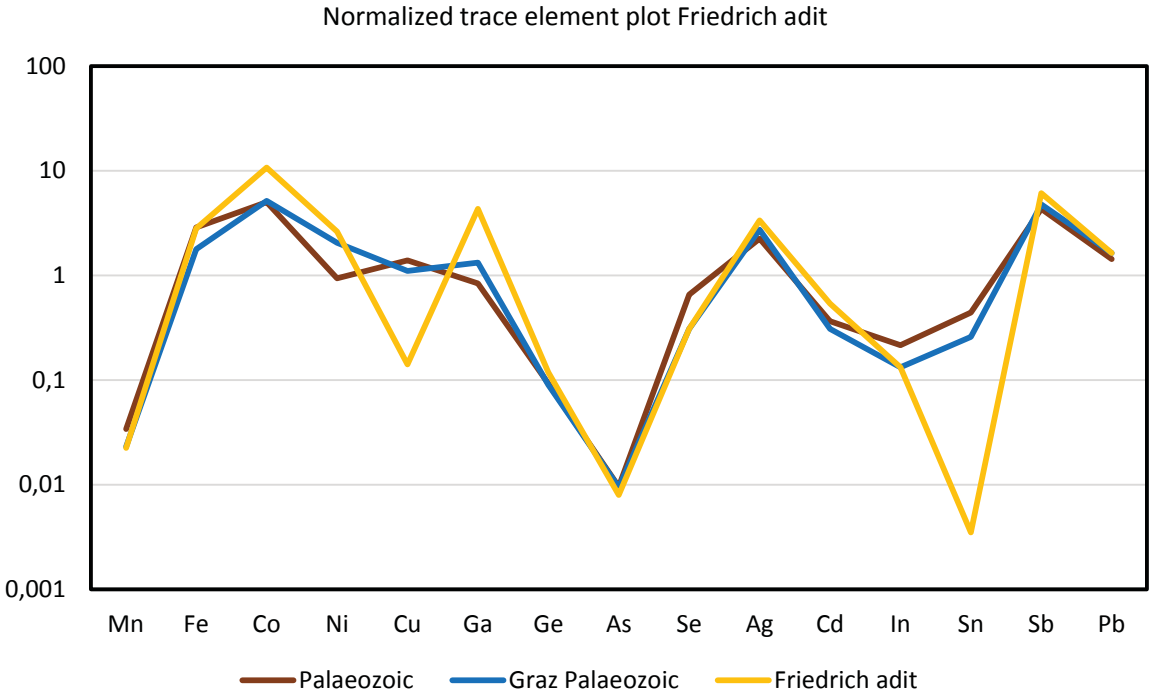

Fig. 68: Spider plot of the median from Friedrich adit and all measured Paleozoic and Graz Paleozoic Pb/Zn deposits normalized to the CTEM.

The elements Fe, Cd, Mn, Co, Ga and In in Fig. 69A, B, C, D, F and H indicate three different generations of sphalerite. A lognormally distribution can be seen for the elements Cu and Ag (Fig. 69: E, G). The elevated Ga and In values (Fig. 69F, H) show a positive correlation, suggesting sulfosalt micro inclusions.

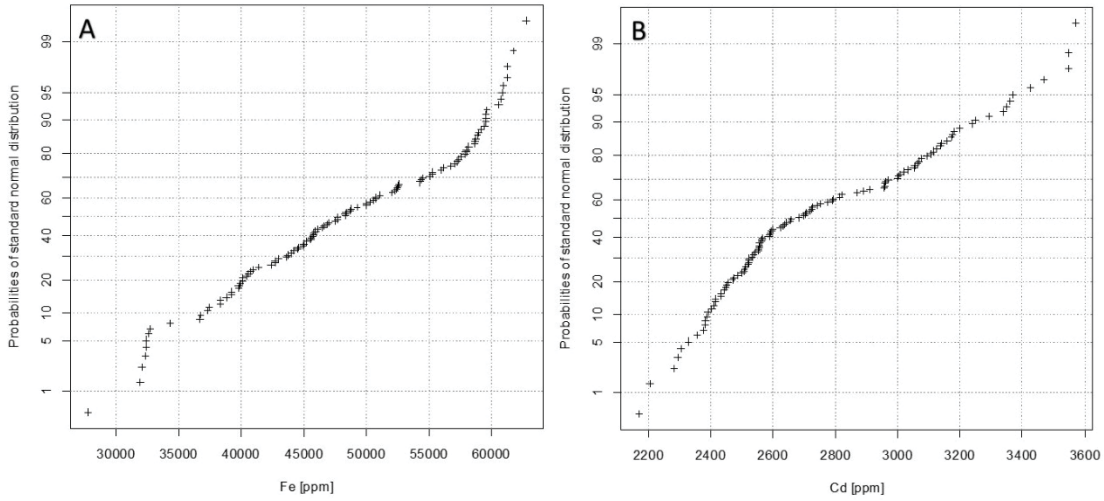

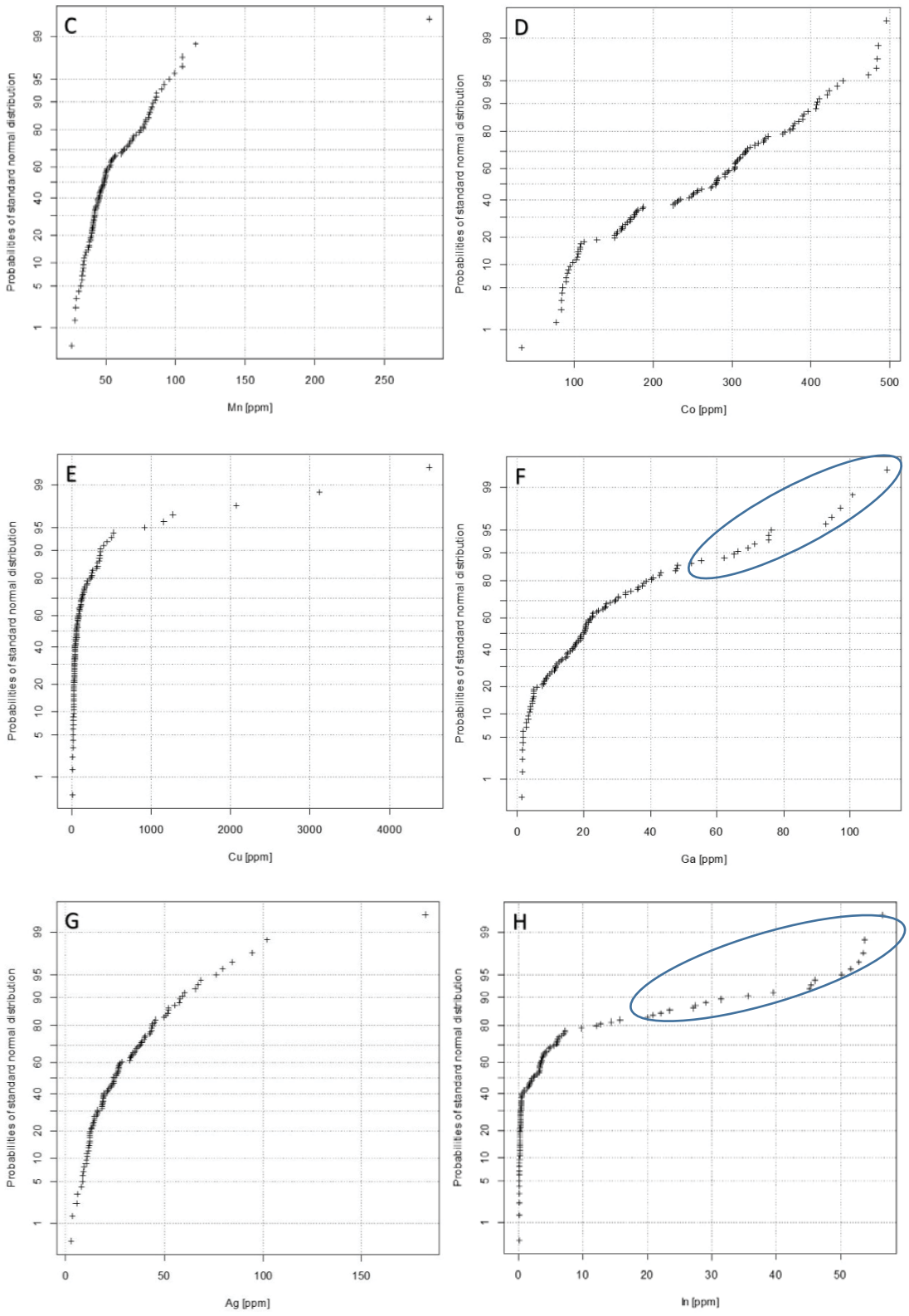

Fig. 69: Probability plots for the elements: A: Fe, B: Cd, C: Mn, D: Co, E: Cu, F: Ga, G: Ag, H: In.

$\delta^{34}S$ measurements (n= 9) performed on sphalerite from the Friedrich adit show a variation between +10 and +13 ‰ (Fig. 70).

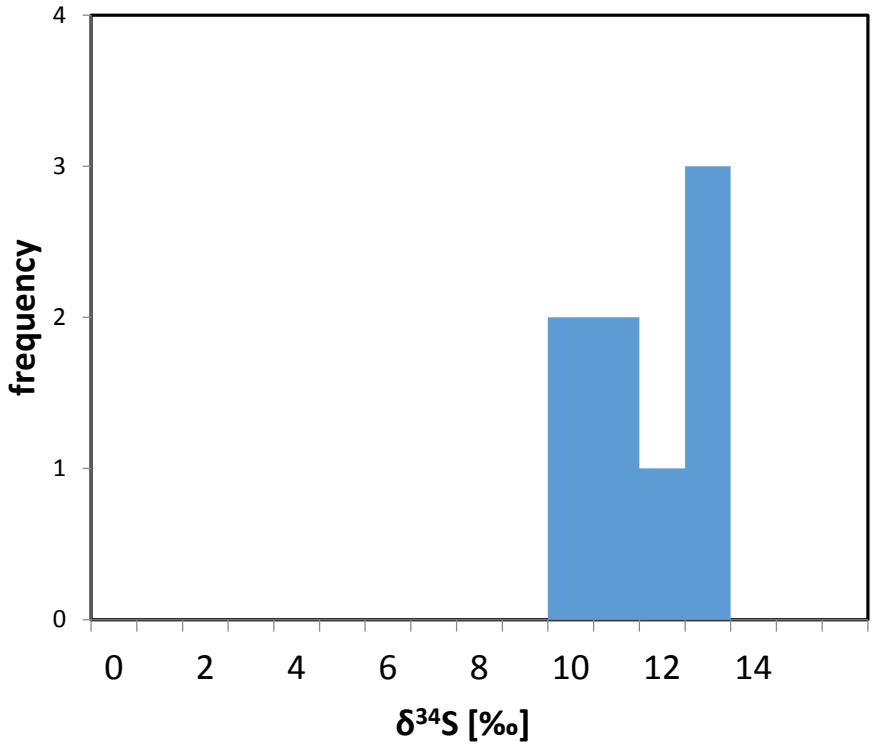

Fig. 70: $\delta^{34}S$ pattern of sphalerite samples from the Friedrich adit.

5.5.3.6 *Silberberg*

The chemical composition of sphalerite from the Silberberg deposit is shown in Table 19, determined by LA-ICP-MS (3 samples, 54 spot analyses) for the major, minor and trace elements.

Table 19: Statistics summarizing table of trace element contents from 54 LA-ICP-MS measurements on sphalerite hosted in the Silberberg mineralization (values reported in µg/g).

	^{55}Mn	^{56}Fe	^{59}Co	^{63}Cu	^{71}Ga	^{74}Ge	^{82}Se	^{107}Ag	^{111}Cd	^{115}In	^{121}Sb	^{208}Pb
Q90	48.8	34227	136	2257	13.9	0.5	4.4	27.5	3835	9.2	10.3	147
Q75	28.7	32828	127	1180	11.4	0.2	3.4	22.7	3308	6.7	7.8	48.8
Median	12.3	30295	86	490	6.1	0.1	2.3	20	2650	3.2	5.2	28.5
Q25	bdl	7890	8	236	1.4	bdl	1.8	16.8	2535	2.4	3.1	19.7
Q10	bdl	5842	bdl	136	0.2	bdl	1.4	13	2397	2	2.4	12.6
Min	bdl	5217	bdl	46.7	0.1	bdl	0.9	4.8	2158	1.6	0.4	3.7
Max	3230	40100	353	4020	26.2	7.2	5.7	34.4	4155	11.4	28	9300

In contrast to the CTEM, samples of the Silberberg show enrichment in Fe, Co, Ga, Ag, Sb and Pb. The samples are depleted in Mn, Ni, Ge, As, Se, Cd, In and Sn. In comparison to the median of all Paleozoic deposits, sphalerite from Silberberg depleted in all trace elements except Ga (Fig. 71). Compared to the Graz Paleozoic

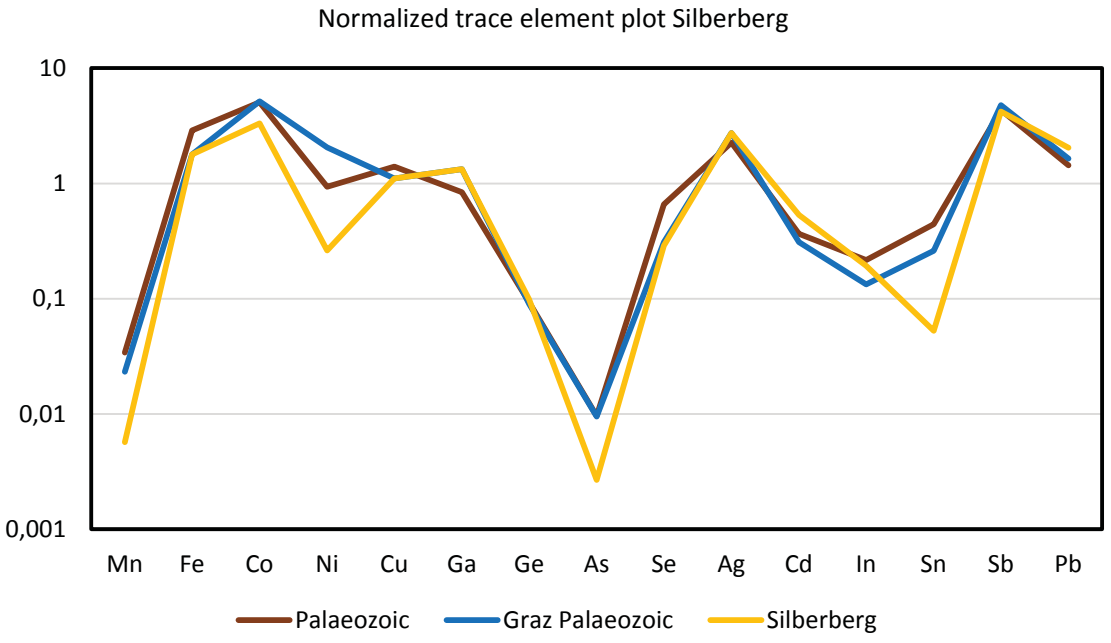

Fig. 71: Spider plot of the median from Silberberg mineralization and all measured Paleozoic and Graz Paleozoic Pb/Zn deposits normalized to the CTEM.

5.5.3.7 *Haufenreith*

The chemical composition of samples from the Haufenreith deposit shown in Table 20, determined by LA-ICP-MS (6 samples, 80 spot analyses) for selected major, minor and trace

elements represent the highest In median value of all investigated Pb-Zn deposits of the Graz Paleozoic.

Table 20: Statistics summarizing table of trace element contents from 80 LA-ICP-MS measurements on sphalerite hosted in the Haufenreith mineralization (values reported in µg/g).

	^{55}Mn	^{56}Fe	^{59}Co	^{63}Cu	^{71}Ga	^{82}Se	^{107}Ag	^{111}Cd	^{115}In	^{121}Sb	^{208}Pb
D90	343	9476	160	440	5.9	7.3	11.1	1849	33.7	4.2	63
D75	137	20010	155	434	3.3	2.8	6.2	1114	29.2	2.1	20.2
Median	110	15870	147	424	1.5	1.7	3	892	20.9	1.3	9.7
D25	93	14700	132	413	0.5	1.1	1.1	849	16.1	0.7	6.4
D10	86	13959	117	29.4	0.2	0.7	0.6	828	14.1	0.3	2.5
Min	76	13570	11.8	15.3	0.2	0	0.3	815	12.6	bdl	0.1
Max	1180	116600	167	750	11.9	10.8	64	3527	82	58	23100

In contrast to the CTEM samples from Haufenreith show enrichment in Co, Ni, Cu, In and are depleted in Mn, Ga, Ge, As, Se, Ag, Cd, Sn, Sb and Pb. In comparison to the median of all Paleozoic deposits, sphalerite from Haufenreith is enriched in Mn, Ni, As, In and depleted in all other elements (Fig. 71).

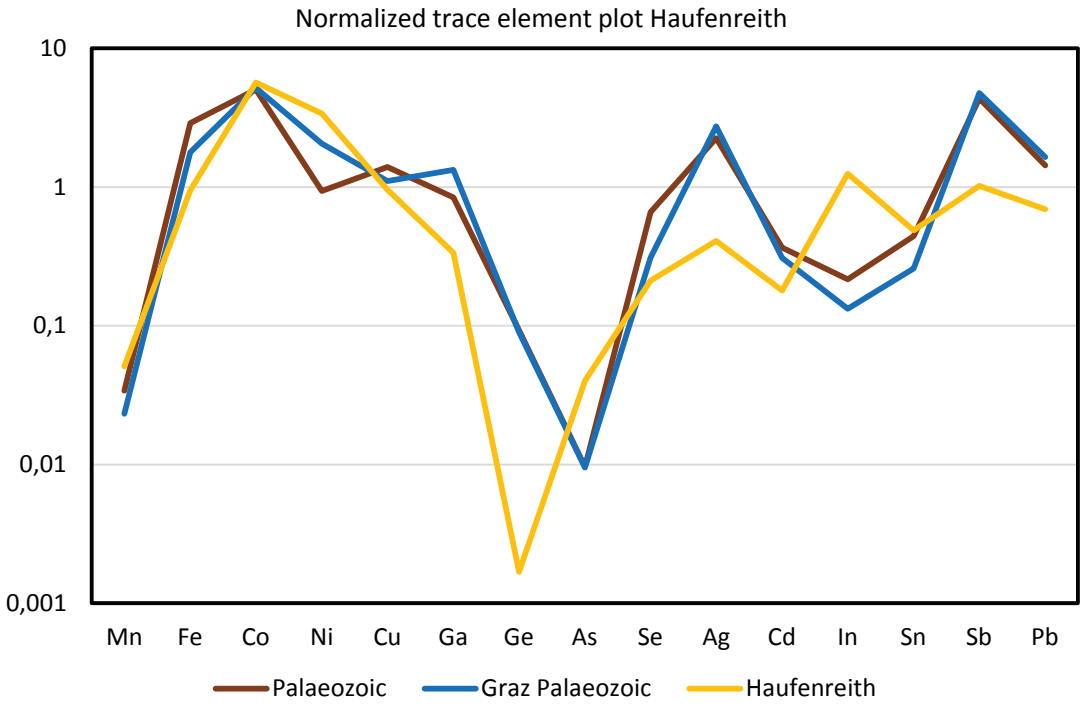

Fig. 72: Spider plot of the median from Haufenreith mineralization and all measured Paleozoic and Graz Paleozoic Pb/Zn deposits normalized to the `Eastern Alpine Median`.

The probability plots for all the plotted elements give evidence for at least two sphalerite populations (Fig. 73). The copper diseases of the investigated sphalerite can be seen in Fig. 73 where the data points on the left side stand for the sphalerite with tiny Ccp inclusions and on the right side for sphalerite without copper diseases.

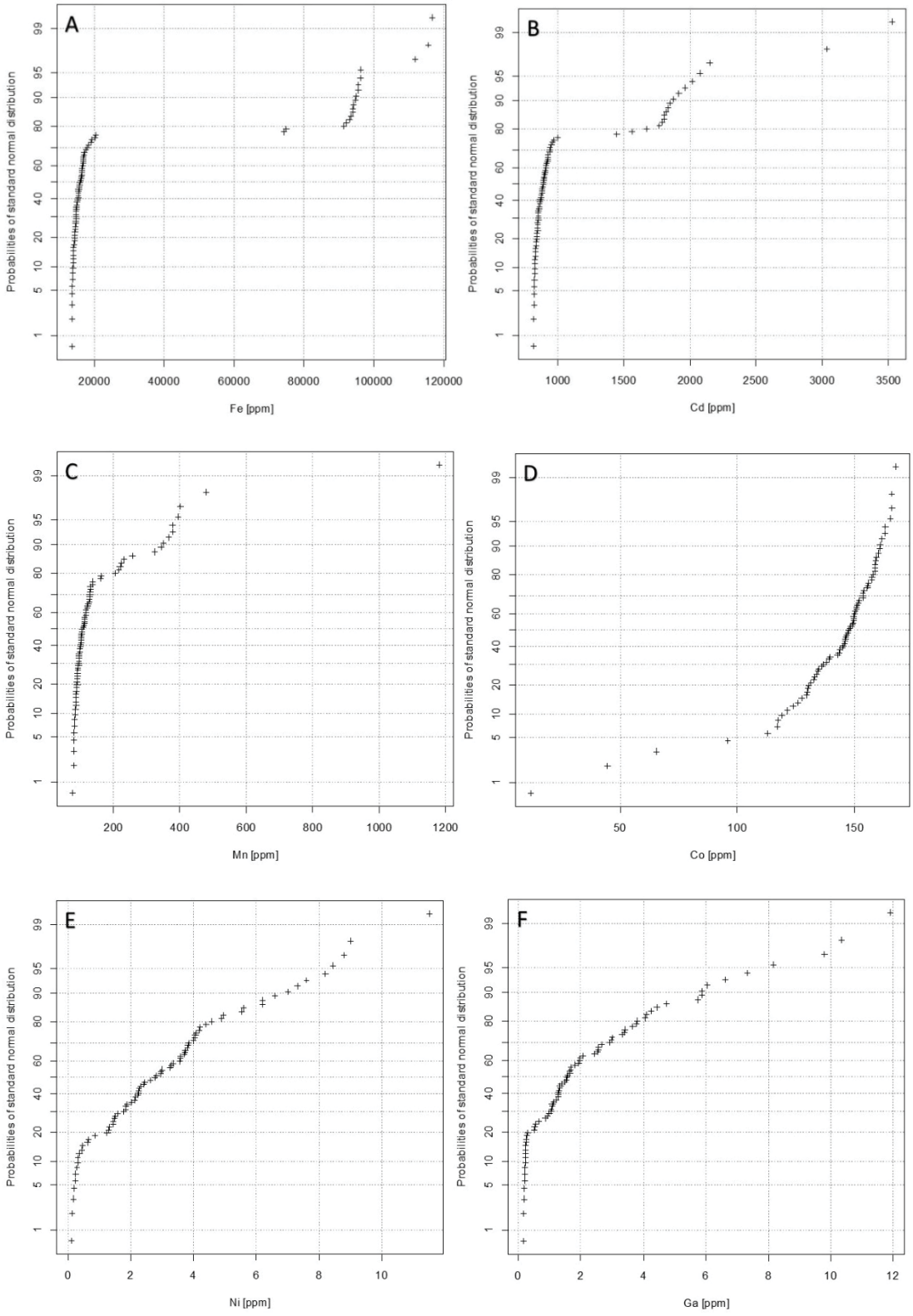
A
Probabilities of standard normal distribution
1
5
10
20
40
60
80
90
95
99
20000
40000
60000
80000
100000
120000
Fe [ppm]
B
Probabilities of standard normal distribution
1000
1500
2000
2500
3000
3500
Cd [ppm]
C
Probabilities of standard normal distribution
200
400
600
800
1000
1200
Mn [ppm]
D
Probabilities of standard normal distribution
50
100
150
Co [ppm]
E
Probabilities of standard normal distribution
0
2
4
6
8
10
Ni [ppm]
F
Probabilities of standard normal distribution
0
2
4
6
8
10
12
Ga [ppm]

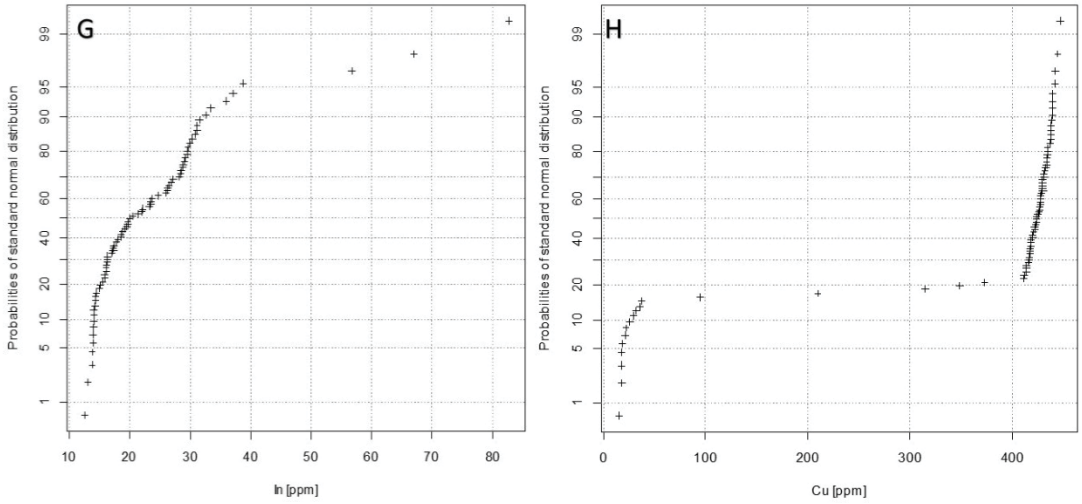

Fig. 73: Probability plots for the elements: A: Fe, B: Cd, C: Mn, D: Co, E: Ni, F: Ga, G: In, H: Cu.

The $\delta^{34}S$ composition from Haufenreith samples show a unimodal distribution with a maximum at +5 ‰, ranging from +2 to +9 ‰ (Fig. 74).

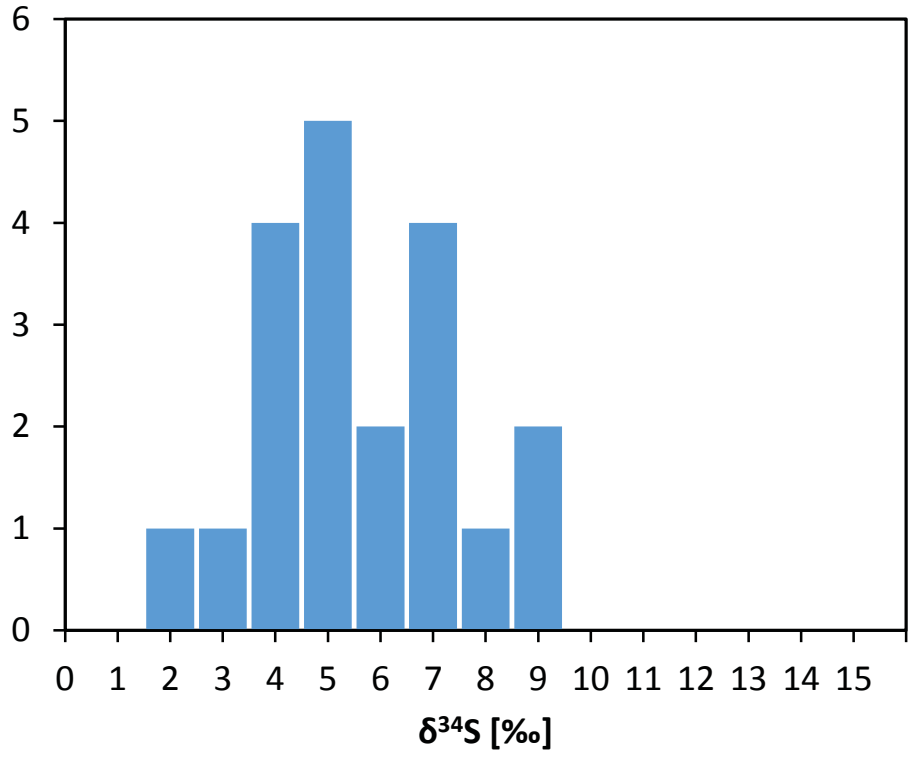

Fig. 74: $\delta^{34}S$ pattern of sphalerite samples from the Haufenreith adit.

5.5.3.8 Meiselding

Table 21 displays the chemical composition of sphalerite from the Meiselding deposit, determined by LA-ICP-MS (19 samples, 302 spot analyses) for selected major, minor and trace elements.

Table 21: Statistics summarizing table of trace element contents from 302 LA-ICP-MS measurements on sphalerite hosted in the Meiselding deposit (values reported in µg/g).

	^{55}Mn	^{56}Fe	^{59}Co	^{63}Cu	^{71}Ga	^{74}Ge	^{107}Ag	^{111}Cd	^{115}In	^{121}Sb	^{208}Pb
D90	860	96390	326	1168	1	0.5	52	4918	52	25.9	4320
D75	668	91975	301	919	0.9	0.3	28.8	4532	23.1	13.1	197
Median	453	88300	213	747	0.7	0.1	13.2	3960	15.7	5.5	12.3
D25	331	83025	139	586	0.5	bdl	7.4	3603	10.2	2	3.1
D10	269	77330	87	175	0.4	bdl	4.1	3391	7	0.6	1.5
Min	157	66300	28.1	16.6	0.2	bdl	1.2	2330	5.5	bdl	bdl
Max	5610	151000	381	5220	10.2	0.9	266	6830	88	158	88000

Trace element pattern from Meiselding shows nearly no correlation with the Paleozoic and the CTEM. In contrast to the CTEM, all elements except Cr and Ni show an enrichment. Compared to the median of all Paleozoic deposits, sphalerite from Meiselding is depleted in Cr and Ni. All other elements are enriched in this deposit (Fig. 75).

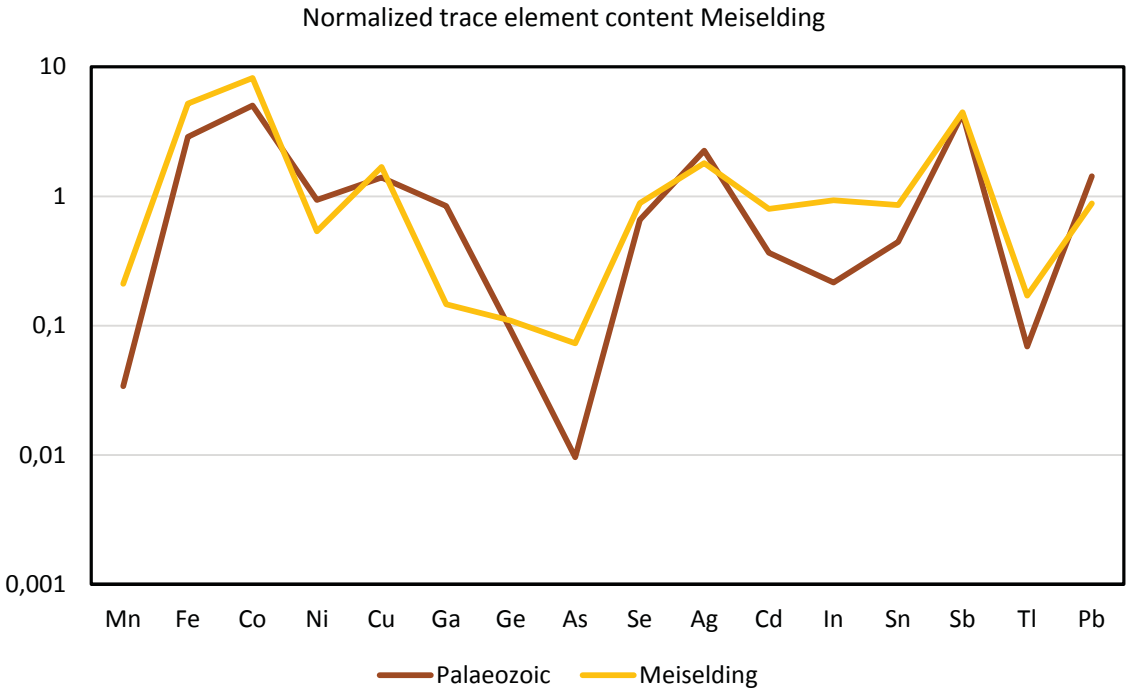

Fig. 75: Spider plot of the median from The Meiselding deposit and all measured Paleozoic Pb/Zn deposits normalized to the CTEM.

The probability plots of the Meiselding deposit for the elements Fe, Cd and Co (Fig. 76A, B and D) give evidence for at least two sphalerite populations. The elements In and Ag measured on sphalerite give a lognormally distribution (Fig. 76E, F).

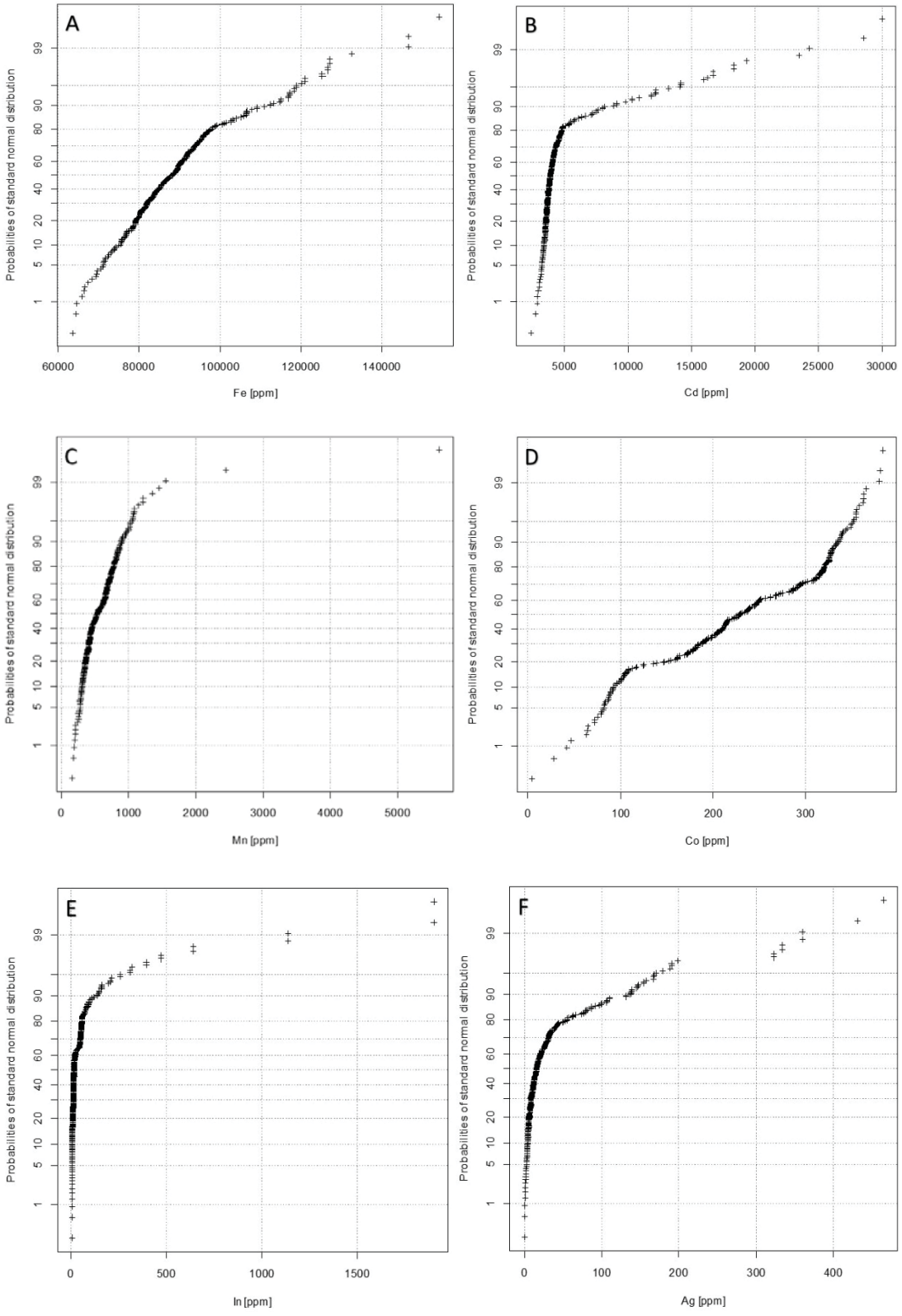

Fig. 76: Probability plots for the elements: A: Fe, B: Cd, C: Mn, D: Co, E: In, F: Ag.

The $\delta^{34}S$ composition of samples from Meiselding shows a tight spread ranging between -2 and +3 ‰ and a maximum at 0 ‰ (Fig. 77).

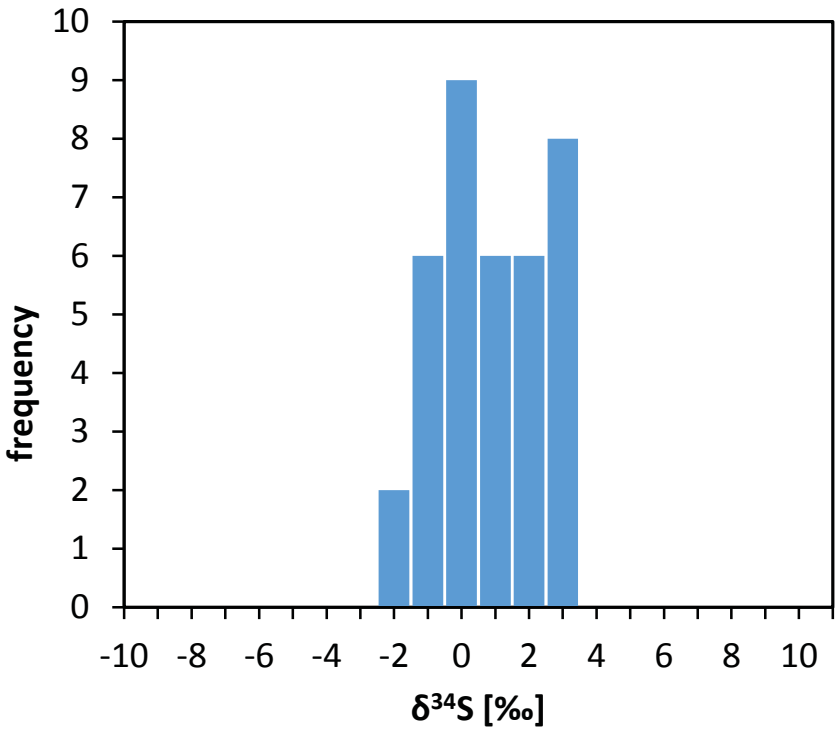

Fig. 77: $\delta^{34}S$ pattern of sphalerite samples from the Meiselding deposit.

5.5.3.9 *Walchen*

Table 22 displays the chemical composition of sphalerite from the Walchen deposit, determined by LA-ICP-MS (10 samples, 109 spot analyses) for selected major, minor and trace elements. Noticeable in the Walchen deposit are the high In values with a maximum of 352 µg/g.

Table 22: Statistics summarizing table of trace element contents from 109 LA-ICP-MS measurements on sphalerite hosted in the Walchen deposit (values reported in µg/g).

	^{55}Mn	^{56}Fe	^{59}Co	^{63}Cu	^{71}Ga	^{107}Ag	^{111}Cd	^{115}In	^{118}Sn	^{121}Sb	^{208}Pb
D90	362	97420	130	1574	8	38.5	2261	254	16.7	17.9	1793
D75	131	88700	97	690	4.3	19.7	2092	172	3.7	8.4	265
Median	72	84300	55	288	1.5	11.9	1592	98	1.1	3.1	11.5
D25	41.6	77900	11.8	178	0.9	8.6	1364	64	0.5	1.1	3
D10	28.5	55500	1.2	104	0.7	5.9	1260	bdl	0.3	0.5	1
Min	5.9	14040	0.2	9.2	0.2	0.6	1096	bdl	0.1	bdl	0.1
Max	2130	138400	148	5030	60	366	2622	352	510	60	71000

Compared to the CTEM all elements except Fe, Co, Se, Ag, In and Sb are enriched. In contrast to the median of all Paleozoic deposits, sphalerite from Walchen is enriched in Fe, Se, In and Sn all other elements are depleted in this deposit (Fig. 78).

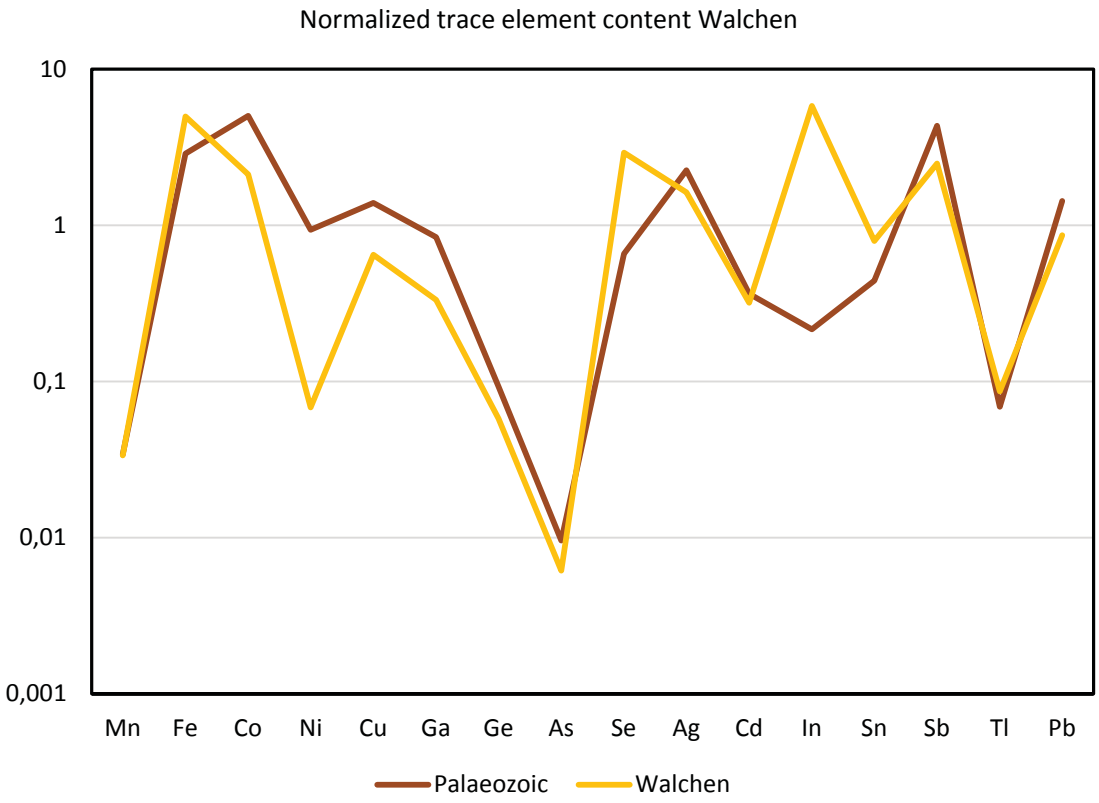

Fig. 78: Spider plot of the median from the Walchen deposit and all measured Paleozoic Pb/Zn deposits normalized to the CTEM.

Geochemical sphalerite data show that sphalerite from the Walchen deposit consists of at least two generations (Fig. 79). The trace elements Ag and Cu (Fig. 79G, H) show a lognormally distribution.

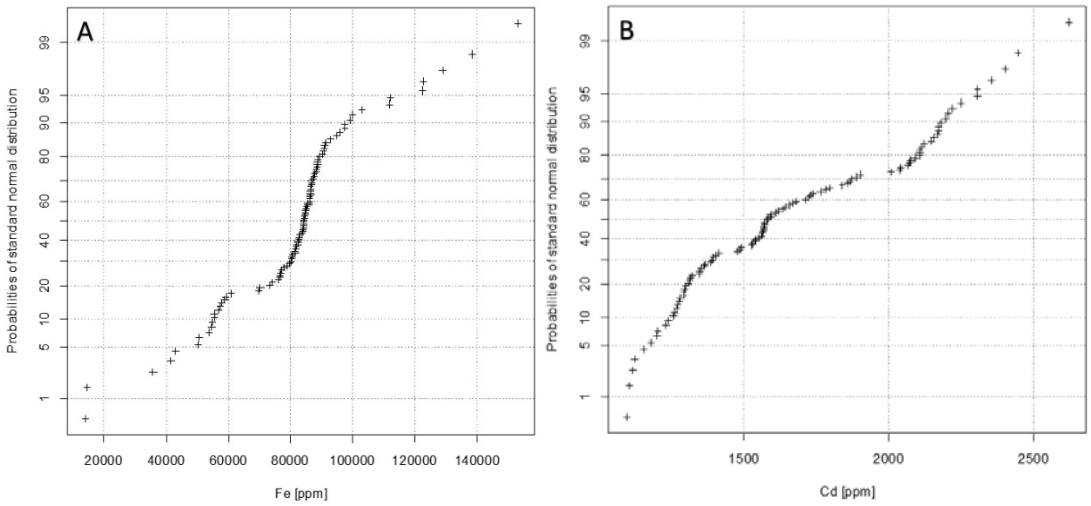

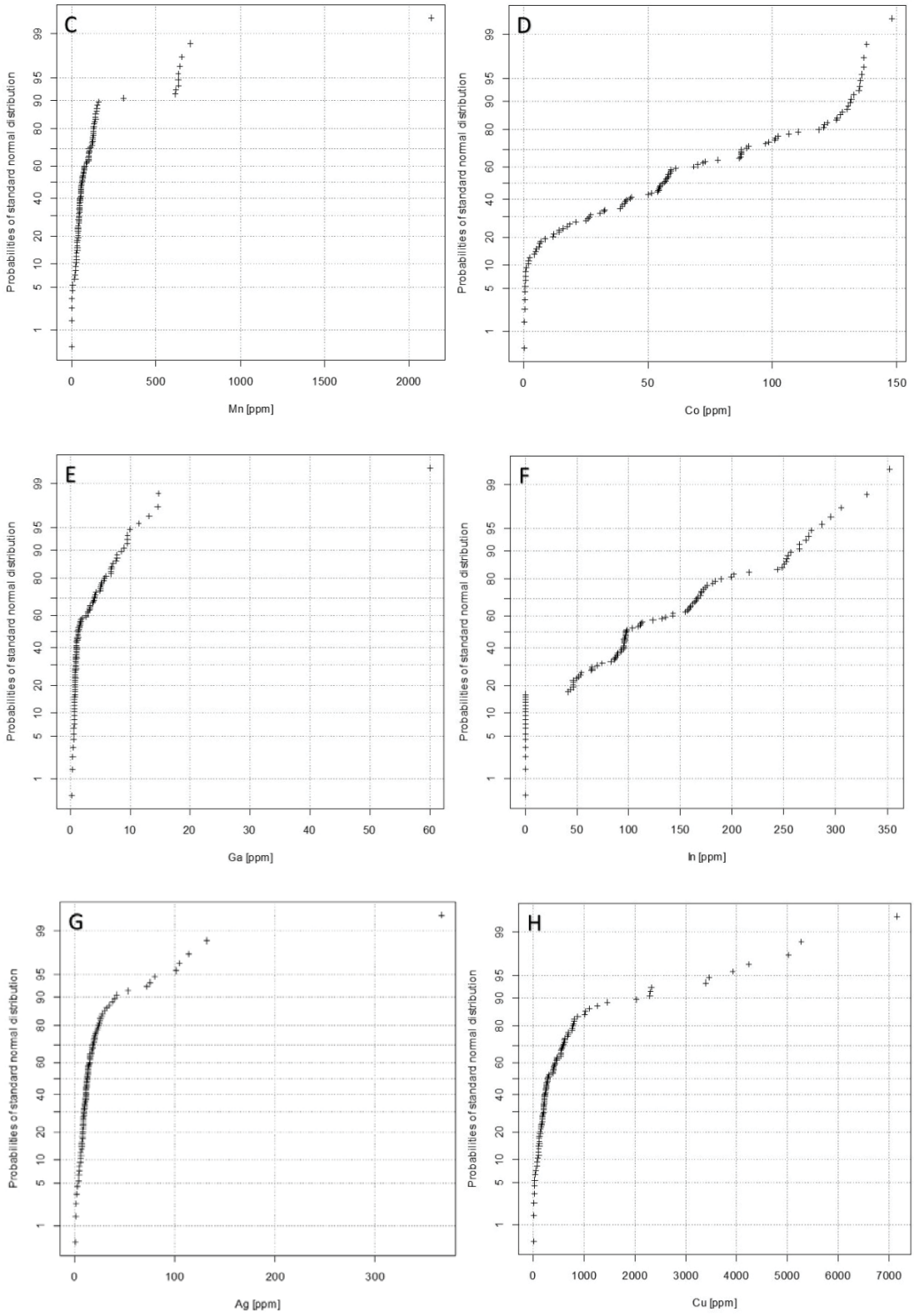

Fig. 79: Probability plots for the elements: A: Fe, B: Cd, C: Mn, D: Co, E: Ga, F: In, G: Ag, H: Cu.

5.5.3.10 *Leogang/Schwarzleo*

Table 22 displays the chemical composition of sphalerite from the Leogang/Schwarzleo deposit, determined by LA-ICP-MS (5 samples, 78 spot analyses) for the major, minor and trace elements. The Leogang deposit is characterized by the highest In median value (246 µg/g) of all investigated sphalerites of the Eastern Alpine.

Table 23: Statistics summarizing table of trace element contents from 78 LA-ICP-MS measurements on sphalerite hosted in the Leogang/Schwarzleo deposit (values reported in µg/g).

	^{55}Mn	^{56}Fe	^{59}Co	^{63}Cu	^{71}Ga	^{107}Ag	^{111}Cd	^{115}In	^{121}Sb	^{208}Pb
D90	676	99290	155	4780	13.6	46.8	4202	279	11.1	587
D75	235	91063	147	2325	1.6	26.8	2560	270	5.4	85
Median	143	79985	127	864	1	10.8	2042	246	2.7	17.1
D25	57	23040	79	225	0.7	4.3	1734	4	1.2	5.1
D10	44.6	14746	51	114	0.3	1.3	1611	3.3	0.7	2.7
Min	30.5	11610	6	83	0.2	0.5	1506	2	0.4	0.6
Max	1170	106000	311	8500	252	360	11260	332	80	74000

Trace element pattern from Leogang follow the Paleozoic and the CTEM. In contrast to the CTEM the elements except Fe, Co, Cu, Se, Ag, In and Sb are enriched. In contrast to the median of all Paleozoic deposits, sphalerite from Walchen is enriched in Fe, Cu, Se, In and Sn. All other elements are depleted in this deposit (Fig. 80).

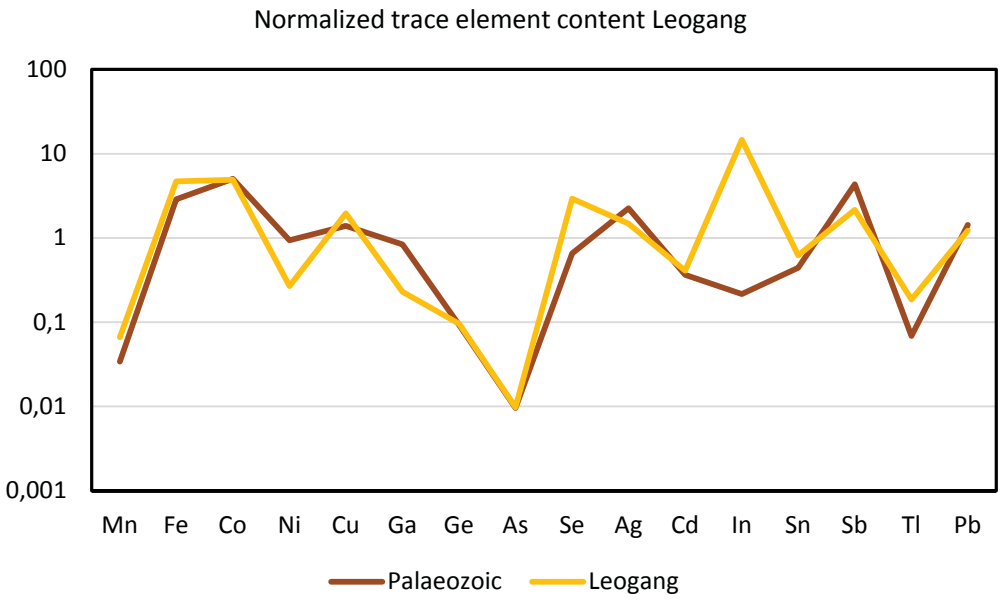

Fig. 80: Spider plot of the median from the Leogang/Schwarzleo deposit and all measured Paleozoic Pb/Zn deposits normalized to the CTEM.

The chemical data of sphalerite from the Leogang deposit show two populations, none of the elements shows a linear- or lognormally distribution.

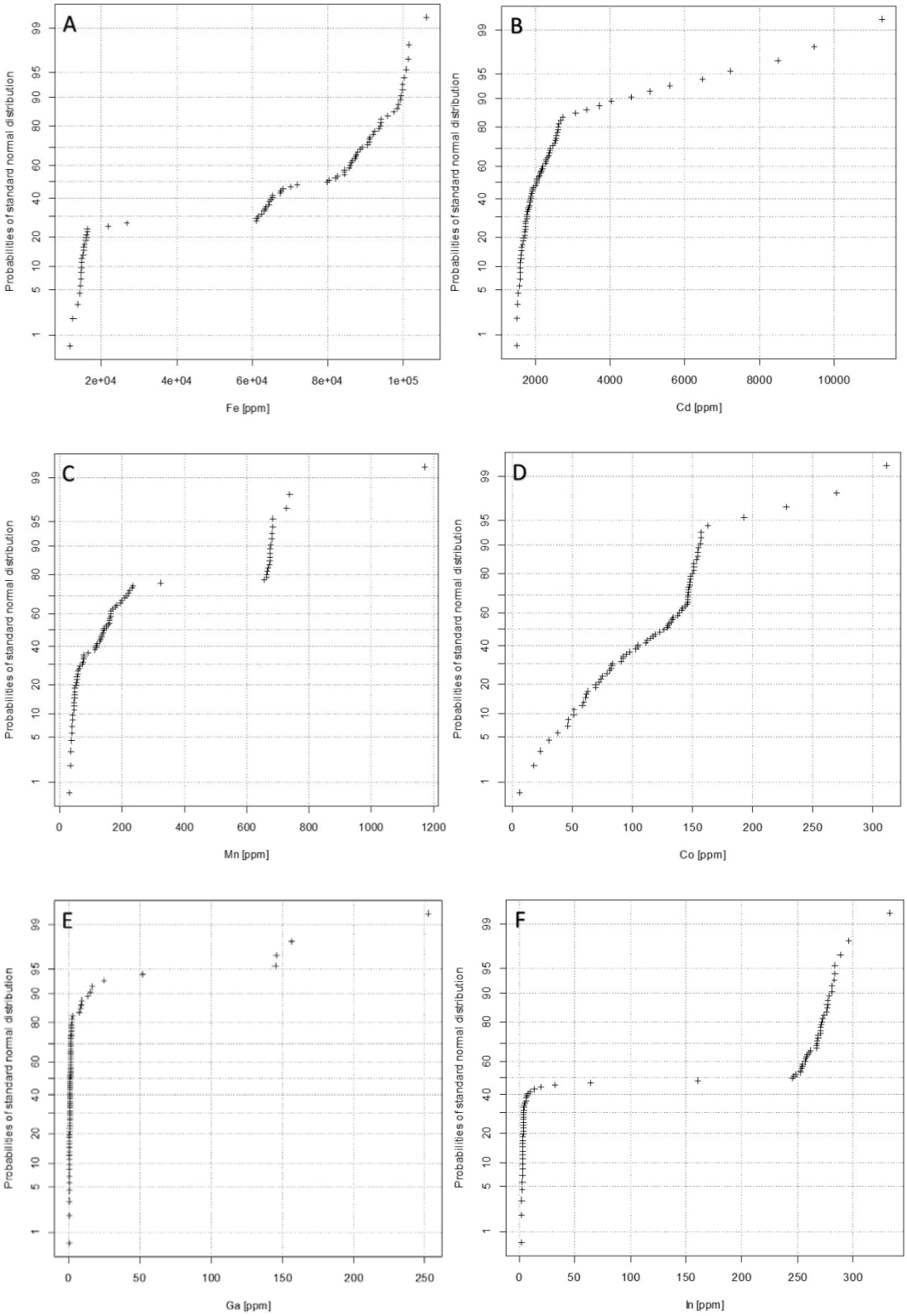
A
Probabilities of standard normal distribution
Fe [ppm]
B
Cd [ppm]
C
Mn [ppm]
D
Co [ppm]
E
Ga [ppm]
F
In [ppm]

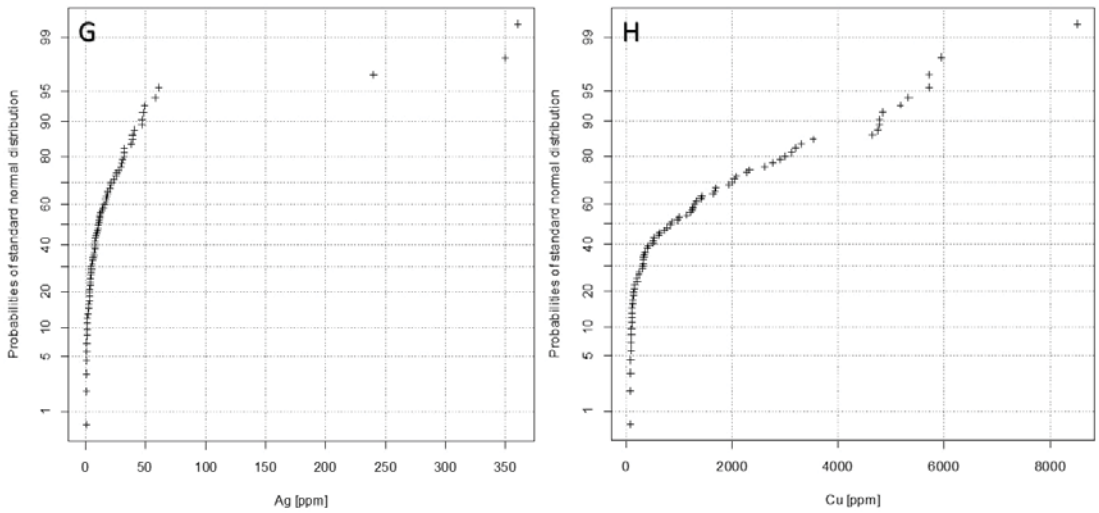

Fig. 81: Probability plots for the elements: A: Fe, B: Cd, C: Mn, D: Co, E: Ga, F: In, G: Ag, H: Cu.

5.5.4 Sphalerite chemistry of Pb/Zn vein type mineralizations hosted in Paleozoic units

Samples median values from the deposits Koprein, Metnitz, Flecktrogalm and Achselalm normalized to the CTEM show enrichment of the elements Fe, Co, Ga, Ag, Sn, Sb and are depleted in Mn, Ni, Cu, Ge, As, Cd, In, Tl and Pb (Fig. 82).

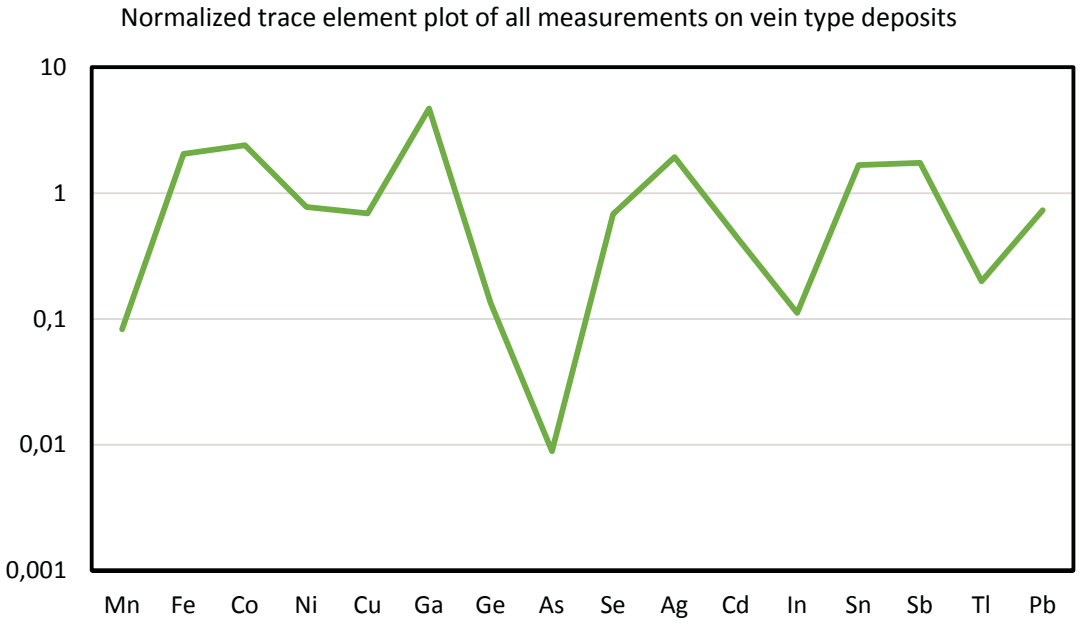

Fig. 82: Normalized trace element data from all measured Eastern Alpine vein type Pb/Zn deposits (4) normalized to the CTEM.

Table 24 shows median values of all in situ trace elements measurements (1575) of all measured samples (92) were calculated and summarized to a ´vein-type trace element median`.

Table 24: Trace element median [µg/g] of all measured Eastern Alpine vein type Pb-Zn deposits (4)

V	Cr	Mn	Fe	Co	Ni	Cu	Ga	Ge	As
0.003	0.37	178	17808	145	2.64	105	24.26	0.09	0.13

Se	Mo	Ag	Cd	In	Sn	Sb	Tl	Pb	Bi
6.06	bdl	3.95	2216	1.78	0.82	2.68	0.01	5.06	0.01

5.5.4.1 Koprein

Table 25 displays the chemical composition of sphalerite from the Koprein deposit, determined by LA-ICP-MS (21 samples, 399 spot analyses) for selected major, minor and trace elements.

Table 25: Statistics summarizing table of trace element contents from 399 LA-ICP-MS measurements on sphalerite hosted in the Koprein deposit (values reported in µg/g).

	^{55}Mn	^{56}Fe	^{59}Co	^{63}Cu	^{71}Ga	^{74}Ge	^{107}Ag	^{111}Cd	^{115}In	^{118}Sn	^{121}Sb
D90	96	47520	785	1305	7.2	0.8	99	3402	88	287	37.8
D75	74	43300	733	607	5.7	0.5	49.8	3135	34.3	107	19.2
Median	55	34720	644	306	4.1	0.3	27.9	2890	17.1	35.8	9
D25	37.5	28100	553	135	2.6	bdl	15.2	2620	10.6	12.6	4.9
D10	28.4	23524	478	89	1.4	bdl	10	2351	6.6	5	2.1
Min	8.9	8040	87.2	24.7	0.1	bdl	5.2	553	0.9	bdl	0.2
Max	1060	56400	1416	3950	15.4	2	222	4070	373	1052	1254

In contrast to the CTEM trace element pattern from Koprein are enriched in the elements Fe, Co, Cu, Ag, Cd, In, Sn Sb and depleted in V (below detection limit), Cr, Ni, Ga, Ge, As, Se, Tl and Pb. Compared to the median of all vein type deposits, sphalerite from Koprein is enriched in Fe, Co, Cu, Ge, As, Ag, Cd, In, Sn, Sb, Tl, Pb and depleted in V, Cr, Ni, Ga and Se (Fig. 83).

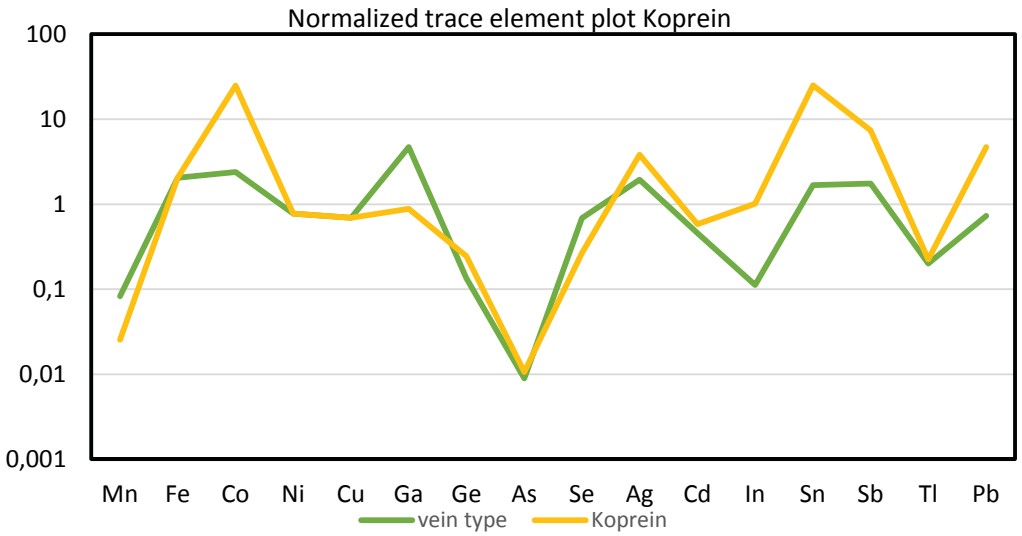

Fig. 83: Spider plot of the median from the Koprein deposit and all measured vein type Pb/Zn deposits normalized to the CTEM

The samples from Koprein show for the elements In, Ag and Sn a lognormal distribution (Fig. 84F, G, H). The elements Fe, Cd, Mn, Cu and Ga show normal distribution (Fig. 84A, B, C, D, E).

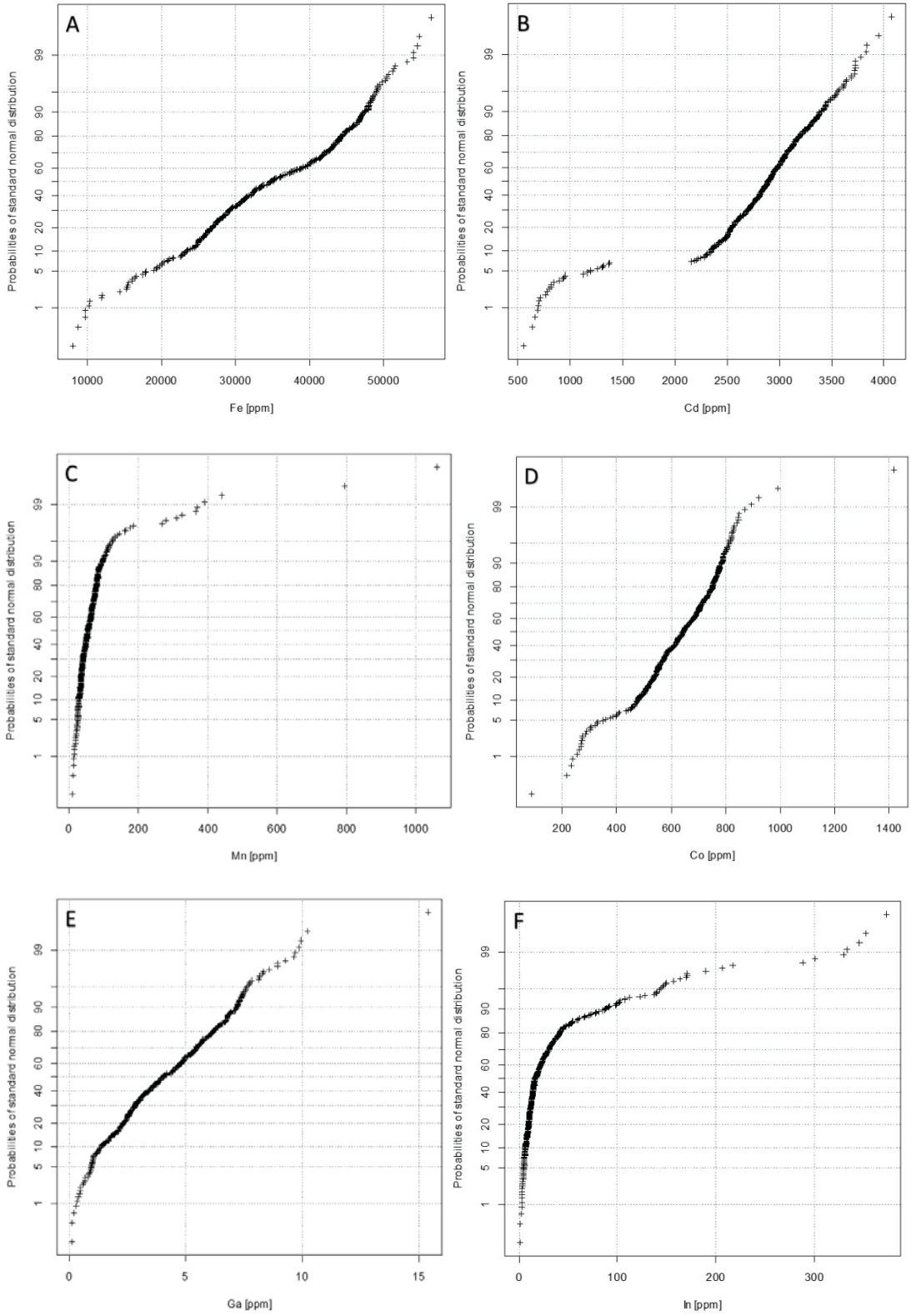

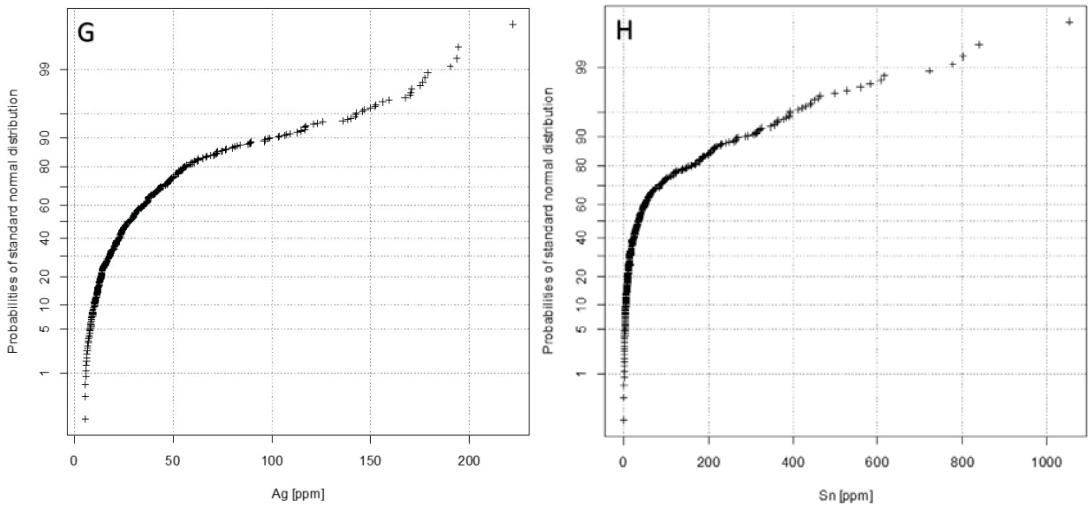

Fig. 84: Probability plots for the elements: A: Fe, B: Cd, C: Mn, D: Co, E: Ga, F: In, G: Ag, H: Sn.

Samples from the Koprein dump site show medium heavy $\delta^{34}S$ composition ranging from +10 to +18 ‰ with a maximum at +15 ‰ (Fig. 85).

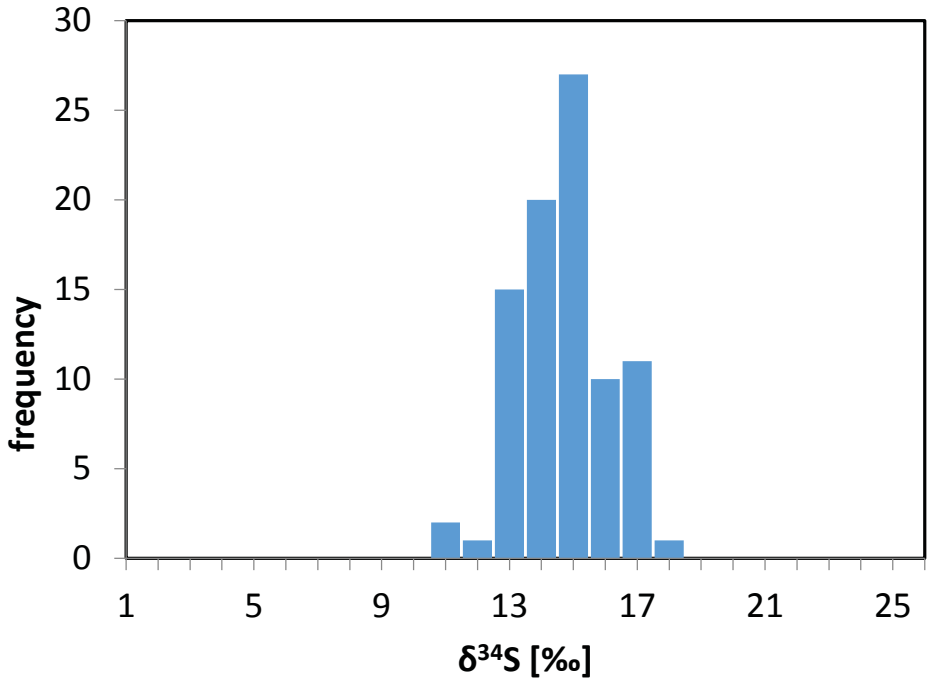

Fig. 85: $\delta^{34}S$ pattern of sphalerite samples from the Koprein dumpsite.

5.5.4.2 Metnitz

Table 26 shows the chemical composition of sphalerite from the Metnitz deposit, determined by LA-ICP-MS (14 samples, 364 spot analyses) for selected major, minor and trace elements. The Metnitz deposit shows elevated median values for Co, Ga and Ge compared to the other investigated vein-type deposits.

Table 26: Statistics summarizing table of trace element contents from 364 LA-ICP-MS measurements on sphalerite hosted in the Metnitz deposit (values reported in µg/g).

	^{55}Mn	^{56}Fe	^{59}Co	^{63}Cu	^{71}Ga	^{74}Ge	^{107}Ag	^{111}Cd	^{115}In	^{118}Sn	^{121}Sb	^{208}Pb
D90	100	70870	505	2078	123.9	527	43.5	2454	1.1	17.3	51	137
D75	86	64900	469	1733	74	373	27.2	2199	0.2	4.4	27.3	35.8
Median	73	58950	404	1220	37.6	149	14.1	1931	0.1	2.4	13.1	10.2
D25	63	52600	346	927	10.4	26.3	6.6	1673	0.1	1.6	4.9	3.3
D10	55	46100	300	786	5.1	0.9	3	1389	0.1	1.2	1.9	1.1
Min	41.2	30300	158	471	0.3	bdl	0.5	892	bdl	0.6	bdl	bdl
Max	411	84900	679	2992	381	910	182	4660	65	198	182	26800

In contrast to the CTEM trace element pattern from Metnitz is enriched in the elements Cr, Fe, Co, Cu, Ga, Ge, Ag, Sn, Sb and depleted in V (below detection limit), Mn, Ni, As, Se, Cd, Tl and Pb. Compared to the median of all vein type deposits, sphalerite from Metnitz is enriched in Cr, Fe, Co, Cu, Ga, Ge, As, Ag, Sn, Sb, Tl, Pb and depleted in V, Mn and Ni (Fig. 86).

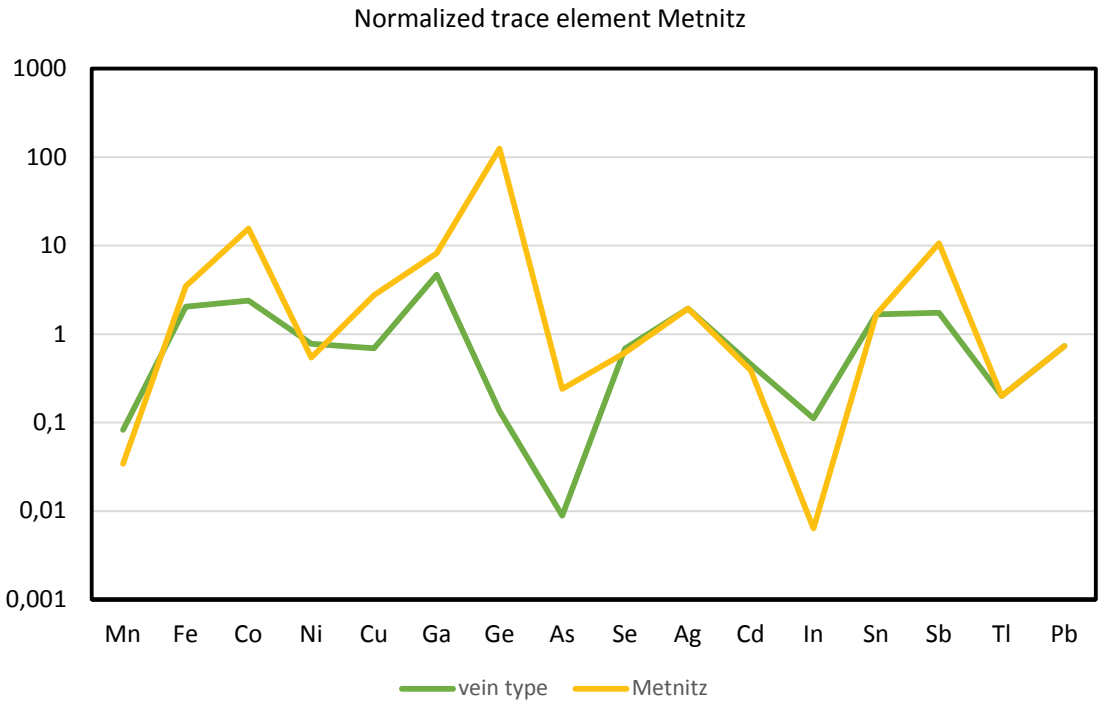

Fig. 86: Spider plot of the median from the Metnitz deposit and all measured vein type Pb/Zn deposits normalized to the CTEM.

The chemical data of sphalerite from Metnitz show no normal distribution for the elements Fe, Cd, Mn, Co and Ga (Fig. 87A, B, C, D, E). The elements In, Ag and Sn are lognormally distributed (Fig. 87F, G, H).

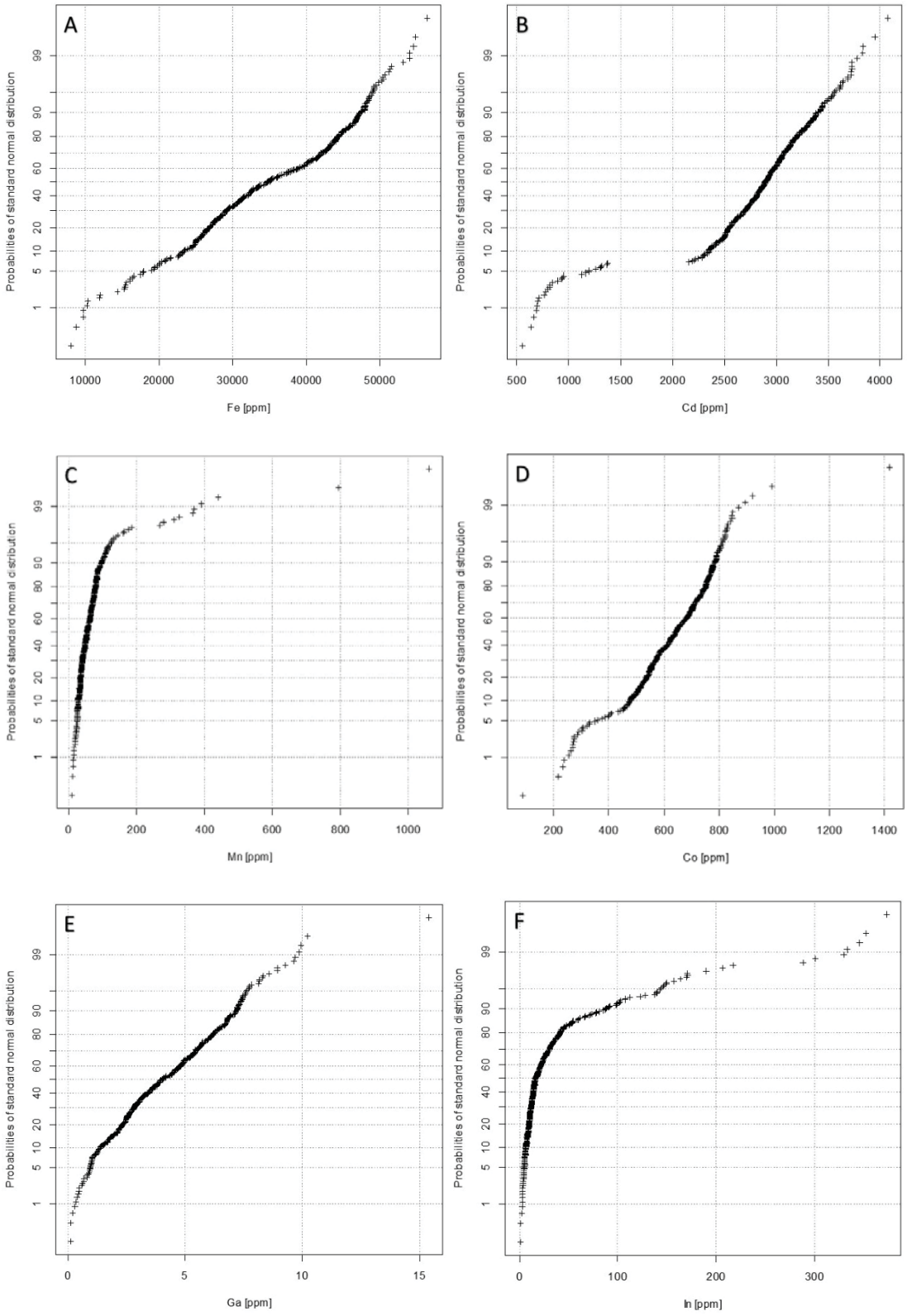
A
Probabilities of standard normal distribution
1
5
10
20
40
60
80
90
99
10000
20000
30000
40000
50000
Fe [ppm]
B
Probabilities of standard normal distribution
500
1000
1500
2000
2500
3000
3500
4000
Cd [ppm]
C
Probabilities of standard normal distribution
0
200
400
600
800
1000
Mn [ppm]
D
Probabilities of standard normal distribution
200
400
600
800
1000
1200
1400
Co [ppm]
E
Probabilities of standard normal distribution
0
5
10
15
Ga [ppm]
F
Probabilities of standard normal distribution
0
100
200
300
In [ppm]

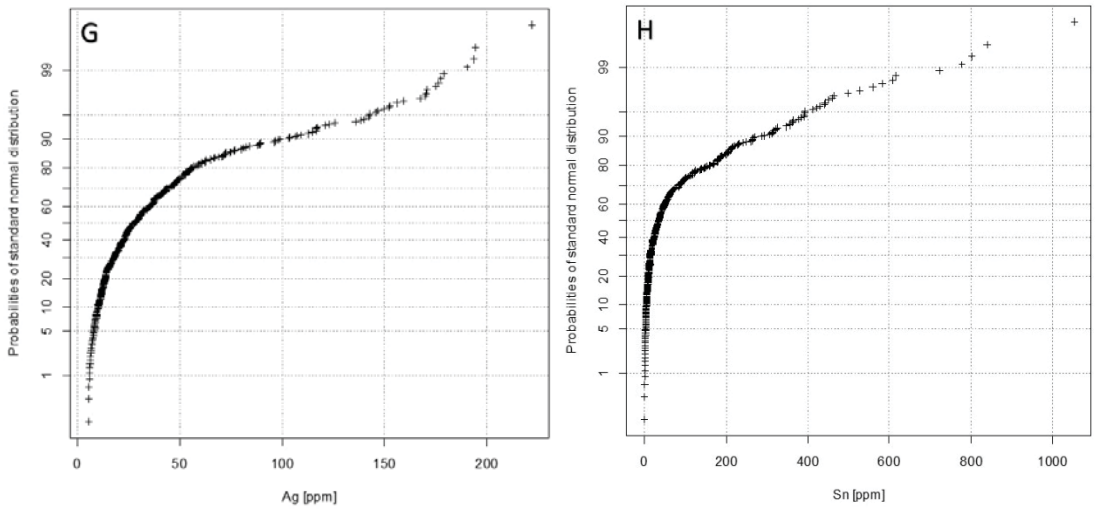

Fig. 87: Probability plots for the elements: A: Fe, B: Cd, C: Mn, D: Co, E: Ga, F: In, G: Ag, H: Sn.

Samples from the Metnitz adit show a small spread in the $\delta^{34}S$ isotopic composition between -3 and +3 ‰ and a maximum at -1 ‰ (Fig. 88).

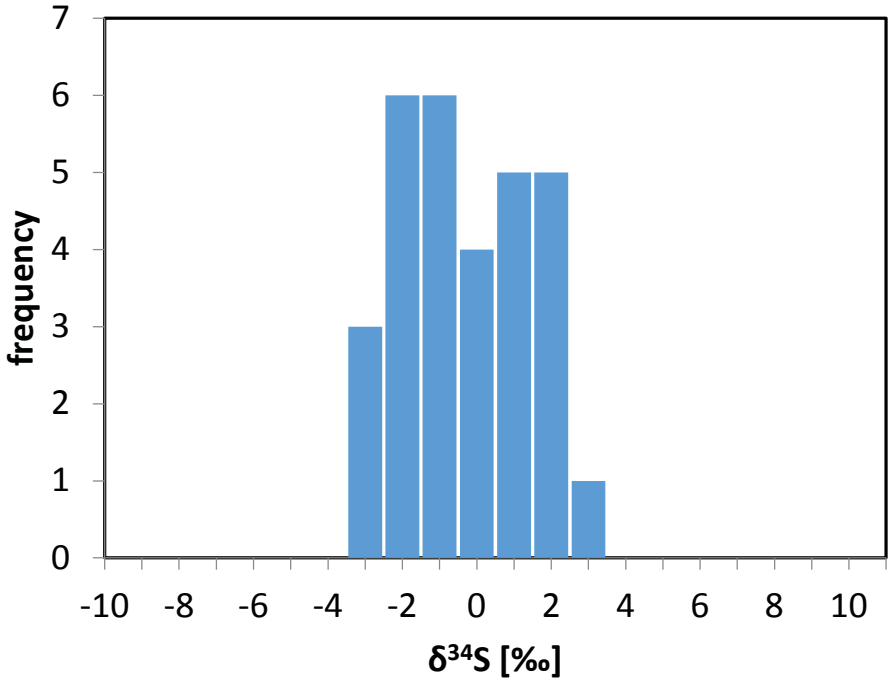

Fig. 88: $\delta^{34}S$ pattern of sphalerite samples from the Metnitz adit.

5.5.4.3 Achselalm

Table 27 shows the chemical composition of sphalerite from the Achselalm deposit, determined by LA-ICP-MS (21 samples, 426 spot analyses) for the major, minor and trace elements.

Table 27: Statistics summarizing table of trace element contents from 812 LA-ICP-MS measurements on sphalerite hosted in the Achselalm deposit (values reported in µg/g).

	^{55}Mn	^{56}Fe	^{59}Co	^{63}Cu	^{71}Ga	^{82}Se	^{107}Ag	^{111}Cd	^{115}In	^{118}Sn	^{121}Sb	^{208}Pb
D90	321	56850	116	112	81	81.2	2.2	3427	5.3	1.2	3.9	22.3
D75	272	28665	70	83	45.3	45.3	1.5	2893	3.2	0.5	1.6	8.7
Median	231	12170	58	38.1	22.3	22.3	0.6	2201	1.9	0.3	0.5	3.1
D25	180	6858	44.2	21.2	7.3	7.3	0.3	1947	1.1	0.2	0.1	1.1
D10	143	3242	38.8	12.5	3.5	3.4	0.3	1464	0.7	0.1	0.1	0.4
Min	48	2748	34.1	0	1	1	0.2	943	0.2	0.1	bdl	0.1
Max	11800	71630	914	255	284	248	36.2	3949	22.9	12	47.2	1500

In contrast to the CTEM trace element pattern from Achselalm is enriched in the elements Mn, Ni, Ga, In and depleted in V, Cr, Fe, Co, Cu, Ge, As, Se, Ag, Sn, Sb, Tl and Pb. In contrast to the median of all vein type deposits, sphalerite from Achselalm is enriched in V, Mn, Ni, Se, In and depleted in Fe, Co, Cu, Ga, Ge, Ag, Sn, Sb, Tl and Pb (Fig. 89).

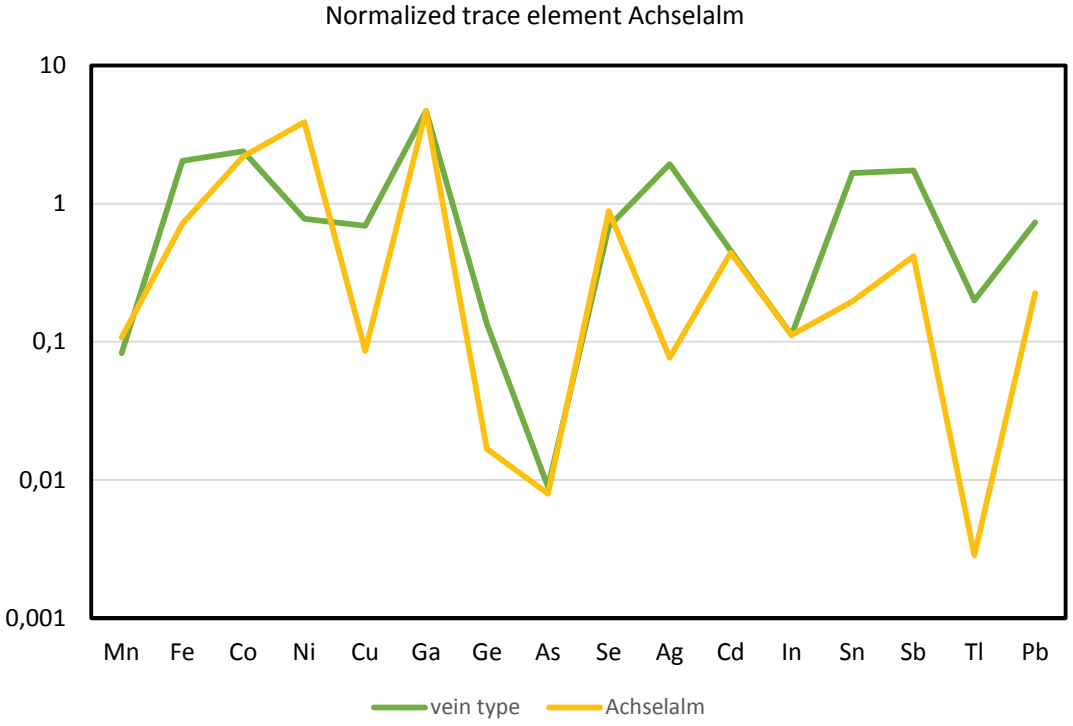

Fig. 89: Spider plot of the median from the Achselalm deposit and all measured vein type Pb/Zn deposits normalized to the CTEM.

Sphalerite from the Achselalm adit shows geochemically in the elements Fe, Cd, Mn and Co at least four populations (Fig. 90A, B, C, D). The elements Ga and In are lognormally distributed over all measured samples (Fig. 90E, F).

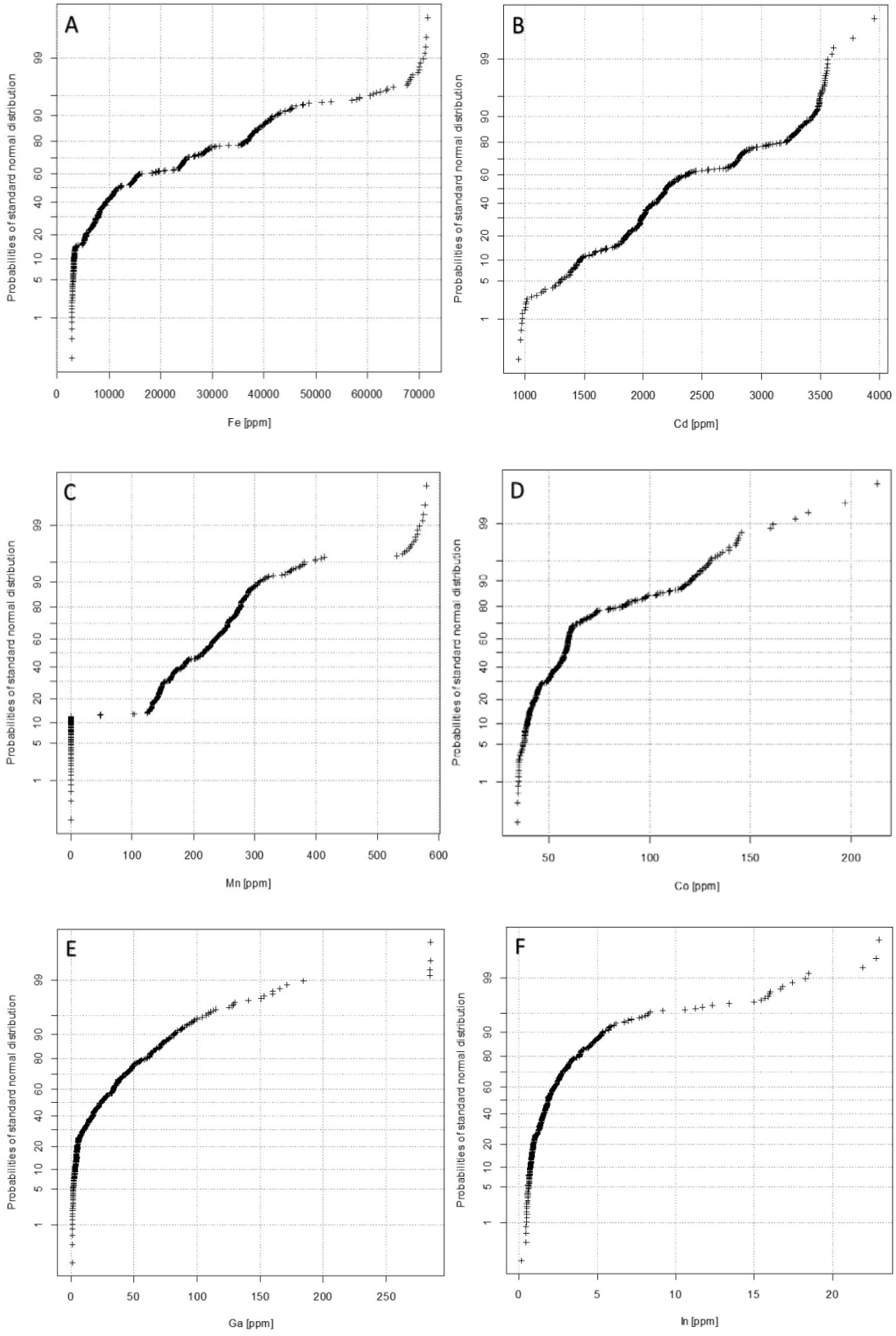

Fig. 90: Probability plots for the elements: A: Fe, B: Cd, C: Mn, D: Co, E: Ga, F: In.

Samples from the Achselalm adit show a $\delta^{34}S$ maximum at +1 ‰ and have a range between -1 and +3 ‰ (Fig. 91).

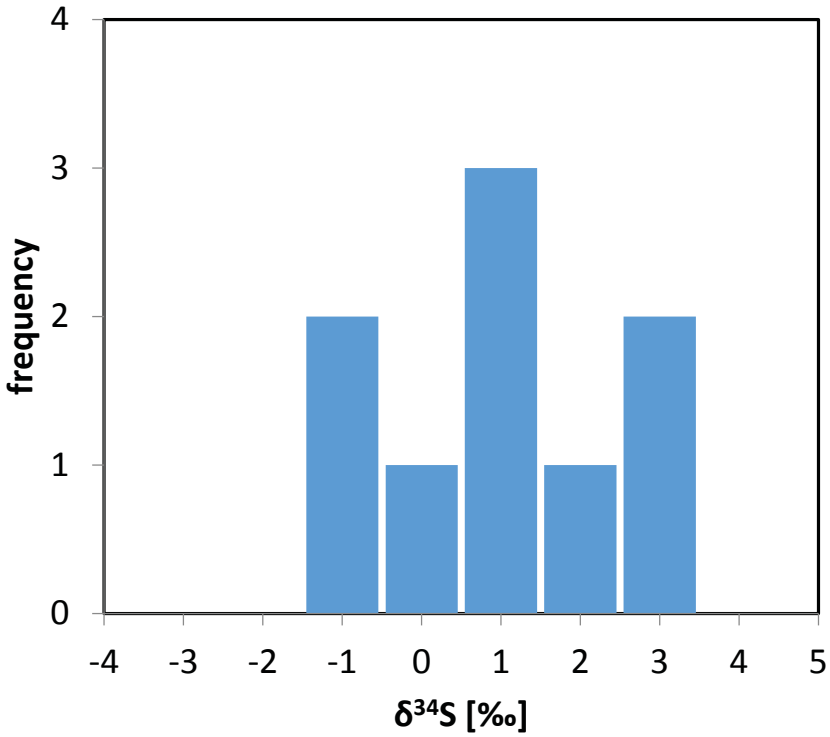

Fig. 91: $\delta^{34}S$ pattern of sphalerite samples from the Achselalm deposit (n= 8).

5.5.4.4 *Flecktrogalm*

Table 28 shows the chemical composition of sphalerite from the Flecktrogalm deposit, determined by LA-ICP-MS (22 samples, 386 spot analyses) for the major, minor and trace elements.

Table 28: Statistics summarizing table of trace element contents from 386 LA-ICP-MS measurements on sphalerite hosted in the Flecktrogalm deposit (values reported in µg/g).

	^{55}Mn	^{56}Fe	^{59}Co	^{63}Cu	^{71}Ga	^{74}Ge	^{82}Se	^{107}Ag	^{111}Cd	^{115}In	^{121}Sb
D90	303	26120	81	107	109	0.1	8.4	2	3346	6.6	4.4
D75	267	19605	73	78	85	0	7.4	1.2	2927	2.6	2
Median	178	10865	62	35.6	32.4	0	5.4	0.5	2263	1.5	0.6
D25	145	4656	50	13.7	8	0	2.1	0.3	1898	0.4	0.2
D10	65	3274	44	9.6	3.3	bdl	bdl	0.2	1761	0.1	0.1
Min	21	2208	34.8	3.5	1.4	bdl	bdl	bdl	1316	bdl	bdl
Max	538	37790	152	201	230	1.8	12.4	10.5	4673	22.3	22.9

In contrast to the CTEM The spider diagram from Flecktrogalm shows enrichment of the elements Mn, Ni, Ga, In and depletion of V, Cr, Fe, Co, Cu, Ge, As, Se, Ag, Sn, Sb, Tl and Pb. Compared to the median of all vein type deposits, sphalerite from Flecktrogalm is enriched in V, Mn, Ni, Se, In and depleted in Fe, Co, Cu, Ga, Ge, Ag, Sn, Sb, Tl and Pb (Fig. 89).

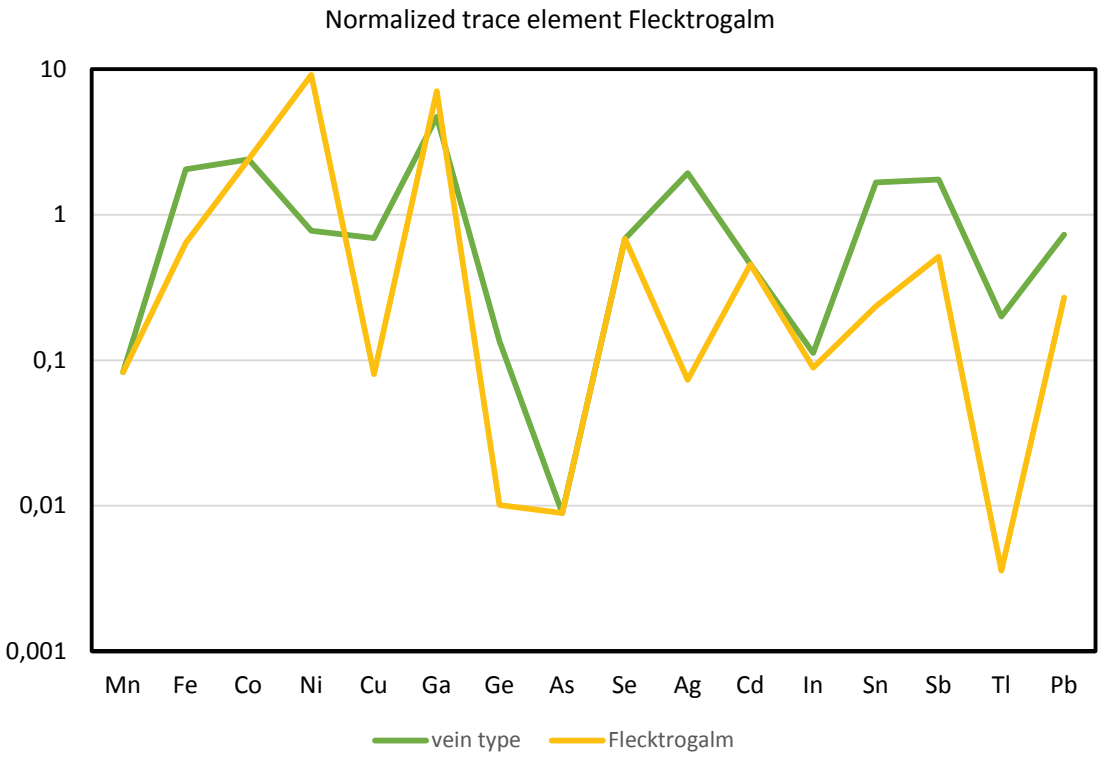

Fig. 92: Spider plot of the median from the Flecktrogalm deposit and all measured vein type Pb/Zn deposits normalized to the CTEM.

Sphalerite from the Flecktrogalm adit shows geochemically four populations of the elements Fe, Cd, Mn and Co at least (Fig. 93A, B, C, D). The elements Ga and In indicate at least two different sphalerite populations (Fig. 93E, F).

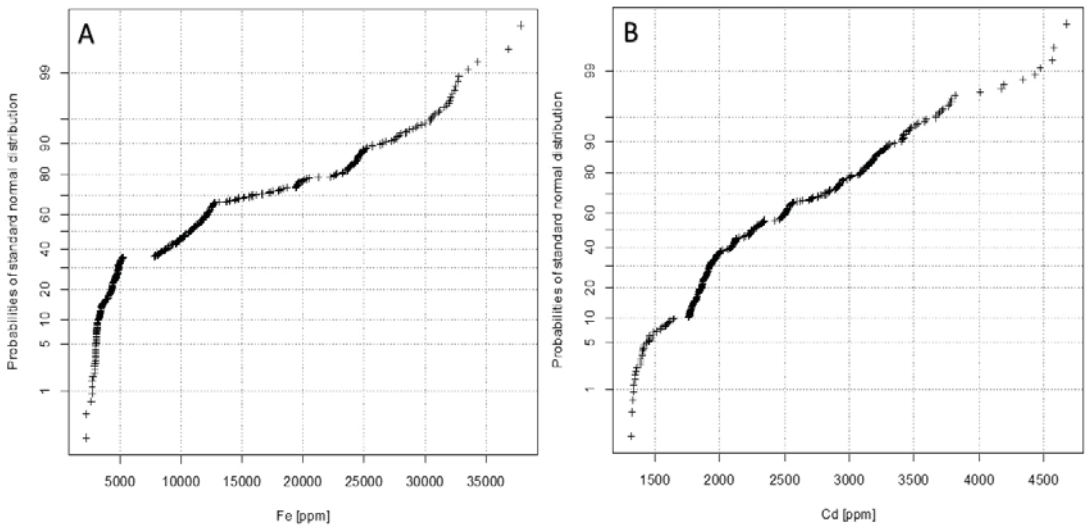

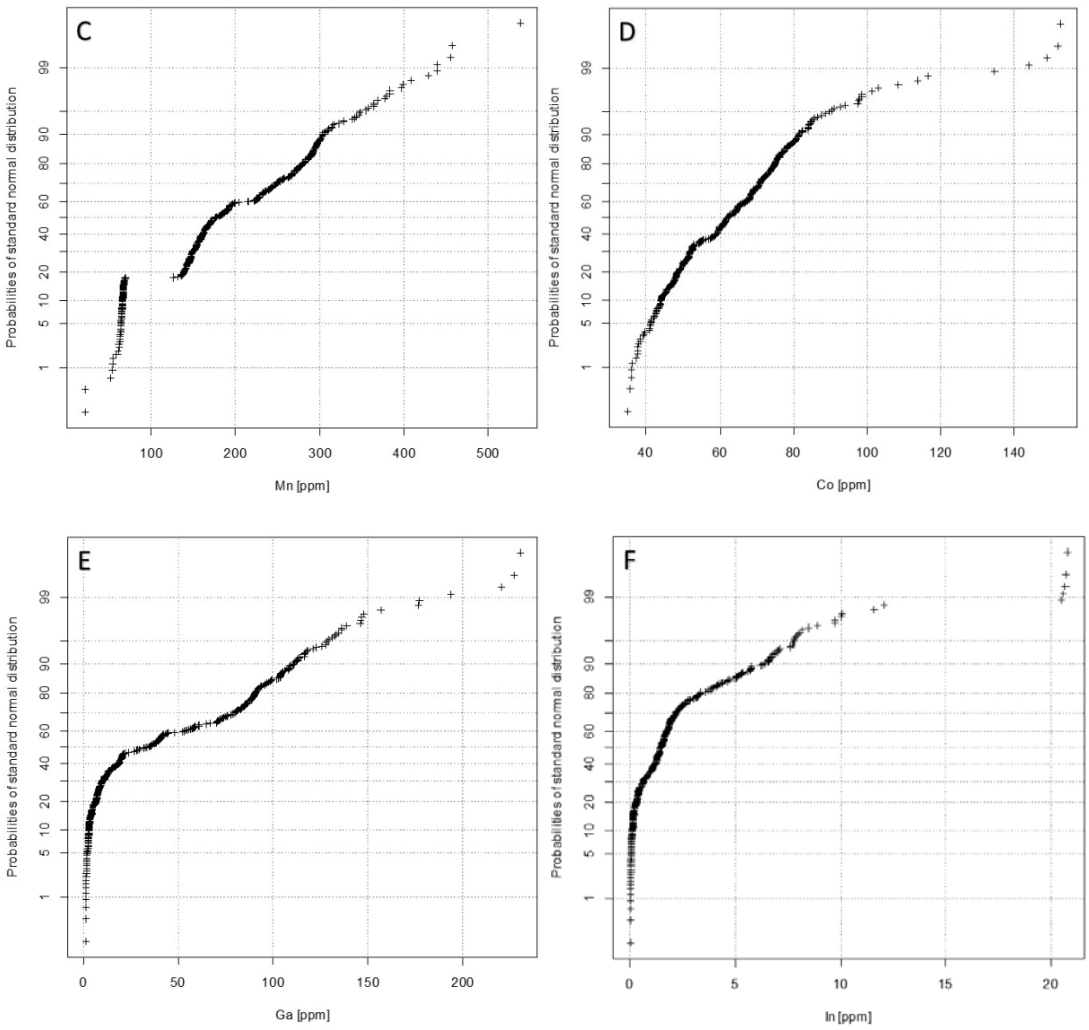

Fig. 93: Probability plots for the elements: A: Fe, B: Cd, C: Mn, D: Co, E: Ga, F: In.

Samples from the Flecktrogalm adit show a $\delta^{34}S$ maximum at +1 ‰ and have a range between -3 and +3 ‰ (Fig. 94). The Achselalm and Flecktrogalm show an overlap in the $\delta^{34}S$ and the trace element values, indicating that they have the same origin.

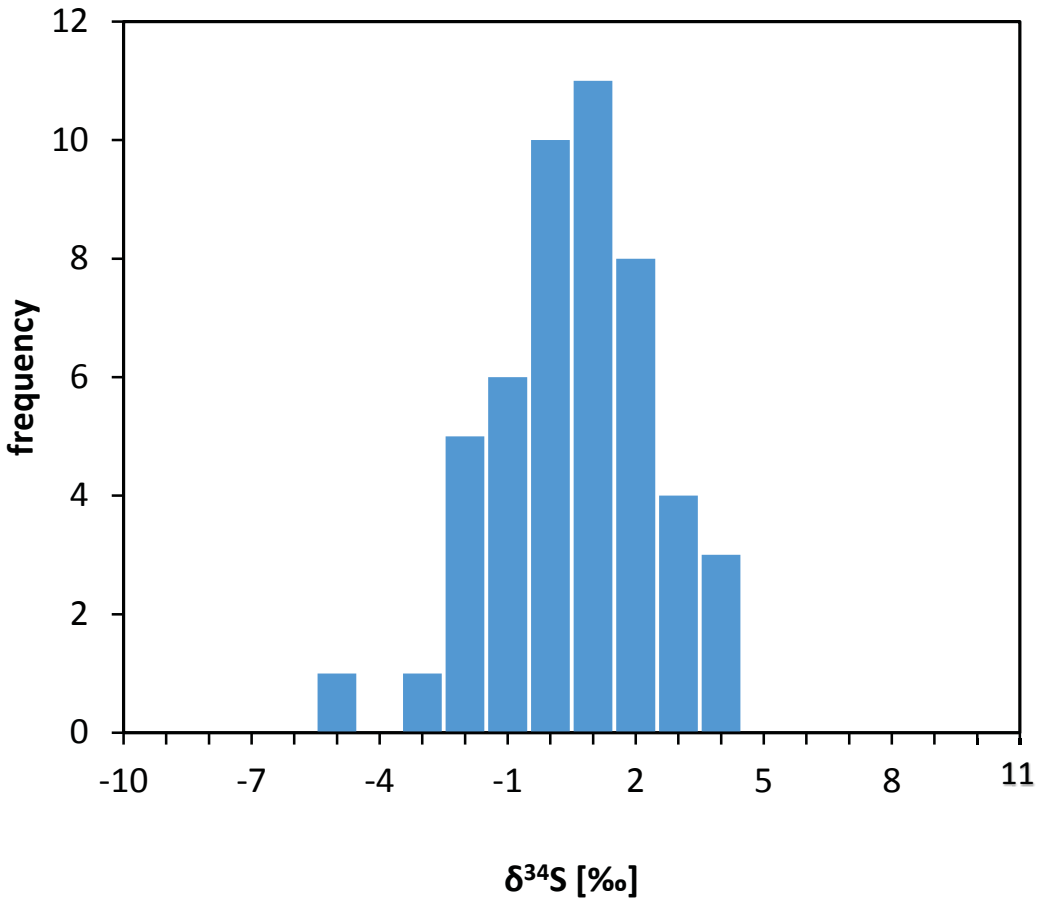

Fig. 94: $\delta^{34}S$ pattern of sphalerite samples from the Flecktrogalm adit (n= 49).

6 Discussion

6.1 Trace element variation of different ore types and locations

6.1.1 Carbonate hosted Mesozoic Pb-Zn deposits

The carbonate hosted Pb-Zn deposits of the Eastern Alps are divided into two groups, Ag bearing and nearly Ag free deposits. The analyzed sphalerites from the Drau Range are nearly Ag free, whereas Lafatsch from the Northern Calcareous Alps contains up to 106 µg/g Ag. Further sphalerite from the Northern Calcareous Alps shows 10 times lower median concentrations for Mn, Fe and Ge. The concentrations of V, Mo, In and Bi are below the limit of detection. Sphalerites from carbonate hosted Pb-Zn deposits are commonly poor in Fe and Mn. However, in contrast to all other investigated ore-types, sphalerite from Mesozoic Pb-Zn deposits show elevated trace-element concentrations of Ge, Cd, As and Tl. The elements Mn, Fe, Co, Ni, Ga, In, Sn and Sb (Table 29, Table 33 and Table 35) have low values compared to other ore types.

Table 29: P75, Median and P25 values of sphalerite from Mesozoic Carbonate hosted Pb/Zn deposits (all values in µg/g).

		Cr	Mn	Fe	Co	Ni	Cu	Ga	Ge	As	Ag	Cd	Sb	Tl	Pb
Bleiberg	P75	0.8	28.1	7160	0.2	0.2	64	3.2	530	554	3.5	2538	0.5	162	1531
	Md	0.6	14.8	2551	0.1	0.1	54	1	229	172	0.7	1379	0.2	52	724
	P25	0.5	7	643	0	0	48.5	0.3	94	34.4	0.3	769	0.1	16.8	271
Fladung	P75	0.9	20.4	8318	0.2	0.5	158	27.8	1127	445	1.6	7323	2.9	219	770
	Md	0.6	16.9	5196	0.1	0.1	93	10.3	846	310	0.5	5515	0.5	137	594
	P25	0.5	12.7	865	0	0	63	3.1	356	86	0.4	4099	0.2	25.4	396
Jauken	P75	0.8	51.5	5880	0.2	0.3	568	2.8	556	65	0.5	1496	0.3	45.3	467
	Md	0.7	39.3	4508	0.2	0.2	555	1.6	389	37.8	0.3	1249	0.1	23.1	246
	P25	0.5	29	3351	0.1	0.1	49.1	0.6	230	22.7	0.3	929	0.1	14	158
Radnig	P75	0.7	34.6	7573	0.1	0.1	50	5	523	129	0.7	1794	0.3	38.1	436
	Md	0.5	24.3	4229	0.1	0	40.6	1.9	325	56	0.4	1383	0.2	16.4	243
	P25	0.4	7.4	1277	0	0	1.4	0.8	121	6.1	0.3	955	0.1	2.5	57
Lafatsch	P75	1.4	2.2	962	0.1	0.1	702	5.2	72	939	106	3443	3.5	87	1199
	Md	0.7	0.9	520	0	0	133	1.2	41.7	273	43.4	1911	1	15.6	330
	P25	0.5	0.2	192	0	0	69	0.3	25.3	75	17.6	1093	0.3	2.6	95

The probability diagrams in Fig. 95A illustrate that the median values for Ga in the investigated carbonate hosted Pb-Zn deposits are below 1 µg/g, except Fladung. This deposit not only shows elevated Ga values, it is also enriched in Ge (Fig. 95B), 70 % of the data are above 700 µg/g. Silver plotted in Fig. 95C demonstrates that more than 50% of the data from the Drau Range are below 1 µg/g. Lafatsch contains the highest Ag concentrations (Md =43 µg/g) in sphalerite of all investigated carbonate-hosted deposits, (Fig. 95C). The highest median Ge value were found in Fladung (1000 µg/g), the lowest in Lafatsch (ca. 50 µg/g); Bleiberg, Jauken and Radnig have very similar median values (ca. 200-400 µg/g) and show lognormal Ge distributions (Fig. 95B).

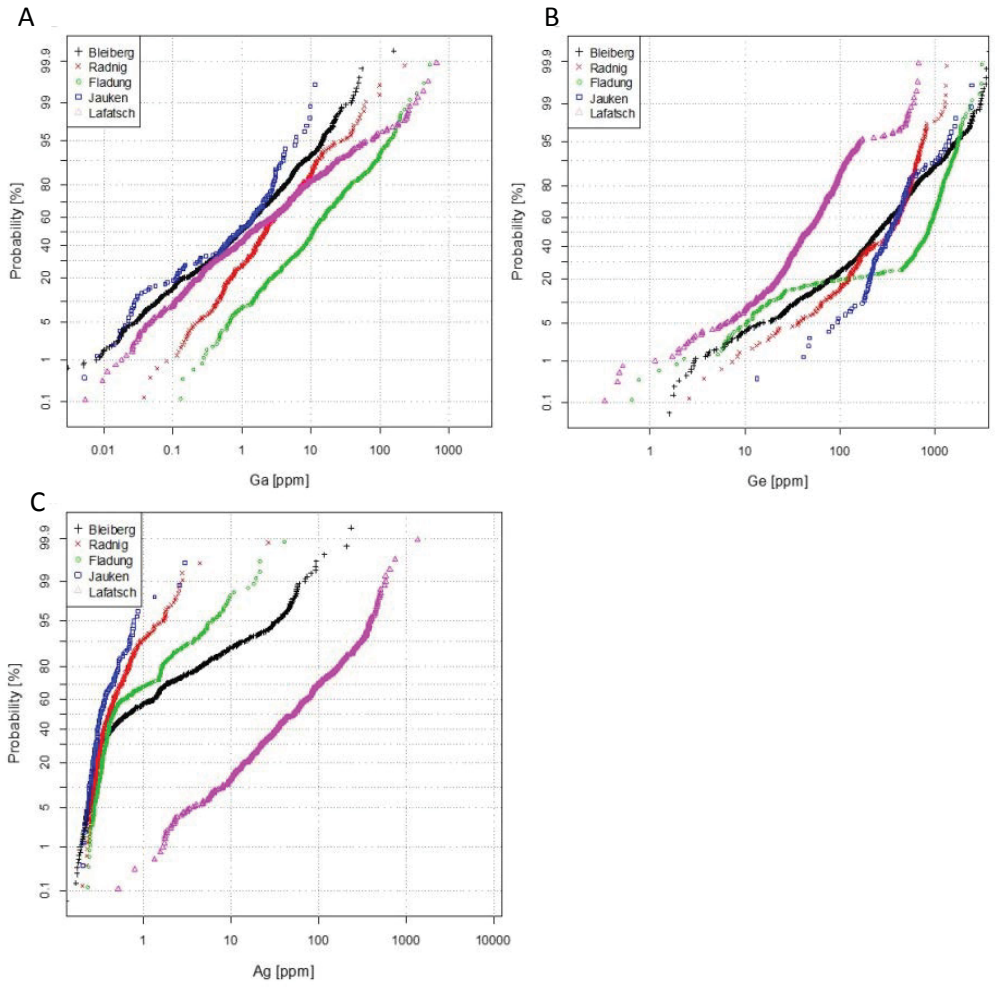

Fig. 95: Probability plot of all A: Ga; B: Ge; C: Ag data from carbonate hosted Pb-Zn deposit.

The sequence for the most important trace elements with decreasing median values from Mesozoic Pb-Zn deposits is listed in Table 30.

Table 30: Sequence of Pb-Zn deposits with decreasing trace element content values in µg/g.

Ga (Md)	Fladung (10.3) > Radnig (1.9) > Jauken (1.6) > Lafatsch (1.2) > Bleiberg (1)
Ge (Md)	Fladung (846) > Jauken (389) > Radnig (325) > Bleiberg (229) > Lafatsch (41)
Ag (Md)	Lafatsch (43) > Bleiberg (0.7) > Fladung (0.5) > Radnig (0.4) > Jauken (0.3)

Probability diagrams for the Mesozoic Pb-Zn deposits (Fig. 96) illustrate lognormal distribution and the presence of subpopulations (indicated by blue arrows). Sphalerite hosted by Mesozoic carbonate rocks of the Drau Range shows similarities in the element distribution and variability, e.g. Cd in Jauken and Fladung; Gallium values in Radnig and Fladung are within the same range (Fig. 96). Most trace elements in Bleiberg, for which a large data set is given, are lognormally distributed except for Fe (second population at higher Fe levels, representing Schalenblende samples). The trace element distribution from the Bleiberg deposit shows an extreme variability of more than three orders of magnitude for all elements. The kink in Cu is probably/likely due to chalcopyrite inclusions, the rest of the data are lognormally distributed

over the three different ore types (Fig. 96A). Sphalerite from Fladung is most enriched in Cd, Ga and Ge. Germanium, Cd and Mn are lognormal distributed in the Fladung deposit. Iron, Ge, As and Tl show a kink at the element concentrations between 5 and 50 µg/g for Tl, 500 and 2000 for Fe and Ge between 100 and 500 µg/g (Fig. 96B:). Those kinks indicate multiple sphalerite generations. The variability in the trace-element content is high (e.g. Ge 0.1 to 120 µg/g) but not as high as in Bleiberg. The Cu curve from the Jauken deposit shows a step between 30 and 500 µg/g due to chalcopyrite micro inclusions. The rest of the plotted elements in Fig. 96C are lognormally distributed. Radnig shows only a lognormal distribution for Mn and Cd and high variability (3 to 4 orders of magnitude depending on the element). The kink in the probability plot for the elements Tl, Ge, As and Fe point to at least two different sphalerite generations (Fig. 96D: blue arrow). Except Cu the trace elements plotted in Fig. 96E, from the Lafatsch deposit are lognormally distributed. Lafatsch is the only investigated Mesozoic carbonate hosted Pb-Zn deposit where sphalerite shows significant Ag values (Fig. 96E). For Tl, Bleiberg and Fladung have similar median values > 70 µg/g, whereas the other investigated deposits show significant lower median values for Tl of around 20-30 µg/g (Fig. 96A, B) .

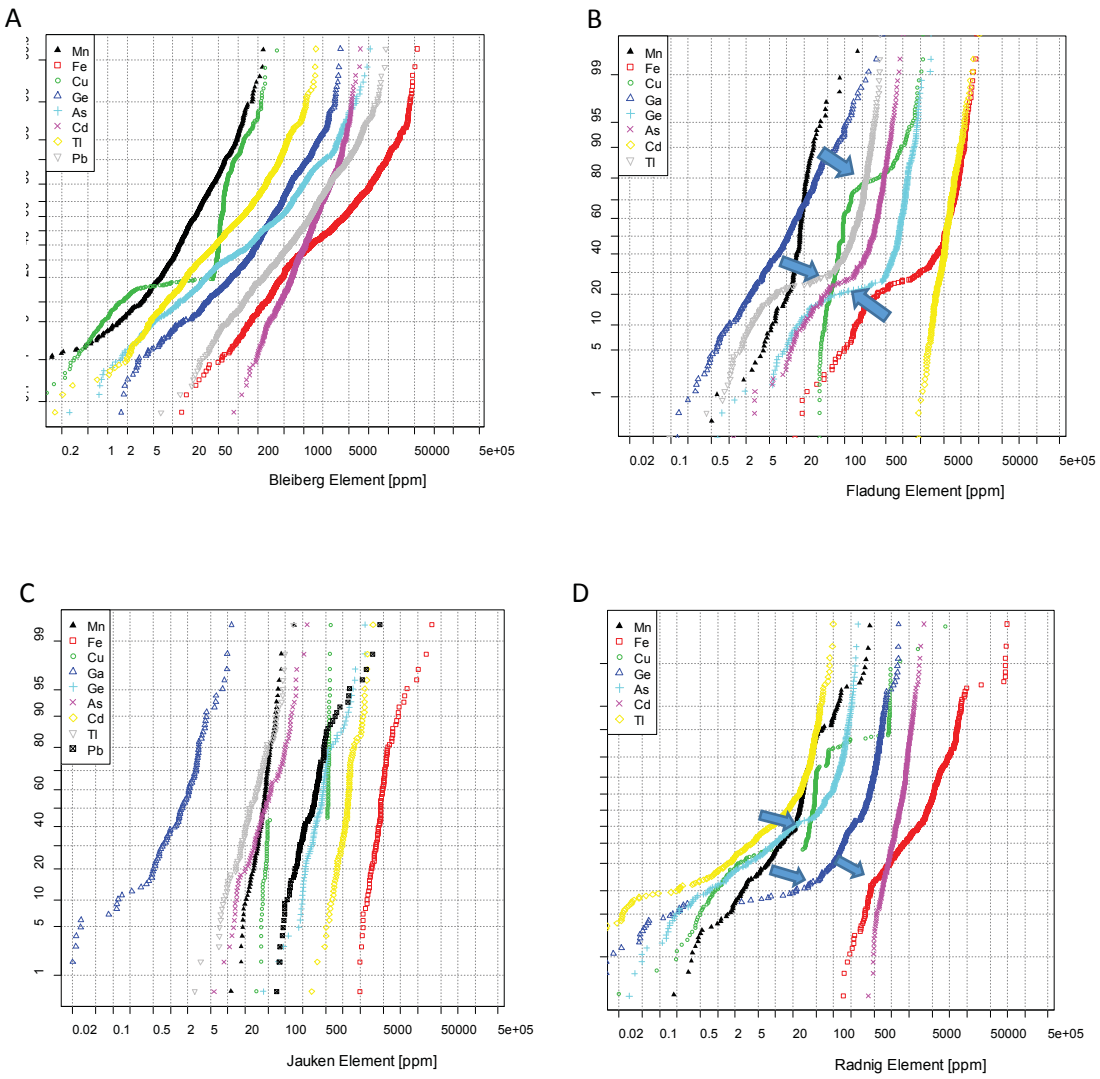

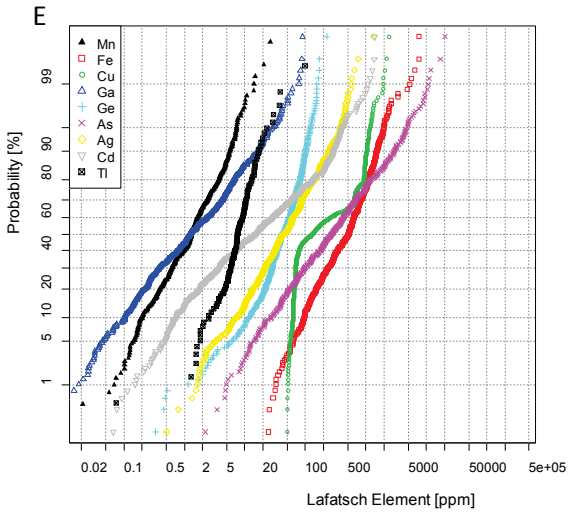

Fig. 96: Probability diagrams for significant trace elements in sphalerite from different Carbonate hosted Pb-Zn deposits; A, Bleiberg; B, Fladung; C, Jauken; D, Radnig; E, Lafatsch. Blue arrows mark kinks in the probability plots.

Seen from a distance (ore deposit), the variation of the trace elements shows a wide spread. For example, the two investigated ore types (Cardita ore, Wetterstein ore) from the Bleiberg deposit show no significant differences. The data points overlap in a wide range (Fig. 97A, B). The different grain sizes and colors of sphalerite described in chapter 5.1.3 show geochemically lognormally distributed data. Germanium shows a positive correlation with Fe (Fig. 97A), whereas Cd correlates negatively with Fe (Fig. 97B).

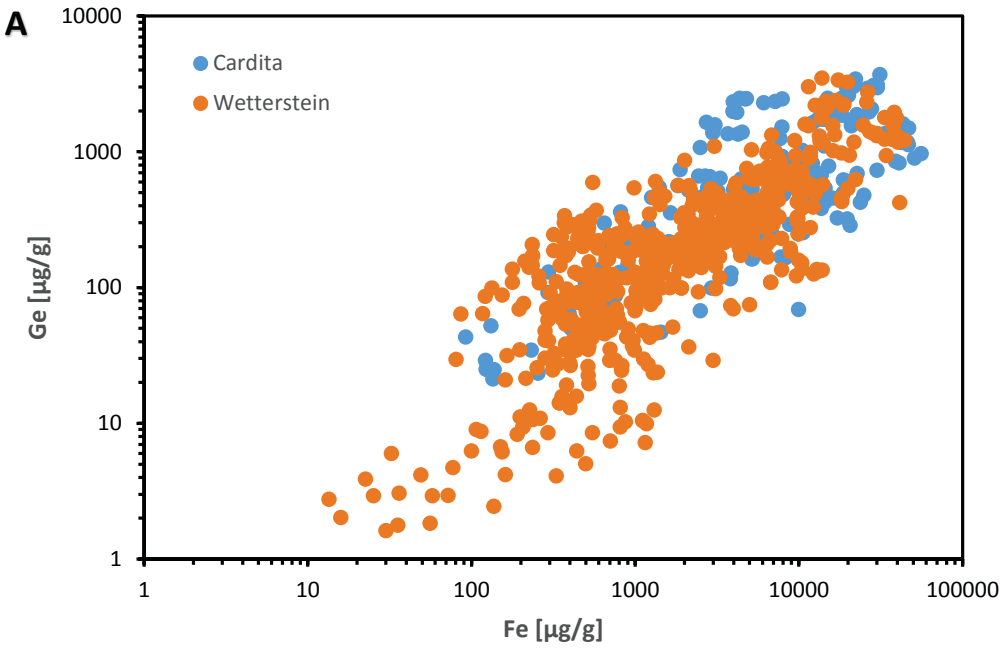

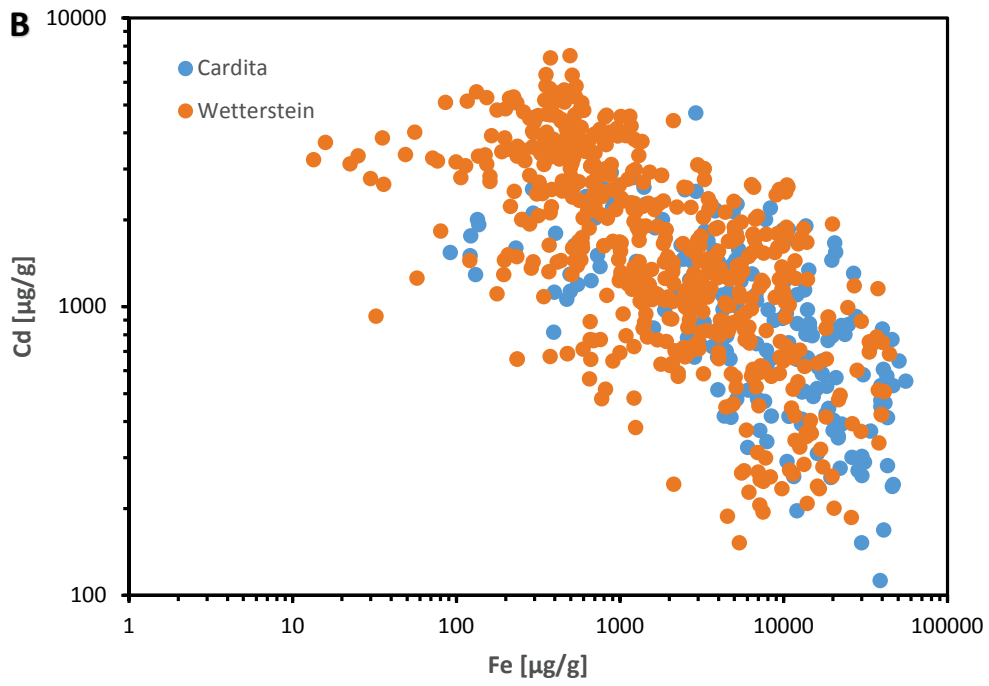

Fig. 97: Plot of all Ge, Fe and Cd sphalerite data from Bleiberg, A: Ge vs. Fe, B: Cd vs. Fe.

Within a single ore type, a grouping of different samples is visible, but the within sample elemental variation is still large. In the Wetterstein ore (Fig. 98A) e.g. Fe ranges from 50 to 20000 µg/g and Ge from 1.5 to ~1000 µg/g. The Cardita ore, plotted in Fig. 98B also shows a huge variation (e.g. four orders of magnitude for Fe and 3 orders of magnitude for Ge) in the trace element content. However, in this ore type, a grouping of the different samples is better visible than in the Wetterstein ore.

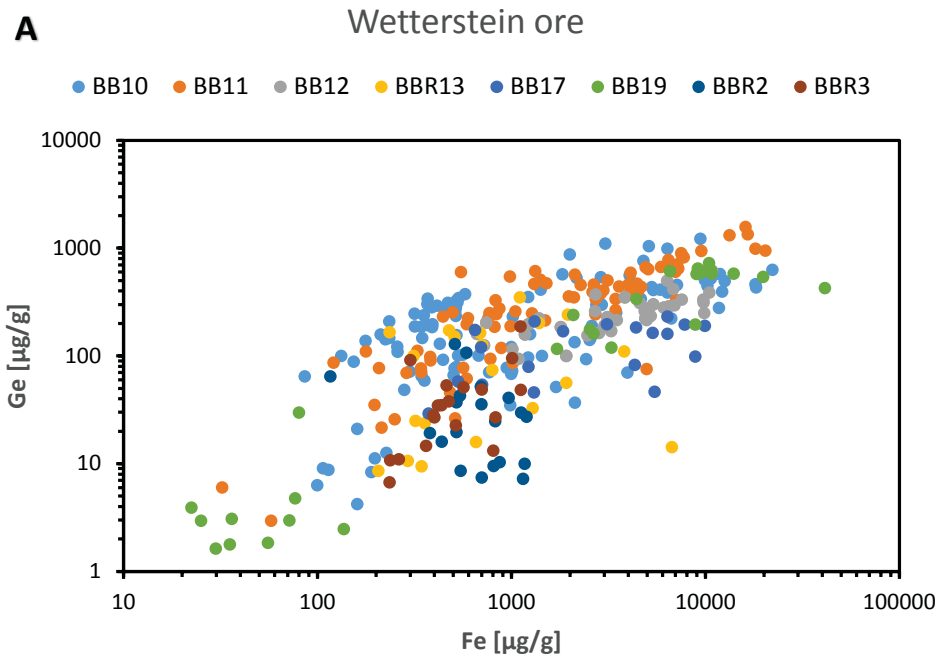

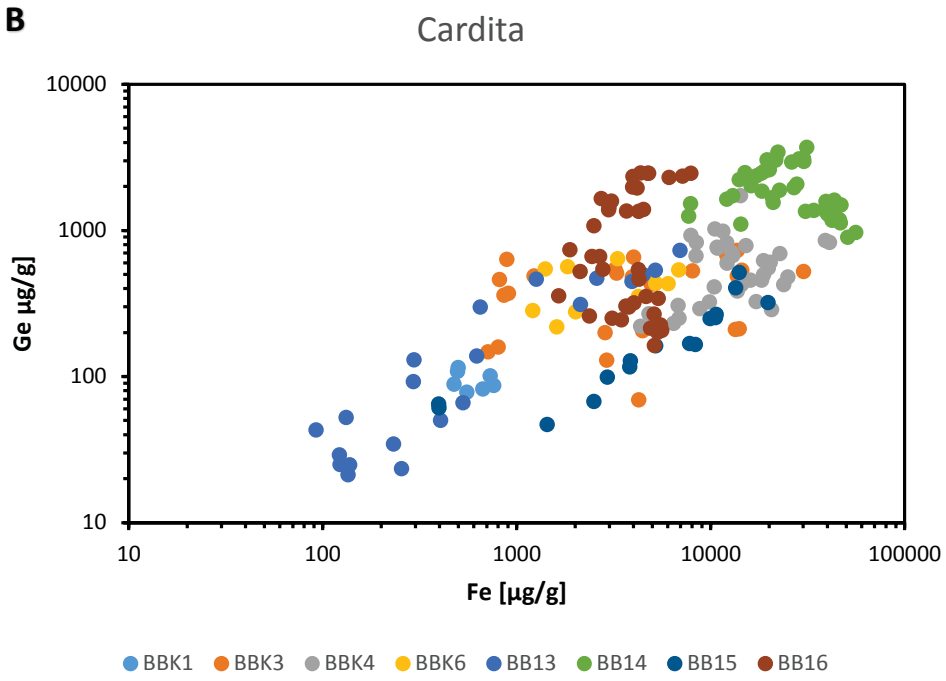

Fig. 98: Fe vs. Ge plot of A: samples from the Wetterstein ore, B: samples from the Cardita ore.

At the scale of a single sample, the trace element variation is still high, but different sphalerite generations, respectively the color variation (Fe is the coloring element) can be identified and explained. For example, samples BBR8 and BB19, both from the Ramser area (Wetterstein ore) (Fig. 99A) clearly show the different coloring (by different Fe mass fraction) of the measured sphalerite. The trace element variation of Schalenblende (Fig. 99B) show a wide variation, e.g. Fe 2 orders of magnitude. This plot also shows that yellow sphalerite is poor in Fe and the Ge content is around 200µg/g lower than in the Fe rich (brown) sphalerite.

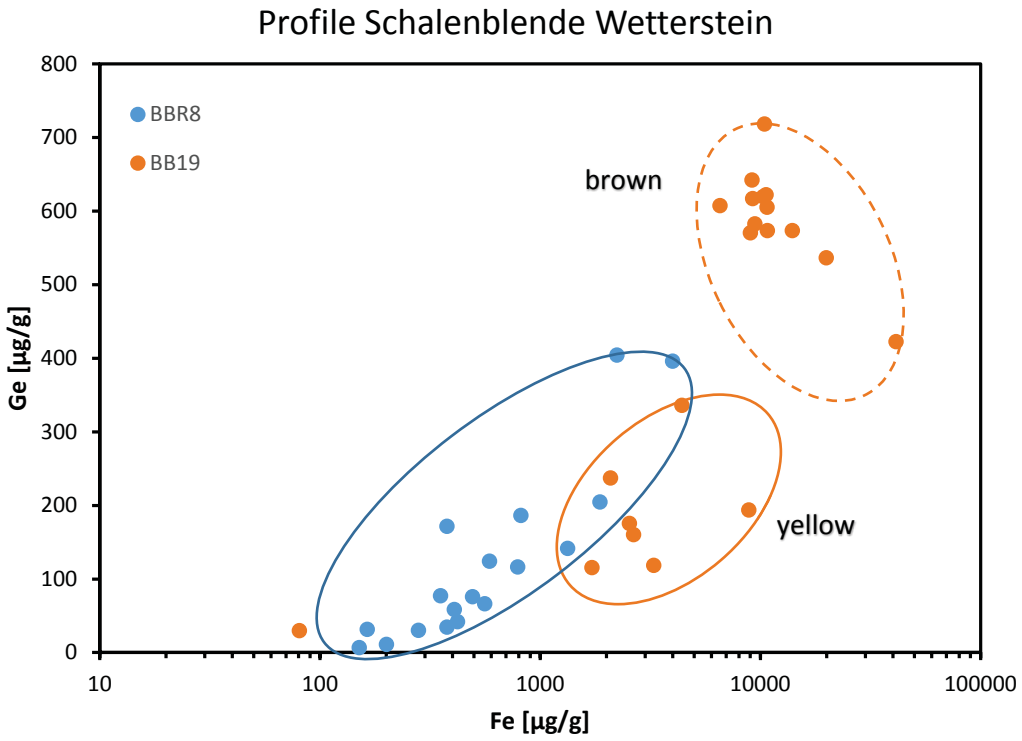

Fig. 99: Fe vs. Ge plot of two profiles through two colloform sphalerite, blue dots stand for mostly yellow sphalerite of sample BBR8, orange dots show the variability within a yellow and brown Schalenblende of sample BB19.

The above-mentioned observations reveal that an identification of different sphalerite generations based on trace element alone is only possible on a small scale. On the scale of ore type or an ore deposit an identification of different generations in the xy-plot is nearly impossible, due to the wide spread of the different trace elements and the large amount of data.

The probability plots in Fig. 96 give a clearer overview of the trace element variability where different generations or varieties are indicated by a kink in the curve. In the following, the different kinks in the probability plots (Fig. 96) are illustrated in ternary diagrams (Fig. 97A, B) to identify the different generations of sphalerite.

The elements that form kinks in the probability diagrams (Fig. 97B,D) of the Radnig and Fladung deposit are plotted in the ternary plots (Fig. 100A,B). The kink in probability plot Fig. 96B from the Fladung deposit for the elements Fe, Ge, As, Tl and Cu, indicates geochemical differences between fine and coarse-grained sphalerite crystals, described in 5.1.4, where the fine-grained sphalerite is represented by concentration levels below Tl~100 µg/g, As~ 700 µg/g and Cu~500 µg/g. Schalenblende (blue ellipse) and coarse-grained sphalerite represent the concentration levels above these levels (yellow ellipse) in Fig. 100A. The blue ellipse in Fig. 100B represents the small-grained brownish sphalerite. The yellow ellipse displays the chemical data of coarse-grained yellow sphalerite described in chapter 5.1.2.

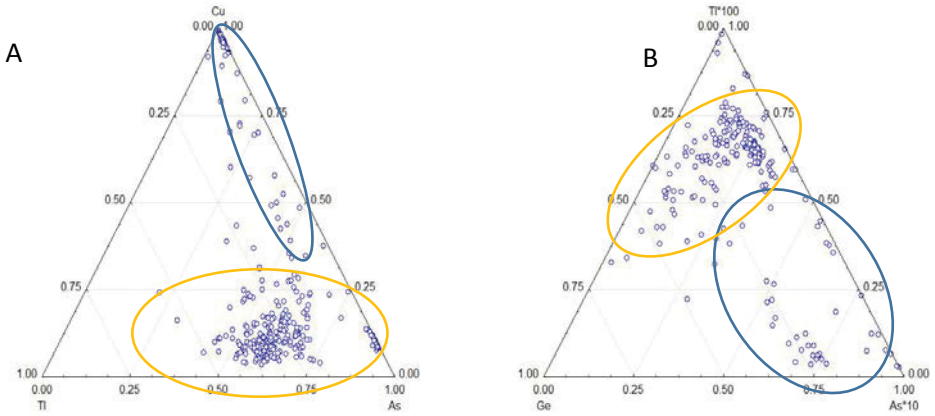

Fig. 100: Ternary element plot: A, Fladung: blue ellipse represents the Schalenblende, yellow ellipse the coarse grained sphalerite ; B, Radnig: blue ellipse represents the small grained and the yellow ellipse the coarse grained sphalerite.

All investigated sphalerites from Mesozoic carbonate hosted Pb-Zn deposits of the Eastern Alps have in common, that the values for Fe, Ge, As, Cd and Tl are elevated compared to the CTEM. None of them has significant values of In, Co and Ga (except Fladung and Lafatsch). A further similarity is that sphalerite from carbonate hosted Mesozoic Pb-Zn deposits is enriched in Ge and depleted in Cd in the Fe rich variety. Lafatsch is a special case within this type of deposits, bearing elevated Ag concentration, but is depleted in Fe and Ge.

From the critical metal point of view, the dark sphalerite variety of carbonate hosted Mesozoic Pb-Zn deposits is to prefer for the production of critical metals, due to the higher Ge and lower Cd content. All investigated Pb-Zn deposits of the Drau Range have Ge contents of economic interest; Fladung shows the highest median values, Bleiberg the lowest (Fig. 101). Although Bleiberg shows the lowest Ge median values, it is the target number one for Ge due to its size (after Cerny and Schroll (1995): Reserve of 2 million tons of ore).

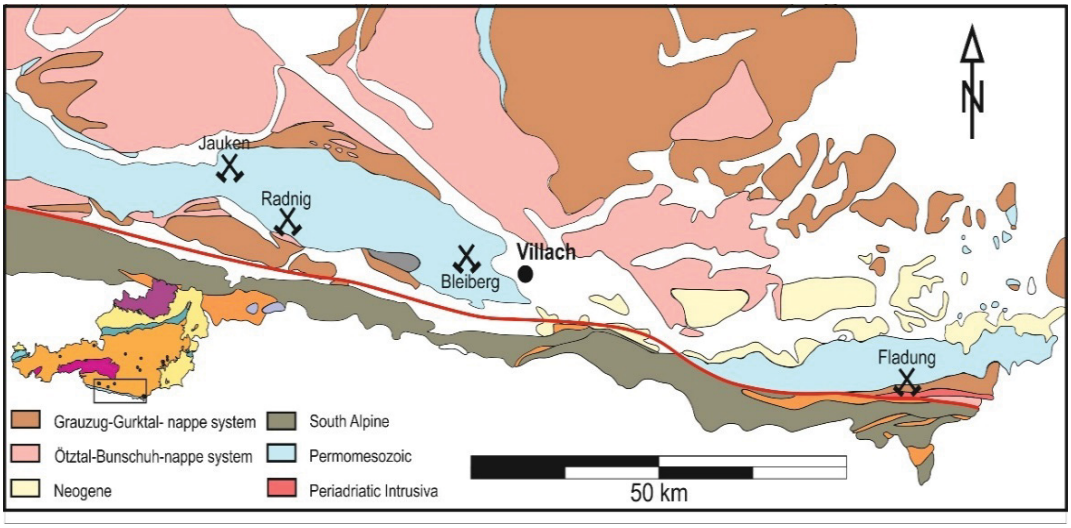

Fig. 101: Simplified geological sketch of a part of the Drau Range (modified after GBA: IRIS Online 2017) and a summary of critical metal median values. PAL (Peri-Adriatic-Lineament)

6.1.2 Sediment-hosted Pb-Zn deposits of the Graz Paleozoic

Sphalerites in sediment-hosted deposits of the Graz Paleozoic exhibit large variations in trace elements among the different deposits. The Graz Paleozoic thus serves as an example of heterogeneity within and between individual deposits in a geological province.

Sphalerite from Pb-Zn deposits of the Graz Paleozoic are commonly rich in Fe (>1 wt. %) and poor in Mn (Md < 100 µg/g) (Table 31). Samples from Friedrich, Elisabeth, Haufenreith and Guggenbach are highest in Co, and Haufenreith sphalerite has In > 20 µg/g. Copper and Ag concentrations are highest at Arzberg, probably partly due to intergrowth with Ag-bearing fahlore and chalcopyrite.

Table 31: P75, Median and P25 values of sphalerite from Sediment-hosted Pb-Zn deposits of the Graz Paleozoic (all values in µg/g).

		Cr	Mn	Fe	Co	Ni	Cu	Ga	Ge	As	Se	Ag	Cd	In	Sn	Sb	Pb
Arzberg	P75	0.79	163	16870	137	0.77	1760	10.23	0.21	0.33	9.00	180	1851	8.42	0.66	13.89	330
	Md	0.45	98	14010	19	0.17	1012	1.64	0.13	0.15	7.10	78	1292	4.03	0.37	5.87	70
	P25	0.17	34	9915	10	0.04	180	0.55	0.05	0.06	5.80	11	975	2.56	0.21	2.41	15
Elisabeth adit	P75	0.41	83	61000	175	1.89	55	21.52	0.58	0.00	3.20	23	2035	0.29	1.13	11.75	55
	Md	0.27	60	56300	158	0.96	29	9.69	0.39	0.00	2.40	14	1894	0.17	1	7.15	27
	P25	0.13	44	52650	122	0.30	19	3.89	0.25	0	1.70	9	1788	0.00	0	3.80	15
Friedrich adit	P75	0.33	70	53380	303	2.98	142	32.54	0.64	0.12	3.80	37	2672	5.61	2.28	10.24	47
	Md	0.22	49	45800	232	2.07	59	18.89	0.44	0.00	2.45	22	2415	1.90	2	7.06	24
	P25	0.12	39	39903	139	1.37	31	9.17	0.32	0.00	1.70	14	2207	0.20	1	4.95	15
Guggenbach	P75	0.99	104	54800	157	3.02	1005	20.84	0.24	1.30	5.50	30	1558	2.96	1.35	8.69	60
	Md	0.68	74	49800	134	1.75	919	7.41	0.09	0.50	4.50	19	1132	0.19	0.85	4.31	23
	P25	0.47	65	44143	103	0.95	602	2.78	0.03	0.26	3.20	10	981	0.13	0.62	1.62	9
Haufenreith	P75	0.26	245	35175	188	10.70	625	6.42	0.38	3.73	2.83	12.39	2219	47	2.31	4.37	36.88
	Md	0.21	214	32600	178	7.85	616	3.60	0	3.00	1.67	5.65	2155	37	1.86	3.05	24.02
	P25	0.15	193	29238	163	5.32	599	2.23	0	2.10	1.12	2.59	2065	28	1.55	1.89	17.88
Rabenstein	P75	0.94	72	56440	151	2.48	1060	9.91	0.51	0.56	6.80	34	1107	3.30	0.81	6.94	95
	Md	0.64	67	52000	130	1.43	994	5.05	0.34	0.35	5.90	25	1032	0.18	0.67	4.25	27
	P25	0.36	60	47850	81	0.77	931	2.80	0.24	0.16	5.00	14	904	0.13	0.55	1.64	11
Silberberg	P75	1.36	30	32150	116	0.32	1190	13.74	0.39	0.11	3.37	22	2871	2.42	0.79	5.50	30
	Md	0.50	24	31000	93	0.20	770	12.34	0.28	0.00	2.29	19	2317	1.84	0	3.73	25
	P25	0.07	17	29400	77	0.12	225	6.62	0.00	0	1.84	17	2186	1.69	0	2.69	20

The probability diagrams in Fig. 102 demonstrate that the curves for Co, Ga, In and Ag for the Elisabeth and Friedrich adit are parallel indicating an affinity that can be described due to the geographical proximity of these two deposits. The Friedrich adit shows the highest Co median values, Arzberg the lowest. Gallium shows the highest median in the Friedrich adit and the lowest in Haufenreith. The most elevated In median was measured in Haufenreith and the highest Ag median in the former Pb-Zn-Ag mine of Arzberg (Md = 78 µg/g).

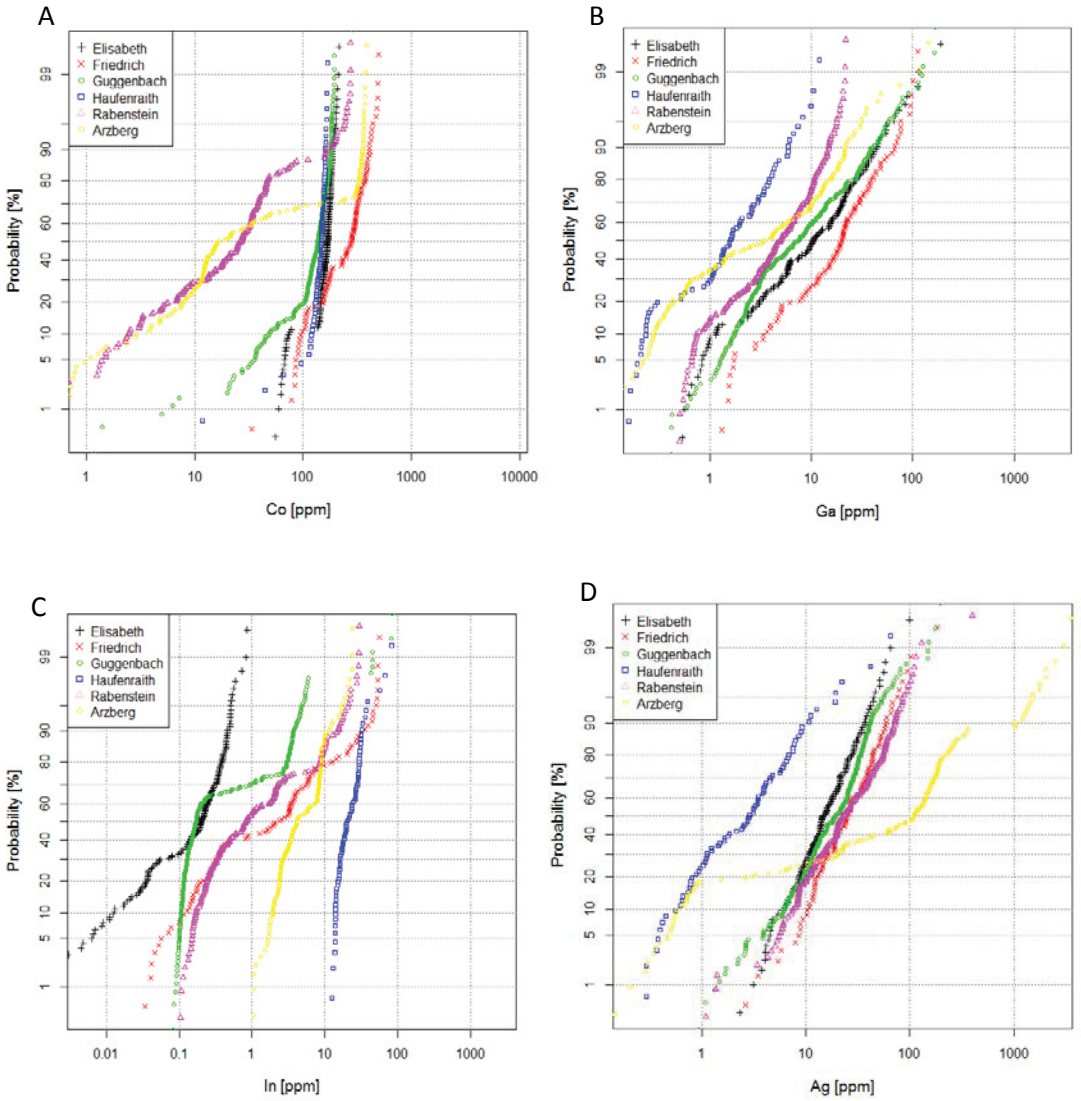

Fig. 102: Probability plot of all A: Co; B: Ga; C: In; D: Ag data from the Graz Paleozoic.

The sequence of decreasing trace element median values from Pb-Zn deposits of the Graz Paleozoic is listed in Table 32. The critical metal contend from ore deposits of the Graz Paleozoic show nearly the same range, except Arzberg for Co and Ag, and Haufenreith for In.

Table 32: Sequence of Pb-Zn deposits with decreasing trace element content values in µg/g.

Co (Md)	Friedrich (232) > Haufenreith (178) > Elisabeth (158) > Guggenbach (134) > Rabenstein (130) >Silberberg (93) > Arzberg (19)
Ga (Md)	Friedrich (18.9) > Silberberg (12.3) > Elisabeth (9.7) > Guggenbach (7.4) > Rabenstein (5.1) > Haufenreith (3.6)> Arzberg (1.6)
In (Md)	Haufenreith (37) > Arzberg (4) > Friedrich (1.9) > Silberberg (1.8) > Rabenstein (0.2) > Guggenbach (0.19) > Elisabeth (0.17)
Ag (Md)	Arzberg (78) > Rabenstein (25) > Friedrich (22) > Silberberg/Guggenbach (19) > Elisabeth (14) > Haufenreith (5.6)

Binary diagrams (Fe vs. Co and Fe vs. Ga) of all data from the Graz Paleozoic demonstrate a variability for Fe of three orders, for Co and Ga nearly four orders of magnitude (Fig. 103). The data show an overlap in a wide field, but clusters of populations can be identified, e.g. Friedrich adit (Fig. 103).

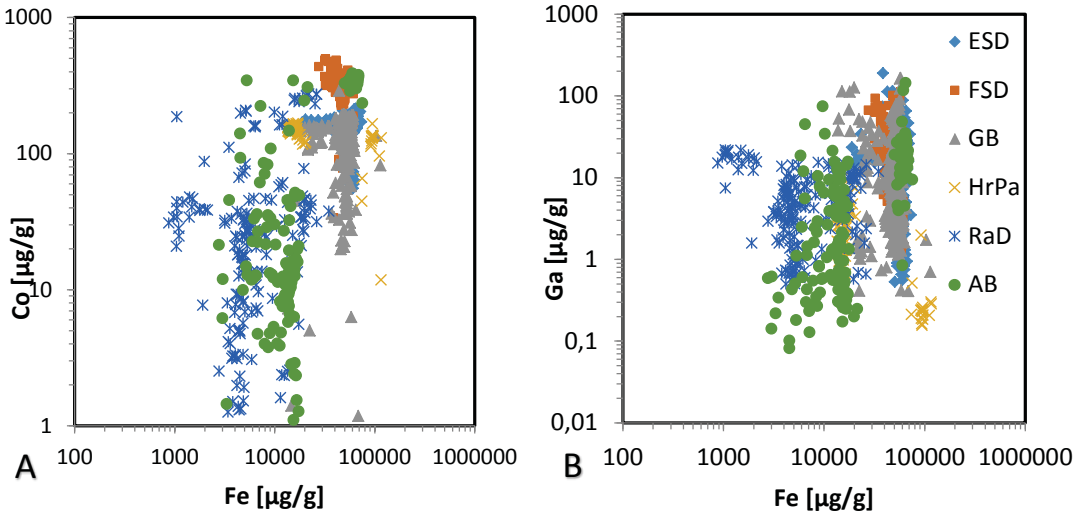

Fig. 103: Fe vs. Co (A) and Fe vs. Ga (B) of all data from the Graz Paleozoic. ESD, Elisabeth-Adit; FSD, Friedrich Adit; Gb, Guggenbach; HrPa, Haufenreith-Passail. RaD, Rabenstein-Deutschfeistritz, Ab, Arzberg;

A closer view to a single ore deposit, in this case Rabenstein-Deutschfeistritz, still shows a high variability, but individual samples can be identified as clusters (Fig. 104). Fig. 104A demonstrates that most of the samples show only one generation, except the samples RaD 3 (grey ellipse) and RaD 7 blue ellipse), where two generations are identified using Fe and Co concentrations.

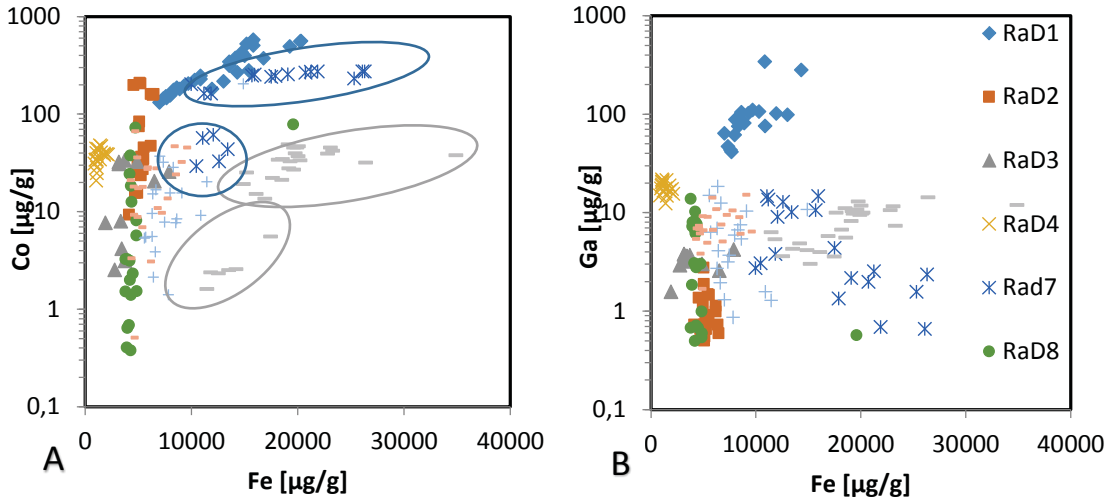

Fig. 104: Fe vs. Co (A) and Fe vs. Ga (B) of all data from sphalerite collected at the Rabenstein-Deutschfeistritz dumpsite.

The probability plot of sphalerite from Arzberg shows two kinks, giving evidence for at least two sphalerite generations. One is Fe, Mn, In and Co poor and one generation is enriched in those elements (kink in Fig. 105A: arrow; at e.g. Fe between 10000 and 50000 µg/g and Co at ~200 µg/g). The probability plot of sphalerite from the Elisabeth adit shows a parallel trend of all elements above Co ~100 µg/g, Ga ~2 µg/g and Fe ~50000 µg/g representing the first generation (except a Pb kink at 50 µg/g due to galena inclusions). Sphalerite from the Elisabeth

adit showing Fe concentrations below 5 wt% are also depleted in Co, Mn, Ag, Sb and Ga (Fig. 105B) and represents the second sphalerite generation. Sphalerite from Friedrich adit localized next to the Elisabeth adit shows nearly parallel probability curves indicating only one sphalerite generation (Fig. 105C). The kink in Cu the plot of the Guggenbach adit (Fig. 105D) at ~200 µg/g is ascribed to the copper disease found in sphalerite from Guggenbach. The other elements in this plot give no evidence for more than one sphalerite generation. Sphalerite from Haufenreith shows a lognormal distribution; the variability is small, due to the small number of data (Fig. 105E). The probability plot of Rabenstein shows only slight kinks for Fe at ~4000 µg/g, Cd at 600 µg/g, In at 5 µg/g and Co between 50 and 120 µg/g, indicating at least two sphalerite generations.

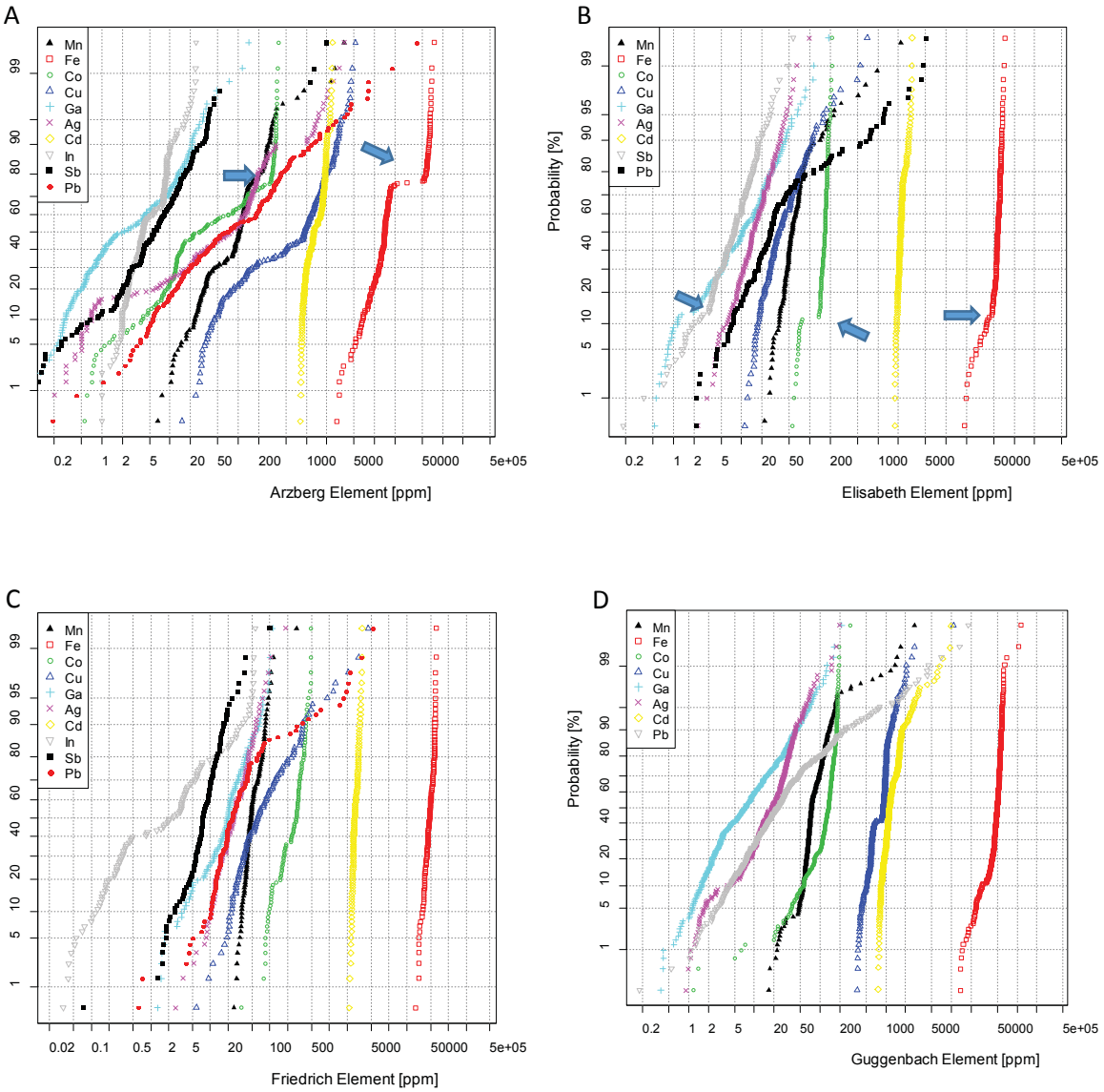

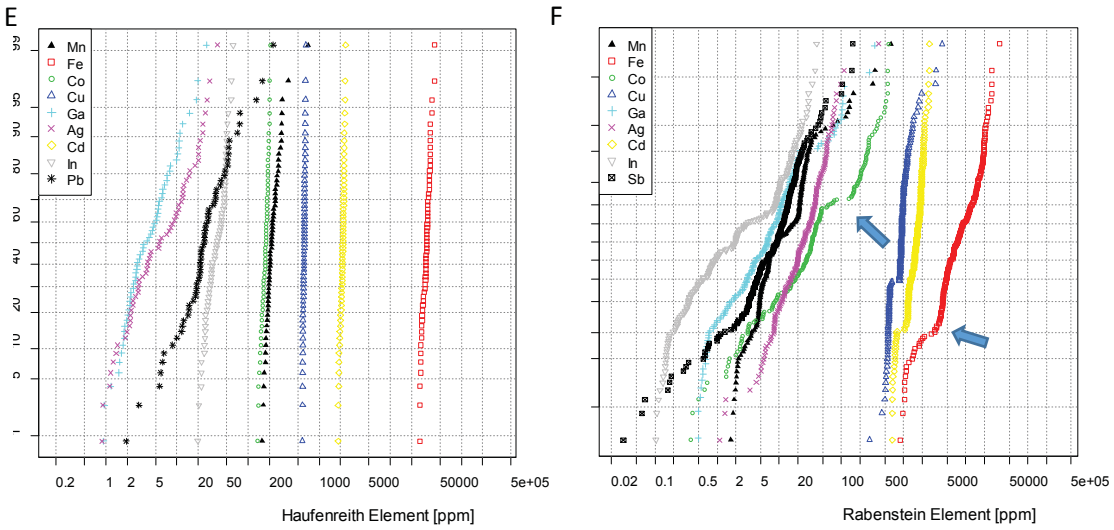

Fig. 105: Probability diagrams for significant trace elements in sphalerite from different SEDEX Pb-Zn deposits hosted in the Graz Paleozoic; A, Arzberg; B, Elisabeth adit; C, Friedrich adit; D, Guggenbach; E, Haufenreith; F, Rabenstein.

Chemical data of sphalerite (Table 31) from Arzberg can be divided into three groups (i) Fe poor (below 2 wt.%), enriched in Co and Cd, (ii) Fe and Co poor, but Cd enriched, representing the reddish brown sphalerite and (iii) Fe rich (above 2 wt.%) enriched in Co and Cd representing brown sphalerite (Fig. 106A). The enrichment of Ga depends on the Fe content: Fe rich sphalerite from Arzberg is enriched in Ga (10 to 100 µg/g).

The three kinks in the plot of the Elisabeth adit (Fig. 106B) for the elements Fe, Cu and Ga give evidence for two sphalerite generations, one Fe, Co and Cu poor (brown sphalerite) and a Fe, Co and Cu rich generation (dark brown sphalerite) Fig. 106B.

Two sphalerite generations were identified in the Rabenstein deposit, an Fe, Cu and Cd poor (yellow sphalerite) and a Fe, Cu and Cd rich (reddish sphalerite) generation (Fig. 106C).

Haufenreith shows two groups in the In-Ag-Fe ternary plot, an Fe r - In poor (orange ellipse) and an Fe - In rich group (Fig. 106D). Both sphalerite groups show a reddish brown color and can not be distinguished using reflected microscopy.

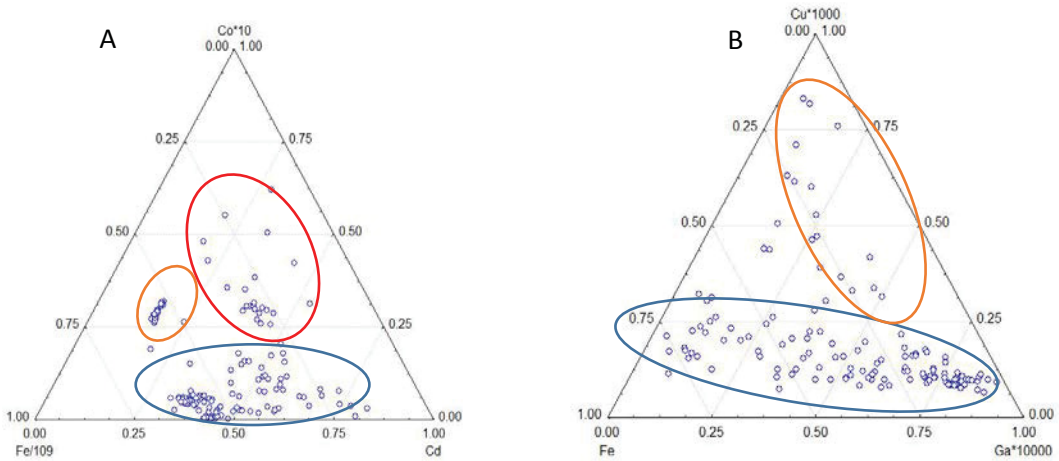

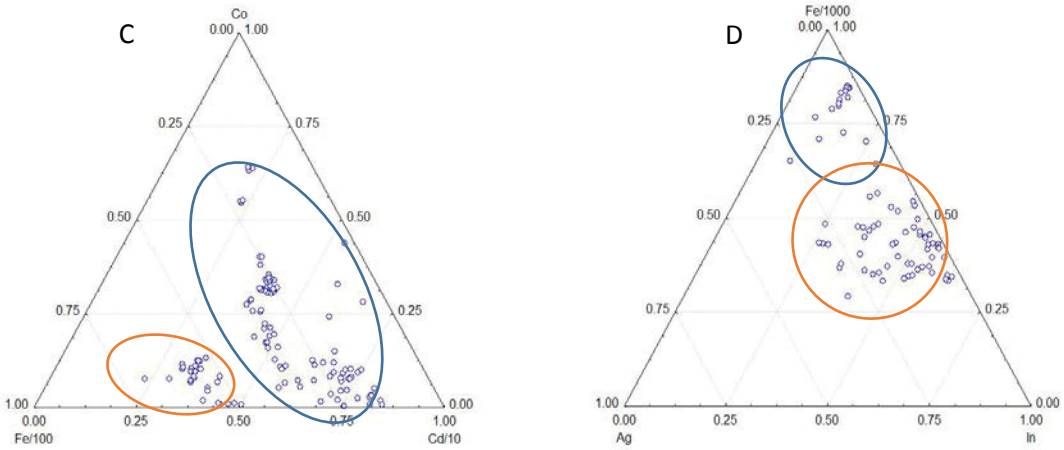

Fig. 106: Ternary element plot: A, Arzberg; B, Elisabeth; C, Rabenstein; D, Haufenreith . The different ellipses indicate the different sphalerite populations in these deposits.

Enrichments in Ag and In were measured in the deposits Arzberg and Silberberg. Elevated Ga values (> 10 µg/g) were found in Elisabeth adit, Friedrich adit and Silberberg. Compared to the CTEM, Co is enriched in Guggenbach, Elisabeth adit, Friedrich adit, Silberberg and Haufenreith, Ga is enriched in Friedrich adit, Ge and In is depleted in all investigated ore deposits. From the critical metal point of view, the investigated ore deposits of the Graz Paleozoic do not show critical element concentrations of economic interest (Fig. 107).

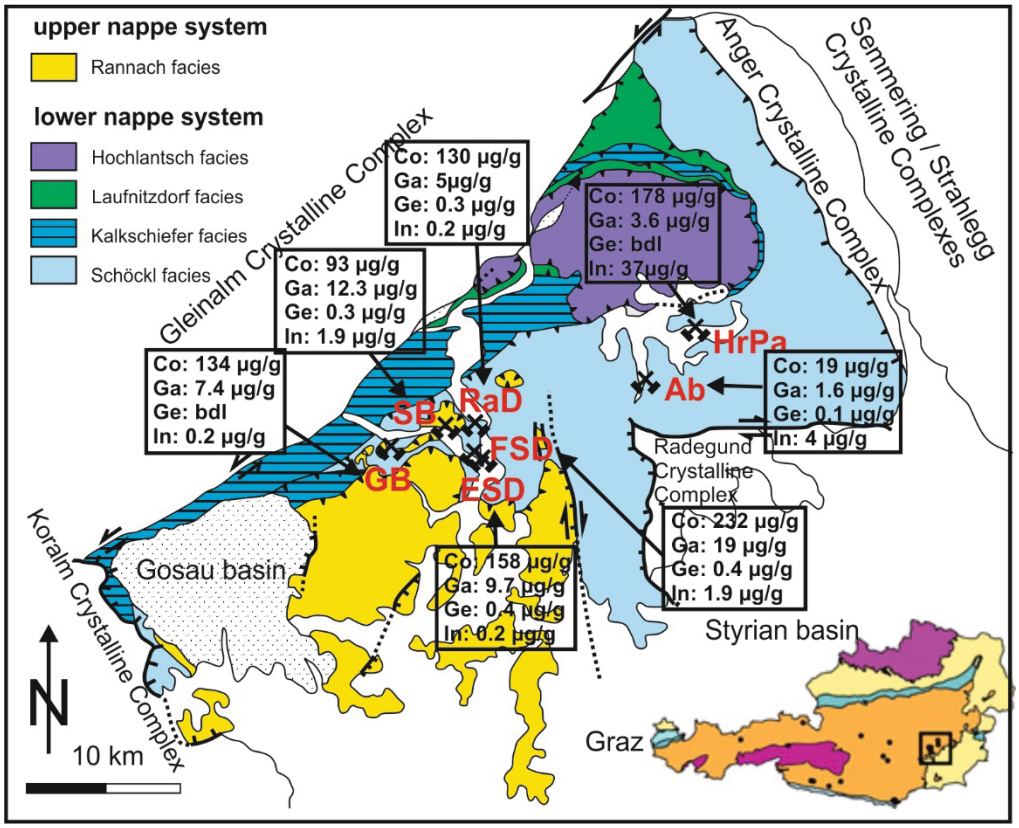

Fig. 107: Simplified geological map of the Graz Paleozoic (modified after Gasser et al. 2010), summarizing the critical metal content of the investigated Pb-Zn deposits.

6.1.3 Sediment-hosted Pb-Zn deposits hosted in other Paleozoic units

The sediment-hosted deposits of Leogang, Walchen and Meiselding show similar Fe median values of approximately 8 wt. %. However, Walchen is considerably enriched in Ga and In, whereas Meiselding is elevated in Cd, Mn and Co. The highest In content measured in Leogang (Md= 247 µg/g) are probably partly due to intergrowth with bornite and chalcopyrite that may carry In (Cook et al. 2011; George et al. 2017) (Table 33).

Table 33: P75, Median and P25 values of sphalerite from Paleozoic Sediment-hosted Pb-Zn deposits (all values in µg/g).

		Cr	Mn	Fe	Co	Cu	Ga	Ge	As	Ag	Cd	In	Sn	Sb	Pb
Leogang	P75	1	235	91063	148	2325	1.6	0.2	0.2	27	2560	270	1.9	5.4	86
	Md	0.8	143	79985	128	865	1	0.1	0.1	11	2042	247	0.9	2.7	17
	P25	0.7	57	23040	79	226	0.7	0	0.1	4	1734	4	0.6	1.2	5
Meiseldin	P75	0.7	669	91975	301	920	0.9	0.3	1.8	29	4532	23	1.5	13.1	198
	Md	0.5	454	88300	213	748	0.7	0.1	1.1	13	3960	16	1.2	5.5	12
	P25	0.3	331	83025	139	586	0.5	0	0.3	7	3603	10	0.9	2	3
Walchen	P75	0.4	131	88700	97	690	4.3	0.1	0.2	20	2092	173	3.7	8.4	270
	Md	0.4	73	84300	55	288	1.5	0.1	0.1	12	1592	98	1.1	3.1	12
	P25	0.3	42	77900	12	178	0.9	0	0	9	1364	64	0.5	1.1	3

The probability plots of Co, In and Ag in Fig. 108 representing the deposits of Meiselding, Walchen and Leogang, demonstrate that the curves are nearly parallel and show a lognormal distribution. The spread of the In trace element distribution (Fig. 108B) rises over nearly six orders of magnitude for the Walchen deposit with a gap between 0.1 and 50 µg/g. The values on the left side of the gap can be discarded, because they are close at the limit of detection, but are shown in this diagram to demonstrate that the Walchen deposit also hosts In free sphalerite.

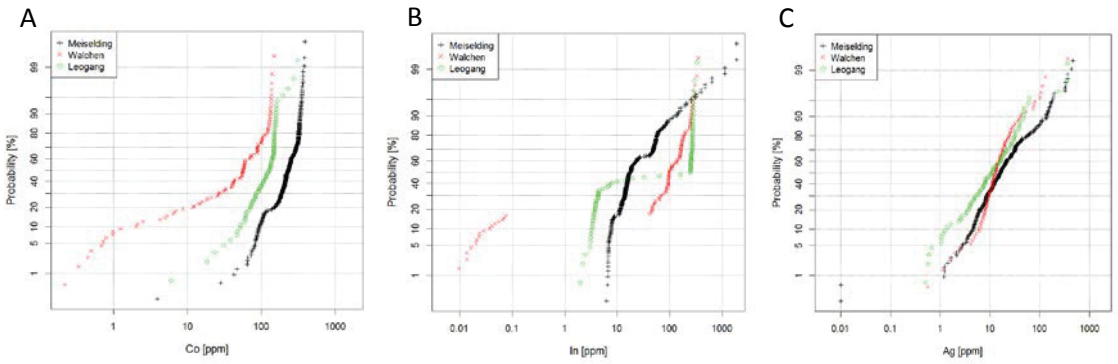

Fig. 108: Probability plot of A: Co; B: In; C: Ag data from different Pb-Zn deposits hosted in Paleozoic units outside the Graz Paleozoic.

Decreasing median trace element contents from Pb-Zn deposits hosted in Paleozoic units outside the Graz Paleozoic are listed in Table 34. The variation between Co and In is high, ehereas Ag is in the same range in all three deposits.

Table 34: Sequence of Pb-Zn deposits with decreasing trace element content values in µg/g.

Co (Md)	Meiselding (454) > Leogang (128) > Walchen (55)
In (Md)	Leogang (247) > Walchen (98) > Meiselding (16)

Ag (Md)	Meiselding (13) > Walchen (12) > Leogang (11)

Plots of all Co and In data of sediment hosted Pb-Zn deposits outside the Graz Paleozoic against Fe in Fig. 109 show an overlap of most data, except the Co poor sphalerite from Walchen and the Fe poor sphalerite from Leogang. In the plot In vs. Fe, the data from Walchen form a distinct cluster above most of the data from Meiselding. The Meiselding data in Fig. 109 demonstrate, that increasing In values correlate with increasing Fe. Comparison of the In and Fe values with the microscopic observations on the samples, indicates that sphalerite that suffers more from copper disease, shows higher In values. Data from Leogang (excluding the data where the In content is close to the limit of detection) form three clusters depending on the Fe content (Fig. 109B).

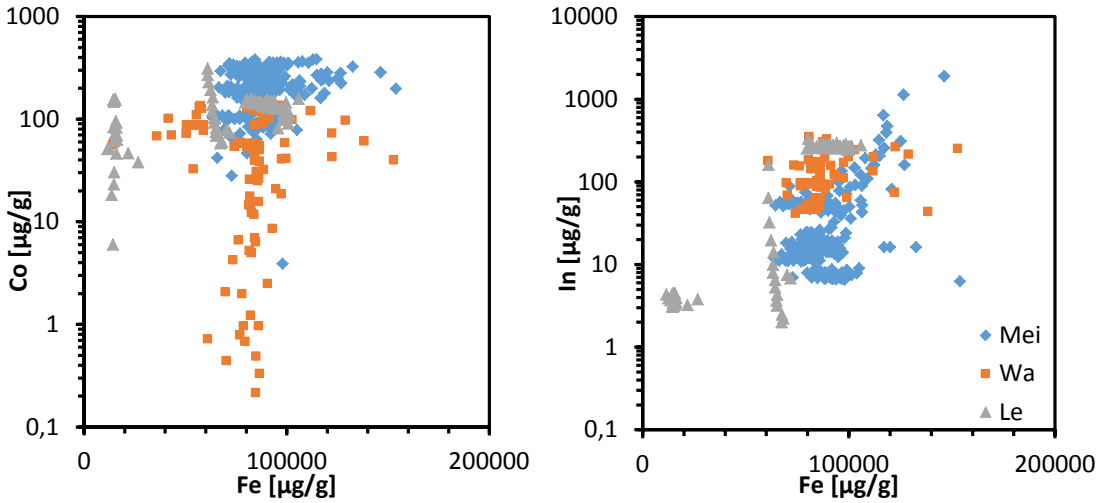

Fig. 109: Fe vs .Co (A) and Fe vs. In (B) of all data from the Sediment hosted Pb-Zn deposits outside the Graz Paleozoic. Mei, Meiselding; Wa, Walchen; Le, Leogang.

On the scale of a single ore deposit, e.g. Leogang, a discrimination of different samples can be done by plotting Fe vs. Mn and Fe vs. In. The variation of Fe and Mn of the investigated samples is within one order of magnitude; In shows higher variation with two orders of magnitude (Fig. 110B). These large variations show the variability within a single ore deposit and also with single samples.

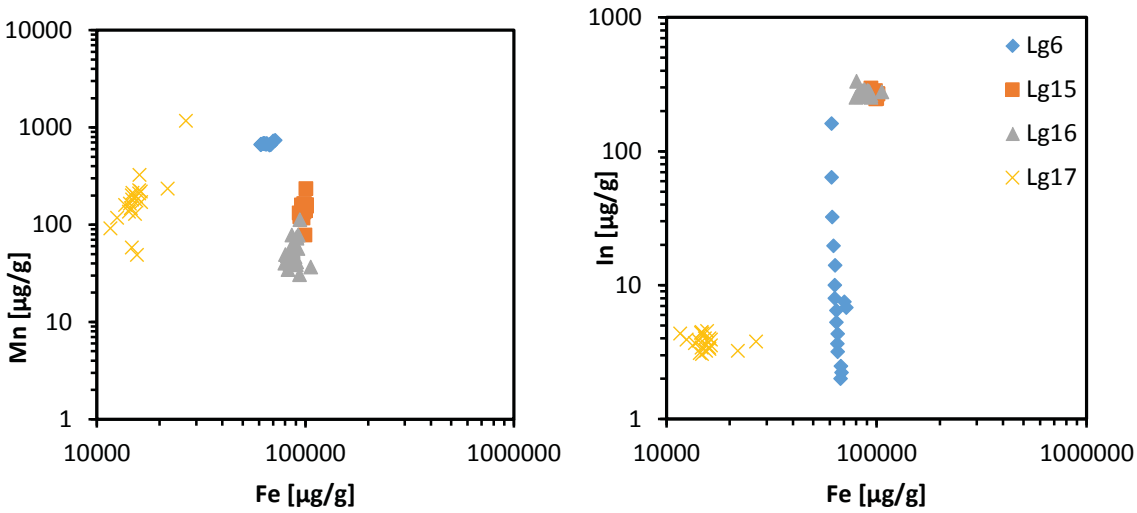

Fig. 110: Fe vs .Co (A) and Fe vs. In (B) of samples from Leogang.

Sphalerite from Leogang shows a kink in Fe between 10000 and 50000 µg/g and Mn between 200 and 500 µg/g indicating two sphalerite generations. The kink between 5 and 200 µg/g in the In curve is probably due to chalcopyrite micro-inclusions (Fig. 111A). The strong kink for Cu at 500 µg/g in Fig. 111B indicates that sphalerite from Meiselding often shows copper disease (Chapter 5.2.9), the kink at 20 µg/g for In and 100 µg/g for Co gives evidence for at least two sphalerite generations. The element content of sphalerite from the Walchen deposit are lognormally distributed (Fig. 111C).

A

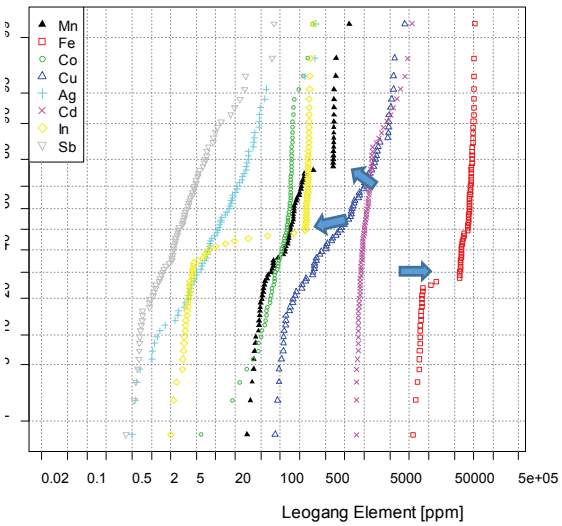

B

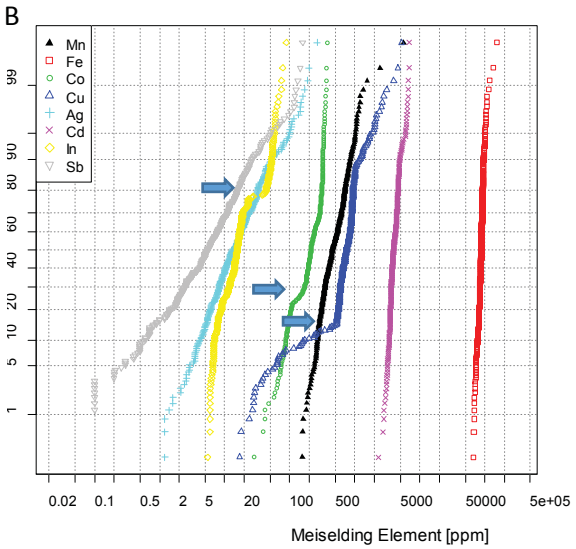

C

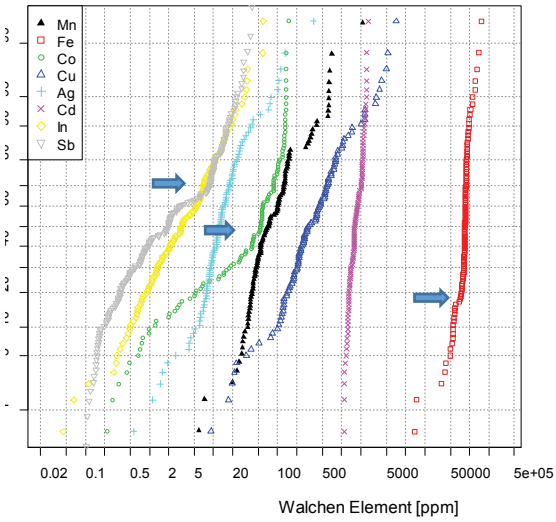

Fig. 111: Probability diagrams for trace elements in sphalerite from different Pb-Zn deposits hosted in Paleozoic units outside the Graz Paleozoic: A, Leogang; B, Meiselding; C, Walchen.

The kinks in the probability plots (Fig. 111A) for Fe (between 10000 and 50000 µg/g), Mn (between 200 and 500 µg/g) and In (between 5 and 200 µg/g) are visualized in ternary diagram Fig. 112 illustrates three different sphalerite generations, (i) In rich (>200 µg/g), Mn poor (< 50 µg/g), Fe rich (>8 wt.%) sphalerite (blue ellipse), (ii) In rich, medium Mn (~150 µg/g), Fe rich sphalerite (green ellipse) and (iii) In poor (< 10 µg/g), Mn rich (> 600µg/g) and Fe depleted (6 wt.%) sphalerite (orange ellipse).

Chemical data of sphalerite from the Walchen deposit (Fig. 112B) indicate two sphalerite species, a Co, Ag and Sb enriched (orange ellipse) and a Co, Ag and Sb poor (blue ellipse) species.

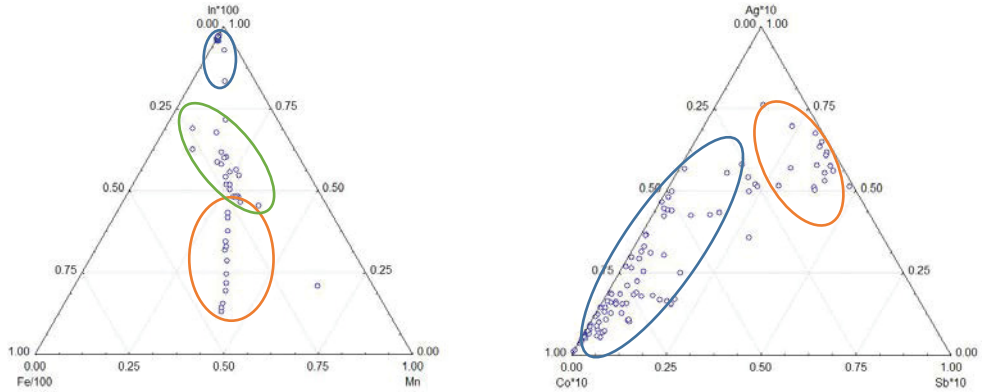

Fig. 112: Ternary plot: A, Leogang; B, Walchen

Compared to the CTEM Leogang and Walchen are enriched in Co, In and Sb (Chapter 5.5.3.9 and 5.5.3.10), Meiselding is enriched in Co, Ag and Sb (chapter 5.5.3.8).

In contrast to sphalerite of the Graz Paleozoic, sphalerites from Leogang, Walchen and Meiselding are enriched in In (Leogang Md= 247 µg/g), depleted in Ga and show the same range of Ge concentrations.

6.1.4 Vein-type deposits

Achselalm and Flecktrogalm in the Subpenninic nappes of the central Tauern Window display similar trace element distributions characterized by low Fe, Co, Ag, Sn compared to Koprein and Metnitz, both located in Austroalpine Paleozoic units. Koprein shows elevated Co, Ag, Sn and Cd, whereas Metnitz is elevated in Fe, Ga and Ge.

Table 35: P75, Median and P25 values of sphalerite from Vein-type deposits (all values in µg/g).

		Cr	Mn	Fe	Co	Ni	Cu	Ga	Ge	As	Se	Ag	Cd	In	Sn	Sb	Pb
Achselalm	P75	0.52	271	28665	70	8.42	84	44.78	0.06	0.32	9.68	1.46	2893	3.22	0.53	1.62	8.75
	Md	0.37	231	12170	57	3.31	38	21.55	0.02	0.12	7.00	0.56	2201	1.88	0.28	0.51	3.14
	P25	0.27	171	6858	43	1.59	21	6.28	bdl	0.05	5.50	0.35	1947	1.05	0.18	0.13	1.05
Flecktrogalm	P75	0.43	268	19605	73	13.87	79	85.68	0.04	0.33	7.40	1.17	2927	2.62	0.59	1.98	8.23
	Md	0.34	178	10865	62	7.77	36	32.41	0.01	0.13	5.40	0.54	2263	1.49	0.33	0.63	3.77
	P25	0.20	145	4656	51	5.04	14	8.01	bdl	0.08	2.10	0.29	1898	0.42	0.19	0.20	1.43
Koprein	P75	0.36	75	43300	734	1.12	608	5.73	0.49	0.37	2.90	50	3135	34	107	19.17	127
	Md	0.10	55	34720	644	0.66	306	4.06	0.29	0.16	2.10	28	2890	17	36	9.04	66
	P25	bdl	37	28100	553	0.35	136	2.58	0.03	0.06	1.40	15	2620	11	13	4.85	32
Metnitz	P75	0.85	86	64900	470	0.67	1733	74.63	374	4.70	6.80	27	2199	0.22	4.43	27.30	36
	Md	0.70	73	58950	405	0.46	1220	37.60	149	3.60	4.85	14	1931	0.11	2.38	13.06	10
	P25	0.56	63	52600	347	0.31	928	10.37	26	2.40	3.40	7	1673	0.08	1.62	4.94	3

The probability plots in Fig. 113 for the elements Co, Ga and Ag show mostly parallel curves with no significant kinks. The curves from Achselalm and Flecktrogalm overlap over a wide range, indicating a close relation. The Co and Ag contents in Koprein show the highest values, the lowest values are observed for Achselalm and Flecktrogalm (Fig. 113: A, C). The Ga mass fraction shows the highest values in Achselalm and Flecktrogalm, whereas the lowest median values for Ga are indicated in Koprein (Fig. 113: B).

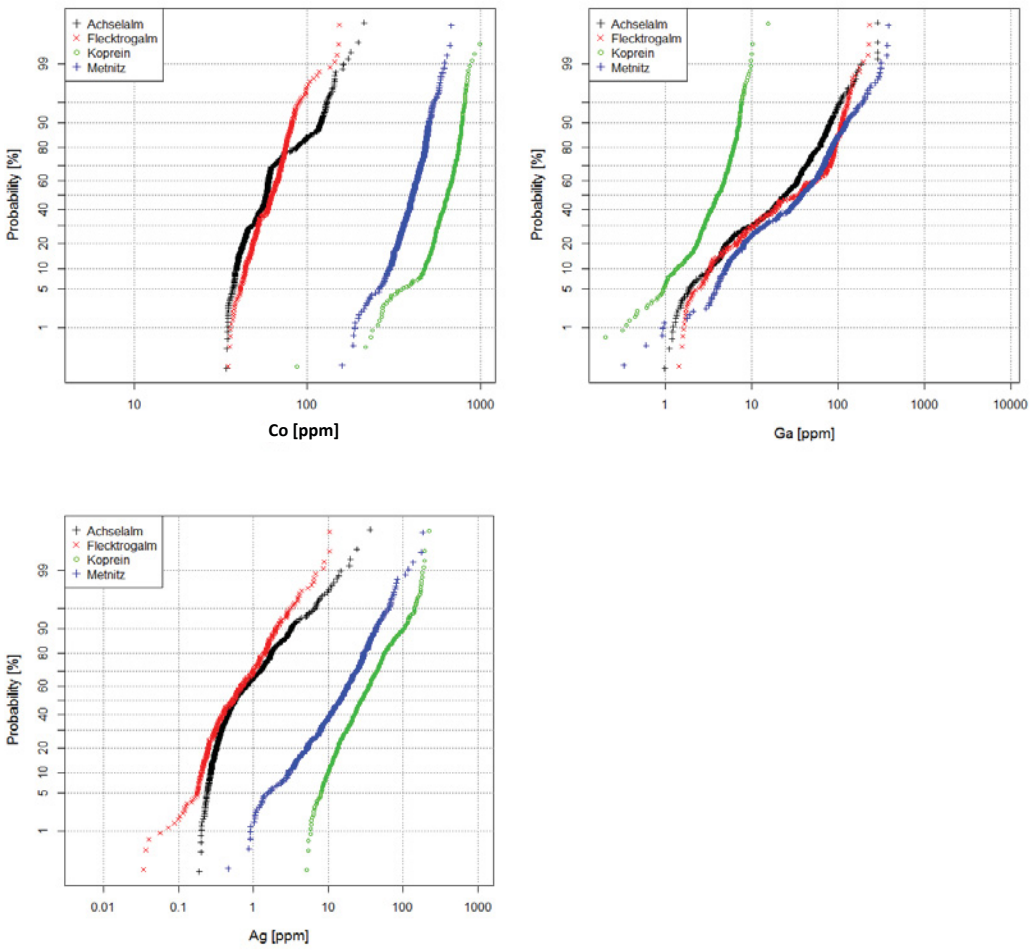

Fig. 113: Probability plot of all A: Co; B: Ga; C: Ag data from the investigated vein-type Pb-Zn deposits.

The sequence of decreasing trace element contents from the vein-type deposits is listed in Table 36.

Table 36: Sequence of vein-type Pb-Zn deposits with decreasing trace element content, values in µg/g.

Co (Md)	Koprein (644) > Metnitz (405) > Flecktrogalm (62) > Achselalm (57)
Ga (Md)	Metnitz (38) > Flecktrogalm (32) > Achselalm (22) > Koprein (4)
Ag (Md)	Koprein (28) > Metnitz (14) > Achselalm (0.6) > Flecktrogalm (0.5)
In (Md	Koprein (17) > Achselalm (1.88) > Flecktrogalm (1.49) > Metnitz (0.11)

The diagrams in Fig. 114 illustrate the variability of vein-type deposits hosted in Paleozoic units of the Eastern Alps. The three mineralisations can be clearly divided and show only a small overlap. Fe content varies most in the Achselalm-Flecktrogalm deposit, due to the different varieties of sphalerite. The data with values of ~ 2000 to 5000 µg/g represent the white to yellow, 5000 to 10000 µg/g the orange to light brown and above 10000 the brown sphalerite

variety. Gallium ranges from 1 to ~90 µg/g, Co from 20 to ~100 µg/g (Fig. 114B). Metnitz shows a smaller variation in Fe and Co but Ga ranges from 0.2 to 150 µg/g, whereas the variation in Koprein for Fe is around one order of magnitude and for Ga and Co smaller than in Metnitz and Achselalm-Flecktrogalm.

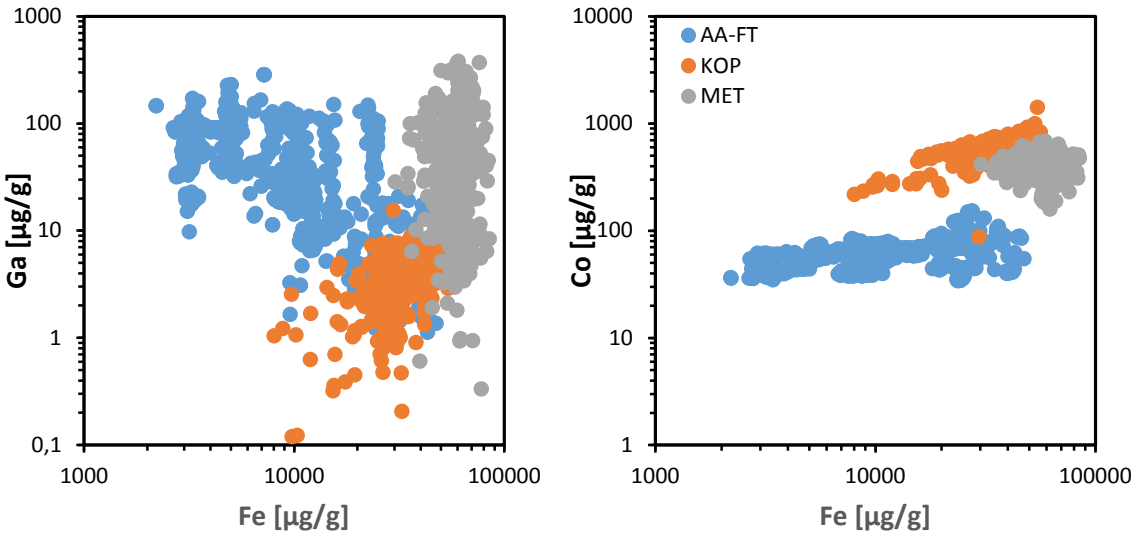

Fig. 114: Fe vs. Ga and Co, of vein-type deposits hosted in Paleozoic units showing the variability of critical metals within vein-type deposits; AA-FT: Achselalm-Flecktrogalm; KOP: Koprein; MET: Metnitz.

The variability of Ga follows a weak negative trend with increasing Fe content of sphalerite (Fig. 115A). However, the range of Ga is still high, depending on the sample ranging from a few µg/g to nearly 400 µg/g. In contract to Ga, Co shows a small variability that is obviously not related to the Fe content of sphalerite (Fig. 115B).

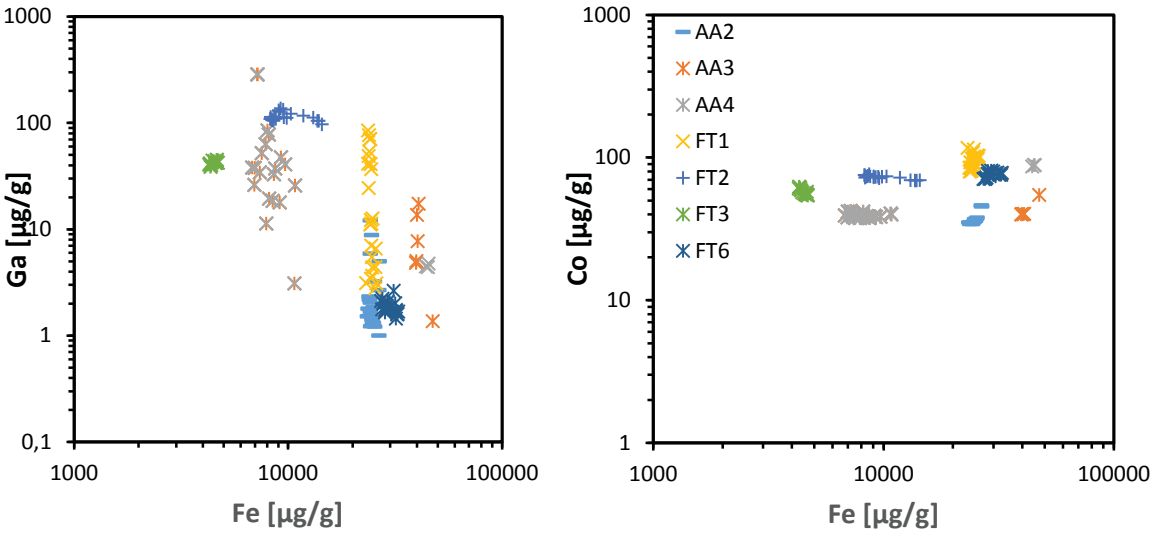

Fig. 115: Fe vs. Ga and Co diagram of samples from Achselalm Flecktrogalm, showing the variability within a single deposit.

The adjacent deposits Achselalm and Flecktrogalm show geochemical similarities and a lognormal element distribution (Fig. 116A, B). They can be merged together to one deposit with two fields Achselalm/Flecktrogalm. Chemical data from Koprein and Metnitz plotted in Fig. 116C, D show a lognormal distribution. None of the curves in Fig shows significant kinks, indicating more than one sphalerite generation. All curves plotted in Fig. 116 exhibit steep slopes implying a small element variability (< two orders of magnitude).

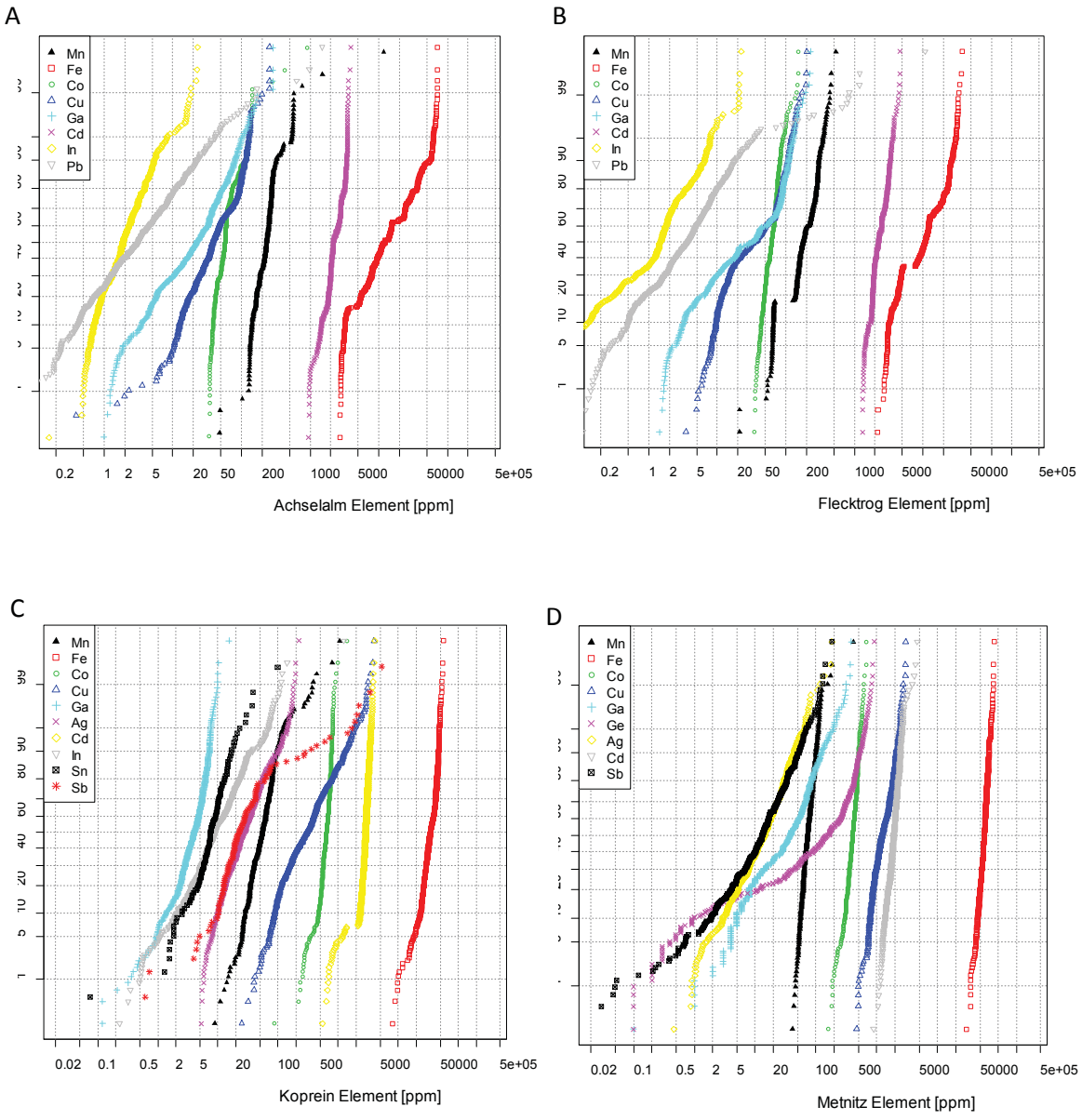

Fig. 116: Probability diagrams for trace elements in sphalerite from different vein type Pb-Zn deposits: A, Achselalm; B, Flecktrogalm; C, Koprein; D, Metnitz.

The Achselalm/Flecktrogalm deposit, compared to Metnitz, is poor in Fe, Co, Ga and Ge but enriched in Mn and In. Metnitz shows the highest values for Ga and Ge of all investigated vein-type deposits (Table 35). Koprein displays the highest Co, Ag and Sn values (Table 35). Compared to the CTEM, sphalerite hosted in vein-type deposits hosted in Paleozoic units of the Eastern Alps are enriched in Fe, Co, Ga, Ag, Sn, Sb and depleted in the elements Mn, Ni, Cu, Ge, As, Se, Cd, In, Tl and Pb. Sphalerite from the Koprein deposit is enriched in Fe, Co, Ag, Sn,

Sb, Pb and depleted in Mn, Ni, Cu, Ga, Ge, As, Se, Cd, In and Tl. Sphalerite from Metnitz is in contrast to the CTEM enriched in Fe, Co, Cu, Ga, Ge, Ag, Sn, Sb and depleted in Mn, Ni, As, Se, Cd, In, Tl and Pb. The deposits Achselalm/Flecktrogalm is only enriched in the elements Ni and Ge, and depleted in all other measured elements.

6.2 Trace element incorporation in sphalerite

The chemical data of sphalerite indicate a huge variation between different ore types, locations and even within a single sample. Sphalerite is known to incorporate numerous trace elements in different concentrations. Several authors have investigated and discussed the trace element distribution of sphalerite. However the incorporation mechanism for some elements is still under debate (Belissont et al. (2014); Belissont et al. (2016); Cook et al. (2009); Cook et al. (2011); Cook et al. (2015)). The variability of each trace element reaches several orders of magnitude. The reason of this is explained by at least two different mechanisms, i.e. lattice incorporation and contamination by micro inclusions (Cook et al. (2009); Belissont et al. (2014)).

Frenzel et al. 2016 developed a geothermometer to calculate the precipitation temperature of sphalerite based on minor and trace elements (Ga, Ge, Fe, Mn and In). Calibration was done using fluid inclusion data from gangue minerals like: quartz, calcite, fluorite, dolomite from the literature. The component PC1 was derived from factor analysis:

$$\mathrm{PC}\ 1^{*} = ln\left(\frac{\mathrm{C}_{\mathrm{Ga}}^{0.22}.\mathrm{C}_{\mathrm{Ge}}^{0.22}}{\mathrm{C}_{\mathrm{Fe}}^{0.37}.\mathrm{C}_{\mathrm{Mn}}^{0.20}.\mathrm{C}_{\mathrm{In}}^{0.11}}\right)$$

The element concentrations for the PC1* equation are to expressed for Ga, Ge, In and Mn in µg/g and for Fe in wt.%. The empirical relationship between PC1* and the homogenization temperature is then described as:

$$T[°C] = -(54.4 \pm 7.3) \cdot PC1^{*} + (208 \pm 10)$$

Frenzel et al. (2016) assumed that the metamorphic overprint of Pb-Zn deposits even at lower greenschist facies conditions leads to a decrease in Ga and Ge concentrations and an increase in Fe and Mn. Therefore, they suggest that the thermometer only gives reasonable values below 310°C (“closing temperature of sphalerite”). Due to the fact, that this thermometer is the only one for sphalerite that gives reasonable precipitation temperature values (at low temperature), it was applied in this study and the effect of T could be evaluated.

6.2.1 Lattice incorporation

The direct substitution of iron (Fe^{2+}) for Zn^{2+} is the most common mechanism. Iron varies between a few hundred µg/g (Carbonate hosted Pb-Zn deposits) up to 14 wt.% in SEDEX and vein type deposits (Cook et al. 2009 and references therein). The plot in Fig. 117 shows the correlation between Fe and the formation temperature of sphalerite. The diagram in Fig shows

a nearly linear relationship between precipitation temperature, calculated after Frenzel et al. (2016) and Fe content.

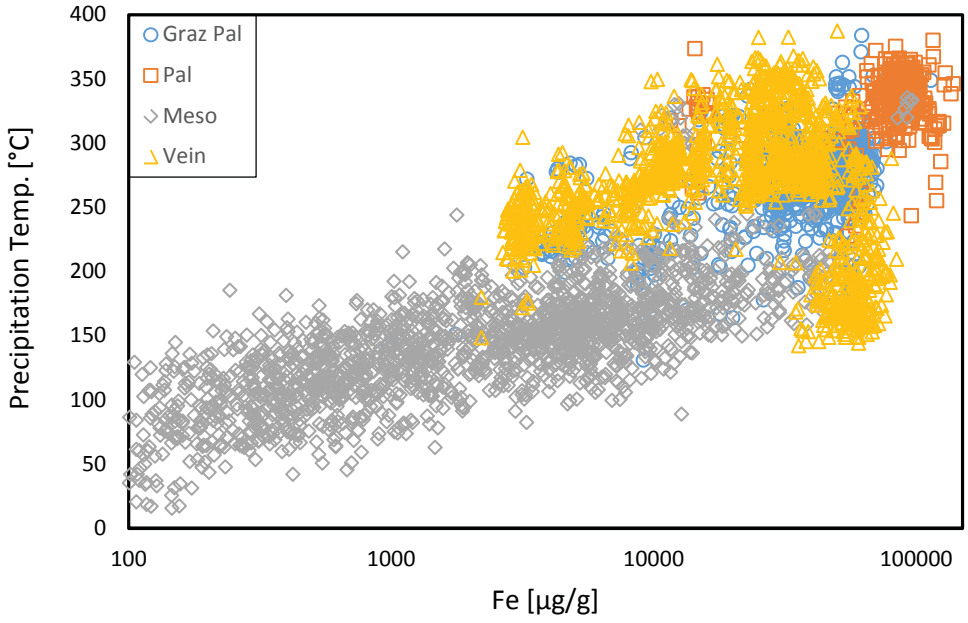

Fig. 117: Fe vs. precipitation temperature of all measurements, calculated after (Frenzel et al. 2016).

The enrichment of Cd in sphalerite is considered to be a solid solution substitution between $Zn^{2+} \leftrightarrow Cd^{2+}$, Cook et al. 2009 reported variations of Cd by a factor of maximum five. The investigated samples show that the variation depends on the ore type and reaches from ~1000µg/g up to 1.8 wt.%. The interpretation that Cd is a lattice bound element is supported by the studies of Cd zonation by Belissont et al. (2016) and Cook et al. (2011). During this study, a slightly negative correlation between Cd and Fe was found in carbonate hosted Pb-Zn deposits (Fig. 118).

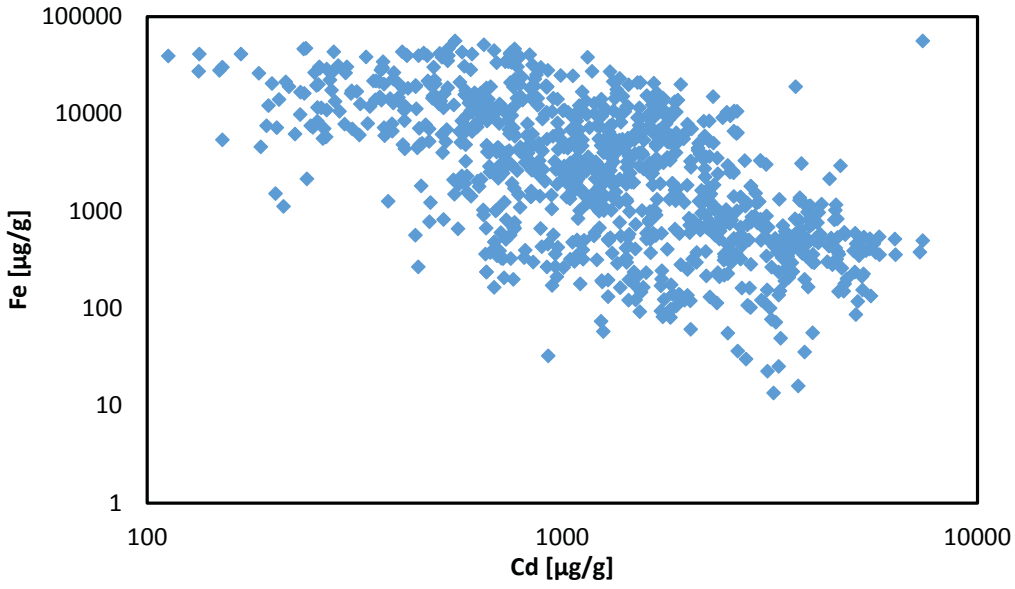

Fig. 118: Cd vs. Fe plot of all data from carbonate hosted Mesozoic Pb-Zn deposits

The incorporation of Mn^{2+} is a direct exchange $Zn^{2+} \leftrightarrow Mn^{2+}$. Together with Cd and Fe, Mn is the most common for element that exchanges Zn. Kubo et al. (1992) found in their experimental studies the order Cd>Zn>Fe>Mn for the preferential partitioning in metamorphically overprinted sphalerite. The partition becomes more relevant with rising metamorphic grade. This relation can be seen in Fig. 119, where the deposits with the higher metamorphic grade (Pal and Graz Pal) show the highest Mn and Fe values. Investigations by Di Benedetto (2005) and Fowler et al. (1996) on compositionally zoned sphalerite attributed the Fe, Mn and Cd variation to a fast self-organization of elements during the deposition or as partitioning during crystal growth along crystallographic faces.

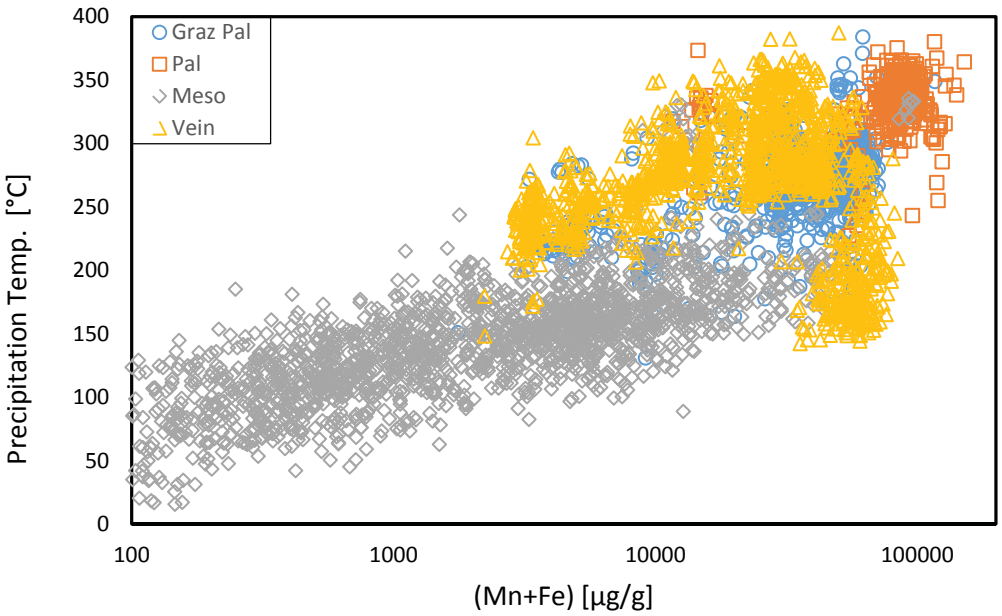

Fig. 119: (Mn+Fe) against precipitation temperature. Temperature is calculated after Frenzel et al. (2016).

After Cook et al. (2009) and Belissont et al. (2014) only a few hundred µg/g of Pb can be incorporated into the sphalerite lattice (Fig. 120A). Values above 1000 µg/g are proposed to be caused by small galena inclusions. In this study Pb values were measured up to 1.7 wt. %; suchhigh values point to the presence of galena inclusion. Evidence for galena inclusions is providet by spikes in the LA-ICP-MS spectra (Fig. 120B).

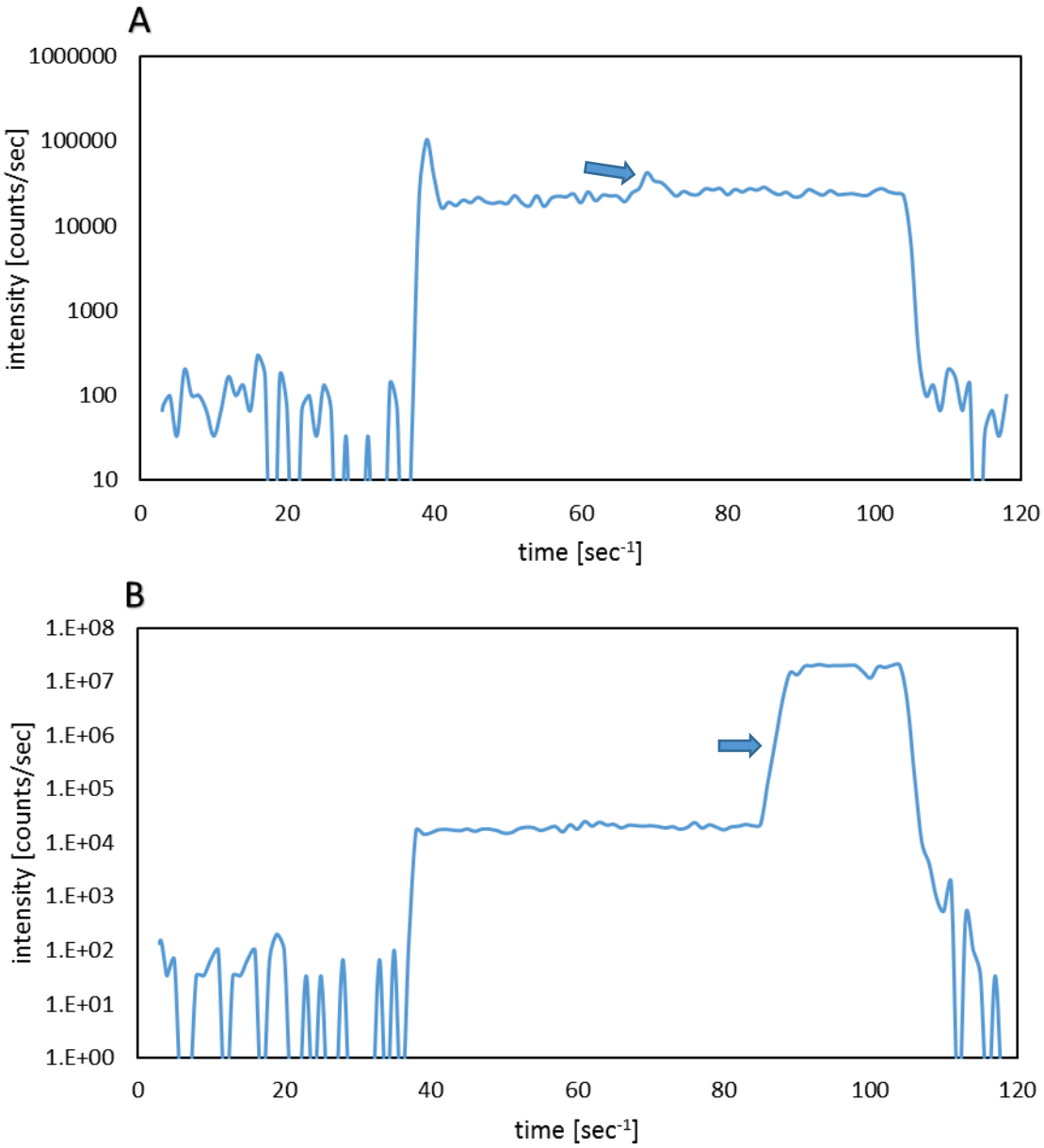

Fig. 120: A: Pb spectra of sample RaD 9-13 (52 µg/g of lead) showing a small galena inclusion at 70 sec. B: Pb spectra of Sample RaD 9-17 (9700 µg/g) showing a large galena inclusion starting from ~90 sec up to the end of the spectra. Blue arrows mark galena inclusions.

The incorporation of Ge into the sphalerite lattice is controversially debated. (Cook et al. (2009); Pfaff et al. (2011); Bonnet et al. (2017); Belissont et al. (2014); Belissont et al. (2016). Cook et al. (2009), Belissont et al. (2014) and Belissont et al. (2016) investigated sphalerite from different Pb-Zn deposits and proposed that Ge is directly incorporated into the sphalerite lattice via solid solution as Ge^{+4} ion together with other mono- and divalent cations. Bonnet et al. (2017) investigated sphalerite samples from MVT deposits in Central and Eastern Tennessee and found three different configurations: (i) Ge^{+2} plus S in tetrahedral coordination: (ii) Ge^{+4} associated with S in tetrahedral coordination and (iii) Ge^{+4} associated with O, interpreted as GeO non-inclusion. In this study, a positive correlation between Fe and Ge was found only in Mesozoic Pb-Zn deposits (Fig. 122).

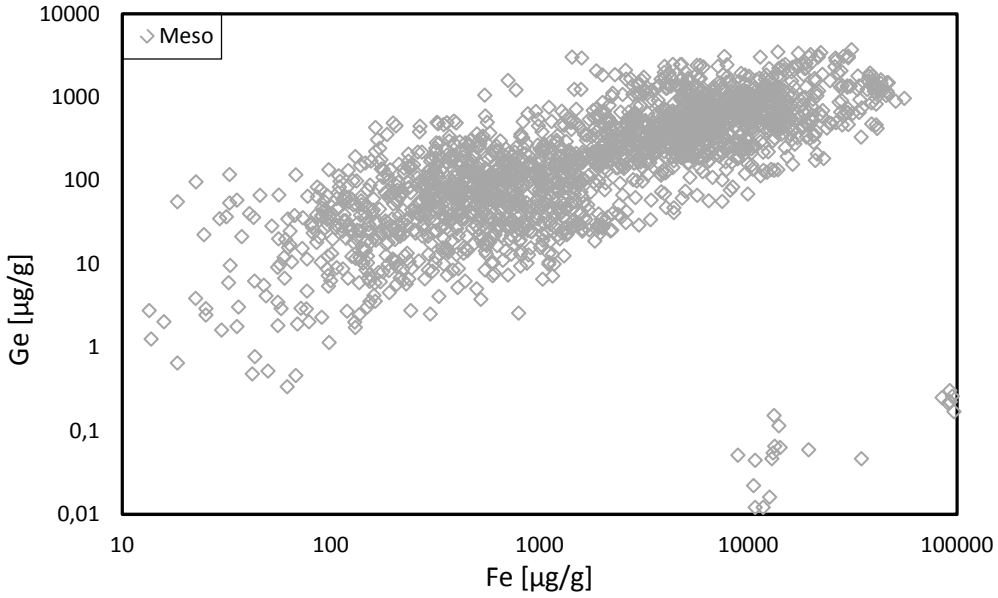

Fig. 121: Plot of all measurement performed on sphalerite from Mesozoic Pb-Zn deposits showing a positive correlation between Fe and Ge.

A correlation of Ge with other elements in other Pb/Zn ore types (vein Type and Palaeozic) could not be found in this study. Bernstein (1985) described sphalerite enriched in Ge in organic rich (bituminous) nonmetamorphic carbonate hosted Pb/Zn deposits (Fig. 122), whereas Ge is low in sphalerite from metamorphic Pb/Zn deposits (Fig. 122). Ge may become enriched in silicate and oxides during metamorphism (Bernstein 1985). Fig. 122 shows the dependence of Ge versus precipitation temperature (after Frenzel et al. 2016) with a depletion of Ge in sphalerite with increasing precipitation/ metamorphism temperature. The samples from the Metnitz deposit that extend into the field of Mesozoic deposits are formed at lower precipitation temperature (150 to 250 °C) than the other investigated vein-type deposits (Fig. 122).

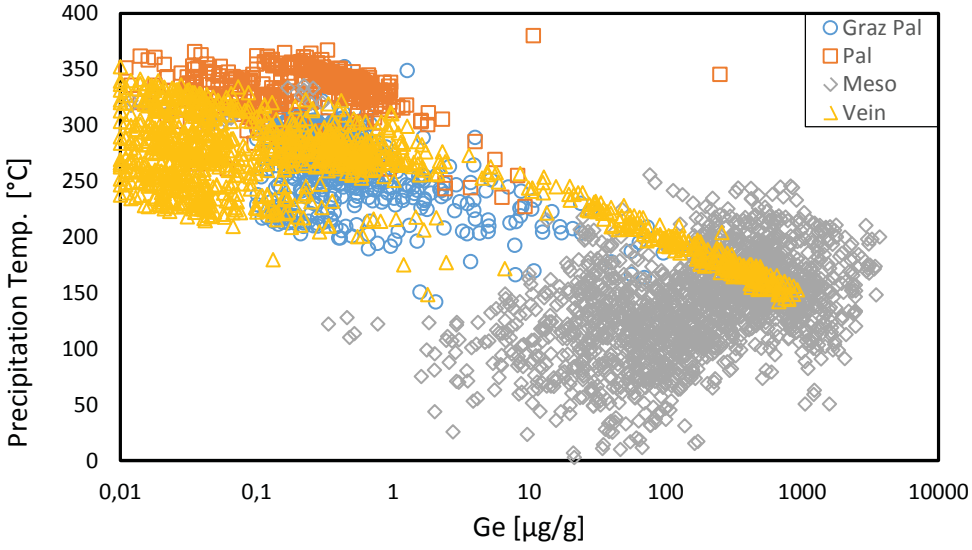

Fig. 122: Plot of all sphalerite data from different ore districts. Samples from the Graz Paleozoic, Paleozoic and vein-Type deposits show a negative correlation between temperature and Ge in sphalerite. Samples from Mesozoic deposits display a positive trend.

Gallium shows no tendency to higher Fe content in sphalerite (Fig. 123), and an indistinct correlation to Ge, giving a strong suspicion that the variation in the Ga (Fig. 124) trace element content depends on the fluid source and the Ga content therein. Möller, Dulski (1993, 1996) described the temperature dependent behavior of Ge and Ga during leaching processes in the host rock, and proposed that Ga behaves like Al and Ge like Si. They developed a thermometer that calculates the leaching temperature of Ga and Ge in the host rock. The calculated leaching temperatures were 50 to 100°C higher than the precipitation temperatures after Frenzel et al. 2016, but were not taken into account in this study, due to the fact that leaching factors like salinity, pH value or S_f are not considered in these calculations and do not reflect the ore forming temperature.

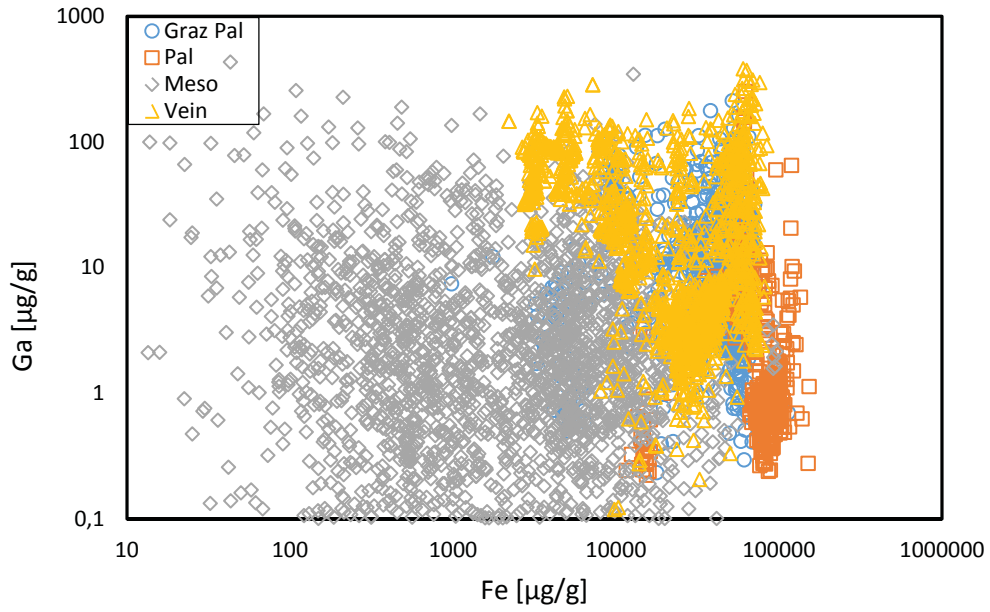

Fig. 123: Plot Ga against Fe of all sphalerite analyses and different ore types.

The Ge/Ga plot in Fig. 124 shows cluster depending on the ore type, but there is no trend in general or within an ore deposit visible. The Mesozoic carbonate hosted Pb-Zn deposits show an independent signature with the tendency to higher Ge values (grey circles). Vein-type deposits in Fig. 124 are separated in two groups, one group with low Ge and a second group with high germanium content. The group with high Ge values represents the Metnitz deposit.

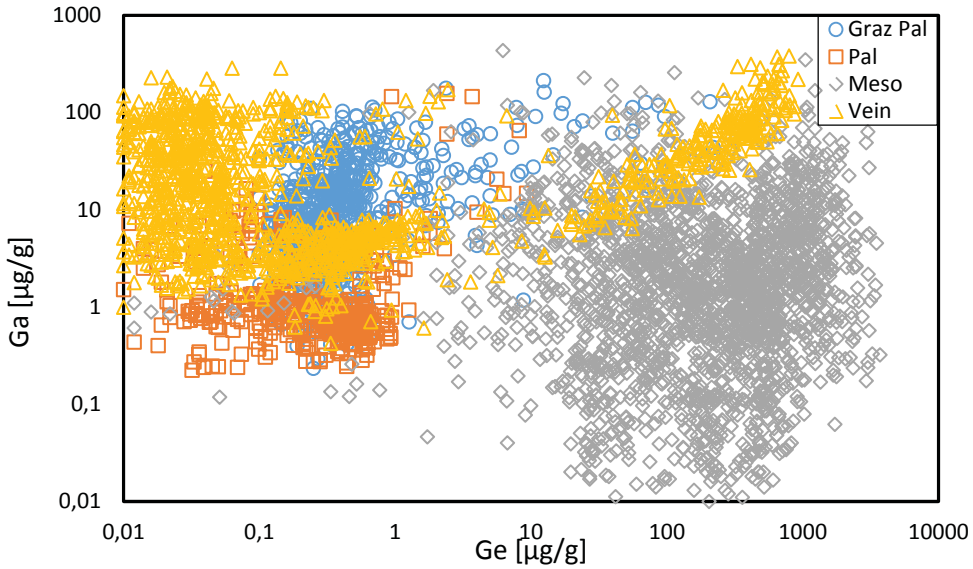

Fig. 124: Plot Ga against Ge of all sphalerite analyses and different ore types.

Gallium plotted against the precipitation temperature after Frenzel et al. (2016) indicates that the Ga content in sphalerite decreases with increasing precipitation temperature (Fig. 125). This leads to the question why the Ga content of carbonate hosted Pb-Zn deposits is low (mostly below 10 µg/g), although they show the lowest precipitation temperatures (calculated after Frenzel et al. (2016)). Two possibilities are discussed, (i) the source rock is poor in Al and Ga, (ii) the Frenzel thermometer does not work well because the empirical formula is based on old sphalerite data (some Ga data in Cerny and Schroll (1990) are too high) and fluid inclusion data of gangue minerals and not of sphalerite. The second possibility is supported by studies of Rantitsch (2001), who calculated temperatures (e.g. Bleiberg) based on the Vitrinite reflectance ~50°C lower than the calculated temperatures using the method after Frenzel et al. 2016.

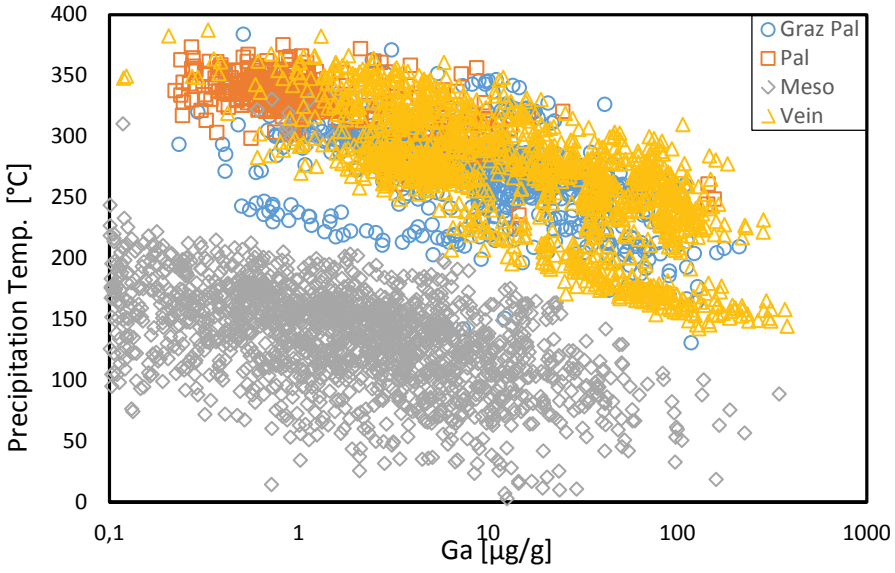

Fig. 125: Plot Ga against temperature (after Frenzel et al. 2016) of all sphalerite analyses and different ore types.

Arsenic is incorporated in sphalerite however, higher amounts only at formation temperatures below 200°C (Clark 1970; Cook et al. 2009). The highest As concentration (2.04 wt.%) was found in samples of Lafatsch, a deposit that shows a formation temperature calculated after Frenzel et al. (2016) of ~80 °C. In general the concentrations of As decrease with increasing temperature and reach a sub µg/g level at formation temperatures higher than 260 °C (Fig. 126). However, an incorporation of small amounts of As into the sphalerite lattice is also possible at higher formation temperatures.

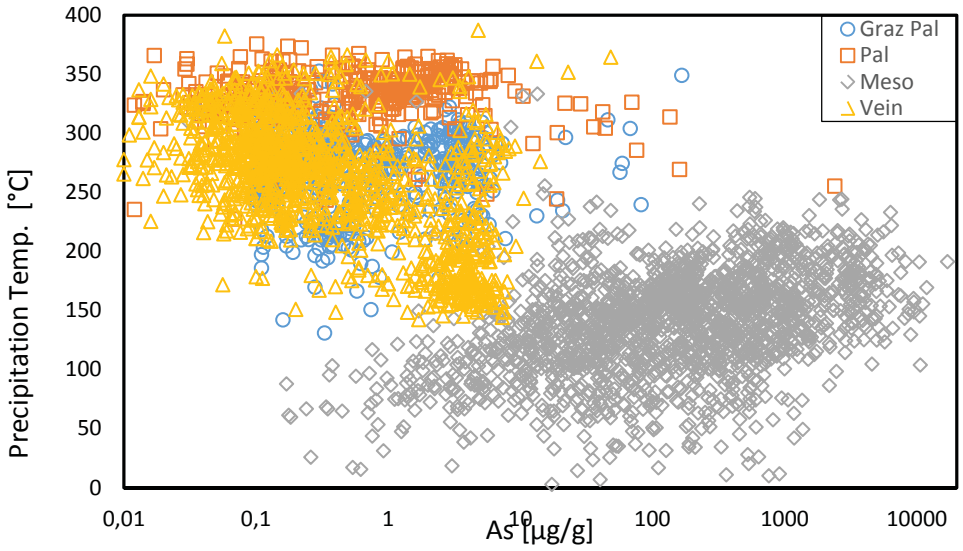

Fig. 126: Plot of all As concentrations against the precipitation temperature calculated after (Frenzel et al. 2014)

The substitution of Cu in the sphalerite lattice is very limited and controversially discussed (Cook et al. (2009); Belissont et al. (2016); Barton and Bethke (1987); Cook et al. (2012)). Cook et al. (2009) found a positive correlation between Cu and In, whereas Belissont et al. (2016) found no evidence for the incorporation of Cu into the sphalerite lattice. Barton and Bethke (1987) proposed that Cu in sphalerite is present in micro inclusions; form and occurrence depend on the S activity. Cook et al. (2012) discussed that Cu is substituted together with In into the sphalerite lattice via the substitution $2Zn^{2}+\rightarrow Cu^{+}+In^{3+}$. In the present study, no such correlation between Cu+In was found.

A substitution mechanism of Tl together with As is reported by Kelley et al. (2004) and Xiong (2007) in a low-temperature environment. Thallium concentrations above the detection limit only were found in samples from carbonate hosted Pb-Zn deposits during this study. The measured samples show a positive trend in the plot Tl/As (Fig. 127).

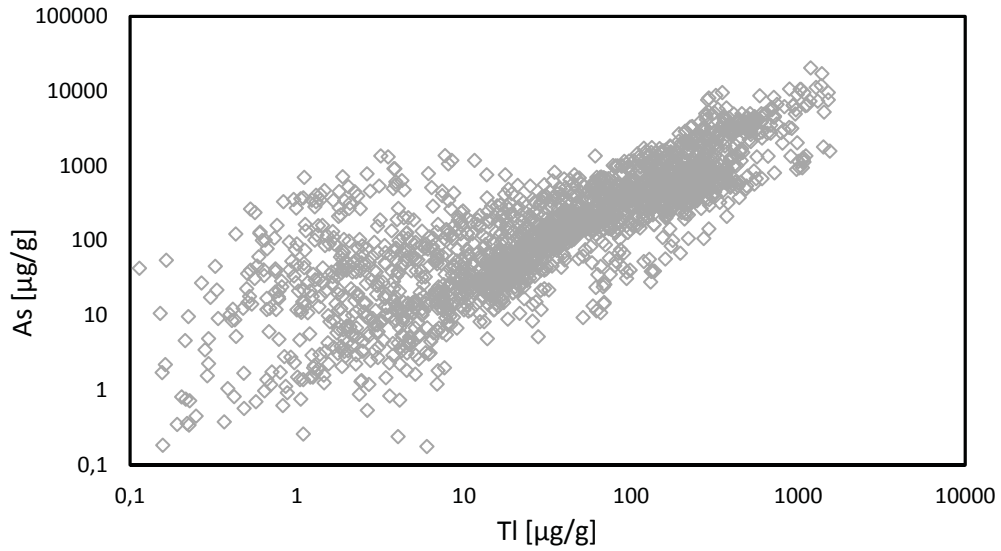

Fig. 127: Plot Tl/As of carbonate hosted Pb-Zn deposits.

Thallium data plotted against the formation temperature, (Fig. 128) show that the Tl content increases with increased temperature up to 250°C. Higher temperature (above 250°C) shows Tl values below the detection limit; this follows therefore the investigations of Xiong (2007) and Kelley et al. (2004). There a two possible explanation for this behavior (i) above 250°C Tl is too volatile to be incorporated in the sphalerite lattice and will be swept away with the fluid, (ii) due to the similar behavior of Tl^{1+} and K, sphalerite is depleted in Tl during metamorphic processes above 250°C

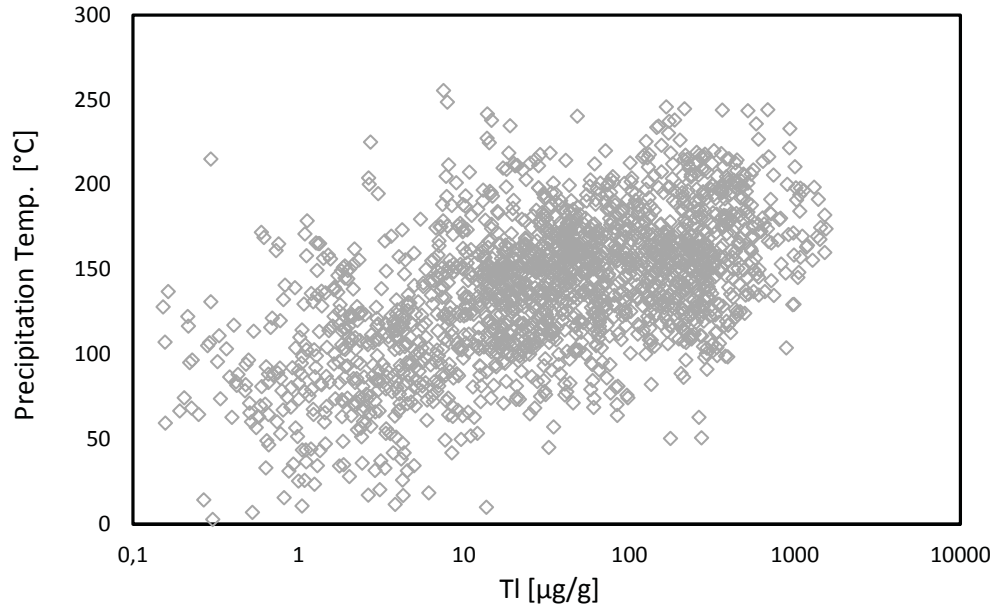

Fig. 128: Tl values plotted against the precipitation temperature (Frenzel et al. 2016) of samples from carbonate hosted Pb-Zn deposits.

6.2.2 Trace element variability of sphalerite in different ore types

In order to compare trace element concentrations in sphalerite between different deposit types the CTEM was used to compare median concentration values individual deposits. Enrichment (+) and depletion (-) factors are graphically illustrated for reasons of better readability (Table 37). A grouping of sphalerite compositions into two major groups becomes obvious. Group 1 comprises sphalerite hosted by Mesozoic carbonate rocks; these sphalerites are, with few exceptions, highly enriched in Ge, As, Tl and Pb, but also highly depleted in Mn, In, Co, Ni, Sn and Ag. Fe, Ga and Cd are slightly depleted compared to CTEM; the median values for Cu and Sb scatter. Group 2 comprises sphalerite hosted by Paleozoic sedimentary and volcanic rocks, either as stratiform ore bodies or as vein-type ore bodies. Sphalerite of the second group is generally enriched in Fe, Co, Cu, Ag, Sb, but values scatter between individual deposits; median values of In and Sn may be highly elevated, but scatter widely. Ge concentrations are elevated only in one deposit (Metnitz), and associated with Co and Sb. In concentrations are elevated in the Leogang deposit, otherwise, group 2 sphalerite is low in Ge, As, and Tl. Concentrations of Pb, Cd and Se are comparable to CTEM.

Table 37: Summary of trace element median from different Eastern Alpine Pb/Zn deposits in comparison to the median values published by Cook et al. 2009 (CTEM).

Location	Mn	Fe	Co	Ni	Cu	Ga	Ge	As	Se	Ag	Cd	In	Sn	Sb	Tl	Pb
median Cook et al. 2009	2152	16959	26	0.85	443	4.59	1.19	14.95	7.9	7.3	4968	16.8	1.425	1.23	0.14	13.95
Bleiberg	----	-	--	--	-	-	+++	++	~	--	-	----	--	-	++	++
Lafatsch	----	--	--	--	-	-	++	++	~	+	-	----	--	~	++	++
Radnig	----	-	--	--	--	-	+++	+	~	--	-	----	--	-	++	++
Jauken Süd	----	-	--	-	~	-	+++	+	~	--	-	----	-	-	++	++
Fladung	----	-	--	--	-	+	+++	++	~	--	~	----	--	-	++	++
Meiselding	--	+	+	~	~	-	-	--	~	~	~	~	~	+	-	~
Silberberg	----	~	+	-	~	~	--	----	-	+	~	-	--	+	-	++
Friedrichstollen	--	+	++	+	-	+	-	----	-	+	~	-	----	+	bdl	~
Elisabethstollen	--	+	+	+	--	+	-	----	-	+	-	-	----	+	bdl	~
Arzberg	--	~	~	-	+	-	--	--	~	++	-	-	-	+	-	+
Haufenreith	--	~	+	+	~	-	----	--	-	~	-	~	-	~	--	~
Rabenstein	----	-	~	+	+	~	--	--	~	+	-	--	-	+	--	~
Guggenbach	--	+	+	+	+	~	--	----	~	+	-	--	~	+	-	~
Leogang	--	+	+	-	~	-	--	----	+	~	-	++	~	+	-	~
Walchen	--	+	+	--	~	-	--	--	+	~	-	+	~	+	--	~
Draßnitz	+	+	~	-	++	+	-	--	~	+	~	+	+	~	-	~
Koprein	--	~	++	~	~	~	-	-	-	+	~	~	+	+	-	+
Metnitz	--	+	++	-	+	+	+++	-	~	~	-	----	~	++	-	~
Flecktrogalm	--	~	+	+	--	+	--	----	~	--	-	--	-	~	bdl	-
Achselalm	--	~	+	+	--	+	--	----	~	--	-	--	-	-	bdl	-

Legend	compare to median after Cook et al. 2009
+++	> 100 times
++	> 10 times
+	> 2 times
~	equal
-	< 2 times
--	< 10 times
----	< 100 times

Mesozoic carbonate hosted Pb-Zn deposits show an independent trend in the P25-P75 pattern (Fig. 129), showing low Fe, Co, Ni, Se, In and Sn values. Compared to vein type, Paleozoic and Graz Paleozoic ore deposits Germanium and As are more than three orders of magnitude elevated (Fig. 129 blue field). Vein type, Paleozoic and deposits from the Graz Paleozoic show similarities in most element concentrations. The Graz Paleozoic (Fig. 129 grey field) differs in Ge, As and Sb where the P25 is close to the limit of detection. Vein type and Paleozoic deposits overlap in all elements, whereas the range of variability is higher in vein type deposits (Fig. 129 green field) than in Paleozoic deposits (Fig. 129 red field).

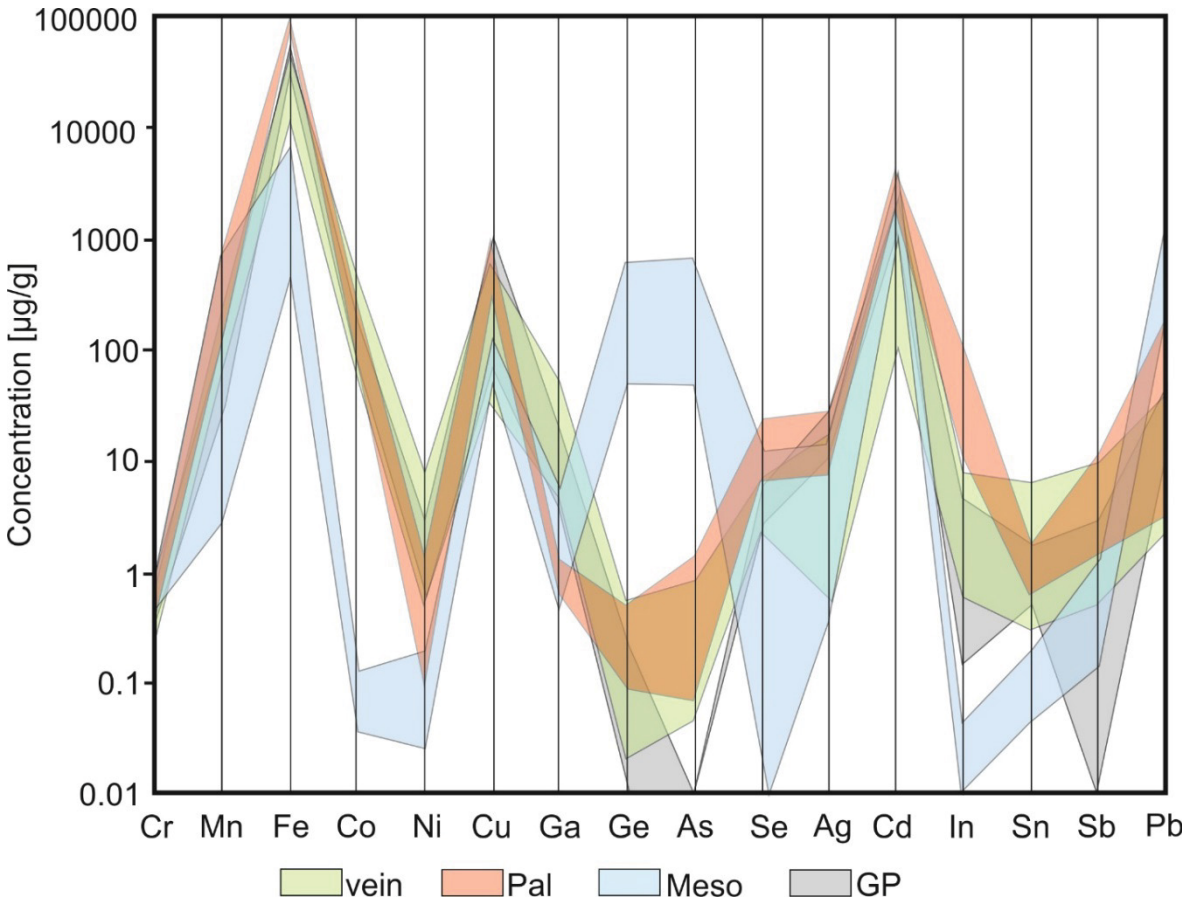

Fig. 129: P25 and P75 element concentrations of the different investigated ore types.

6.3 Sulfur isotopes

Factors that control the sulfur isotope fractionation have been discussed by several authors (Ault and Kulp (1960); Ohmoto (1972); Ohmoto and Lasaga (1982); Seal et al. (2000)). The most important factors that control the $\delta^{34}S$ composition are oxidation-reduction reaction, temperature, pH value, bacterial sulfate reduction, thermal sulfate reduction, pressure, sulfur fugacity and the mineral chemistry. All these controlling factors are different in different ore types, and therefore all of these show individual $\delta^{34}S$ compositions/signatures, e.g. temperatures below 110°C and the influence of seawater sulfate promote the bacterial seawater sulfate reduction, leading in a light $\delta^{34}S$ composition.

6.3.1 Mesozoic Pb-Zn deposits

6.3.1.1 Bleiberg

The sulfur-isotope composition of sphalerite from the Bleiberg deposit (n= 151) is characterized by medium to light $\delta^{34}S$ values, showing a huge variation ranging from -1 to -34 ‰. This variation is independent from the different investigated ore-types (Fig. 130). All ore-types show a bimodal distribution with a first maximum at ~ -9 ‰ and a second maximum at around -26 ‰ (Fig. 130). Schalenblende is represented by the light $\delta^{34}S$ values, the fine-grained sphalerite by the heavier $\delta^{34}S$ values. The data correlate with the literature (Schroll and Rantitsch (2005); Henjes-Kunst et al. (2017); Kucha et al. (2005)). The first peak at around -6 ‰ can be interpreted as sulfur from a hydrothermal fluid (Schroll and Rantitsch 2005), the

second peak at around between – 20 and -34 ‰ (Fig. 130) can be ascribed to bacteriogenic reduction of seawater sulfate (Kucha et al. 2010)

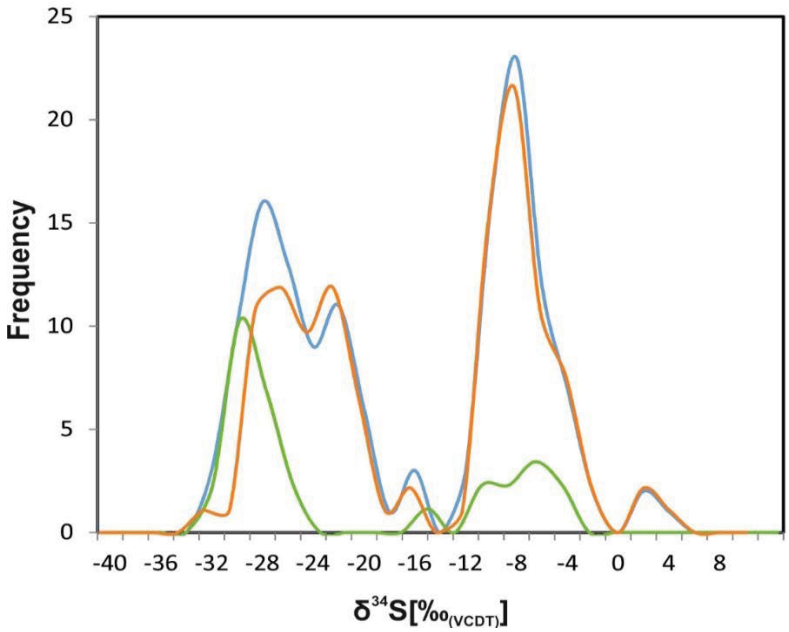

Fig. 130: $\delta^{34}S$ isotopic pattern of sphalerite from Bleiberg (n=151): Blue line cumulative pattern of all measurements; Orange: Wetterstein ore; Green: Cardita ore.

6.3.1.2 Jauken, Radnig, Fladung

The Pb-Zn deposit Jauken (n=22) is characterized by the heaviest $\delta^{34}S$ composition (maximum at +4 ‰) of all investigated Mesozoic Pb-Zn deposits (Fig. 131). The variation is small (0-7 ‰); thus values indicate that the origin of sulfur is from a hydrothermal fluid. The Radnig (n= 35) deposit in Fig. 131 shows the biggest variation (-8 to -27‰) with a maximum between -14 and -19 ‰. These sulfur isotope values display a combination between hydrothermal fluid and bacteriogenic reduction of seawater sulfate. Sphalerite from the Fladung deposit has a small variation in the $\delta^{34}S$ composition between -16 and -30 ‰, the maximum of 47 measurements is at -23 ‰ relative to the V-CDT (Fig. 131). The new in-situ measurements correlate with the measurements on sphalerite concentrates published by Schroll and Pak (1983) who measured for Jauken -2 to +4 ‰, Radnig -20 to -24 ‰ and Fladung -8 to -18 ‰.

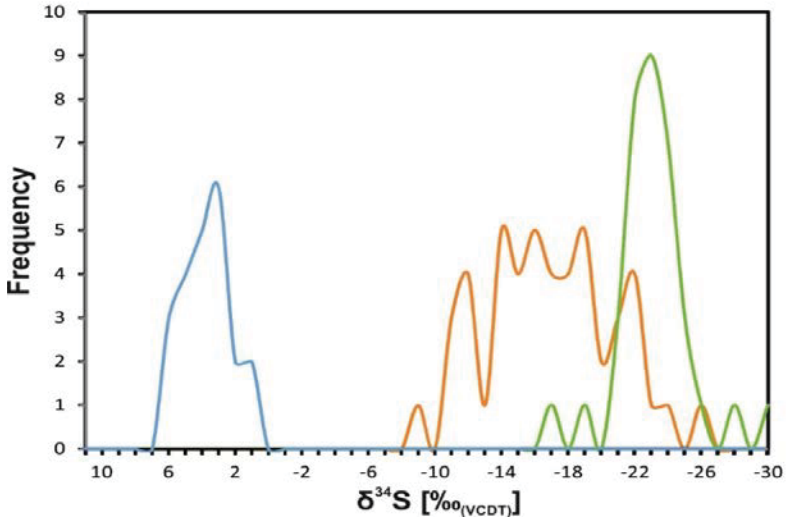

Fig. 131: $\delta^{34}S$ isotopic pattern of sphalerite from the Mesozoic Pb-Zn deposits; Blue: Jauken, Orange Radnig; Green Fladung.

Sphalerite from the Lafatsch deposit shows a large variation (-11 to -35 ‰) with two maxima in the $\delta^{34}S$ pattern (Fig. 132); the first maximum is at -21 ‰, the second at -27 ‰. This signature can be ascribed as to bacteriogenic reduction of seawater sulfate within the sedimentary environment. Schulz (1981) described $\delta^{34}S$ values on sphalerite concentrates from Lafatsch ranging from -12.5 to -27.2 ‰.

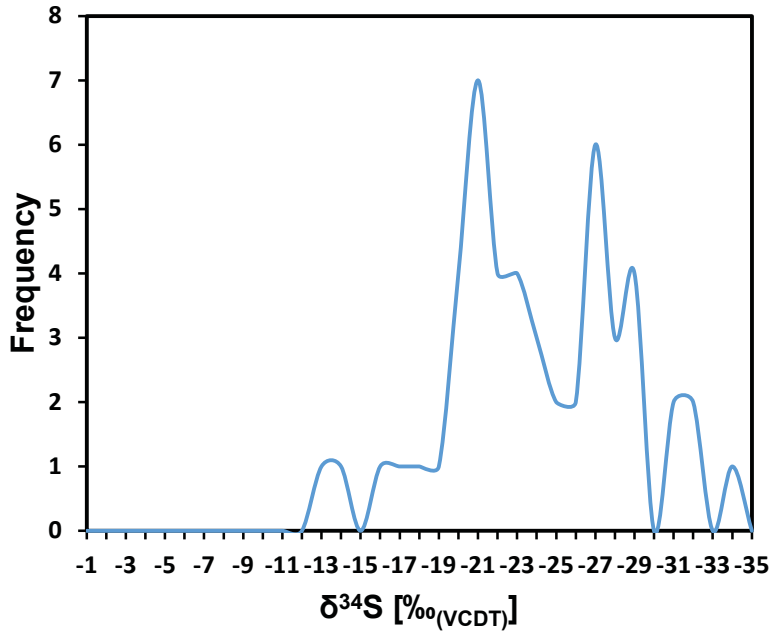

Fig. 132: $\delta^{34}S$ isotopic pattern of sphalerite from Lafatsch

The sulfur isotopic compositions of the investigated Mesozoic Pb-Zn deposits possibly follow a paleogeographic trend (Fig. 133) from north-east to south-west with increasing $\delta^{34}S$ values. The increasing $\delta^{34}S$ values correlate with decreasing precipitation temperatures calculated after Frenzel et al. (2016). One explanation for this inverse trend of temperature and $\delta^{34}S$ composition is, that the heat transfer during the rifting of the Penninic ocean that started in the south-west of the Penninic ocean had more time to heat up the ore bearing fluid than in the north-east. This higher fluid temperature reduced or rather suppressed the bacteriogenic reduction of seawater sulfate. A further explanation for this trend is that the mineralizations with heavier $\delta^{34}S$ compositions are younger and the thermal effect of the overlying formation prevents the BSR. This second mineralization event also could explain the bimodal $\delta^{34}S$ distribution that was already discussed by (Schroll, Rantitsch 2005; Schroll 2006, 1978, 1983).

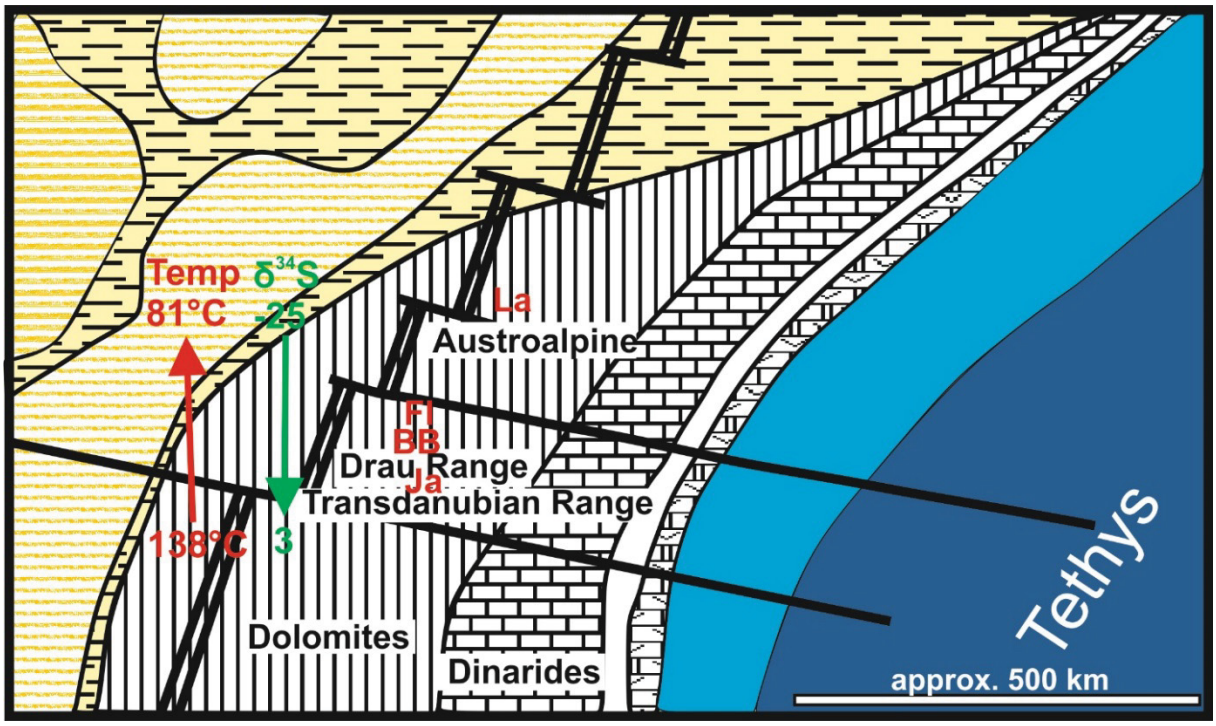

Fig. 133: Simplified paleogeographic reconstruction of the western Tethys during late Triassic modified after Mandl (2000): La: Lafatsch; Fl: Fladung; BB: Bleiberg; Ja: Jauken

The $\delta^{34}S$ composition is one of the factors that differs APT from MVT deposits (Schroll 1995, 2006, 2008). MVT deposits are characterized by heavier (> 0‰) $\delta^{34}S$ values whereas APT deposits show a wide range between -35 to +10 ‰.

6.3.2 Graz Paleozoic Pb-Zn deposits

The $\delta^{34}S$ composition of the investigated Pb-Zn deposits from the Graz Paleozoic plot all in the same range from -2 to +14 ‰. The Guggenbach deposit shows a bimodal distribution, the first maximum is between 0 and +3 ‰, the second between +6 and +12 ‰. This bimodal distribution may reflect two sphalerite generations, with primary sphalerite having δ34S values between +6 and +12 ‰, and remobilised sphalerite between 0 and +3 ‰ (Fig. 134). The $\delta^{34}S$ pattern Arzberg, Rabenstein and Haufenreith give evidence for exhalative-sedimentary enhancement of metals from a hydrothermal fluid (Weber 1990).

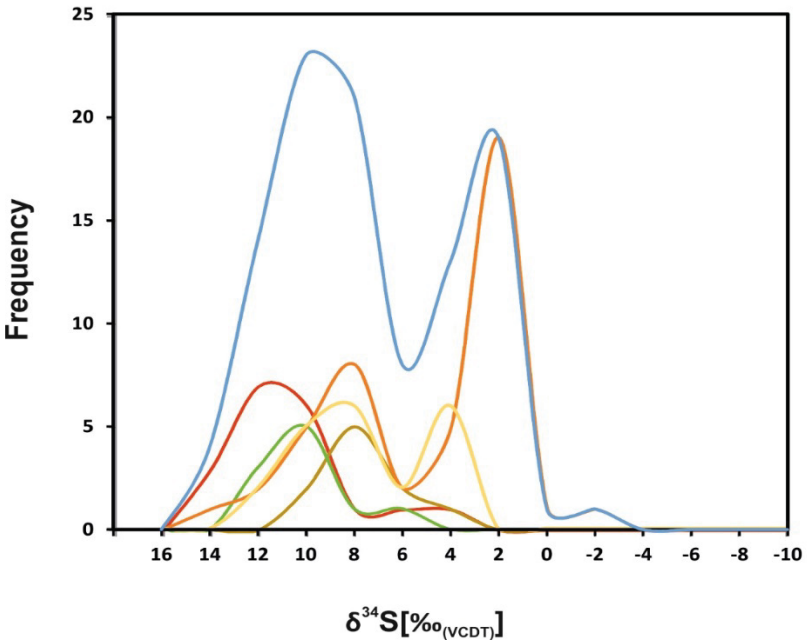

Fig. 134: $\delta^{34}S$ isotopic pattern of sphalerite from the Graz Paleozoic: Blue line cumulative pattern of all measurements; Orange: Guggenbach; Yellow: Arzberg; Red: Rabenstein; Green: Elisabeth; Brown Haufenreith

6.3.3 Sediment-hosted Pb-Zn deposits hosted in other Paleozoic units

In contrast to deposits of the Graz Palaeozoic, the sulfur isotopic pattern of Meiselding (Fig. 135) shows a unimodal distribution with values around zero. These values point to a hydrothermal sulfur source, although a magmatic sulfur source cannot be excluded. The Walchen deposit shows a similar $\delta^{34}S$ pattern like the deposits from the Graz Paleozoic; note that the turbulent curve in Fig. 135 is due to the low quantity of confident measurements.

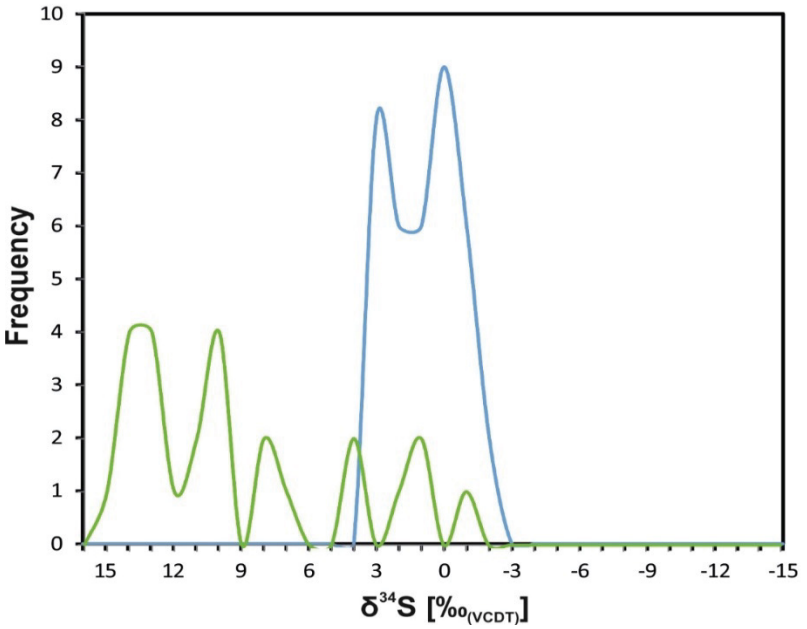

Fig. 135: $\delta^{34}S$ isotopic pattern of sphalerite from Paleozoic Pb-Zn deposits outside the Graz Paleozoic; Blue: Meiselding; Green Walchen

6.3.4 Vein-type deposits

The vein-type deposits Achselalm/Flecktrogalm and Metnitz show $\delta^{34}S$ values around zero, as expected for hydrothermal deposition (Fig. 136). The heavy sulfur isotope composition (15 ‰) from sphalerite of the Koprein deposit provides the heaviest signature of all investigated vein-type deposits. The combination with the precipitation temperature of ~290°C calculated after Frenzel et al. (2016), this strongly argues for thermochemical sulfate reduction.

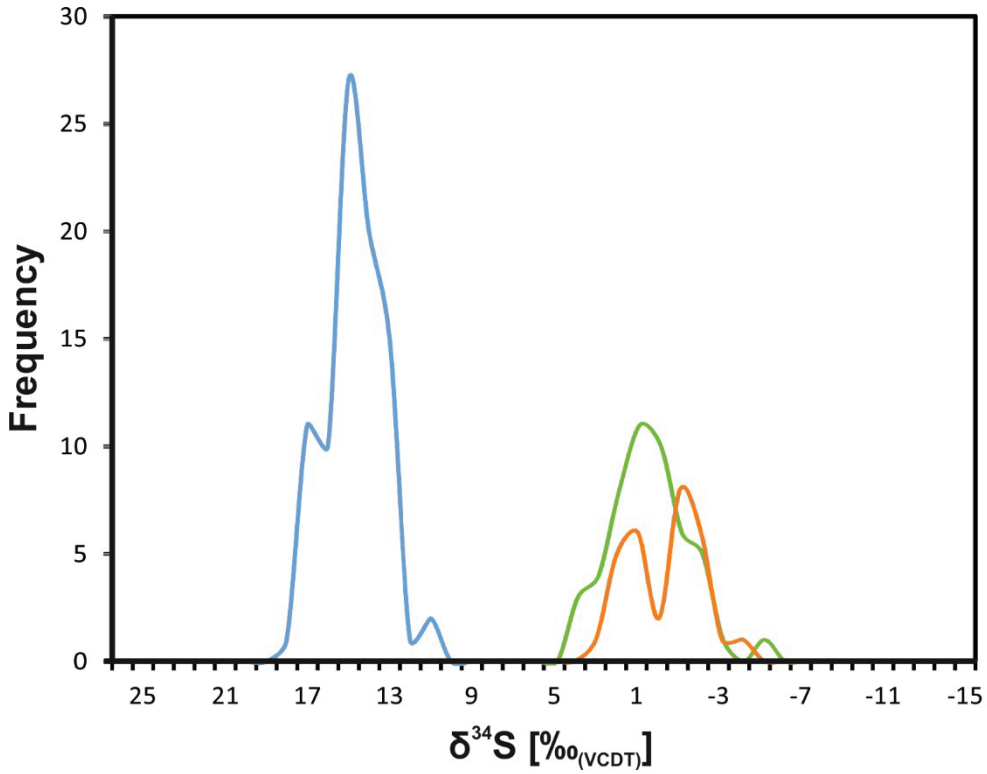

Fig. 136: $\delta^{34}S$ isotopic pattern of sphalerite from vein-type deposits hosted in Paleozoic units; Green: Achselalm/Flecktrogalm; Orange: Metnitz; Blue: Koprein

6.3.5 Correlation between $\delta^{34}S$ and trace element content

Henjes-Kunst (2016) found out that the trace element content in sphalerite shows no correlation with the $\delta^{34}S$ values. Fig. 137 illustrates the Ge, Ga, Cd and Tl content .vs. $\delta^{34}S$ for the Bleiberg deposit indicating no relation between the sulfur isotopic composition and the trace element content over a wide range. This leads to the result that the sulfur source respectively the sulfate reduction process has no influence on the trace element content in sphalerite and therefore this variable can be excluded as fractionation factor.

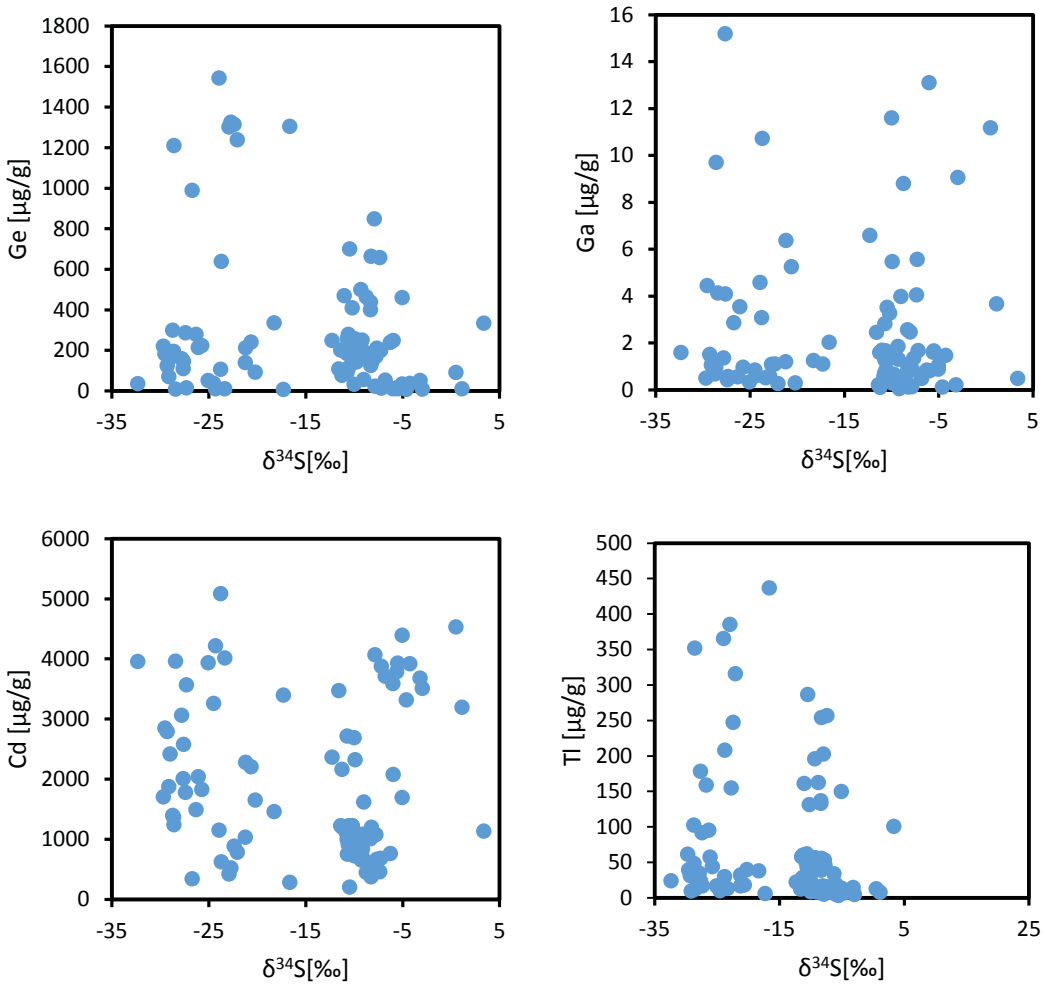

Fig. 137: Correlation between Ga, Ge, Cd and Tl vs. δ34S sulfur isotopic composition in the Bleiberg deposit.

6.3.6 Comparison between ore deposits that share the same basement.

There a several factors that influence leaching processes of elements from the source rock e.g. temperature, pH value, pressure, type of source rock, chemical behavior of the leached element and many more. In the following the focus is on the solubility of Ge, Ga, In and Ag as a function of temperature and pH value.

The behavior of Ge is similar to Si in most geological environments. Silicates like quartz and mica are the responsible source for Ge in a hydrothermal fluid. The Ge/Si ratios in most bedrocks is small (typically < 1 µmol/mol). However, in hydrothermal fluids the Ge/Si ratios are often very high, ranging from 2 to 1000 µmol/mol (Murnane, Stallard 1990). Germanium is transported in hydrothermal fluids as aqueous Ge(IV) hydroxide complexes $Ge(OH)_4$ and Si as silica acid $Si(OH)_4$ (Mortlock, Froelich 1986). The solubility of Ge (Fig. 138 dashed line) at temperatures of ~100 °C is relatively higher than the solubility of Si (Fig. 138 full line) leading to a higher Ge/Si ratio (Fig. 138 red line). Higher temperatures result in a higher Ge solubility compared to Si leading to lower Ge/Si ratios (Evans, Derry 2002) (Fig. 138). During the

precipitation of silicates from a low temperature fluid, Si will be depleted relative to Ge resulting in a positive Ge balance.

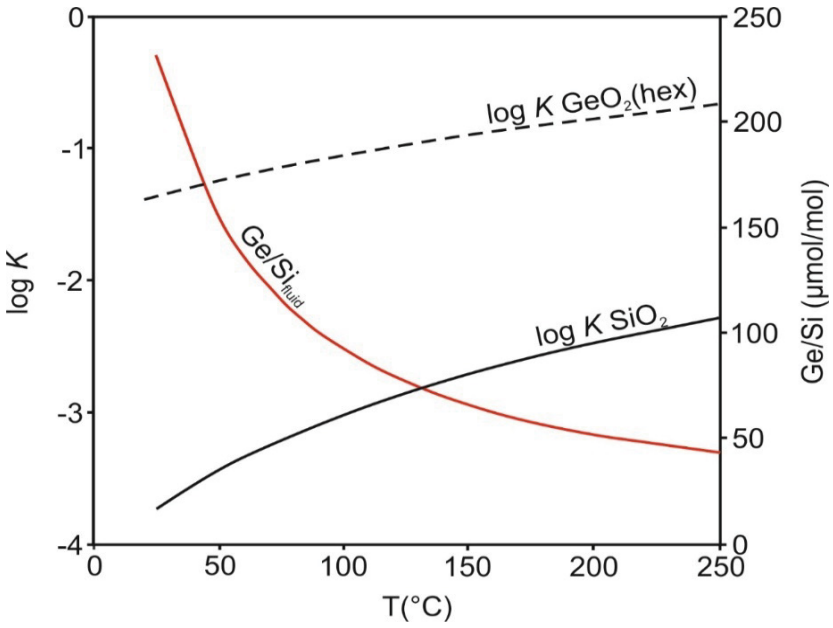

Fig. 138: Solubility of GeO_2 and SiO_2 and Ge/Si fluid as a function of temperature after Evans and Derry (2002).

The geochemical behavior of Ga is analogous to that of Al. As a source for Ga, Al silicates, bauxite and coal play a major role. The solubility of Ga in a hydrothermal fluid depends on the pH and the temperature. At pH values of ~3.5 solubility is the lowest independent of the fluid temperature (Fig. 139). The fluid temperature has the highest influence on the solubility of Ga, in comparison to fluid temperatures of 100°C (Fig. 139: black line) and 300°C (Fig. 139: red line). The solubility increases ~ two orders of magnitude. These facts lead to the conclusion that hot hydrothermal fluids that leach a Al silicates, bauxite or coal will carry substantial amounts of Ga.

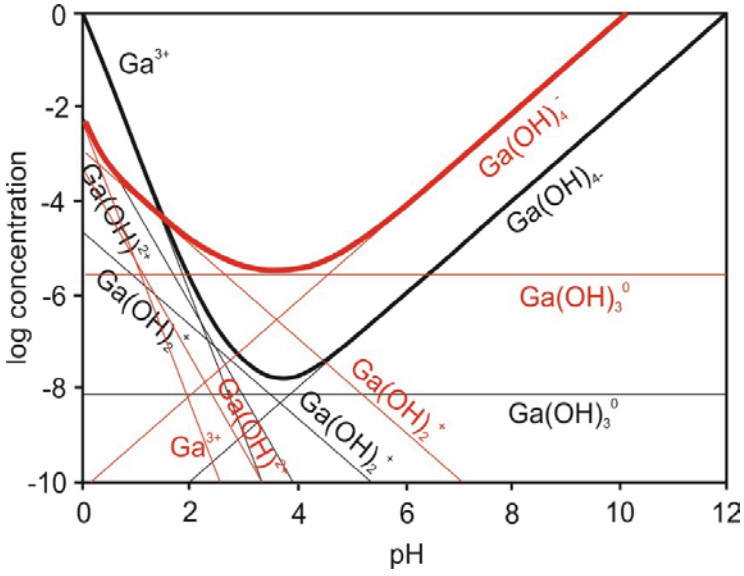

Fig. 139: Solubility of GaOOH vs. pH at temperatures of 100°C (black line) and 300°C red line modified after Wood and Samson (2006).

The geochemical properties of In are similar to of Al and Ga. Biotite and hornblende are the source of In in hydrothermal fluids during leaching processes (Wager et al. 1958). The most important factors for the solubility of In are the pH value and temperature of the fluid. Indium shows a low solubility at pH values between 4 and 9 (Fig. 140). High In concentration in fluids, are coupled to acidic and high alkaline conditions.

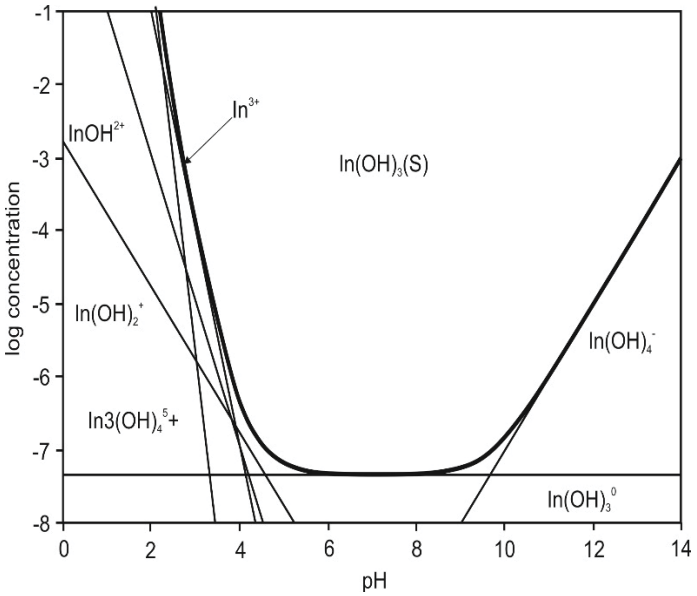

Fig. 140: Solubility of $In(OH)_3(S)$ species as a function of pH after at 25°C after Wood and Samson (2005)

Silver is transported in hydrothermal fluids as $AgCl_2^-$ complex; the solubility depends mostly on temperature and the pH value (Fig. 140).

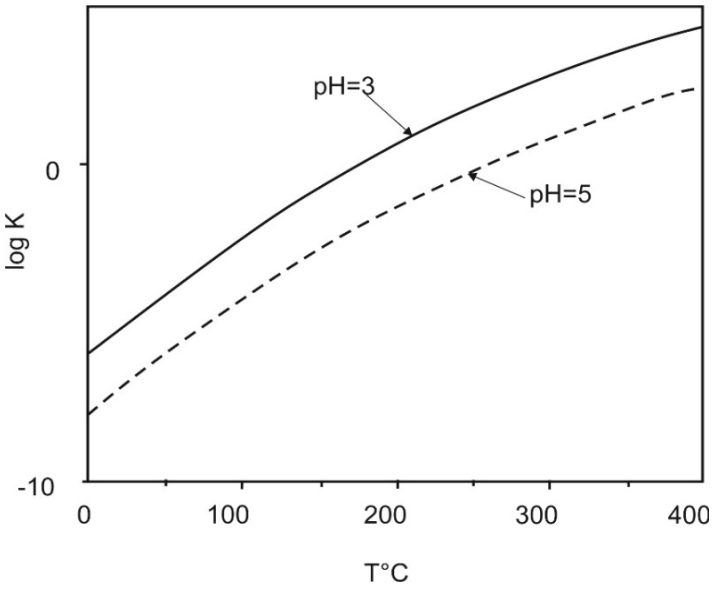

Fig. 141: Solubility of Ag ($AgCl_2^-$) as a function of pH and temperature (modified after Gammons, Williams-Tones (1995)).

Low pH, high temperature lead to a higher concentration of Ag, In and Ga in the fluid, low temperatures increase the Ge content due to a smaller Ge/Si ratio.

The Drauzug-Gurktal nappe system is the basement of the three investigated Pb-Zn deposits Bleiberg, Meiselding and Metnitz. This implies that these three deposits may have the same source rock where the fluid leached the ore forming elements, but show extreme different trace element compositions in sphalerite (Table 38).

Table 38: List of key parameters for the deposits Bleiberg Meiselding and Metnitz.

Location	Bleiberg	Meiselding	Metnitz
Type	ATP	SEDEX	Vein-type
Age (Ma)	200	Paleozoic	unknown
pH	~6	~3	below 5
Temp (°C)	~100	~360	~175
Ge (md)	200	0.1	149
Ga (md)	1	0.7	37.6
In (md)	bdl	15.7	0.1
Ag (md)	0.7	13.1	14.1

A explanation for these differences could be the different fluid parameters (e.g. temperature, pH, Eh, pressure and so on) during formation of the ore deposits (Table 38).

A probable result of these observations could be that at low temperatures a sequential leaching of Ge from quartz and mica of the basement happened, resulting in high Ge contents in sphalerite (Bleiberg and Metnitz). High temperatures like in Meiselding resulting in a lower Ge/Si ratio (Fig. 138), leading into precipitation of quartz, where Ge was incorporated into the lattice (Mortlock and Froelich 1986). A second potential mechanism for the depletion of Ge in Meiselding is that during the greenschist facies metamorphism Ge was remobilized and incorporated in mica and oxides (Bernstein 1985).

An explanation for higher In (transported in the fluid as Indium hydroxide $In(OH)_3$) values in Meiselding compared to Bleiberg and Metnitz could be that the solubility of In is higher at low pH- values and higher temperature (Wood, Samson 2000) (Fig. 140). Indium is also coupled to Cu during precipitation of sphalerite, resulting in the observation that sphalerite showing high Cu values are often enriched in In.

The Metnitz deposit is hosted in carbonates and mica schist as vein type deposit. The fluids of vein type deposits show commonly pH values below 5. The precipitation temperature calculated after Frenzel et al. (2016) shows a median temperature of 176°C. This temperature is high enough to leach Ge and Ga (Fig. 138, Fig. 139) from the source rock, but the solubility of In at this temperature and pH range is too low to leach significant amounts of In from the host rock (Fig. 140). As seen in Fig. 138, the Ge/Si ratio in Metnitz was still low (higher than in Bleiberg, but lower than Meiselding) and significant Ge values were incorporated in sphalerite. When the fluid penetrated the carbonates it was buffered (pH increases), the fluid lost its metal load and the ore forming minerals precipitated.

A possible explanation for the nearly Ag free sphalerite in Bleiberg and the elevated Ag contents in Meiselding and Metnitz is that the temperature and pH value of the leaching fluid in Bleiberg was too low to absorb significant amounts of Ag.

To proof these theories, especially for the incorporation of Ge in quartz, further LA-ICP-MS investigation on the Ge content of quartz should be done on samples of the source rock and the alteration zone and on quartz of the host rock.

6.3.7 Comparison with data of Cerny and Schroll (1992, 1995)

Cerny and Schroll (1992, 1995) and Schroll (1950, 1955) analysed sphalerite from a number of different deposits in the Eastern Alps. These analyses mainly performed were on sphalerite concentrates using spectrometric analysis for small ore samples and wet chemical methods for bulk analyses. Electron microprobe investigations for in-situ analyses started in the 1970ies and Proton Induced X-ray Emission (PIXE) in the 1980ies. Most of the analyses were carried out at the "Österreichische Forschungs- und Prüfanstalt Arsenal" in Vienna. The median LA-ICP-MS median data of the elements Co, Ge, Ga, In, Tl and Cd produced in this study from different deposits were compared with data published by (Cerny, Schroll 1992, 1995).

The diagrams in Fig. 142 displays the correlation between LA-ICP-MS location median data of this study and concentrate data analysed by Cerny and Schroll (1992, 1995). The comparison between the two datasets gives the best correlation for Co (R^2=0.99) (Fig. 142: A). The correlation for Ga (R^2= 0.94), Cd (R^2= 0.91), In (R^2= 0.90) and Tl (R^2= 0.97) are still in a reasonable range for heterogeneous geochemical samples (Fig. 142: B, D, E, F). Germanium shows a poor correlation (R^2= 0.61) due to an outlier (red arrow) for the Jauken deposit where data from Cerny and Schroll (1992, 1995) give a value for Ge of 1260 µg/g (Fig. 142). Without this outlier the comparison would show R^2 = 0.91.

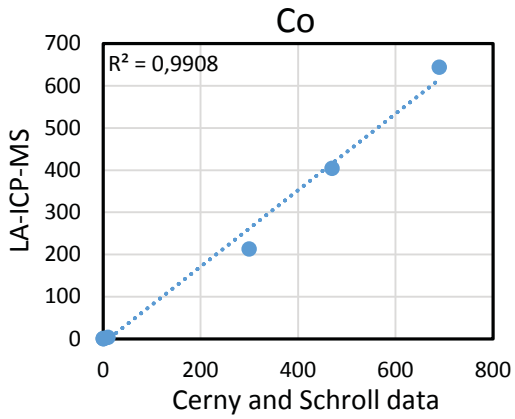
Co
R² = 0,9908
LA-ICP-MS
Cerny and Schroll data
0
100
200
300
400
500
600
700
0
200
400
600
800

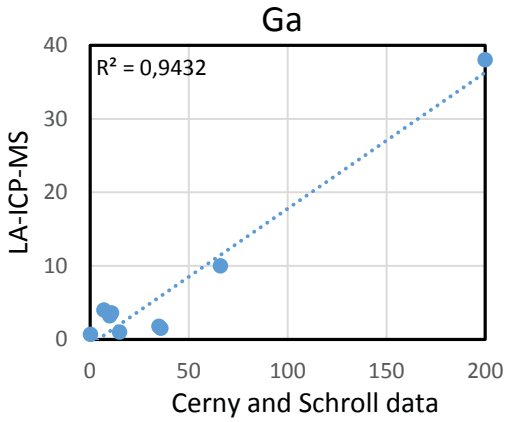
Ga
R² = 0,9432
LA-ICP-MS
Cerny and Schroll data
0
10
20
30
40
0
50
100
150
200

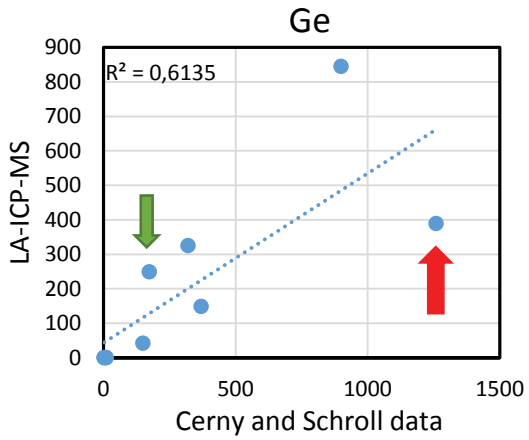
Ge
R² = 0,6135
LA-ICP-MS
Cerny and Schroll data
0
100
200
300
400
500
600
700
800
900
0
500
1000
1500

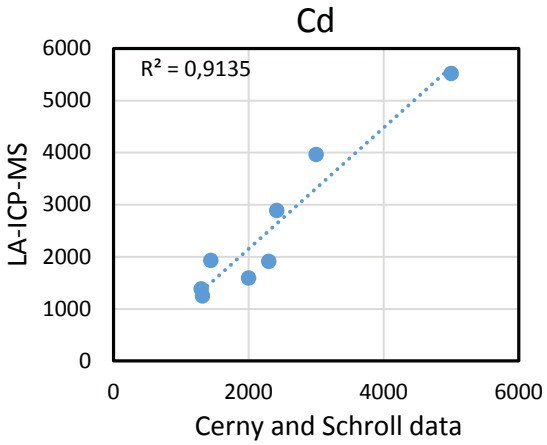
Cd
R² = 0,9135
LA-ICP-MS
Cerny and Schroll data
0
1000
2000
3000
4000
5000
6000
0
2000
4000
6000

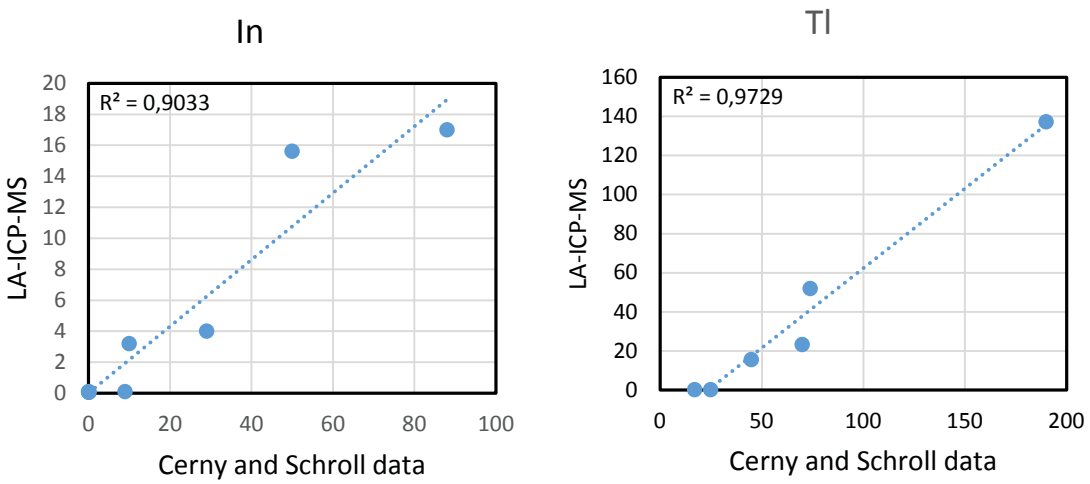

Fig. 142: Comparison of sphalerite concentrate analyses from Cerny and Schroll (1992 and 1995) and the median values for sphalerite analysed by LA-ICP-MS from this study.

The diagrams for Co, Ga, Cd, In and Tl in Fig. 142 illustrate a good correlation and accuracy between the historical and LA-ICP-MS data, whereas the correlation and accuracy for Ge has a bad quality. The bad accuracy for Ge can be explained by different values published by the same authors. Schroll (2006) published long-term Ge values for Bleiberg of 200 µg/g, Cerny and Schroll (1995) 249 µg/g for sphalerite concentrates and LA-ICP-MS median data from Bleiberg show 173 µg/g (Fig. 142: green arrow). The differences for the Jauken (Fig. 142: red arrow) deposit can be explained by the low amount of available samples in this study. If the data of Bleiberg were corrected to 200 µg/g and the Jauken deposit is excluded the correlation shows a better fitting R^2=0.92 and the also the accuracy of the data is better. The bad accuracy for In can be explained by the low amount of measurements in the historical data set.

6.3.8 Multivariate statistics (factor analysis)

Factor analyses were performed using the R software. In Fig. 143, median data of all ore deposits were plotted. Four factors are distinguished accounting for 82% of the ariance in the sample suite. These factors are attributed to geological/mineralogical processes. Factor 1, by far the dominant, combines Ge-Tl-As and minor Pb and Cd. showing the influence of low temperature Mesozoic Schalenblende in factor one. Factor two with the elements Co,Ga,Sb, Sn and Fe indicates the influence of higher temperatures, probably pointing to Paleozoic and vein type deposits. The elements Cu-Ag-Sb point to a sulfosalt komponent in sphalerite (e.g. polybasite $Cu(Ag,Cu)_6Ag_9Sb_2S_{11}$). In factor four hosting the elements Fe,In and Sn a sakuraiite $(Cu,Zn,Fe)_3(In,Sn)S_4$ (sulfosalt) component is indicated

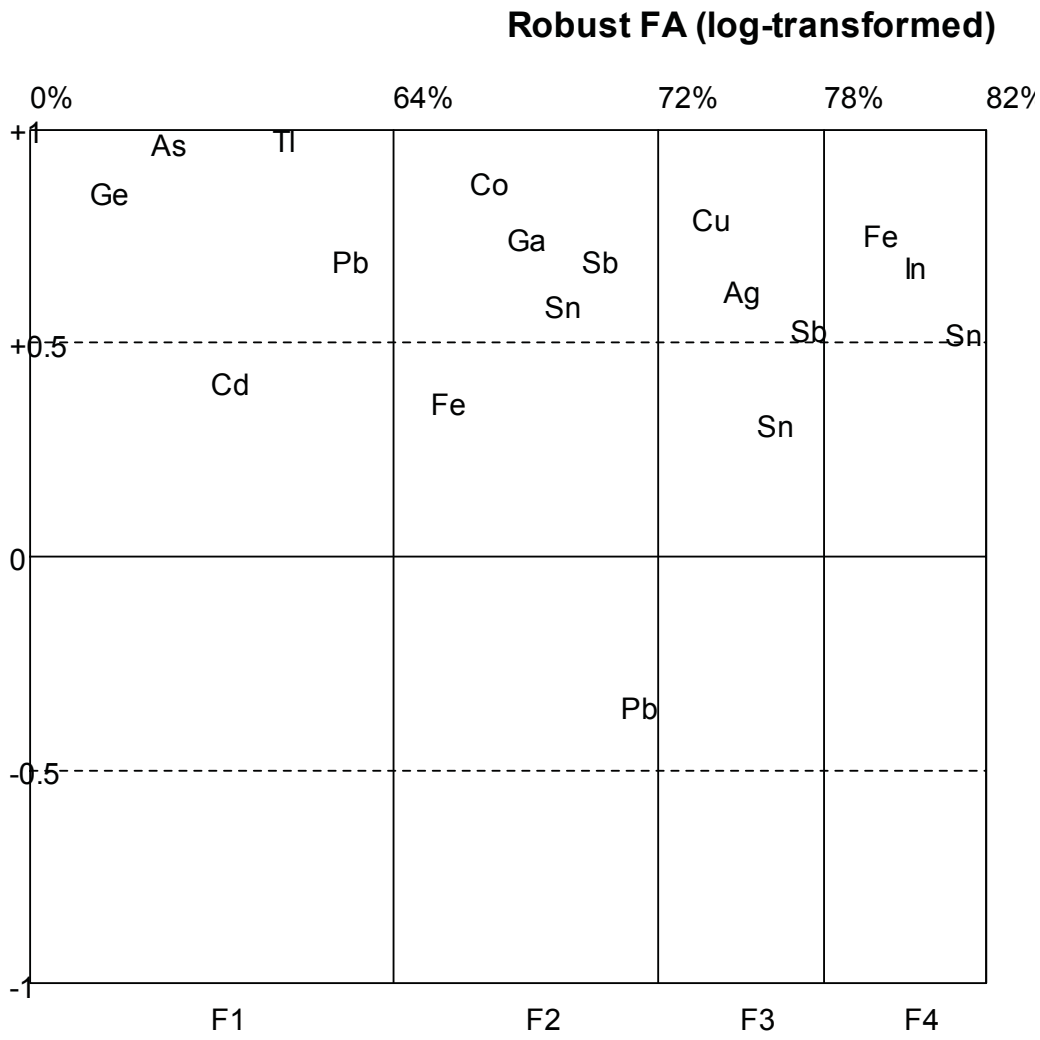

Fig. 143: Factor analysis of all trace element median values of Austro Alpine Pb-Zn Deposits.

The Schalenblende factor, especially the temperature dependency of Tl is illustrated in the temperature vs. Tl plot in Fig. 128. The association of Tl and As in the Schalenblende factor can be seen in Fig. 127 as a positive correlation in Mesozoic Pb-Zn deposits.

Further factor analyses using all data of the different ore types were performed. As examples, Mesozoic ores and data of the Graz Paleozoic are given in the following.

Mesozoic sphalerite from the Drau Range and the Northern Calcareous Alps illustrate in factor one the Schalenblende factor hosting the elements Mn, Fe, Ge and Tl (Fig. 144). The elements As, Tl and Pb (Fig. 144) give evidence for a richardsollyite ($TlPbAsS_3$) component, Factor three (Cu, Ag, Sb) shows similar elements like in Fig. 144 and is summarized as polybasite factor. Cadmium and Tl in factor four was often described by Schroll E. as a element accociation in Mesozoic Pb-Zn deposits and is therefore called “Schroll factor” (Schroll 1992, 1995)

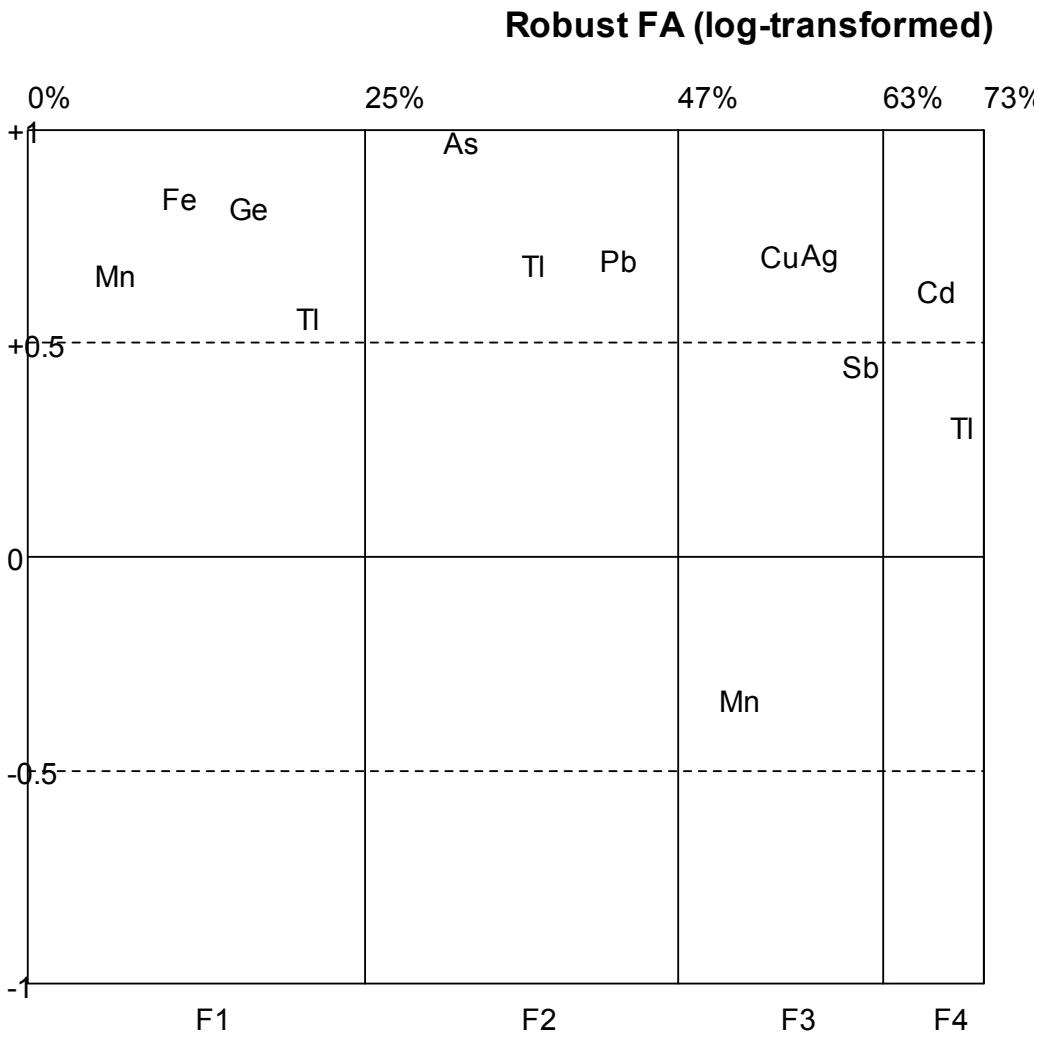

Fig. 144: Factor analysis of all data from the Drau Range and the Northern Calcareous Alps.

The factor analysis in Fig. 144, reflects in an impressive way the characterizing element composition of sphalerite hosted in Mesozoic Pb-Zn deposits which are commonly rich in Ge, Tl and As, but poor in Fe and Mn. The Ag component in the polybasite factor (factor 3) is mainly related to elevated Ag content in sphalerite from Lafatsch. The Element relations of Fe-Mn, Fe-Ge and the temperature dependence of Tl can be seen in the xy-plott in Fig. 128. Thallium and As in the richardsollyite factor can be seen in Fig. 127 as positive correlation.

The factor analysis of the Graz Paleozoic gives a different view in factor one and two compared to the analysis of Mesozoic Pb-Zn deposits. Manganese, Fe and Co show the highest influence on data of the Graz Paleozoic (Fig. 145), where Fe, Mn and Co are elevated compared to Mesozoic Pb-Zn deposits (Fig. 144), Cu and Ag indicate a negative correlation indicating that Cu and Ag enriched sphalerite is slightly depleted in Fe. Factor 2 illustrates that Cu rich sphalerite is depleted in Cd due to copper disease (Fig. 145). A sulfosalt component is illustrated in factor three hosting the elements Ag, Sb and Pb. The positive correlation of Ge vs. Fe was found in Mesozoic Pb-Zn deposits (Fig. 121), due to the low Ge concentrations in sphalerite from the Graz Paleozoic no such correlation was observed.

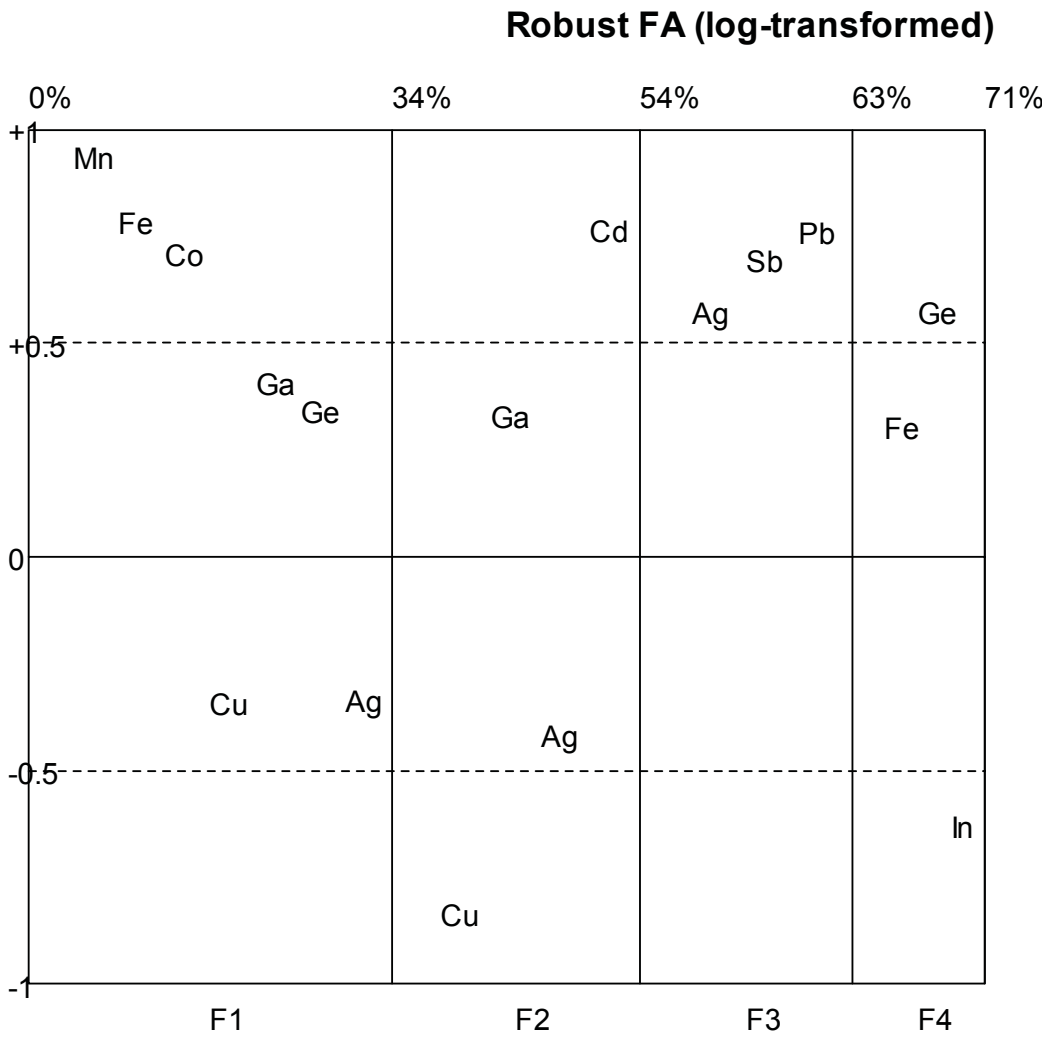

Fig. 145: Factor analysis of all sphalerite data from the Graz Paleozoic.

6.3.9 Economic Potential

Fig. 146 illustrates the high-tech metal content of the investigated Pb-Zn deposits, the red numbers indicate economically interesting trace metal contents of sphalerite.

Deposits of economic potential for Ge are mainly hosted in the Drau Range where Fladung shows the highest Ge values and Bleiberg the lowest (Fig. 146). These lower Ge content in sphalerite from Bleiberg can be compensated by the large size of this deposit. Cerny and Schroll (1995) estimated the remaining tonnage with 2 million tons of ore resulting in 496 tons Ge metal. The Lafatsch deposit in the Northern Calcareous Alps might be a target for Ge (42 µg/g) in combination with Ag (43 µg/g). For Ga no potential target was found in Mesozoic Pb-Zn deposits. Metnitz is the only deposit outside the group of carbonate hosted Pb-Zn deposits that has significant Ge values (Metnitz 149 µg/g). In combination with the elevated Co content (400 µg/g) Metnitz could be a potential target for critical metals as a byproduct.

The highest In values were found in Leogang (247 µg/g) followed by Walchen (98 µg/g) that seem to be potential targets in combination with Cu and for Walchen with Au as byproducts (Fig. 146). Due to the lack of reliable reserve data, no economic potential could be calculated. The In content of Mesozoic carbonate hosted Pb-Zn deposits is below the limit of detection and therefore they can be excluded as target for this element.

For Co, sphalerite from Koprein holds the highest Co content (664 µg/g) of the investigated deposits. However due to the remote location and probably small size of this deposit, an economic production is very unlikely. In the near future

Deposits of the Graz Paleozoic show no potential for critical metals, the small size and the mining activities over centuries in this area, combined with the small size of the different deposits and the uncertain reserve data make it very unlikely that mining and exploration activities will be started in the future. The Achselalm-Flecktrogalm deposit can be excluded as targets for three reasons, (i) the low content of trace elements, (ii) they are located in a natural heritage area and (iii) the extremely remote location.

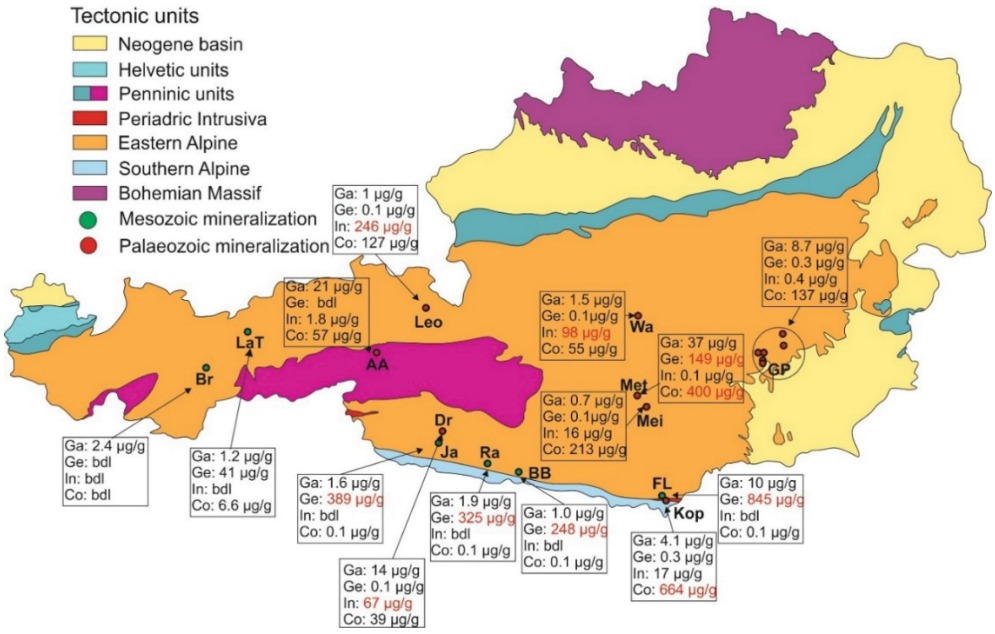

Fig. 146: Geological overview of Austria with median values of critical elements in sphalerite, modified after (Egger et al. 1999). AA, Achselalm; BB, Bleiberg-Kreuth; Fl, Fladung-Hochobir; GP, Graz Paleozoikum; Ja, Jauken; KOP, Koprein; LaT, Lafatsch; Leo, Leogang; Mei, Meiselding; Met, Metnitz;

7 Conclusion

Base metal deposits in the Eastern Alps may be grouped into at least three types based on their geological position. Group 1 comprises Pb-Zn deposits hosted by Triassic platform carbonates; type locality is Bleiberg. The mineralogy comprises only galena, Fe-poor sphalerite and minor Fe sulfides. Sphalerite was formed under low temperature condition with a maximum precipitation temperature of 138°C (Jauken). The sulfur isotope pattern shows a light signature (except Jauken) indicating BSR. This group is enriched in Ge, Cd and Tl. The second type comprises stratiform deposits hosted by Paleozoic clastic and volcanoclastic sequences that have been metamorphosed under medium-grade conditions (greenschist facies). This group is generally enriched in Cu and Ag, hosted by chalcopyrite, fahlore and other phases; sphalerite is Fe-rich. Type locality of this type is Arzberg in the Graz Paleozoic. Slightly differing deposits of this group are hosted by metacarbonates (Leogang) and are polymetallic and polymineralic. Leogang shows high In values (up to 330 µg/g). These high values are most probably caused by chalcopyrite and stannite micro inclusions in sphalerite. However, sphalerite compositions are similar to typical stratiform deposits such as Walchen. The sulfur isotope signature illustrates medium to heavy $\delta^{34}S$ ratios indicating a hydrothermal sulfur source. A third genetic type includes vein-type deposits in various geological units. These deposits may have characteristics of both, stratiform type-II and carbonate-hosted type-I deposits. A good example is Metnitz, where sphalerite is elevated in Co, Ge and Sb. Some vein-type deposits show elevated In, Sn and Sb (e.g. Drassnitz, Koprein). Sulfur isotope ratios are around 0 ‰ suggesting a hydrothermal sulfur source, except those of Koprein ($\delta^{34}S$= +15‰). The heavy $\delta^{34}S$ ratios of the Koprein deposit points to a thermo chemical sulfate reduction.

From the trace element contents in sphalerite indicate that, base metal deposits in the Eastern Alps may be grouped into two major types. The first group (Mesozoic carbonate hosted PB-Zn deposits) is characterized by highly elevated concentrations of Ge, As, Tl and Pb, and low Co, Ga, In and Ag. The recovery of Ge may be economic, but As and Tl, along with Cd are deleterious elements to be considered for metallurgical recovery. Type locality is Bleiberg. The second group is highly variable in trace elements, but tends to be more enriched in Co, Cu, Fe, Ag and Sb compared to CTEM; Ga, In and Sn may be elevated as well. This type is generally low in Ge, As, Tl and Pb. Compared to CTEM, all deposits have depleted Mn concentrations in sphalerite, due to the lack of skarn and epithermal deposits that are most enriched in Mn in the data of Cook et al. (2009).

The calculation of resource numbers using the data presented in this study is not possible because there are no valid reserve data available. The data in Table 39 are presented in g/t sphalerite. The author suggests at this point that the samples investigated in this study are not representative for the ore deposits due to the restricted accessibility of some deposits and the samples were taken with the focus on high sphalerite content.

Table 39: Summary of base metal ore types and their trace metal content in sphalerite [g/t].

Unit	Location	ore type	Co	Ga	Ge	In	Ag	As	Cd	Tl
Mesozoic	Bleiberg	APT	0.06	1.05	229.1	bdl	0.74	172	1379	51.79
	Fladung	APT	0.1	10.33	845.5	bdl	0.47	310	5515	137.1
	Jauken	APT	0.17	1.55	389.1	bdl	0.34	37.75	1249	23.1
	Radnig	APT	0.08	1.86	325.3	bdl	0.44	56.1	1383	16.4
	Lafatsch	APT	0.04	1.22	41.7	bdl	43.4	273	1911	15.55
Graz Palaeozoic	Arzberg	SEDEX	19	1.64	0.13	4.03	78	0.15	1292	bdl
	Elisabeth adit	SEDEX	158	9.69	0.39	0.17	14	bdl	1894	bdl
	Friedrich adit	SEDEX	232	18.89	0.44	1.9	22	bdl	2415	bdl
	Guggenbach	SEDEX	134	7.41	0.09	0.19	19	0.5	1131	bdl
	Haufenreith	SEDEX	178	3.6	1.67	37	5.65	3	2155	bdl
	Rabenstein	SEDEX	130	5.05	0.34	0.18	25	0.35	1032	bdl
	Silberberg	SEDEX	93	12.34	0.28	1.84	19	bdl	2317	bdl
Palaeozoic	Leogang	SEDEX	128	1.05	0.11	247	11	0.15	2042	0.03
	Meiselding	SEDEX	213	0.67	0.13	16	13	1.09	3960	0.02
	Walchen	SEDEX	55	1.53	0.07	98	12	0.09	1592	0.01
	Achselalm/Flecktrogalm	vein-type	59.5	29.98	0.01	1.69	0.55	0.12	2232	bdl
	Koprein	vein-type	644	4.06	0.29	17	28	0.16	2890	bdl
	Metnitz	vein-type	405	37.6	149	0.11	14	3.6	1931	bdl

Carbonate-hosted Pb-Zn deposits have the highest potential for Ge. For Ga, the potential is small and lower than predicted in the previous study conducted by Cerny and Schroll (1992, 1995), these authors investigated sphalerite concentrates over many years and locations that are not accessible anymore. Indium is enriched only in a few deposits like Leogang and Walchen, mainly hosted by Paleozoic sedimentary rocks. In addition to sphalerite, significant concentrations of In may reside in chalcopyrite. Cobalt, becoming an increasingly important critical element, is present as a trace element only in sphalerite of some vein-type and stratiform deposits; most of the Co in these deposits is hosted by pyrite, pyrrhotite, Fe-Co-Ni sulfoarsenides and other minerals. In addition to the critical elements, elevated concentrations of Ag, Cd and Tl hosted by sphalerite in some deposit types may add to the economic value of sulfide deposits in the Eastern Alps.

To confirm the economic potential of the recommended ore deposits, representative bulk samples should analyzed. Depending on the results visibility studies including drilling programs and reserve calculations should be done.

8 Publication bibliography

Ault, W. U.; Kulp, J. L. (1960): Sulfur isotopes and ore deposits. In Economic Geology 55 (1), pp. 73–100.

Barton Jr., P. B.; Bethke, P. M. (1987): Chalcopyrite disease in sphalerite. Pathology and epidemiology. In American Mineralogist 72 (5-6), pp. 451–467.

Belissont, R.; Boiron, M.-C.; Luais, B.; Cathelineau, M. (2014): LA-ICP-MS analyses of minor and trace elements and bulk Ge isotopes in zoned Ge-rich sphalerites from the Noailhac – Saint-Salvy deposit (France). Insights into incorporation mechanisms and ore deposition processes. In Geochimica et Cosmochimica Acta 126, pp. 518–540.

Belissont, R.; Muñoz, M.; Boiron, M.-C.; Luais, Béatrice; Mathon, Olivier (2016): Distribution and oxidation state of Ge, Cu and Fe in sphalerite by µ-XRF and K-edge µ-XANES. Insights into Ge incorporation, partitioning and isotopic fractionation. In Geochimica et Cosmochimica Acta 177, pp. 298–314.

Bente, K.; Doering, T. (1993): Solid-state diffusion in sphalerites. An experimental verification of the "chalcopyrite disease". In European Journal of Mineralogy 5 (3), pp. 465–478.

Bernardini, G. P.; Borgheresi, M.; Cipriani, C.; Di Benedetto, F.; Romanelli, M. (2004): Mn distribution in sphalerite. An EPR study. In Physics and Chemistry of Minerals 31 (2), pp. 80–84.

Bernstein, L. R. (1985): Germanium geochemistry and mineralogy. In Geochimica et Cosmochimica Acta 49 (11), pp. 2409–2422.

Bonnet, J.; Cauzid, J.; Testemale, D.; Kieffer, I.; Proux, Olivier; Lecomte, A; Bailly, L. (2017): Characterization of Germanium Speciation in Sphalerite (ZnS) from Central and Eastern Tennessee, USA, by X-ray Absorption Spectroscopy. In Minerals 7 (5), p. 79.

Brandner, R.; Sperling, M. (Eds.) (1995): Zur "Terrane"-Geschichte der Lienzer Dolomiten (Drauzug) aus stratigraphischer und strucktureller Sicht. With assistance of Geologische Bundesanstalt. Geologie von Osttirol. Lienz, 2.-6. Oktober 1995.

Cerny, I.: Die karbonatgebundenen Blei-Zink-Lagerstätten des alpinen und außeralpinen Mesozoikums Die Bedeutung ihrer Geologie, Stratigraphie und Faziesgebundenheit. Die Bedeutung ihrer Geologie, Stratigraphie und Faziesgebundenheit für Prospektion und Bewertung. In : Archiv für Lagerstättenforschung der Geologischen Bundesanstalt, vol. 11, pp. 5–125.

Cerny, I. (1989a): Current prospecting strategy for carbonate-hosted Pb-Zn mineralizations at Bleiberg-Kreuth (Austria). In Economic Geology 84 (5), pp. 1430–1435.

Cerny, I. (1989b): Die karbonatgebundenen Blei-Zink-Lagerstätten des alpinen und außeralpinen Mesozoikums. Die Bedeutung ihrer Geologie, Stratigraphie und Faziesgebundenheit für Prospektion und Bewertung (11).

Cerny, I.; Scherer, J.; Schroll, E. (1982): Blei-Zink-Verteilungsmodell in stilliegenden Blei-Zink-Revieren der Karawanken (Archiv für Lagerstättenforschung der Geologischen Bundesanstalt, 2).

Cerny, I.; Schroll, E. (1992): Beurteilung der Verfügbarkeit von Lagerstätten bzw. Vorkommen von Pb-Zn-Rohstoffen sowie der mit diesen assoziierten Nebenelementen in Österreich im

Hinblick auf neue Anwendungsbereiche und neue Technologien. - Studie im Rahmen des Projektes Rohstoffe für Zukunftstechnologien. Teilschritt II der Kommission für Grundlagenforschung der Mineralrohstoff-Forschung der Österreichischen Akademie der Wissenschaften.

Cerny, I.; Schroll, E. (1995): Heimische Vorräte an Spezialmetallen (Ga, In, Tl, Ge, Se, Te und Cd) in Blei-Zink- und anderen Erzen. Wien: Geologische Bundesanst (Archiv für Lagerstättenforschung der Geologischen Bundesanstalt, 18).

Cerny, Immo (1989c): Die karbonatgebundenen Blei-Zink-Lagerstätten des alpinen und außeralpinen Mesozoikums. Die Bedeutung ihrer Geologie, Stratigraphie und Faziesgebundenheit für Prospektion und Bewertung. Leoben, Montanuniv., Habil.-Schr., 1989. Leoben.

Clark, A. H. (1970): ARSENIAN SPHALERITE FROM MINA-ALCARAN, PAMPA-LARGA, COPIAPO, CHILE. In American Mineralogist 55 (9-10).

Cook, N. J.; Ciobanu, C. L.; Brugger, J.; Etschmann, B.; Howard, D. L.; Jonge, M. D. de et al. (2012): Determination of the oxidation state of Cu in substituted Cu-In-Fe-bearing sphalerite via -XANES spectroscopy. In American Mineralogist 97 (2-3), pp. 476–479.

Cook, N. J.; Ciobanu, C. L.; Pring, A.; Skinner, W.; Shimizu, M.; Danyushevsky, L. V. et al. (2009): Trace and minor elements in sphalerite. A LA-ICPMS study. In Geochimica et Cosmochimica Acta 73 (16), pp. 4761–4791.

Cook, N. J.; Ciobanu, C. L.; Williams, T. (2011): The mineralogy and mineral chemistry of indium in sulphide deposits and implications for mineral processing. In Hydrometallurgy 108 (3), pp. 226–228.

Cook, N. J.; Etschmann, B.; Ciobanu, C. L.; Geraki, K.; Howard, D.; Williams, T. et al. (2015): Distribution and Substitution Mechanism of Ge in a Ge-(Fe)-Bearing Sphalerite. In Minerals 5 (2), pp. 117–132.

Danyushevsky, L. V.; Robinson, P.; Gilbert, S. E.; Norman, M.; Large, R.; McGoldrick, P.; Shelley, M. (2011): Routine quantitative multi-element analysis of sulphide minerals by laser ablation ICP-MS. Standard development and consideration of matrix effects. In Geochemistry: Exploration, Environment, Analysis 11 (1), pp. 51–60.

Di Benedetto, F. (2005): Compositional zoning in sphalerite crystals. In American Mineralogist 90 (8-9), pp. 1384–1392.

Egger, H.; Krenmayer, H. G.; Mandl, G. W.; Matura, A.; Nowotny, A.; Pascher, G. et al. (1999): Geologische Übersichtskarte der Republik Österreich. Edited by Geologische Bundesanstalt. Wien. Available online at https://www.geologie.ac.at/forschung-entwicklung/kartierung-landesaufnahme/geologie/geologische-karte-12000000/, checked on 3/22/2017.

Eichhorn, R.; Loth, G.; Kennedy, A. (2001): Unravelling the pre-Variscan evolution of the Habach terrane (Tauern Window, Austria) by U-Pb SHRIMP zircon data. In Contrib Mineral Petrol 142 (2), pp. 147–162.

European Commission (2017): Study on the review of the list of critical raw materials. Edited by European Commision. Available online at https://publications.europa.eu/en/publication-detail/-/publication/08fdab5f-9766-11e7-b92d-01aa75ed71a1/language-en.

Evans, Matthew J.; Derry, Louis A. (2002): Quartz control of high germanium/silicon ratios in geothermal waters. In Geology 30 (11), p. 1019.

Feichter, M. M.; Mogessie, A. (2003): Die Sulfidmineralisationen von Arzberg (Steiermark): Ergebnisse petrographischer, mineralchemischer und geochemischer Untersuchungen. In Mitteilungen der Österreichischen Mineralogischen Gesellschaft (148), pp. 133–135.

Feitzinger, G.; Günther, W.; Brunner, A. (1998): Bergbau- und Hüttenstandorte im Bundesland Salzburg: Land Salzburg.

Figueiredo, M. O.; Silva, T.; Oliveira, D.; Rosa, D. R.N. (2012): Indium-Carrier Minerals in Polymetallic Sulphide Ore Deposits. A Crystal Chemical Insight into an Indium Binding State Supported by X-ray Absorption Spectroscopy Data. In Minerals 2 (4), pp. 426–434.

Fowler, A. D.; L'Heureux, I. (1996): Self-organized banded sphalerite and branching galena in the Pine Point ore deposit, Northwest Territories. In The Canadian Mineralogist 34 (6), pp. 1211–1222.

Frenzel, M.; Hirsch, T.; Gutzmer, J. (2016): Gallium, germanium, indium, and other trace and minor elements in sphalerite as a function of deposit type ? A meta-analysis. In Ore Geology Reviews 76, pp. 52–78.

Frenzel, M.; Ketris, M. P.; Gutzmer, J. (2014): On the geological availability of germanium. In Miner Deposita 49 (4), pp. 471–486.

Gammons, C. H.; Williams-Tones, A. E. (1995): The solubility of Au□Ag alloy + AgCl in HCl/NaCl solutions at 300°C. New data on the stability of Au (1) chloride complexes in hydrothermal fluids. In Geochimica et Cosmochimica Acta 59 (17), pp. 3453–3468.

Gasser, D.; Stüwe, K.; Fritz, H. (2010): Internal structural geometry of the Paleozoic of Graz. In Int J Earth Sci (Geol Rundsch) 99 (5), pp. 1067–1081.

GBA: IRIS Online (2017): GBA-Webapplikation:IRIS Online-Interaktives-rohstoffinformationssystem. Available online at http://www.geologie.ac.at/services/webapplikationen/geofast/iris-interaktives-rohstoffinformationssystem, updated on 3/30/2017.

George, L.L.; Cook, N. J.; Ciobanu, C. L. (2016): Partitioning of trace elements in co-crystallized sphalerite–galena–chalcopyrite hydrothermal ores. In Ore Geology Reviews 77, pp. 97–116.

George, L.L.; Cook, N. J.; Ciobanu, C. L. (2017): Minor and Trace Elements in Natural Tetrahedrite-Tennantite. Effects on Element Partitioning among Base Metal Sulphides. In Minerals 7 (2), p. 17.

Grammatikopoulos, T. A.; Valeyev, O.; Roth, T. (2006): Compositional variation in Hg-bearing sphalerite from the polymetallic Eskay Creek deposit, British Columbia, Canada. In Chemie der Erde-Geochemistry 66 (4), pp. 307–314.

Günther, D.; Heinrich, C. A. (1999): Enhanced sensitivity in laser ablation-ICP mass spectrometry using helium-argon mixtures as aerosol carrier. In J. Anal. At. Spectrom. 14 (9), pp. 1363–1368.

Haditsch, J.G; Mostler, H. (1970): Die Kupfer-Nickel-Kobalt-Vererzung Im Bereich Leogang. In Archiv f. Lagerstättenfg. in den Ostalpen (11), pp. 161–209.

Henjes-Kunst, E. (2014): The Pb-Zn deposits in the Drau Range (Easter Alps, Austria/Slovenia): A multi-analytical research approach for investigation of ore-forming mechanisms. PhD Thesis, Leoben. Lagerstättenmineralogie.

Henjes-Kunst, E.; Raith, Johann G.; Boyce, Adrian J. (2017): Micro-scale sulfur isotope and chemical variations in sphalerite from the Bleiberg Pb-Zn deposit, Eastern Alps, Austria. In Ore Geology Reviews 90, pp. 52–62.

Höll, R.; Kling, M.; Schroll, E. (2007): Metallogenesis of germanium—A review. In Ore Geology Reviews 30 (3-4), pp. 145–180.

Johan, Z. (1988): Indium and germanium in the structure of sphalerite. An example of coupled substitution with copper. In Miner Petrol 39 (3-4), pp. 211–229.

Keil, M.; Neubauer, F. (2011): The Miocene Enns Valley basin (Austria) and the North Enns Valley fault. In Austrian Journal of Earth Sciences 104 (1), pp. 49–65.

Kelley, K. D.; Leach, D. L.; Johnson, C. A.; Clark, J. L.; Fayek, M.; Slack, J. F. et al. (2004): Textural, Compositional, and Sulfur Isotope Variations of Sulfide Minerals in the Red Dog Zn-Pb-Ag Deposits, Brooks Range, Alaska. Implications for Ore Formation. In Economic Geology 99 (7), pp. 1509–1532.

Kozlik, M. (2015): Mineralogical, petrological and (isotope-) geochemical studies on the Felbertal scheelite deposite, Austria: Development of an epigenetic model for W mineralization in the context of Variscan magmatism in the Tauern Window. Dissertation. Montanuniversität, Leoben. Rohstoffmineralogie.

Kreis, H. H.; Unger, Heinz Josef (1971): Die Bleiglanz-Zinkblende-Flußspat-Lagerstätte der Achsel-und Hinteren Flecktrogalm bei Hollersbach, Oberpinzgau/Salzburg: na.

Krouse, H. R.; Coplen, T. B. (1997): Reporting of relative sulfur isotope-ratio data (Technical Report). In Pure and Applied Chemistry 69 (2).

Kubo, T.; Nakato, T.; Uchida, E. (1992): An Experimental Study on Partitioning of Zn, Fe, Mn and Cd between Sphalerite and Aqueous Chloride Solution. In Shigen-Chishitsu 42 (235), pp. 301–309.

Kucha, H.; Schroll, E.; Raith, J. G.; Halas, S. (2010): Microbial Sphalerite Formation in Carbonate-Hosted Zn-Pb Ores, Bleiberg, Austria. Micro- to Nanotextural and Sulfur Isotope Evidence. In Economic Geology 105 (5), pp. 1005–1023.

Kucha, H.; Schroll, E.; Stumpfl, E. F. (2005): Fossil sulphate-reducing bacteria in the Bleiberg lead-zinc deposit, Austria. In Miner Deposita 40 (1), pp. 123–126.

Leach, D. L.; Bradley, D. C.; Huston, D.; Pisarevsky, S. A.; Taylor, R. D.; Gardoll, S. J. (2010a): Sediment-Hosted Lead-Zinc Deposits in Earth History. In Economic Geology 105 (3), pp. 593–625.

Leach, D. L.; Sangster, D. F.; Kelley, K. D.; Large R. R.; Garven, G.; Allen, C. R. (2005): Sediment-hosted Pb-Zn Deposits: a global perspective. In Economic Geology 100, pp. 561–608.

Leach, D. L.; Taylor, R. D.; Fey, D. L.; Diehl, S. F.; Saltus, R. W. (2010b): A deposit model for Mississippi Valley-Type lead-zinc ores: Chapter A in Mineral deposit models for resource

assessment. With assistance of U. S. Geological Survey. Reston, VA (Scientific Investigations Report, 2010-5070A).

Lepetit, P.; Bente, K.; Doering, T.; Luckhaus, S. (2003): Crystal chemistry of Fe-containing sphalerites. In Physics and Chemistry of Minerals 30 (4), pp. 185–191.

Lockington, J. A.; Cook, N. J.; Ciobanu, C. L. (2014): Trace and minor elements in sphalerite from metamorphosed sulphide deposits. In Miner Petrol 108 (6), pp. 873–890.

Mandl, G. W. (2000): The Alpine sector of the Tethyan shelf - Examples of Triassic to Jurassic sedimentation and deformation from the Northern Calcareous Alps. In Mitteilungen der Österreichischen Geologischen Gesellschaft (92), pp. 61–77.

Melcher, F.; Oberthür, T.; Rammlmair, D. (2006): Geochemical and mineralogical distribution of germanium in the Khusib Springs Cu–Zn–Pb–Ag sulfide deposit, Otavi Mountain Land, Namibia. In Ore Geology Reviews 28 (1), pp. 32–56.

Möller, P.; Dulski, P. (1993): Germanium and gallium distribution in sphalerite. In Formation of Hydrothermal Vein Deposits–Case Study of the Pb-Zn, Barite and Fluorite Deposits of the Harz Mountains. Monograph Series on Mineral Deposits 30, pp. 189–196.

Möller, P.; Dulski, P. (1996): Germanium and gallium distribution in sphalerite a key to the genesis of sediment-hosted sulphide mineralizations. In ZEITSCHRIFT FUR GEOLOGISCHE WISSENSCHAFTEN 24, pp. 527–538.

Mortlock, R. A.; Froelich, P. N. (1986): Hydrothermal germanium over the southern East Pacific Rise. In Science 231 (4733), pp. 43–45.

Mostler, H. (1967): Bemerkungen zur Geologie der Ni-Co-Lagerstätte Nöckelberg bei Leogang, Salzburg: na.

Murnane, Richard J.; Stallard, Robert F. (1990): Germanium and silicon in rivers of the Orinoco drainage basin. In Nature 344 (6268), pp. 749–752.

Neubauer, F. (1987): The Gurktal thrust system within the Austroalpine region—some structural and geometrical aspects. In Geodynamics of the Eastern Alps, pp. 226–236.

Oftedal, I. W. (1941): Untersuchungen über die Nebenbestandteile von Ermineralien norwegischer zinkblendeführender Vorkommen: I Kommisjon hos J. Dybwad.

Ohmoto, H. (1972): Systematics of Sulfur and Carbon Isotopes in Hydrothermal Ore Deposits. In Economic Geology 67 (5), pp. 551–578.

Ohmoto, Hiroshi; Lasaga, Antonio C. (1982): Kinetics of reactions between aqueous sulfates and sulfides in hydrothermal systems. In Geochimica et Cosmochimica Acta 46 (10), pp. 1727–1745. DOI: 10.1016/0016-7037(82)90113-2.

Ono, S.; Hirai, K.; Matsueda, H.; Kabashima, T. (2004): Polymetallic Mineralization at the Suttsu Vein-type Deposit, Southwestern Hokkaido, Japan. In Resource Geology 54 (4), pp. 453–464.

Onuk, P.; Melcher, F.; Mertz-Kraus, R.; Gäbler, H-E.; Goldmann, S. (2016): Development of a Matrix-Matched Sphalerite Reference Material (MUL-ZnS-1) for Calibration of In Situ Trace Element Measurements by Laser Ablation-Inductively Coupled Plasma-Mass Spectrometry. In Geostand Geoanal Res.

Onuk, P.; Pribil, M. J.; Strauss, H.; Melcher, F. (2017a): MUL-ZnS-SI-1 and MUL-ZnS-SI-2: two matrix matched sulfur isotope reference materials for laser ablation MC-ICP-MS. LA-ICP-MS workshop Lubljana 2017.

Onuk, P.; Walkner, C.; Pribil, M.; Melcher, F. (2017b): In-situ measurement of sulfur isotopic composition (δ34S) in sphalerite using LA-(QQQ)-ICP-MS. Goldschmidt conference 2017

Paar, W. H.; Chen, T. T. (1986): Zur Mineralogie von Cu-Ni (Co)-Pb-Ag-Hg-Erzen im Revier Schwarzleo bei Leogang, Salzburg, Osterreich. In Mitteilungen der Österreichischen Geologischen Gesellschaft (78), pp. 125–148.

Paton, C.; Hellstrom, J.; Paul, B.; Woodhead, J.; Hergt, J. (2011): Iolite. Freeware for the visualisation and processing of mass spectrometric data. In J. Anal. At. Spectrom. 26 (12), p. 2508.

Pfaff, K.; Koenig, A.; Wenzel, T.; Ridley, Ian; Hildebrandt, L. H.; Leach, D. L.; Markl, Gregor (2011): Trace and minor element variations and sulfur isotopes in crystalline and colloform ZnS. Incorporation mechanisms and implications for their genesis. In Chemical Geology.

Piller, W. E.; Egger, H.; Erhart, Ch. W.; Gross, M.; Harzhauser, M.; Hubmann, B. et al. (2004): Stratigraphische Tabelle von Österreich 2004 (sedimentäre Schichtfolgen): Österreichische Stratigraphische Kommission.

Pohl, W.; Belocky, R. (1999): Metamorphism and metallogeny in the Eastern Alps. In Min Dep 34 (5-6), pp. 614–629.

Pohl, W. L. (2011): Economic Geology: Principles and Practice: John Wiley & Sons.

Rantitsch, G. (2001): Thermal history of the Drau Range (Eastern Alps). In Schweizerische Mineralogische und Petrographische Mitteilungen 81 (2), pp. 181–196.

Reuter, M. A.; Verhoef, E. V. (2004): A dynamic model for the assessment of the replacement of lead in solders. In Journal of Elec Materi 33 (12), pp. 1567–1580.

Robb, L. J. (2011): Introduction to ore-forming processes. [Nachdr.]. Malden, MA [u.a.]: Blackwell Publ.

Roberts, S.; Gunn, G. (2014): Cobalt. In G. Gunn (Ed.): Critical Metals Handbook. Indium. Oxford: John Wiley & Sons.

Rudnick, R. L.; Gao, S. (2005): Composition of the Continental Crust. In R. W. Carlson (Ed.): The mantle and core. 1st ed. Amsterdam, Boston: Elsevier (Treatise on geochemistry, vol. 2), pp. 1–64.

Schlüter, J.; Tarkian, M.; Stumpfl, E. F. (1984): Die stratiforme Sulfidlagerstätte Walchen, Steiermark, Österreich. Geochemie und Genese. In TMPM Tschermaks Petr. Mitt. 33 (4), pp. 287–296.

Schmid, S. M.; Fügenschuh, B.; Kissling, E.; Schuster, R. (2004): Tectonic map and overall architecture of the Alpine orogen. In Eclogae geol. Helv. 97 (1), pp. 93–117.

Schmidt, T.; Blau, J.; Kázmér, M. (1991): Large-scale strike-slip displacement of the Drauzug and the Transdanubian Mountains in early Alpine history. Evidence from permo-mesozoic facies belts. In Tectonophysics 200 (1-3), pp. 213–232.

Schönlaub, H. P.; Histon, K. (1999): The Palaeozoic Evolution of the Southern Alps 92, 1999, pp. 15–34.

Schroll, E. (1978): Beitrag der Geochemie zur Kenntnis der Lagerstätten der Ostalpen. In Geol. Bundesanstalt (Austria) Verh (3), pp. 461–470.

Schroll, E. (1983): Geochemical Characterization of the Bleiberg Type and Other Carbonate Hosted Lead-Zinc Mineralizations. In H-J. Schneider (Ed.): Mineral Deposits of the Alps and of the Alpine Epoch in Europe. Proceedings of the IV. ISMIDA Berchtesgaden, October 4-10, 1981. Berlin, Heidelberg: Springer Berlin Heidelberg (Special Publication No. 3 of the Society for Geology Applied to Mineral Deposits, 0723-8835, 3), pp. 189–197.

Schroll, E. (1985): Geochemische Parameter der Blei-Zink-Vererzung in Karbonatgesteinen und anderen Sedimenten. In Arch Lagerstättenforsch Geol Bundesanst Wien 6, pp. 167–178.

Schroll, E. (2006): Neues zur Genese der Blei-Zink-Lagerstätte Bleiberg. In Carinthia II 116, pp. 483–500.

Schroll, E.; Pak, E. (1983): Sulfur isotope investigations of ore mineralizations of the Eastern Alps. In : Mineral Deposits of the Alps and of the Alpine Epoch in Europe: Springer, pp. 169–175.

Schroll, E.; Rantitsch, G. (2005): Sulphur isotope patterns from the Bleiberg deposit (Eastern Alps) and their implications for genetically affiliated lead? Zinc deposits. In Mineralogy and Petrology 84 (1-2), pp. 1–18.

Schroll, Erich (2008): Blei-Zink-Lagerstätte Bleiberg. Die Geschichte ihrer Erforschung. Klagenfurt: Naturwissenschaftlicher Verein für Kärnten (Carinthia / 2 / Sonderheft, 62).

Schulz, O. (1981): Die Pb-Zn-Erzlagerstätte Lafatsch - Vomperloch (Karwendelgebirge, Tirol). In Veröffentlichung Museum Ferdinandeum (61), pp. 55–103.

Schwartz, M. O. (1997): Mercury in Zinc Deposits. Economic Geology of a Polluting Element. In International Geology Review 39 (10), pp. 905–923.

Schwartz, M. O. (2000): Cadmium in Zinc Deposits. Economic Geology of a Polluting Element. In International Geology Review 42 (5), pp. 445–469..

Schwarz-Schampera, U. (2014): Indium. In G. Gunn (Ed.): Critical Metals Handbook. Indium. Oxford: John Wiley & Sons.

Scott, S. D.; Barnes, H. L. (1971): Sphalerite geothermometry and geobarometry. In Economic Geology 66 (4), pp. 653–669.

Seal, Robert R.; Alpers, Charles N.; Rye, Robert O. (2000): Stable isotope systematics of sulfate minerals. In Reviews in Mineralogy and Geochemistry 40 (1), pp. 541–602.

Strunz, H.; Geier, B. H.; Seeliger, E. (1958): Gallit, CuGaS2, das erste selbständige Galliummineral, und seine Verbreitung in den Erzen der Tsumeb-und Kipushi-Mine. In N. Jb. Mineral. Mh. 1958, pp. 241–264.

Unger, H. J. (1969): Detaillierte geologische Aufnahme des Walchengrabens bei Öblarn, Ennstal und des niederöblarner Grabens bis zum Ernestine-Stollen: na.

Wager, L. R.; Smit, J.van R.; Irving, H. (1958): Indium content of rocks and minerals from the Skaergaard intrusion, East Greenland. In Geochimica et Cosmochimica Acta 13 (2-3), pp. 81–86.

Weber, L. (1990): Die Blei-Zinkerzlagerstätten des Grazer Paläozoikums und ihr geologischer Rahmen. Wien: Geologische Bundesanst (Archiv für Lagerstättenforschung der Geologischen Bundesanstalt, Bd. 12).

Weber, L. (2012): Der Österreichische Rohstoffplan. Archiv für Lagerstättenforschung Geologische Bundesanstalt. Wien.

Weber, L.; Cerny, I. (1997): Handbuch der Lagerstätten der Erze, Industrieminerale und Energierohstoffe Österreichs. Wien: Geologische Bundesanst (19,2).

Wilson, S. A.; Ridley, W. I.; Koenig, A. E. (2002): Development of sulfide calibration standards for the laser ablation inductively-coupled plasma mass spectrometry technique. In J. Anal. At. Spectrom. 17 (4), pp. 406–409.

Wood, S. A.; Samson, I. M. (2000): The Hydrothermal Geochemistry of Tungsten in Granitoid Environments. I. Relative Solubilities of Ferberite and Scheelite as a Function of T, P, pH, and mNaCl. In Economic Geology 95 (1), pp. 143–182.

Xiong, Y. (2007): Hydrothermal thallium mineralization up to 300 °C. A thermodynamic approach. In Ore Geology Reviews 32 (1-2), pp. 291–313.

8.1 Appendix

8.1.1 Sample locations

Table 40: Location, GPS data (WGS 84 coordinate), sampling date and sample type of the self-collected samples.

Location	GPS data	Date	underground	dump site
Jauken	13°03.55` 46°42.00`	17.08.2015		X
Radnig	13°22.42` 46°39.70`	09.10.2015		X
Bleiberg Ramser ore	13°38.86` 46°37.78`	06.08.2016	X	
Fladung	14°30.97` 46°29.62`	31.10.2015		X
Guggenbach	15°13.95` 47°12.57`	13.09.2015		X
Arzberg	15°31.15` 47°15.06`	13.11.2015	X	
Rabenstein	15°18.57` 47°14.90`	09.10.2014		X
Elisabeth adit	15°20.06` 47°12.57`	10.10.2014	X	
Friedrich adit	15°19.74` 47°11.97`	10.10.2014	X	
Silberberg	15°13.70` 47°11.91`	09.04.2014	X	
Haufenreith	15°31.55` 47°15.61`	30.04.2016		X
Meiselding	14°22.68` 46°50.95`	02.05.2015	X	
Walchen Thaddäus adit	14°03.34` 47°25.78`		X	
Walchen dump site	14°03.21` 47°25.54`			X
Leogang/Schwarzleo	12°40.41`	26.05.2016	X	

Mariahilf Stollen	47°25.22`			
Koprein	14°41.19` 46°28.68`	20.11.2014		X
Metnitz adit	14°10.75` 46°57.62`	25.05.2015	x	
Metnitz open pit	14°10.77` 46°57.59`	25.05.2015		x
Achselalm	12°23.51` 47°14.43`	29.09.2015	X	
Flecktrogalm	12°23.49` 47°14.35`	29.09.2015	X	

8.1.2 Geographical maps

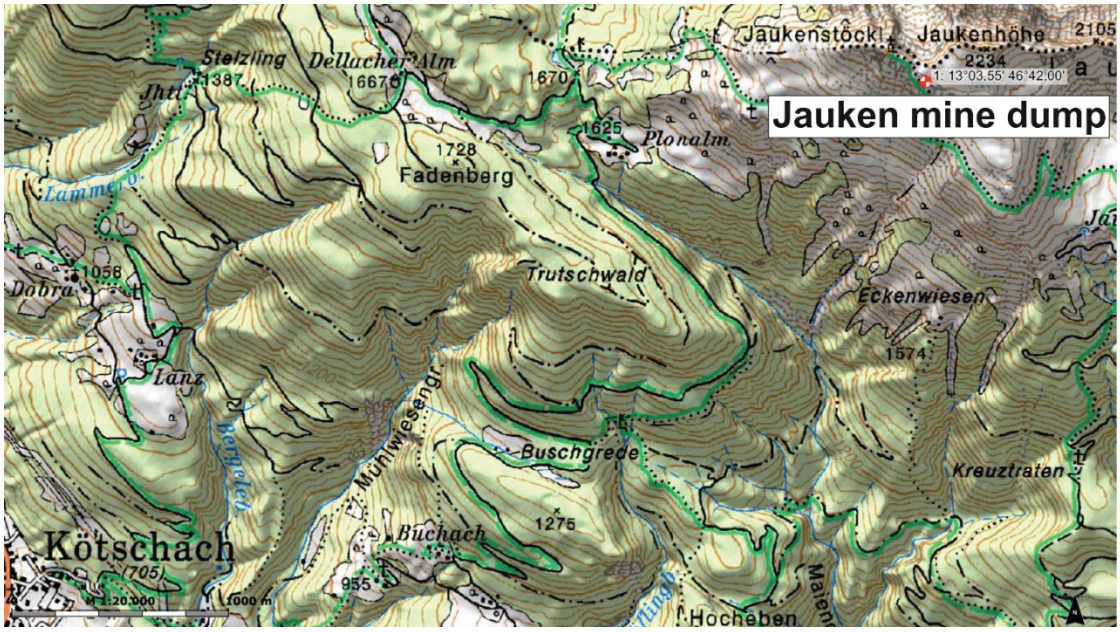

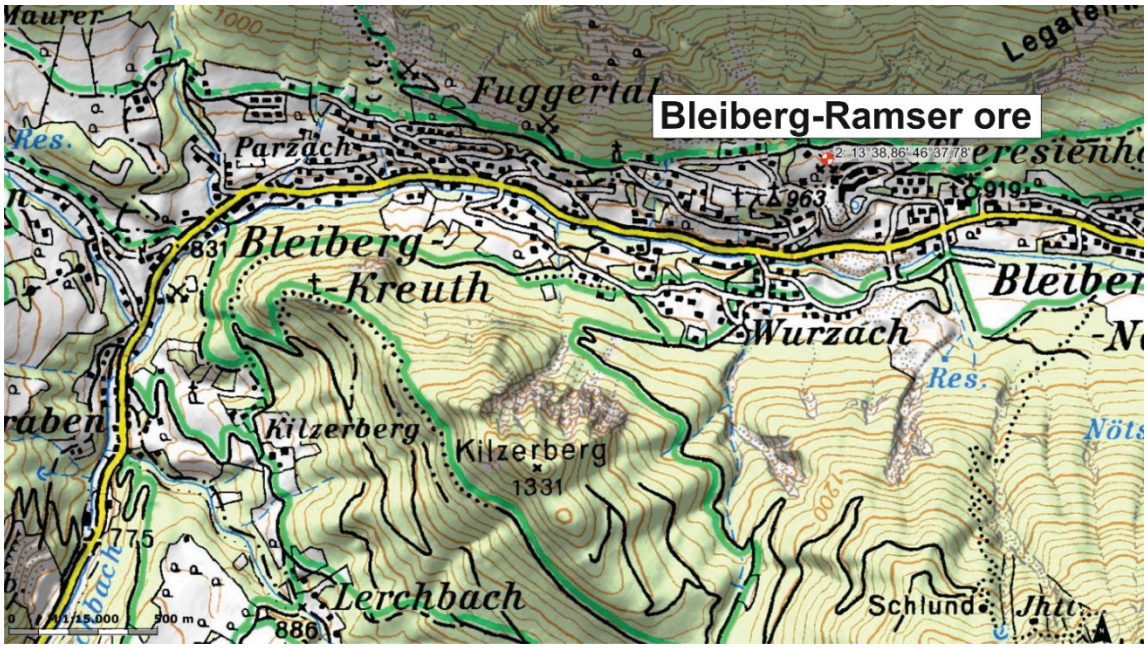
Bleiberg-Ramser ore
Fuggertal
Parzach
Bleiberg-
-Kreuth
Wurzach
Kilzerberg
Kilzerberg
1331
Lerchbach
Schlund
Res.
831
886
775

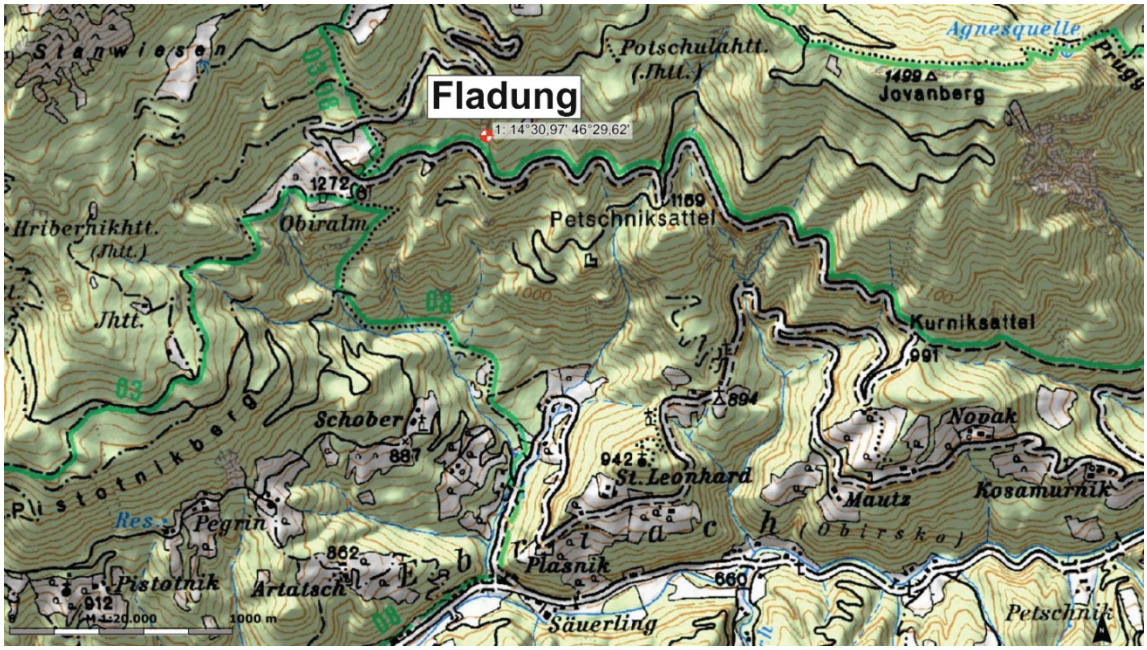
Fladung
Potschulahtt.
(Jhtt.)
Agnesquelle
Jovanberg
1499
Petschniksattel
1169
Obiralm
1272
Hriberhikhtt.
(Jhtt.)
Jhtt.
Kurniksattel
901
Schober
887
St. Leonhard
942
Novak
Mautz
Kosamurnik
Pegrin
Plasnik
Pistotnik
Artatsch
862
912
Säuerling
Petschnik
Res.
894
660

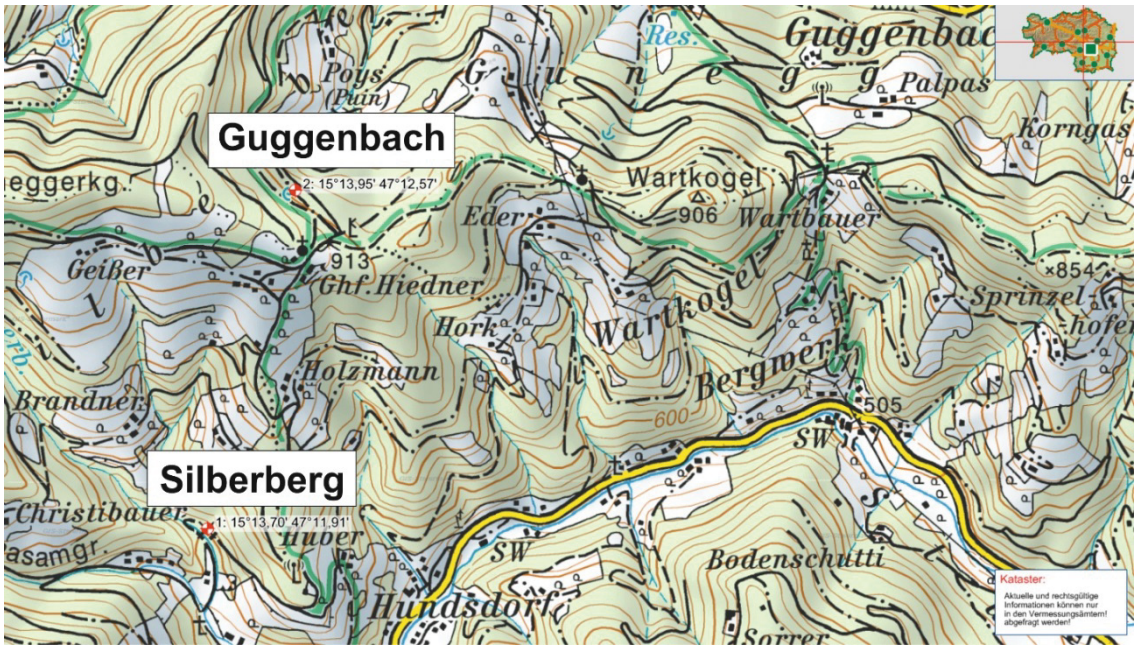
Guggenbach
Silberberg
Wartkogel
Eder
Geißer
Ghf. Hiedner
Holzmann
Brandner
Hork
Bergwerk
Sprinzel
Palpas
Korngas
Wartbauer
Christibauer
Huber
Hundsdorf
Bodenschutti
Sorrer
Kataster:
Aktuelle und rechtsgültige Informationen können nur in den Vermessungsämtern! abgefragt werden!

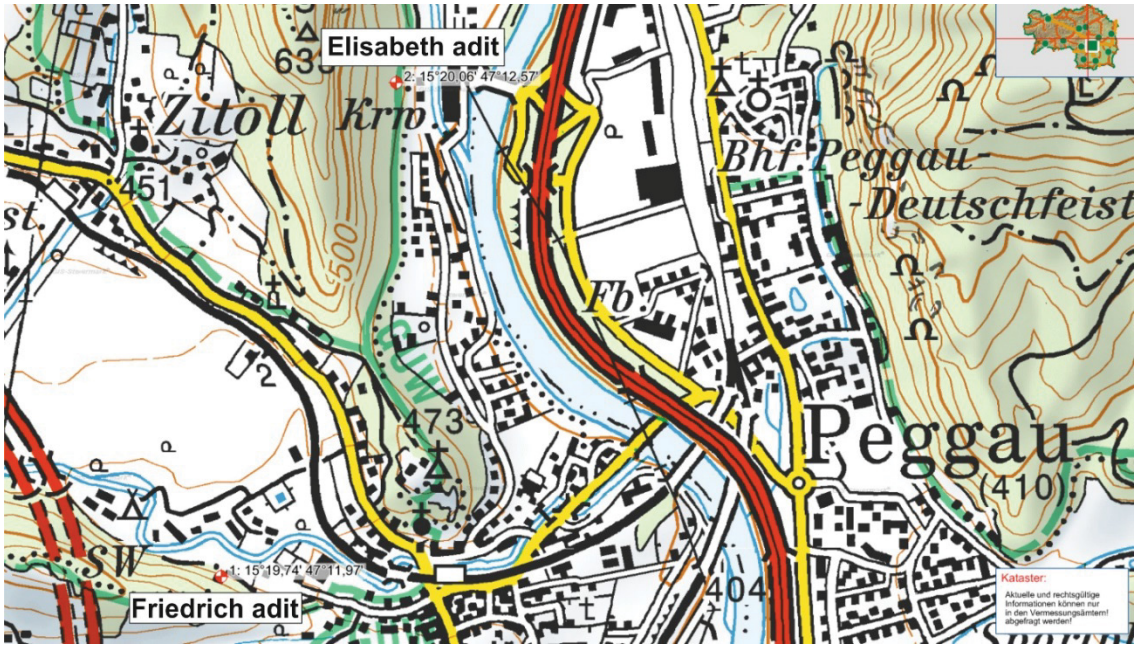
Elisabeth adit
Friedrich adit
Zitoll
Krp.
Bhf. Peggau-
-Deutschfeist
Peggau
(410)
Fb.
473
451
404
Kataster:
Aktuelle und rechtsgültige Informationen können nur in den Vermessungsämtern! abgefragt werden!


Haufenreith
Arzberg
Arzberg
Gösser
Stadlzenzenhalt
1088
592
750
1030
Kataster:

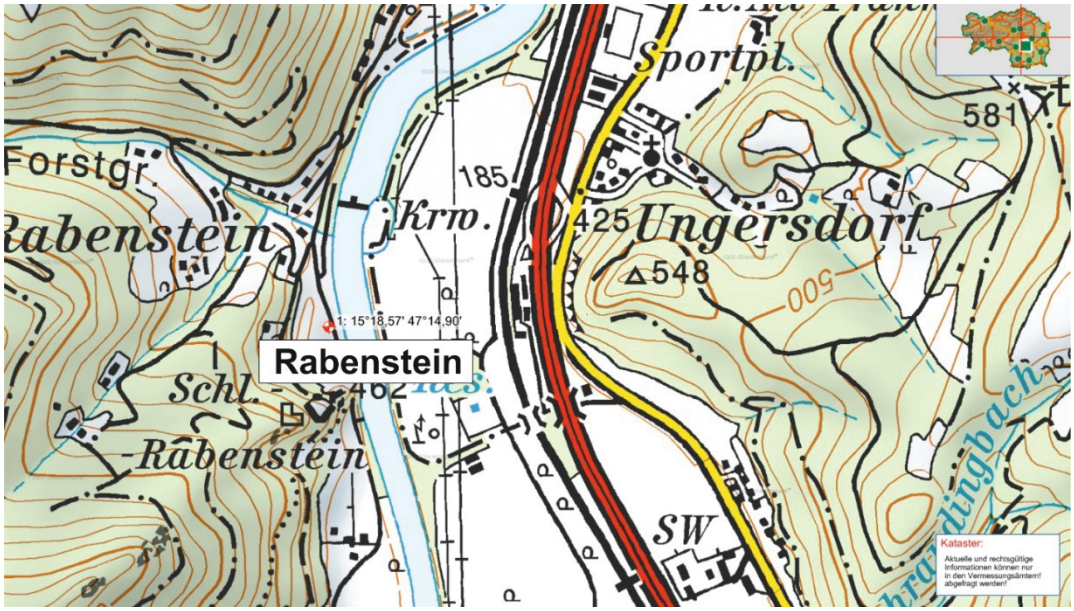
Rabenstein
Rabenstein
Forstgr.
Krrw.
Sportpl.
Ungersdorf
548
581
425
185
SW
Schl.
Kataster:

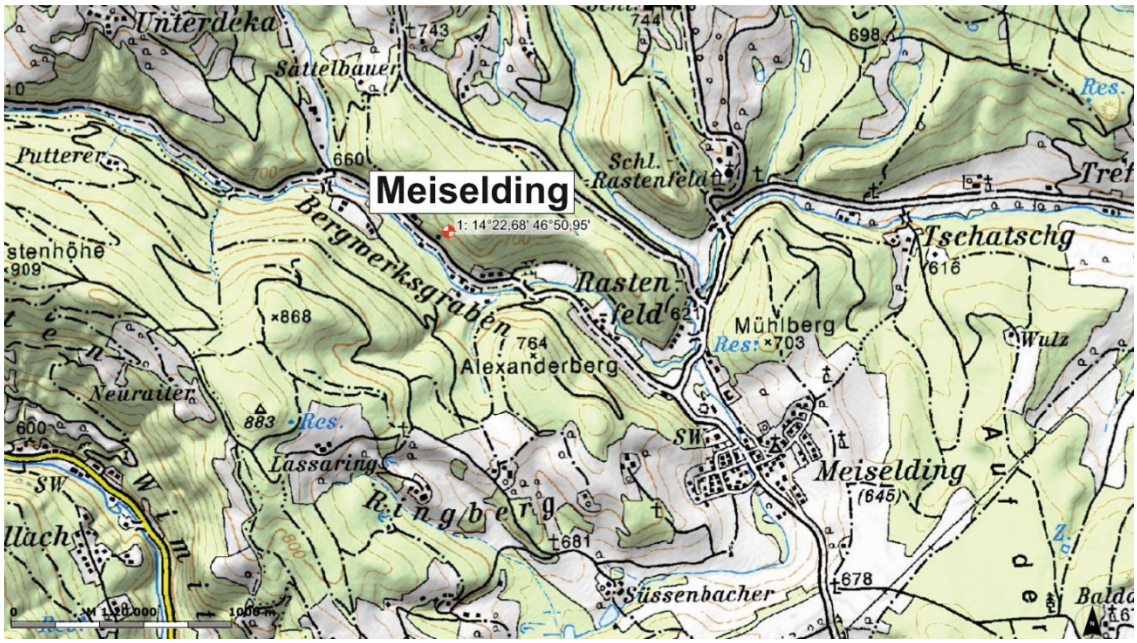
Meiselding
1: 14°22,68' 46°50,95'
Unterdeka
Sattelbauer
Putterer
Bergwerksgraben
Rasten-feld
Alexanderberg
Mühlberg
Tschatschg
Wulz
Neuraiter
Lassaring
Ringberg
Meiselding
Süssenbacher
Schl. Rastenfeld
Res.

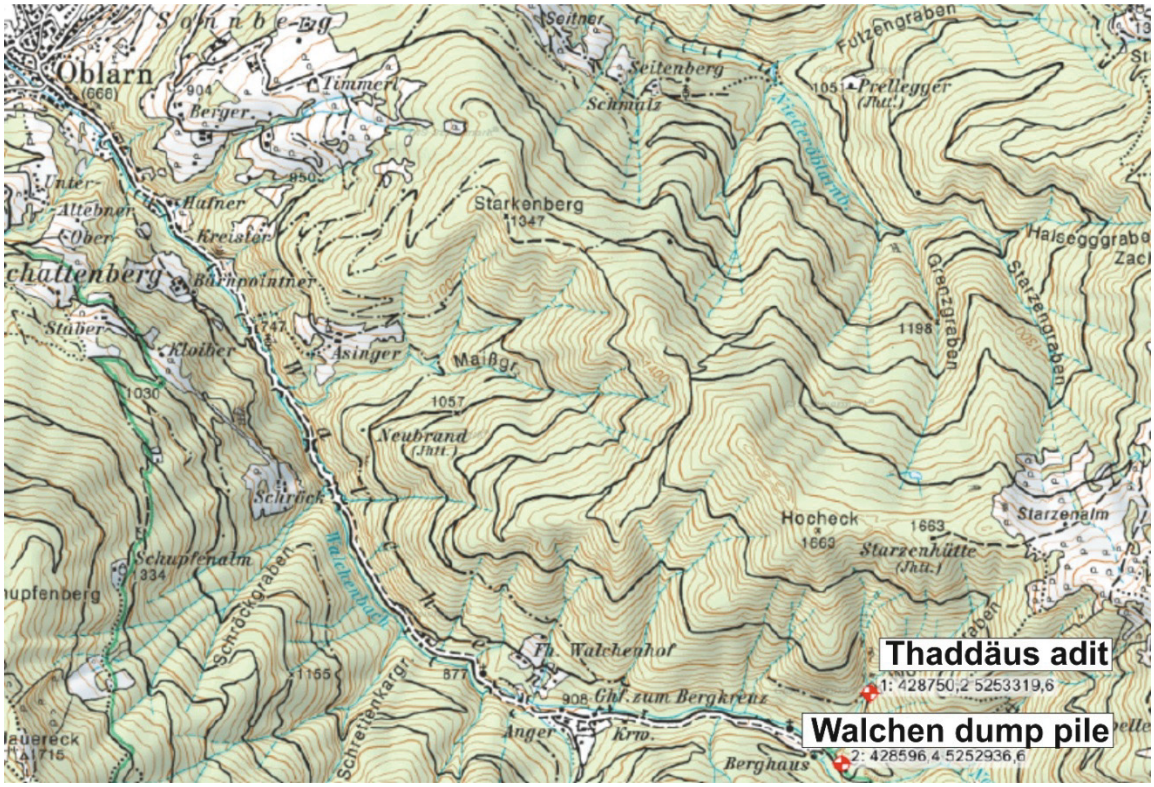
Oblarn
Starkenberg
Neubrand
Hocheck
Starzenalm
Starzenhütte
Schuptenalm
Fh. Walchenhof
Ghf. zum Bergkreuz
Berghaus
Seitenberg
Prellegger
Thaddäus adit
1: 428750,2 5253319,6
Walchen dump pile
2: 428596,4 5252936,6

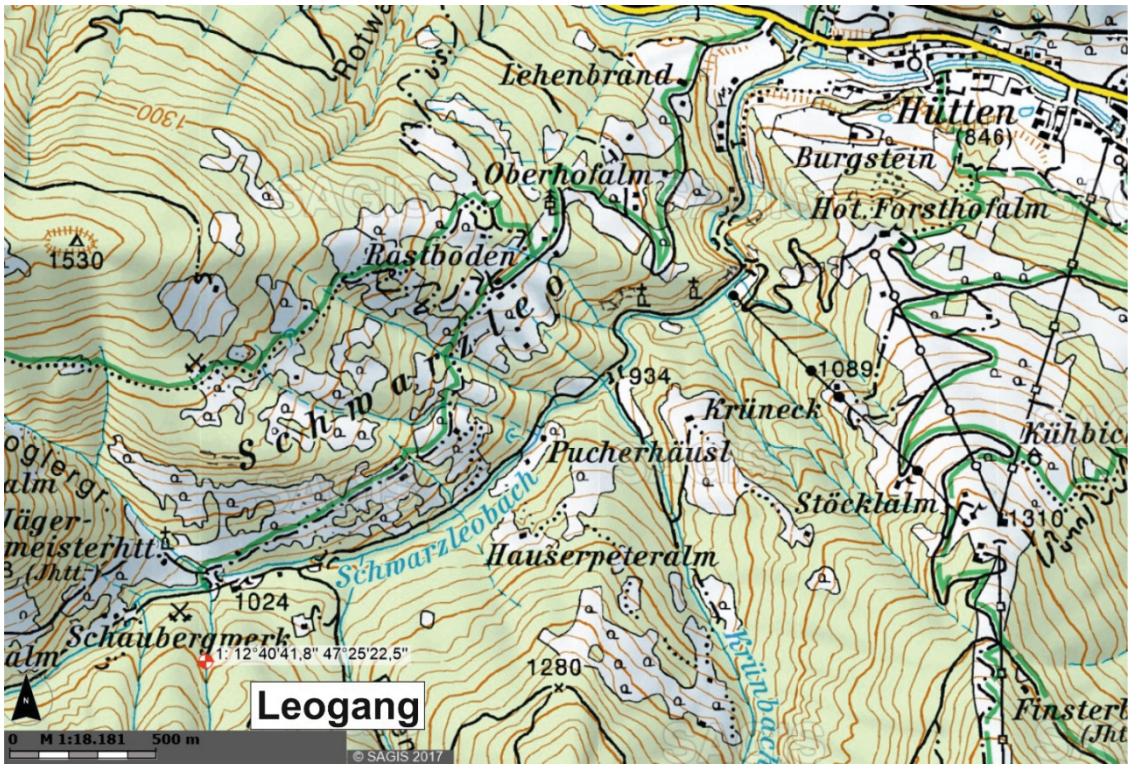
Lehenbrand
Hütten
(846)
Burgstein
Oberhofalm
Hot. Forsthofalm
1530
Rastboden
1934
1089
Krüneck
Pucherhäusl
Stöcklalm
1310
Hauserpeteralm
Schwarzleobach
1024
Schaubergmerk
1: 12°40'41,8" 47°25'22,5"
1280
Leogang
0 M 1:18.181 500 m
© SAGIS 2017


Dertsche
Wenetik
1202
Gorelza
1360
Vinoda
1095
Petschnik
Winkl
Wh. Rastotschnik
827
Koprein-Sonnseite
1228
Auprich
Gregoritsch
748
Koprein
1136
Leppenbach
706
1017
Hrewelnik
1: 14°41,19' 46°28,68'
Riegelnik
Jawornik
1507
Sneschnik
1543
Spitzberg
0 M 1:20.000 1000 m

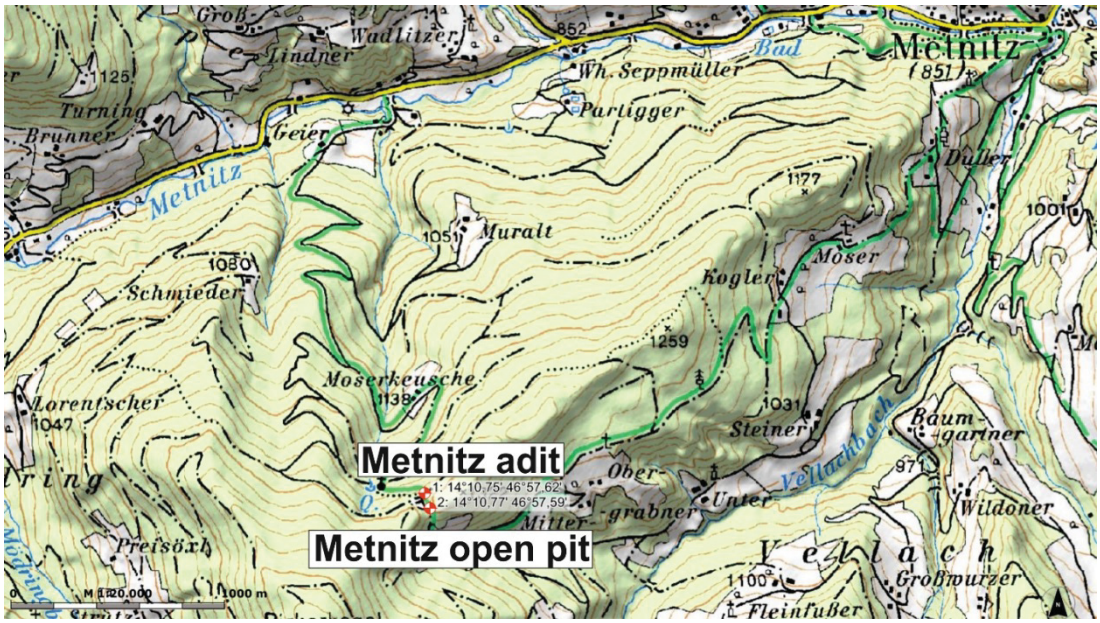
Metnitz adit
1: 14°10'75" 46°57'62"
2: 14°10'77" 46°57'59"
Metnitz open pit
Metnitz
Muralt
Schmieder
Moserkeusche
Kogler
Moser
Steiner
Baumgartner
Wildoner
Großwurzer
Fleintußer
Vellachbach
Vellach
Metnitz
Wh. Seppmüller
Partigger
Duller
Lindner
Wadlitzer
Turning
Brunner
Geier
Lorentscher
Preisöxh
Ober-grabner
Unter-grabner
M 1:20.000
1000 m

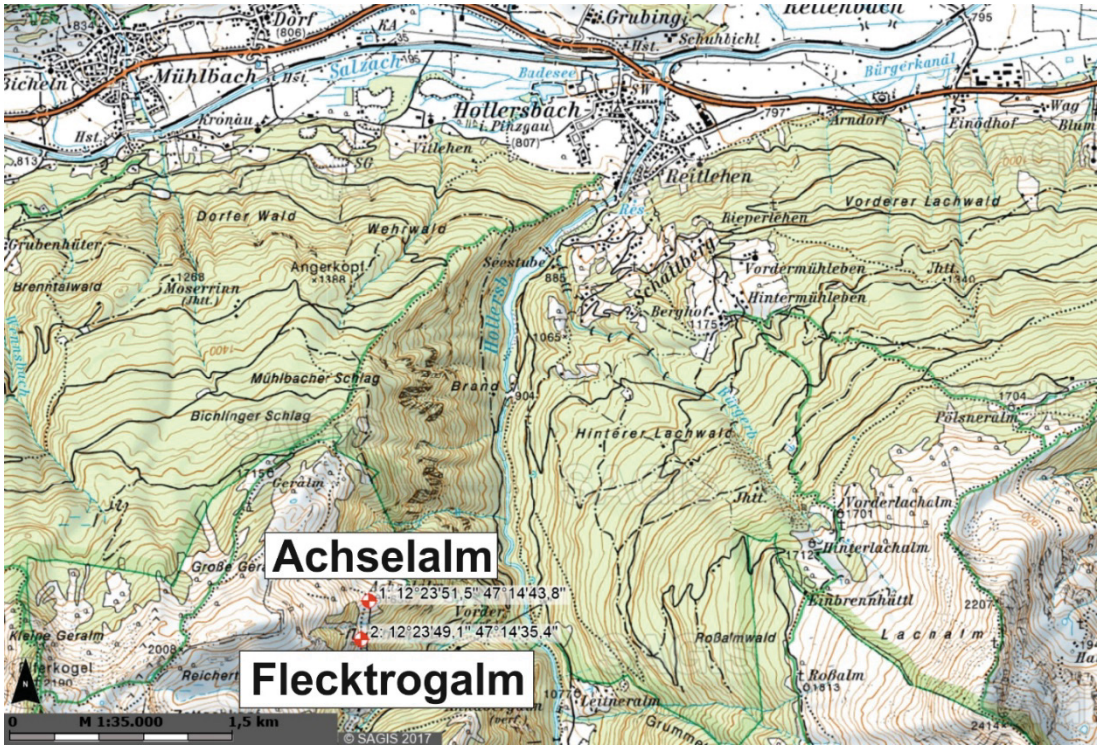
Achselalm
1: 12°23'51,5" 47°14'43,8"
2: 12°23'49,1" 47°14'35,4"
Flecktrogalm
Mühlbach
Hollersbach
Reitlehen
Vorderer Lachwald
Hinterer Lachwald
Dorfer Wald
Wehrwald
Angerkopf
Brenntalwald
Mühlbacher Schlag
Bichlinger Schlag
Brand
Schattberg
Vordermühleben
Hintermühleben
Bergbof
Pölsneralm
Vorderlachalm
Hinterlachalm
Einbrennhüttl
Roßalmwald
Lachalm
Roßalm
Leitneralm
Arndorf
Einödhof
Badesee
Salzach
Hollersbach
Grubingi
Schuhbichl
Bürgerkanal
Seestube
Villehen
Pinzgau
Krönau
Dorf
Grubenhüter
Kleine Geralm
Geralm
Reicherkogel
0 M 1:35.000 1,5 km
© SAGIS 2017